Investigating the effect that disease-linked PLCγ2 variants have on enzymatic activity, and exploring PLCγ2's role within microglia cell function

Thesis submitted for the degree of

Doctor of Philosophy

Student: Daniel Anthony Bull

Supervisors: Professor. Paul Whiting and

Professor. Matilda Katan

Department: Institute of Neurology

Funding: UCL Impact Studentship supported by GlaxoSmithKline Research & Development Limited (GSK)

Declaration

I, Daniel Anthony Bull confirm that the work presented in this thesis is my own. Where information/materials have been gathered from other sources, I confirm that this has been indicated in the thesis.

Abstract

Phospholipase C-gamma 2 (PLCγ2) is highly expressed in immune cells, such as microglia. PLCγ2 hydrolyses phosphatidylinositol 4,5-bisphosphate into inositol trisphosphate (IP_3) and diacylglycerol. Variants of PLCγ2 have been described in several diseases, such as late onset Alzheimer's disease (LOAD), inflammatory bowel disease, as well as rare immune disorders, suggesting a key role for this enzyme in the regulation of immune cell function. To characterise the enzymatic activity of disease-linked PLCγ2 variants, an assay measuring inositol monophosphate (IP_1), a downstream metabolite of IP_3, was adapted and optimised. The S707Y, Δ845-848 and M1141K PLCγ2 variants, linked to a complex immune disorder, have strong hypermorphic activity, whereas the PLCγ2 V1103I variant shows a mild increase in PLC activity.

In the context of LOAD, microglia have been implicated as key mediators of disease pathophysiology. However, the role of PLCγ2 within microglia is still not fully understood. To address this issue, the hypermorphic PLCγ2 S707Y disease linked-variant was introduced into human inducible pluripotent stem cells (hiPSCs) to explore the role that strong gain-of-function PLCγ2 variants have within hiPSC-derived microglia. Based on the IP_1 measurements, PLCγ2 S707Y hiPSC-derived microglia exhibited hypermorphic enzymatic activity under both basal and stimulated conditions, which in turn resulted in increased calcium flux. However, when challenged with apoptotic neuronal cells, a reduction in phagocytosis was observed. Additionally, secretion of IL-1β, IL-8 and TNF-α was shown to be elevated in basal conditions. However, when challenged with lipopolysaccharide, PLCγ2 S707Y hiPSC-derived microglia exhibited a reduction in IL-10, IL-6 and TNF-α secretion, likely due to decreased NF-κB activation and translocation. RNA sequencing of the PLCγ2 S707Y hiPSC-derived microglia revealed a downregulation of genes related to innate immunity and response. Therefore, this thesis demonstrates that despite the increase in PLCγ2 enzymatic activity, the PLCγ2 S707Y hiPSC-derived microglia display a loss of function for key microglial processes.

Impact statement

Alzheimer's disease (AD) is a neurological disorder that causes the brain to shrink and brain cells to die. AD is becoming an increasingly more prevalent condition, especially as human life expectancy is improving. Currently, there is no treatment available to cure AD, and only a handful of medications that temporary improve or slow progression. To combat such issues, genome wide association studies (GWAS) have been implemented to identify genomic variants associated with LOAD, resulting in the identification of PLCγ2 risk (M28L) and protective (P522R) variants.

Microglia have been implicated as key mediators of LOAD pathophysiology. PLCγ2 is highly expressed in microglia, although its role within microglial biology is still not fully defined. To address such questions, PLCγ2 KO and P522R microglial models have been developed and characterised. However, it still remains to be investigated what role the protective PLCγ2 P522R variant has on LOAD pathophysiology, especially given the mild hypermorphic activity it exhibited.

Rare and novel PLCγ2 variants linked to severe inflammation have been identified in literature. To address questions on how the PLCγ2 variants influence enzymatic activity, an artificial transient transfection model was developed and optimised to rank the activity (IP_1 accumulation) of the PLCγ2 variants of interest, allowing for the enzymatic characterisation of the novel PLCγ2 Δ845-848, M1141K and V1103I variants. From the enzymatic activity ranking, the PLCγ2 S707Y variant was selected to be implemented into hiPSC-derived microglia, as strong hypermorphic PLCγ2 variants have not been assessed within microglial biology. Although the PLCγ2 S707Y variant displayed its characteristic hypermorphic enzymatic activity, and subsequent increased calcium flux, it was uncovered that the variant resulted in a decrease of key microglial processes such as phagocytosis and cytokine production (upon LPS exposure). RNASeq analysis showed a significant downregulation of phagocytic receptors (AXL, MERTK and P2RY6) and complement pathway proteins (C1QA, C1QB, C1QC, C3 and C3AR1), as well as genes related to innate immunity and response.

Overall, this thesis provides novel insight into the role PLCγ2 has within microglial biology, concluding that strong hypermorphic PLCγ2 variants drastically alter microglial functionality. Furthermore, this thesis provides a platform for the improved characterisation of the PLCγ2 P522R LOAD protective variant, ultimately providing key valuable knowledge for the development of therapeutics for treatment of LOAD.

Preface

The work in this thesis was carried out at the University College London (UCL) under the supervision of Prof. Paul Whiting, Prof. Matilda Katan and Dr. Lorenza Magno. Throughout my PhD, I was sponsored by the UCL Impact Studentship supported by GlaxoSmithKline Research & Development Limited.

Unless stated otherwise, all work was performed by me. Work conducted with colleagues from the lab, or in collaboration with other labs, is indicated here and mentioned in the relevant parts of the thesis.

In Chapter 3, Prof. Matilda Katan (UCL, England) provided the PLCγ2-pTriEx-4 (PLCγ2-HIS) and peGFP-PLCγ2 (PLCγ2-GFP) vectors which encode the full length wild-type human PLCγ2 cDNA, as well as an empty peGFP-C1 vector. The A708P and Δ845-848 constructs were generated and validated by Dr. Tom Bunney (Katan Lab, UCL, England). Additionally, all PLCγ2 plasmid variants were validated by Sanger Sequencing through Source Bioscience (England). Moreover, an anti-PLCγ2 antibody was kindly provided by Prof. Todd Golde (University of Florida, USA)

In Chapter 7, PLCγ2 WT and S707Y hiPSC lines were generated by Dr. Rebecca McIntyre and Julie Matte (Wellcome Sanger Institute, England). The sequencing of the hiPSC PLCγ2 single nucleotide polymorphisms was performed by GVG Genetic Monitoring GmbH (Germany).

In Chapter 8, RNASeq was performed by University College London Genomics (UCL, England).

Acknowledgements

I would like to thank all members, past and present, of the Alzheimer's Research UK University College London Drug Discovery Institute (ARUK UCL DDI) for their support, help and friendship throughout my PhD. Specifically, I would like to thank Prof. Paul Whiting, Dr. Lorenza Magno and Prof. Matilda Katan for being fantastic mentors and allowing me to have this amazing opportunity!

I would like to give a special thanks to Emma Lovesey, Silvana Silva, Anthony Bull and Carmen Silva for supporting me through this journey. I am incredibly lucky to have them all in my life and would not have been able to do this without their support.

List of publications

The research findings from this thesis and my industrial placement have been published in a series of journals, listed below:

1. Martín-Nalda, A., Fortuny, C., Rey, L., Bunney, T., Alsina, L., Esteve-Solé, A., **Bull, D.**, et al. Severe Autoinflammatory Manifestations and Antibody Deficiency Due to Novel Hypermorphic PLCG2 Mutations. J Clin Immunol 2020, **40**, 987–1000.
2. **Bull, D.**, Schweitzer, C., Bichsel, C., Britschgi, M., Gutbier, S. Generation of an hiPSC-Derived Co-Culture System to Assess the Effects of Neuroinflammation on Blood–Brain Barrier Integrity. Cells 2022, **11**, 419.

Table of contents:

List of figures

List of tables

List of abbreviations/acronyms

^{3}H	Tritium
ACTB	Actin beta
ADP	Adenosine diphosphate
AIF1/IBA1	Allograft inflammatory factor 1/Ionized calcium binding adaptor molecule 1
ANOVA	Analysis of variance
APLAID	Auto-inflammation and phospholipase Cγ2 (PLCγ2)-associated antibody deficiency and immune dysregulation
APOE	Apolipoprotein E
APP	Amyloid precursor protein
ARID2	AT-rich interaction domain 2
ARM	Activated response microglia
ASD	Autism spectrum disorder
ATP	Adenosine 5'-triphosphate
ATP5B	ATP synthase F1 subunit beta
AXL	AXL receptor tyrosine kinase
BCR	B cell receptor
BLNK	B cell linker
BMP4	Bone morphogenetic protein 4
BSA	Bovine serum albumin
BTK	Bruton's tyrosine kinase
C1QA	Complement C1q A
C1QB	Complement C1q B
C1QC	Complement C1q C
C3	Complement component 3
C3AR1	Component 3a receptor 1
Cas9	CRISPR associated protein 9
CD11b/ITGAM	Integrin subunit alpha M
CD14	Cluster of differentiation 14
CD163	Cluster of differentiation 163
CD163L1	Cluster of differentiation 163 like 1
CD45	Protein tyrosine phosphatase receptor type C
CD68	Cluster of differentiation 68
CD79	Cluster of differentiation 79
CD8	Cluster of differentiation 8
CD95	Cluster of differentiation 95
CMV	Cytomegalovirus
CNS	Central nervous system
CO_2	Carbon dioxide
CPM	Counts per million
CR3	Complement receptor 3
CRISPR	Clustered regularly interspaced short palindromic repeats

CSF	Cerebrospinal fluid
CSF1R	Colony stimulating factor 1 receptor
CX3CR1	CX3C chemokine receptor 1
CXCL8	Chemokine (C-X-C motif) ligand 8
DAG	Diacylglycerol
DAM	Disease associated microglia
DAP12/TYROBP	TYRO protein tyrosine kinase-binding protein
DAPI	4′,6-diamidino-2-phenylindole
DEGs	Differentially expressed genes
DMEM	Dulbecco's modified eagle medium
DMSO	Dimethyl sulfoxide
DNA	Deoxyribonucleic acid
EB	Embryoid body
EGF	Epidermal growth factor
EGFR	Epidermal growth factor receptor
ENU	N-ethyl-N-nitrosourea
ERK	Extracellular signal-regulated kinase
FBS	Fetal bovine serum
FcγRIIA	Fc gamma receptor IIa
FDR	False discovery rate
FL	Full length
FOLR2	Folate receptor beta
GAPDH	Glyceraldehyde 3-phosphate dehydrogenase
GAS6	Growth arrest specific 6
GFP	Green fluorescent protein
GO	Gene ontology
GOF	Gain of function
GSEA	Gene set enrichment analysis
GWAS	Genome wide association study
HBSS	Hanks' balanced salt solution
HEK293	Human embryonic kidney 293 cells
HEK293T	Human embryonic kidney 293 cells expressing SV40 large T antigen
HEPES	4-(2-hydroxyethyl)-1-piperazineethanesulfonic acid
hESCs	Human embryonic stem cells
HET	Heterozygous
HIS	Histidine
HOMO	Homozygous
HTRF	Homogeneous time resolved fluorescence
IBD	Inflammatory bowel disease
ICC	Immunocytochemistry
iDEP	Integrated differential expression and pathway analysis.
IFIT1	Interferon induced protein with tetratricopeptide repeats 1
IFITM3	Interferon induced transmembrane protein 3

IFN-γ	Interferon-gamma
IL-10	Interleukin 10
IL-12	Interleukin 12
IL-1β	Interleukin 1 beta
IL-23	Interleukin 23
IL-3	Interleukin 3
IL-34	Interleukin 34
IL-4	Interleukin 4
IL-6	Interleukin 6
IL-8	Interleukin 8
IP_1	Inositol monophosphate
IP_3	Inositol 1,4,5-trisphosphate
IP_3R	Inositol 1,4,5-trisphosphate receptor
iPSCs	Induced pluripotent stem cells
ITAM	Immunoreceptor tyrosine-based activation motif
kDa	Kilodaltons
KI	Knock in
KO	Knock out
LAT	Linker for activation of T cells
LB	Luria-Bertani
LOAD	Late-onset Alzheimer's disease
LPL	Lipoprotein lipase
LPS	Lipopolysaccharides
LYN	LYN proto-oncogene, tyrosine kinase
MERTK	MER proto-oncogene, tyrosine kinase
MX1	MX dynamin like GTPase 1
NFAT	Nuclear factor of activated T-cells
NFT	Neurofibrillary tangles
NGS	Next-generation sequencing
NLRP3	NLR family pyrin domain containing 3
O_2	Oxygen
P2RY12	Purinergic receptor P2Y12
P2RY6	Purinergic receptor P2Y6
PBMC	Human peripheral blood mononuclear cells
PBS	Phosphate buffered saline
PBST	Phosphate buffered saline Tween
PC	Phosphatidylcholine
PCA	Principle component analysis
PCR	Polymerase chain reaction
PEDF/SERPINF1	Pigment epithelium derived factor/Serpin family F member 1
PEI	Polyethylenimine
PFA	Paraformaldehyde
PI	Phosphatidylinositol

PI3K	Phosphatidylinositol 3 kinase
PIP_2	Phosphatidylinositol 4,5-bisphosphate
PIP_3	Phosphatidylinositol 3,4,5-trisphosphate
PKC	Protein kinase C
PL	Phospholipase
PLA	Phospholipase A
PLAID	Phospholipase Cγ2 (PLCγ2)-associated antibody deficiency and immune dysregulation
PLC	Phospholipase C
PLCY1	Phospholipase C gamma 1
PLCY2	Phospholipase C gamma 2
PLD	Phospholipase D
PLIN2	Perilipin 2
PPI	Protein–protein interaction
PTPRC/CD45	Protein tyrosine phosphatase receptor type C/Cluster of differentiation 45
qPCR	Quantitative polymerase chain reaction
RasGRP	RAS guanyl-releasing protein 1
RCU	Red calibrated units
RFU	Relative fluorescence units
RLU	Relative light units
RNA	Ribonucleic acid
ROS	Reactive oxygen species
RPS4Y1	Ribosomal protein S4 Y-linked 1
RT	Reverse transcription
SALL1	Spalt like transcription factor 1
SCF	Stem cell factor
SD	Standard deviation
SIGLEC1	Sialoadhesin
SLC2A5/GLUT5	Solute carrier family 2 member 5
SLP-76	Glucose transporter type 5
SNP	Single nucleotide polymorphism
SPI1/PU.1	Spi-1 proto-oncogene
STRING	Search tool for the retrieval of interacting genes/proteins
SYK	Spleen associated tyrosine kinase
TAM	Tyro3, Axl and MerTK
TGF	Transforming growth factor
TLR4	Toll-like receptor 4
TMEM119	Transmembrane protein 119
TNF	Tumor necrosis factor
TREM2	Triggering receptor expressed on myeloid cells 2
UBC	Ubiquitin C
VEGF	Vascular endothelial growth factor
WT	Wild type

Chapter 1 - Introduction

1.1 Inflammation

Inflammation is a rapid and coordinated response by the hosts immune system to defend against microbial infection, tissue injury and other noxious conditions, by removing the hazardous stimuli and initiating repair[1]. Therefore, inflammation is a defence mechanism essential for health. However, in some instances inflammation is viewed as an unwanted response, as prolonged or overactive inflammation can result in serious repercussions to human health.

During acute inflammation, cellular and molecular events aim to control infection and minimise injury, eventually resulting in homeostasis and the termination of the acute inflammation. However, if uncontrolled acute inflammation can become chronic. Chronic inflammation has been linked to multiple diseases such as diabetes, metabolic syndrome, cardiovascular disease, cancer, rheumatoid arthritis, inflammatory bowel disease (IBD), asthma, chronic obstructive lung disease, as well as neurodegenerative disorders such as Alzheimer's disease (AD)[1]. Hence, the development of novel and efficacious therapies targeting these inflammatory pathways has high potential in preventing and eradicating these diseases.

1.2 Innate immune cells involved in inflammation

1.2.1 Introduction

Humans, and other mammals, live in an environment that is populated by both pathogenic and non-pathogenic microbes that threaten normal homeostasis[2]. If microbes are able to bypass the physical and chemical barriers (e.g. skin and mucus secretion) that mammals possess, the immune system will elicit its "two lines of defence", known as the innate and adaptive response, in order to prevent microbial invasion[2].

The innate system is the first line of defence against microbial incursions. Its role is to prevent infection, eliminate invader microbes and stimulate the acquired immune response. Firstly, innate immune cells recognise foreign cell surface proteins, molecules or deoxyribonucleic acid (DNA) and become activated[3]. This activation elicits a multicellular defence mechanism that uses inflammatory responses, phagocytosis, natural killer cells and the complement system, to damage and remove any foreign substance[4].

The innate immune response also initiates the secondary defence mechanism called the adaptive immune response. The adaptive system is comprised of T- and B-lymphocytes that destroy invading pathogens through antigen-dependent and antigen-specific processes[5]. The hallmark of the adaptive immunity is its ability to "memorise", which enables the host to elicit a more rapid and efficient immune response upon subsequent exposure to the antigen[5]. It is worth noting that there is a 4-7 day lag between antigen exposure and maximal adaptive response[4]. Therefore, the innate immune response plays a critical role in containing infection until the adaptive response comes into effect. As a result, synergy between both immune responses is crucial for effective removal of foreign material.

1.2.2 Macrophages

Macrophages are located in almost every part of the body, and exist in at least three different forms: yolk sack and foetal liver-derived tissue resident macrophages, as well as infiltrating bone marrow (monocyte)-derived macrophages[6,7]. For many years, it was thought that macrophages solely arose from the differentiation of circulating monocytes[8]. However, recent studies have provided evidence that most tissue resident macrophages arise from embryonic yolk-sac progenitors and are replaced with macrophages derived from either foetal monocytes or hematopoietic stem cells[9–11]. This leads to either the complete replacement of the yolk-sac derived macrophages or a mixed population of macrophages dominated by the foetal monocyte or stem cell lineage[10,12]. Depending on the location, different populations of macrophages will be present. Trophic factors from the local environment shape macrophage identity and population resulting in functions specific to their environment, such as tissue development, growth, homeostatic maintenance and remodelling[7,13,14].

Macrophages are an essential part of the innate immune response as they are constantly monitoring for invading microbes, provide effective control and clearance of infections, execute the removal of debris and dead cells, as well as promote tissue repair and wound healing[15]. Furthermore, macrophages also provide a link between the innate and adaptive immune response by capturing and presenting foreign or self-antigens on their surface membrane, before moving towards T cells, to prime and stimulate them[7,16].

Although the classical M1 (pro-inflammatory) and M2 (anti-inflammatory) model has been helpful in conceptualising macrophage activity, transcriptome studies show that the macrophage phenotype is varied and disease-dependent[17]. In fact, we know that

these two extreme states only exist *in vitro* and do not recapitulate the complexity of macrophage biology[18].

1.2.3 Microglia

First described by Rio-Hortega in the early 20th century, microglia are the resident central nervous system (CNS) innate macrophage population accounting for approximately 10% of all CNS cells[19–21]. Although ubiquitously expressed throughout the CNS, microglia densities have been shown to vary across different regions of the brain[22]. Fate mapping strategies have shown that microglia originate solely from primitive progenitors in the yolk sac that migrate into the CNS during early embryogenesis, before maturing into microglia[12,23,24]. However, unlike resident tissue macrophages, microglia achieve self-renewal throughout life, are functionally distinct and possess specific transcriptional signatures distinct from other brain and peripheral immune cells such as the specific markers purinergic receptor P2Y12 (P2RY12), transmembrane protein 119 (TMEM119) and sal-like protein 1 (SALL1)[25–33]. Furthermore, sexual differences in microglial numbers, morphology, as well as transcriptional signatures have also been documented[34–38].

Microglia morphology is one of its most defining features. In their resting state, microglia exhibit a ‘ramified’ morphology characterised by a small cell body with long, thin, branched processes in all directions. Two-photon imaging studies have shown microglia to be highly active in their presumed ‘resting state’, continuously surveying their local environment, with the ability to scan the entire brain over the course a few hours[39,40]. However once activated, microglia adopt a more 'amoeboid' morphology, indicating that they have detected a change in their local environment. Throughout life microglia contribute towards synaptic pruning and modulation[41–43], memory and learning[44,45], phagocytosis[46–48], myelination[49], synaptic plasticity[44,50,51] and vasculature development[52], to ensure healthy CNS development and homeostasis. Single cell RNA sequencing and proteomics studies have identified brain region specific subpopulations of microglia with different responses to triggers, varying degrees of immune vigilance, as well as changes in the gene expression profile[53–56]. It is thought that regional differences may require distinct microglial subtypes or states for healthy CNS homeostasis[57–59].

1.3 Disease Pathology

1.3.1 Alzheimer's Disease (AD)

It has been estimated that around 50 million people globally are living with dementia and that by 2050 this number will increase to 152 million[60]. AD is the most common form of dementia, and is classically characterised by the decline in cognitive function, neuronal loss, inflammation and Tau pathology initiated by amyloid-beta (Aβ) deposition[61–63]. The hippocampus, the part of the brain that plays a major role in learning and memory, is often one of the earliest affected brain regions[64]. As AD spreads throughout the brain, additional areas begin to become affected[65]. Consequently, the cortex becomes thinner, and the brain shrinks in size resulting in patients experience memory and cognitive impairment disorders[65]. AD can be classified as either familial (also known as early onset) or sporadic (also known as late onset), with the latter having multiple risk genes. The Apolipoprotein E (APOE) gene is one of the strongest risk factors for late onset Alzheimer's disease (LOAD) with the ε4 allele present in ~40% of all AD cases[66,67]. With AD prevalence predicted to increase over the coming years, along with the financial burden imposed by AD, the understanding of the mechanisms responsible for pathogenesis, as well as identification of new novel therapeutic targets is urgently needed[68].

Aβ is derived through the processing of the membrane bound amyloid precursor protein by the β- and γ-secretase proteases. Aβ extracellular monomers can aggregate together to form neurotoxic oligomers, protofibrils and amyloid fibrils, with the latter being able to further assemble into plaques[69]. Similar to Aβ plaques, hyperphosphorylated Tau monomers oligomerise to form paired helical filaments that then aggregate to form neurofibrillary tangles (NFTs) that induce neuronal dysfunction[70]. Both forms of pathology are hallmark features of AD.

However, treatments targeting the removal or reduction of Aβ plaques and NFTs have showed little to no effect on the stopping or slowing down of AD pathology prompting a rethink into how AD pathology is initiated and progresses[71]. As a majority of risk genes have been demonstrated to be highly expressed within microglia, it is thought that a long, complex feedback mechanism between microglia, astrocytes and vasculature is causative of AD, with microglial associated neuroinflammation being a significant contributor[63,72].

1.3.2 Inflammatory Bowel Disease (IBD)

Inflammatory bowel disease (IBD) is an umbrella term used for Crohn's disease, ulcerative colitis and other conditions, describing the chronic inflammation of the gastrointestinal tract[73]. As of 2017, it has been estimated that globally 6.8 million people have IBD[74]. Several comprehensive studies have highlighted genetic and environmental factors that contribute towards IBD[75,76]. However, the exact mechanism of IBD is currently unknown. Symptoms of IBD include abdominal pain, ulcers, diarrhoea, bloody stools, weight loss, as well as the influx of neutrophils and macrophages that produce cytokines, proteolytic enzymes and free radicals[77,78].

Although treatments for IBD do exist, e.g. TNF (tumor necrosis factor) monoclonal antibody blockers, many patients do not respond to these clinically approved drugs, prompting the need for more novel therapeutic treatments[79]. It is classically thought that chronically activated intestinal macrophages play a central role in IBD pathology and that enforcing an anti-inflammatory phenotype might be a novel therapeutic approach to control intestinal inflammation and restore tissue function[80,81]. Furthermore, IBD patients have been shown to have an higher chance of developing dementia, suggesting that perhaps the two diseases are somewhat interlinked through the gut-brain axis, which describes the signalling between the gut, its microbiome and the CNS[82].

1.4 Macrophage and microglia disease relevance

1.4.1 Dysfunction of macrophages in disease

Macrophages have been demonstrated to have key roles in the pathogenesis of many chronic inflammatory and autoimmune diseases, such as IBD and rheumatoid arthritis[80,83]. In these diseases, macrophages have been recognised as a source of many pro-inflammatory cytokines that mediate and drive disease pathology[83,84]. In the case of IBD, inflammatory mediators produced in the colon have been shown to transition homeostatic macrophages into pro-inflammatory dendritic ‘like’ cells that produce large quantities of TNF-α, IL-23 and IL-12 that contribute to pathology[85]. Together with this observation, it has been demonstrated that changes in the local environment can influence macrophage differentiation, which in turn has a pivotal role in the pathology of many inflammatory and autoimmune diseases[7]. In addition to microglia, non-parenchyma perivascular, meningeal and choroid plexus brain macrophages also play a role in CNS homeostasis[52]. However, current knowledge of non-parenchymal macrophage function in health and disease is currently limited, with these cells

potentially being a key component of initiating or progressing diseases within the brain[52].

1.4.2 Dysfunction of microglia in disease

The discovery of multiple immune related risk genes in large population studies has resulted in microglia and other innate immune pathways entering the spotlight of pathomechanistic research in sporadic forms of neurodegeneration, specifically Parkinson's disease and AD[86–88]. Furthermore, microglia have been implicated as key mediators of neurodevelopmental disorders such as autism spectrum disorders (ASD) and schizophrenia[89]. Several human post-mortem studies in patients with ASD have found microglia to be dysfunctional, and as such have reported differences in microglial numbers, morphology, neuronal interactions, as well as modified expression of microglial specific genes, especially in those associated with an inflammatory response[90–95]. Additional studies have also implied that dysregulated or overactive microglial synaptic pruning could contribute to abnormal synapse loss and dysfunction in ASD, as well other neurodevelopmental disorders such as schizophrenia[96,97].

Although microglia are classically considered essential for maintaining brain homeostasis, conflicting research has also suggested microglia may also have detrimental effects upon their activation[98,99]. Stimulated microglia produce many pro-inflammatory mediators, such as reactive oxygen species (ROS), cytokines (e.g. TNF-α), chemokines and nitric oxide. Consequently, all these mediators have the potential to be neurotoxic, causing or accelerating disease pathology[23,100]. In the context of AD, microglial protective and detrimental effects have been reported depending on the stage of disease[99]. It has been proposed that as Aβ plaques form, microglia cluster around the Aβ aggregates and clear them through the process of phagocytosis. However, due to aging or genetic susceptibility, microglia function becomes inadequate to prevent the onset and progression of AD. As a result, toxic Aβ aggregates accumulate inducing microglia into a nonconstructive and inflammatory state, in which they over-prune synapses, as well as secrete neurotoxic cytokines that injure neurons[99,101–103]. This process is often referred to as neuroinflammation.

Murine transcriptome studies have uncovered distinct microglial neurodegenerative reaction states known as disease associated microglia (DAM), activated response microglia (ARM) or microglial neurodegenerative phenotype (MGnD)[104–107]. It has been demonstrated that during the progression of AD and other neurodegenerative

diseases, that these disease associated microglial subtypes lose their homeostatic function due to the downregulation of homeostatic genes (such as P2RY12, TMEM119 and SALL1), contributing towards neuronal loss, as well as upregulation of several known AD risk genes, such as APOE and triggering receptor expressed on myeloid cells 2 (TREM2)[27,104,105,108].

Studies have shown that the upregulation of DAM genes does not directly correlate to the progression of neurodegeneration, but the upregulation of APOE may influence neurodegeneration severity[107,108]. However, further evidence is still needed. Additionally, multiple studies have shown that DAM are not only associated with neurodegeneration but also with natural aging[104,105,107]. Further evidence is needed to conclusively prove that a DAM subpopulation exists in human brain, as many DAM genes showed little to no enrichment in human microglia from AD patients[108–111].

1.4.3 Single nucleotide polymorphisms (SNPs)

Most of the human genetic variation is accounted for by single nucleotide polymorphisms (SNPs), in which a single nucleotide is substituted for another[112]. In fact it has been estimated that there are eleven million SNPs in the human genome[113]. Missense non-synonymous SNPs in the coding region of genes can cause a different amino acid to be expressed, potentially resulting in a change of protein function. However, not all single amino acid substitutions alter protein function, as it is estimated that only 20-30% of SNPs result in phenotypic change[112,114].

If SNPs do exhibit a phenotypic change, it is typically because they have either altered the proteins active state (e.g. “residues involved in ligand binding, catalysis, allosteric regulation or post-translational modification”[112]), affected the scaffolding of the protein (e.g. “by deforming and/or destabilising the binding site or the entire protein structure”[112]), influenced promoter activity (gene expression), messenger RNA (mRNA) conformation (stability) or subcellular localisation of mRNAs and/or proteins[115]. It is important to differentiate between beneficial, neutral and harmful mutations to better comprehend each SNPs effect on protein function.

1.4.4 Genome wide association studies

AD and IBD are two complex diseases whereby the pathophysiology is still yet to be fully elucidated. In order to gain better insights into complex diseases, genome wide

association studies (GWAS) have been implemented in order to highlight potential SNPs that may be associated with disease. The AD field is one of many fields that has tremendously benefited from numerous GWAS studies. Multiple SNPs have been found to be associated with increasing the risk of developing LOAD with many of these SNPs located in genes highly expressed by microglia, implicating them as modulators of the disease, as confirmed by proteomic data and microglia enhancer data, whereby enhancers are short regions of DNA that bind transcription factors to enhance messenger RNA expression from target promoters[88,116–124].

TREM2 is a cell surface receptor expressed in cells of the myeloid lineage including macrophages, osteoclasts, dendritic cells and microglia[125]. TREM2 has received much attention due to the identification of the rare R47H risk variant, which has been suggested to cause a 2 to 4.5 fold increased risk of developing AD[126,127]. Since then, TREM2 has been shown to be vital for microglial survival and function with the receptor playing a role in cell proliferation, inflammatory responses, cholesterol metabolism, the phagocytosis of apoptotic cells and myelin debris, as well as the clustering of microglia around Aβ plaques[128–133]. The R47H variant has been suggested to place microglia in a less responsive state with deficits in cholesterol metabolism and glycolytic energy production in response to cell activation observed[133–135]. However, further investigation of into the role of human TREM2 is still needed, as there is disparity in results between mouse and human models[136].

Another identified gene, phospholipase C-γ2 (PLCγ2), has also received much interest due to the identification of the rare LOAD associated P522R protective and M28L risk missense varaints[116,137]. Moreover, two IBD risk variants, R268W and H244R, of PLCγ2 have also been identified, suggesting that perhaps PLCγ2 plays a key role in disease[138]. Furthermore, phospholipase C (PLC) enzymes are potentially druggable proteins, making PLCγ2 a very attractive target for novel therapeutics using a small molecule approach[139].

1.5 Phospholipase C-γ2 (PLCγ2)

1.5.1 Phospholipase enzymes

Phospholipase (PL) enzymes break down phospholipids within the cell membrane into bioactive lipid mediators through hydrolysis[140]. These lipid mediators regulate a variety of functions including proliferation, survival, migration, tumorigenesis, metastasis and inflammation[141]. Phospholipase enzymes are grouped into four main classes: PLA (A1

and A2), PLC and PLD, depending on where they cleave the phospholipid substrate. PL enzymes are capable of hydrolysing multiple glycerophospholipids including phosphatidylinositol (PI) and phosphatidylcholine (PC)[141]. All phospholipase enzymes are composed of multiple isotypes with distinct functions, domains and regulatory mechanisms[142–145].

1.5.2 Domain organisation of PI-PLC enzymes

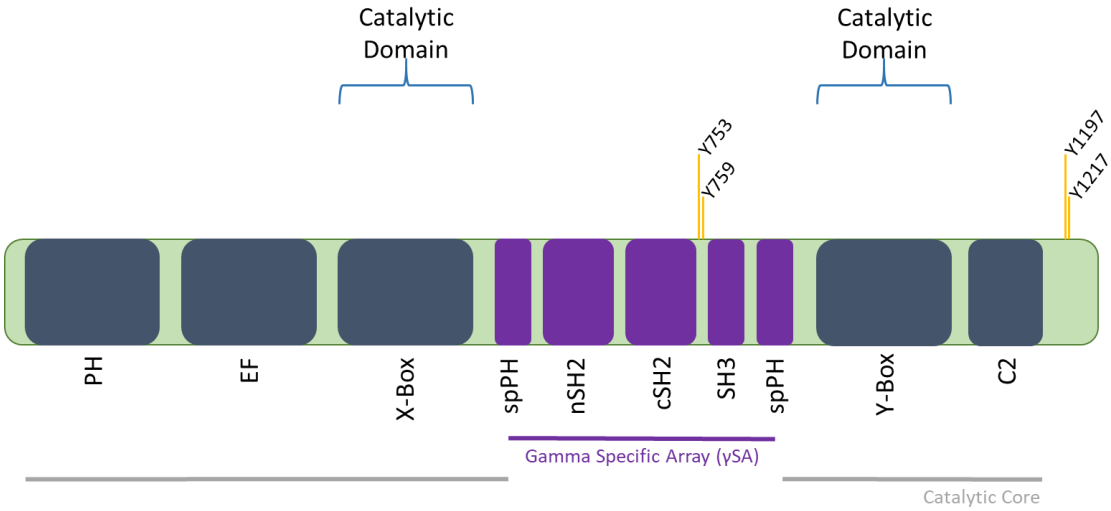

Figure 1.1 PLCγ2 domain structure. The core PLC domains (pleckstrin homology (PH), EF-hands, TIM barrel (X and Y box) and C2 domain) and the regulatory domains unique for PLCγ (split PH domain (spPH), two src-homology 2 (SH2) domains (nSH2 and cSH2) and one src-homolgy 3 (SH3) domain), comprising the gamma specific array (γSA), are coloured dark blue and purple, respectively. Domain location of the four known PLCγ2 tyrosine phosphorylation sites: Y753, Y759, Y1197 and Y1217 (yellow line).

In mammals, phosphoinositide-specific PLC enzymes (PI-PLC) are subdivided into six families (β, γ, δ, ε, ζ and η). All PLC isotypes (except for PLCζ) share a conserved core structure, with the addition of other domains unique to each family. The core PLC catalytic structure is composed of a pleckstrin homology (PH), EF-hands, a catalytic TIM barrel and a calcium binding C2 domain (Figure 1.1).

PLCγ enzymes have a large multi-domain insert between the two parts (X and Y) of the TIM barrels called the ‘gamma specific array’ (γSA). This is composed of a split PH domain (spPH), two src-homology 2 (SH2) domains (nSH2 and cSH2) and one src-homolgy 3 (SH3) domain (Figure 1.1)[146]. The γSA domains play a key role in the

binding of PLCγ to regulatory and scaffold proteins within diverse multiprotein signalling complexes[147]. The known role of each PLCγ domain in cellular function is summarised in Table 1.1.

PLCγ Domain	**Function**	**Reference**
PH	PIP_2 binding (Based on other PLC families)	[148]
EF	Supports catalytic domain structure	[149]
TIM, X-Box	PIP_2 catalysis and autoinhibition	[147]
N-terminal spPH	Rac GTPase activation of PLCγ2 and autoinhibition	[147,150]
N-terminal SH2	Linker for activation of T cells (LAT) binding	[151]
C-terminal SH2	Autoinhibition and B cell signalosome assembly	[147,152]
SH3	Lymphocyte cytosolic protein 2 (SLP-76) and cluster of differentiation 95 (CD95) binding	[153,154]
C-terminal spPH	Rac GTPase activation of PLCγ2 and autoinhibition	[147,150]
TIM, Y-Box	PIP_2 catalysis and autoinhibition	[147]
C2	Structural stabilisation of the TIM domains, membrane interactions and autoinhibition	[147]

Table 1.1 Each domains role in PLCγ function. Abbreviations: (PH) pleckstrin homology, (EF) EF-hands, (X and Y box) TIM barrel, (C2) C2 domain, (spPH) split PH, (nSH2 and cSH2) n and c terminus src-homology 2 and (SH3) src-homolgy 3.

1.5.3 PLCγ expression

PLCγ1 and PLCγ2, which are encoded by the PLCG1 (human chromosome 20) and PLCG2 (human chromosome 16) gene respectively, are both ~150kDa in size, and share high sequence similarity across all domains[155,156]. PLCγ2 is abundantly expressed in hematopoietic cells, such as B lymphocytes, mast cells, natural killer cells, neutrophils, dendritic cells, osteoclasts, macrophages and microglia[157]. In comparison, PLCγ1 is expressed ubiquitously throughout the body and is essential for embryonic development[158]. It is also highly expressed in T cells[151,159]. Both PLCγ isozymes can perform non-overlapping functions in cells that express both forms, and one isozyme generally cannot compensate for depletion of the other[160,161]. To date, no complete tertiary structure of PLCγ2 has been solved, meaning domain interactions are modelled

using homology with other PLC enzymes for which the structure is known, including the recently characterised PLCγ1 isozyme structure[146,147].

1.5.4 PLCγ2 function

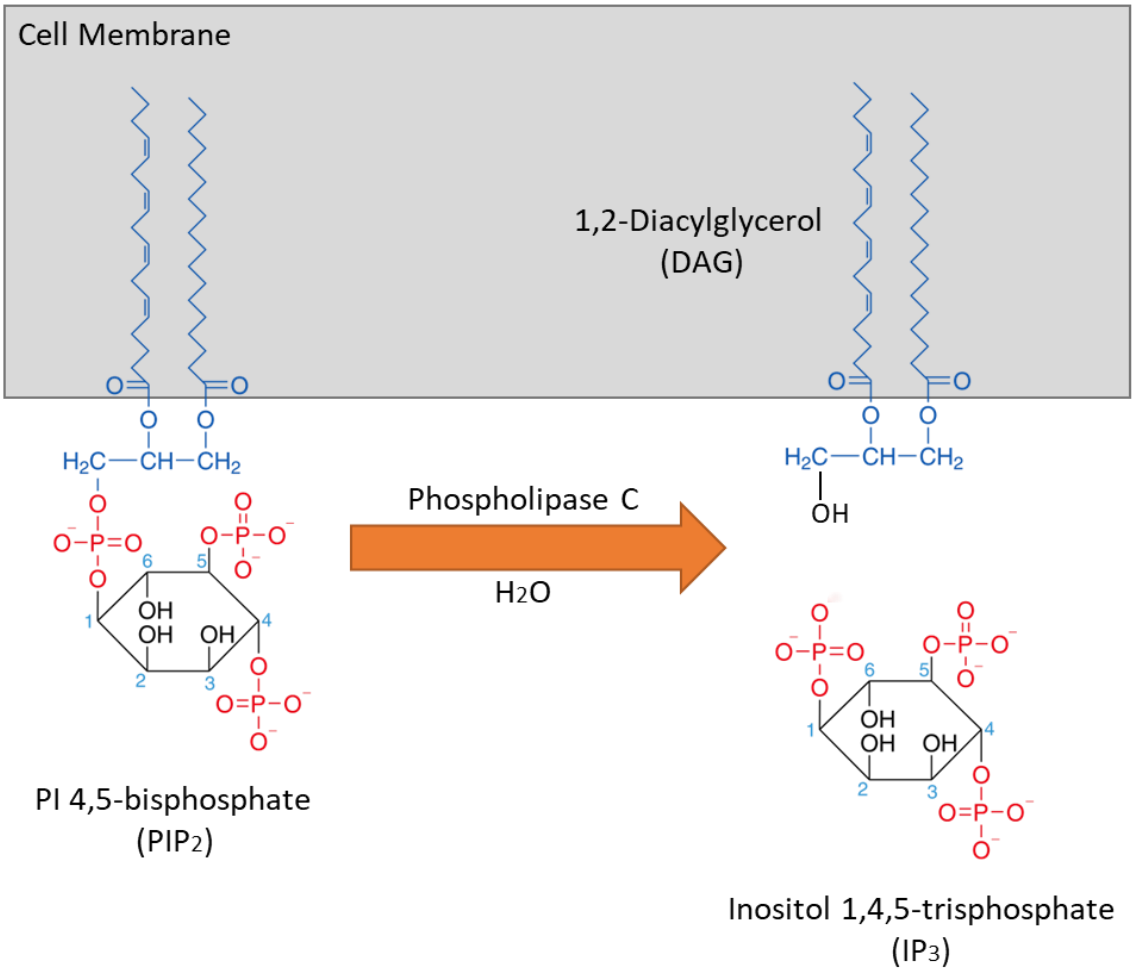

Figure 1.2 Hydrolysis of PIP_2 (phosphatidylinositol 4,5-bisphosphate) by PLC (phospholipase C) enzymes. PLC hydrolyses PIP_2 and generates the intracellular secondary messengers, inositol 1,4,5-trisphosphate (IP_3) and diacylglycerol (DAG). Figure adapted and modified from Seo et al[162].

Phosphoinositides account for around 1% of all membrane phospholipids, with PIP_2 being the most abundant[163–165]. Upon activation, PLCγ2 is recruited to the plasma membrane and, as with all PI-PLC isoforms, catalyses the hydrolysis of the phosphatidylinositol 4,5-bisphosphate (PIP_2) substrate to the secondary messengers; inositol 1,4,5-trisphosphate (IP_3) and diacylglycerol (DAG, Figure 1.2)[166,167]. Both products propagate a wide range of downstream signals that are cell specific. However,

the generation of DAG and IP_3 is not specific to PLC and can occur from other pathways[168,169].

1.5.5 PLCγ2 activation

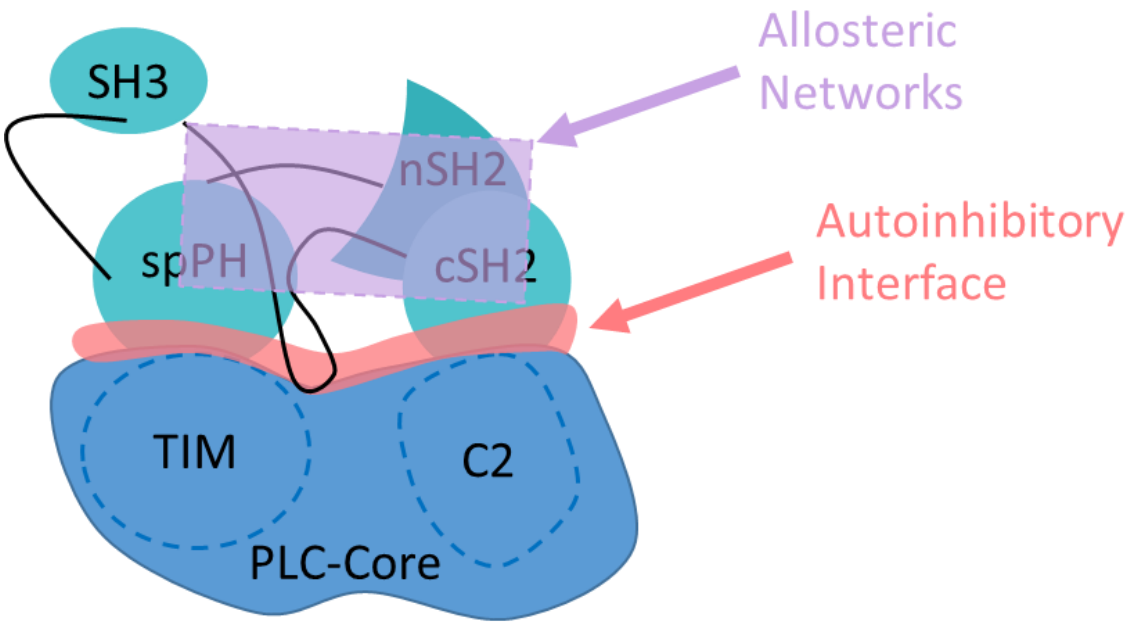

Figure 1.3 The inactive form of PLCγ. Inactive PLCγ is maintained by interactions between the TIM barrel and spPH domains, as well as the C2 and cSH2 domains, at the autoinhibitory interface (red). Physiological stimulation is mediated through allosteric networks to the autoinhibitory interface. Upon phosphorylation, intramolecular interactions change between the Y759 phosphorylated region and the cSH2 domain. Allosteric networks could also have a role to stabilise the active form. PLCγ structural architecture is based on PLCγ1. Figure adapted from Liu et al[147].

PLCγ2 has 4 known tyrosine phosphorylation sites: Y753, Y759, Y1197 and Y1217, with Y1217 appearing to be unique to PLCγ2 (Figure 1.1)[170]. According to the current model, interactions between the TIM-barrel and spPH domains, as well as the C2 and cSH2 domains, results in autoinhibition of PLCγ2, as mutations within either of the two contact points (autoinhibitory interface) can overcome enzymatic autoinhibition (Figure 1.3)[147]. In fact, it has been suggested that both contacts are required to maintain an inhibited form[147]. Phosphorylation of the Y759 residue (between the cSH2-SH3 linker), prevents this autoinhibitory interaction, consequentially allowing PLCγ2 domains to bind to the membrane, allowing the substrate PIP_2 to access the active site (TIM barrel)[152,171]. The PH domain is speculated to be important in docking the enzyme to the inner membrane by binding to PIP_2 or phosphatidylinositol (3,4,5)-trisphosphate

(PIP_3)[148,172]. Phosphorylation of the PLCγ2 Y753 and Y1217 residues has been shown to vary depending on the cell type used, with phosphorylation of the Y759 residue being consistent amongst all cell types tested[170,173]. In the context of B cells, PLCγ2 phosphorylation has been characterised as a rapid event, with the maximal level phosphorylation occurring after 1 minute[170]. Moreover, the tyrosine protein phosphatases that deactivate PLCγ2 have not yet been identified, nor has any method of PLCγ2 dephosphorylation[166].

PLCγ2, in addition to PLCβ2, can also be activated through the GTPase ras-related C3 botulinum toxin substrate (Rac) 1, 2 and 3, whereas PLCγ1 cannot[174]. PLCγ2 has been shown to form hydrophobic interactions with Rac2, through its spPH domain, resulting in plasma membrane recruitment and activation of PLCγ2[150,174,175].

1.5.6 PLCγ2 pathways

1.5.6.1 Introduction

Depending on the specific cell type, PLCγ2 can be activated through tyrosine kinase receptors[139,176,177], toll like receptors (TLR)[178], integrins[179,180], as well as several immunoreceptor tyrosine-based activation motif (ITAM)-linked receptors such as Fcγ receptors[181,182], the B cell receptor complex[170] and the TREM2 receptor complex[183]. ITAM is a highly conserved region in the cytoplasmic domain of signalling chains of adapter proteins and receptors that is involved in the regulation of immune cell proliferation, survival and differentiation[184–186]. Upon specific receptor activation, ITAM regions become phosphorylated, resulting in the recruitment and subsequent phosphorylation of PLCγ2. However, the role of PLCγ2 mediated downstream signalling in some of these pathways is still unclear. PLCγ2 activation, and its subsequent downstream effects, are best characterised in the context of B cells, where PLCγ2 function has been extensively investigated.

1.5.6.2 B cell receptor (BCR) pathway

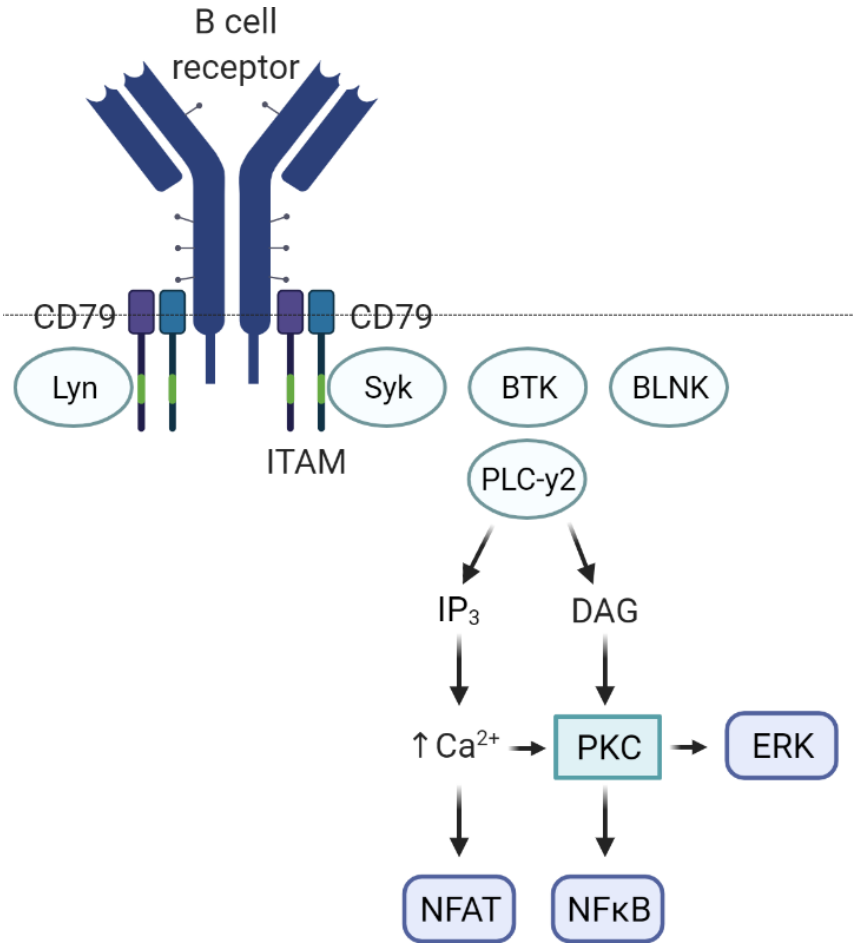

Figure 1.4 Simplified B cell receptor (BCR) signalling complex. BCR activation induces phosphorylation of immunoreceptor tyrosine-based activation motifs (ITAMs) and recruitment of the Lck/Yes novel tyrosine kinase (LYN) and spleen tyrosine kinase (SYK) kinases to activate Bruton tyrosine kinase (BTK). BTK recruits the adapter protein B-cell linker (BLNK), as well as phosphorylates and activates phospholipase C-γ2 (PLCγ2) to hydrolyse phosphatidylinositol 4,5-bisphosphate (PIP_2) into inositol 1,4,5-trisphosphate (IP_3) and diacylglycerol (DAG), which triggers the activation of nuclear factor of activated T-cells (NFAT) and nuclear factor kappa B (NF-κB) transcription factors, as well as extracellular signal-regulated kinase (ERK) through protein kinase C (PKC). Figure adapted from Burger and Wiestner[187]. Figure was created with BioRender.com.

The B cell receptor (BCR) complex is composed of a membrane immunoglobulin, non-covalently bonded to the CD79a(Igα)-CD79b(Igβ) heterodimer. The CD79 heterodimer, bound together by disulphide bridges, has a cytoplasmic ITAM tail. Upon BCR-antigen activation, the ITAM regions of the CD79 heterodimer become phosphorylated by the

Src family kinases (Lck/Yes novel tyrosine kinase (Lyn) and spleen tyrosine kinase (Syk)), resulting in the recruitment of the kinases Syk, Bruton tyrosine kinase (Btk) and Lyn, as well as the adaptor protein B-cell linker (BLNK), towards the BCR complex[188]. BLNK is recruited to the non-ITAM region of the CD79 heterodimer where it is phosphorylated by Syk, so that it can act as a scaffold for Btk and PLCγ2[188]. Once Syk, Btk, BLNK and PLCγ2 are in contact, PLCγ2 is phosphorylated by Btk and/or Syk, resulting in the conversion of PIP_2 into IP_3 and DAG (Figure 1.4)[182].

IP_3 is released into the cytosol and binds to IP_3 receptors (IP_3Rs) on the endoplasmic reticulum, increasing cytoplasmic calcium[189]. The upsurge of calcium leads to the activation of calcium-dependent kinases and calcineurin. Calcineurin dephosphorylates the transcription factor, nuclear factor-activated T-cell (NFAT), inducing its nuclear translocation and promoting cytokine transcription[125]. DAG remains bound to the plasma membrane where it activates a number of different targets, one being protein kinase C (PKC). Once activated, PKC triggers the nuclear factor kappa B (NF-κB) pathway, a protein complex that controls transcription, cytokine production and cell survival[125]. In addition, PKC also stimulates Ras guanyl-nucleotide-releasing proteins (RasGRPs). RasGRPs activate the extracellular signal-regulated kinase (ERK) pathway, which is responsible for cell proliferation and cytoskeletal contraction[190]. It should be noted that downstream signalling pathways are cell-context dependent and will differ amongst the different cell types.

1.5.6.3 TREM2 pathway

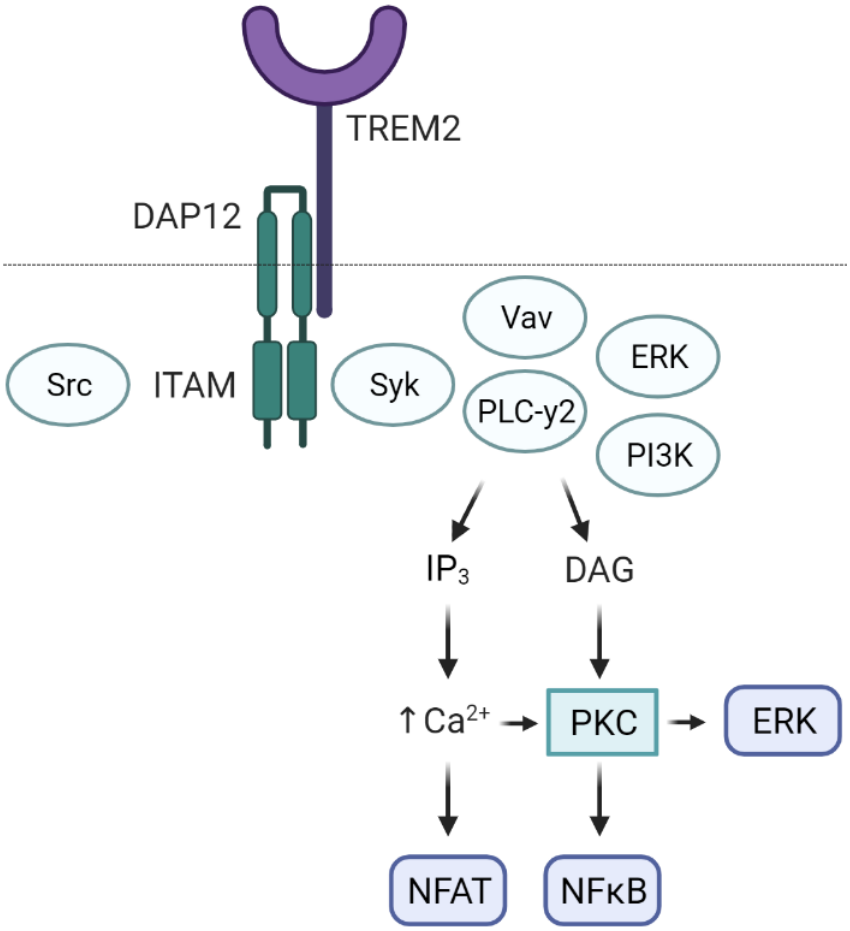

Figure 1.5 Proposed TREM2/PLCγ2 signalling in microglia. Upon ligand binding to TREM2, two tyrosine residues within the ITAM motifs of DAP12 are phosphorylated by Src, which recruits Syk to activate downstream signalling molecules, such as ERK, PI3K, PLCγ2 and Vav. Activated PLCγ2 coverts PIP_2 into IP_3 and DAG, which triggers pathways to activate the NFAT and NF-κB transcription factors, as well as ERK through PKC. Figure adapted from Konishi and Kiyama (2018)[191]. Figure was created with BioRender.com.

TREM2 has been demonstrated to have a minor preference towards anionic substrates, and as a result, activation of TREM2 has been demonstrated with various phospholipids and sphingomyelin[130,133], bacterial lipopolysaccharides[192], lipidated apolipoproteins such as APOE[131], nucleic acids[193] and oligomeric Aβ[194]. TREM2 is known to couple to the DNAX-activating protein 12 (DAP12) through electrostatic interactions[195–197]. Similarly to the B cell CD79 heterodimer, DAP12 is bound together by disulphide bridges and has a cytoplasmic tail containing ITAM motifs[198,199]. Upon TREM2 activation, Src protein tyrosine kinases phosphorylate ITAMs, promoting the

recruitment of Syk, that activates downstream signalling molecules such as PLCγ2, Vav, ERK and phosphatidylinositol 3-kinase (PI3K, Figure 1.5)[191,200,201]. The recruitment of these proteins results in the activation of PLCγ2, and thus the hydrolysis of PIP_2 into IP_3 and DAG. It is hypothesised that the IP_3 and DAG secondary messengers to have the same downstream affects as they do in B cells. This includes changes to transcription, cytokine production, cell survival, cell proliferation, cytoskeletal contraction and phagocytosis[125]. Furthermore, activation of the TREM2 pathway within microglia has been demonstrated to promote anti-inflammatory responses[202].

It must be stated that the microglial TREM2 signalling pathway is still yet to be fully characterised, and that this is the proposed TREM2 pathway based on the current literature[133,203,204]. Additionally, it is also unclear to what extent other adaptor proteins are recruited and associated with PLCγ2 at the membrane[204].

1.6 Identified PLCγ2 disease-linked variants

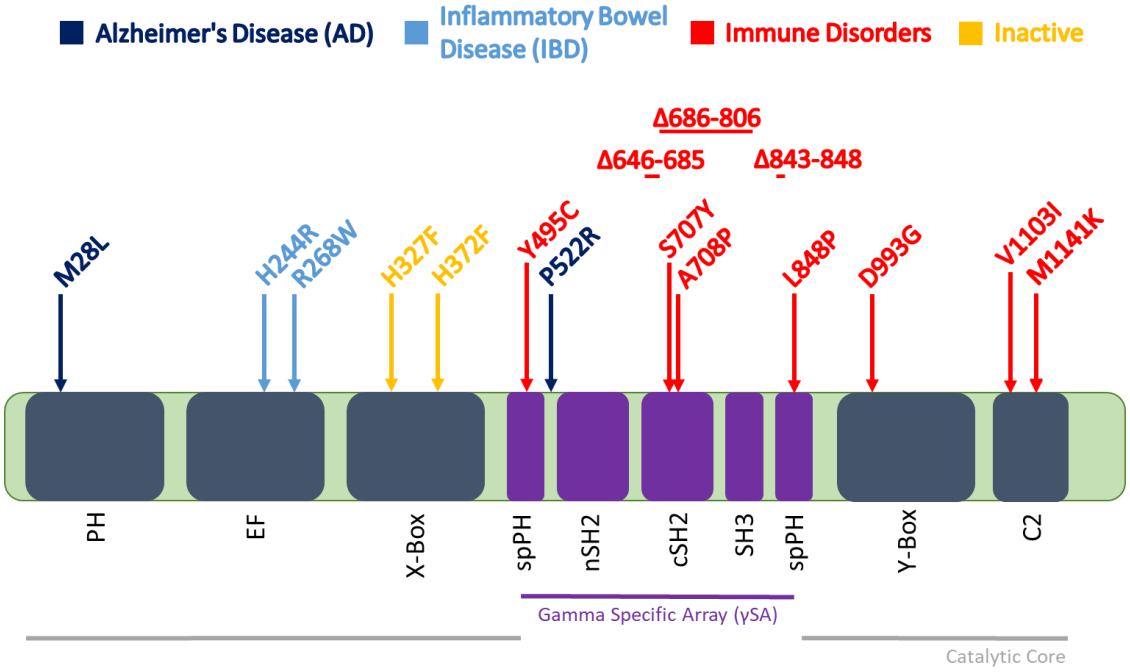

Figure 1.6 PLCγ2 domain structure annotated with the known disease-linked PLCγ2 variants and their associated disease phenotype. Somatic mutations in cancer drug resistance are not included.

1.6.1 Mouse models and inherited immune disorders

Wild type (WT) mice treated with the mutagen N-ethyl-N-nitrosourea (ENU) introduced two independent PLCγ2 gain-of-function (GOF) mutations that caused limb defects and autoimmunity[205–207]. These PLCγ2 variants were identified as D933G and Y495C and are named as abnormal limb 5 and 14 (Ali5 and Ali14), respectively (Figure 1.6)[205–207]. Upon stimulation of B cells, the Ali5 variant showed an increase in inositol phosphate production and enhanced intracellular calcium generation, with the Ali14 mutation displaying similar effects[205–207]. In B cells, both the Ali5 and Ali14 PLCγ2 variants hyper activate external calcium entry causing the expansion of innate inflammatory cells, ultimately resulting in the mice experiencing severe inflammation[206,207]. For the Ali5 mutant, the authors hypothesised that the removal of the negatively charged aspartic acid residue may reduce membrane repulsion[207]. Therefore, perhaps PLCγ2 remains at the membrane longer, increasing its contact time with the PIP_2 substrate, explaining the GOF[205]. Additionally, the Ali14 mutation, which is located in the spPH domain, has been suggested to destabilise the γSA autoinhibition mechanism, resulting in its GOF[208]. In contrast, PLCγ2 deficient mice display functional defects in B cells, platelets, mast cells and NK cells, as well as absent IgM-receptor-induced calcium flux[209].

Cold urticaria is a symptom of multiple inflammatory disorders that commonly causes hives to form on the skin, as well as swelling, after exposure to a cold stimulus[210]. Patients can also experience very low blood pressure, fainting or even shock[210]. An exome (the protein coding regions of genes in a genome) sequencing study of 27 patients with inherited cold urticarial revealed deletions in the PLCG2 gene[211]. Deletions to the cSH2 (Δ646-685) and cSH2/SH3 (Δ686-806) domains were found to disrupt the autoinhibitory mechanism, leading to GOF (Figure 1.6)[211]. However, despite the increase in PLCγ2 enzymatic function, ERK phosphorylation and calcium flux were shown to be reduced in B cells[211]. It was hypothesised that following its activation, WT PLCγ2 stabilises the receptor-adaptor protein complex necessary for signal transduction. Current literature shows that the cSH2 is important for PLCγ2 stability and that mutations in this domain are indirectly affecting autoinhibition[147]. Therefore, the Δ646-685 and Δ686-806 mutations are most likely diminishing the ability of PLCγ2 to stabilise the complex, resulting in a reduction of downstream activity. Additionally, the signalling defect was shown to be temperature sensitive, as decreasing physiological temperatures resulted in an increase of cytosolic calcium levels, as well as ERK

phosphorylation in B cells[211]. The increase in activity at sub-physiological temperatures could be due to intrinsic cold-induced activation which, depending on cell type, can lead to a variety of acute or chronic phenotypes[212]. The term PLAID (PLCγ2-associated antibody deficiency and immune dysregulation) was used to describe the genetic, clinical and functional findings[211]. Interestingly, studies have shown patients to experience PLAID symptoms with no detectable PLCγ2 deletion or mutation suggesting that the PLAID phenotype is not solely due to PLCγ2[213,214].

A father and daughter experiencing skin inflammation, uveitis, colitis and lung inflammation, harboured the PLCγ2 missense variant S707Y (Figure 1.6). This mutation is situated at a highly conserved amino acid residue throughout vertebrates[215]. Since its identification, the PLCγ2 S707Y variant has been demonstrated to disrupt the cSH2 and C2 autoinhibitory mechanism, resulting in increased IP_3 production, intracellular calcium flux and ERK phosphorylation within different cell types[208,215,216]. Furthermore, the pro-inflammatory cytokine interleukin-1 beta (IL-1β) was shown to be elevated in patient peripheral blood mononuclear cells (PBMCs) harbouring the PLCγ2 S707Y variant[217]. IL-1β precursor protein requires proteolytic cleavage by activated caspase-1 through the NLR family pyrin domain containing 3 (NLRP3) inflammasome, a large intracellular multiprotein complex, to generate mature IL-1β[218]. The heightened IP_3-mediated calcium flux generated from the S707Y PLCγ2 variant, was demonstrated to be a key mediator of mature IL-1β production, as increased cytoplasmic calcium promotes the assembly of inflammasome[217]. As the disease was classified as autoinflammatory, the term APLAID (autoinflammation and PLCγ2-associated antibody deficiency and immune dysregulation) was given to classify the genetic, clinical and functional findings[215].

Additionally, four other PLCγ2 missense variants eliciting the APLAID phenotype A708P[219,220], L848P[216], M1141K[221] and Δ845-848[222] have also been demonstrated to increase PLCγ2 activity under both basal and stimulated conditions *in vitro*[216,222,223] (Figure 1.6). Patients harbouring these mutations were experiencing recurrent infections, antibody deficiency and autoimmunity. Characterisation of the PLCγ2 A708P variant shows it to be one of the most hypermorphic PLCγ2 SNPs, producing significantly more IP_3 relative to the WT control[171]. Given its close proximity to the S707Y PLCγ2 variant, the A708P variant most likely disrupts the autoinhibitory mechanism through the same process. Furthermore, the PLCγ2 M1141K variant has also been found to dysregulate the autoinhibitory mechanism resulting in increased

intracellular calcium influx, ERK phosphorylation and increased apoptosis of immature B cell subsets[223,224]. However, for the patients eliciting the PLCγ2 M1141K variant, different phenotypes were observed for each patient, suggesting that perhaps other factors contribute to the disease[224].

1.6.2 Inflammatory bowel disease (IBD)

A GWAS of IBD patients identified two independent PLCγ2 missense variants, H244R and R268W, both located in the EF domain (Figure 1.6)[138]. As no mutations in this domain have previously been characterised, it is hard to predict if they are influencing enzymatic activity. A recent study has reported the R268W variant to cause an increase in calcium influx in peripheral B cells, suggesting that this variant is perhaps hypermorphic[225]. However, further functional studies still need to be performed.

1.6.3 Alzheimer's disease (AD)

A GWAS of LOAD patients identified a protective PLCγ2 variant, P522R[116]. This variant is unique compared to others, as it is located in the linker between the spPH and nSH2 PLCγ2 domains (Figure 1.6). Therefore, it is not clear if this variant is also affecting the autoinhibition mechanism like other variants. Functional characterisation of the variant has shown a mild GOF in activity when stimulated, with increases in IP_3 and DAG production, as well as calcium signalling documented[139,226]. Furthermore, upon comparable overexpression of PLCγ2 WT and P522R, the variant was shown to enhance PLCγ2 dependent cholesterol metabolism in hiPSC-derived microglia cells, suggesting that alterations in microglial lipid metabolism might contribute to LOAD[133]. However, further functional characterisation of the variant is still needed as conflicting phagocytosis data has been published, with substrate dependent increases and decreases in phagocytosis reported[226,227]. Studies have shown dementia and mild cognitive impairment (MCI) patients carrying the P522R variant to have lower phosphorylated Tau 181 ($pTau_{181}$) concentrations and total Tau levels in their cerebrospinal fluid (CSF), classical hallmarks of AD, compared to non-carriers[228,229]. Additionally, the variant has been associated with an increased likelihood of longevity, as well as counteracting the harmful effect of the APOE ε4 allele[230].

To the contrary, a rare missense variant of PLCγ2, M28L, has been suggested to confer increased AD risk[231]. Previous characterisation of the PLCγ2 M28L variant showed no

change in enzymatic activity[176]. As this variant has activity comparable to PLCγ2 WT it could act as a control for future studies.

1.6.4 Engineered PLCγ2 mutations that affect enzymatic activity

It is helpful to identify inactive forms of PLCγ2 to act as negative controls for subsequent experiments. Human embryonic kidney 293 (HEK293) cells transfected with PLCγ2 cDNA harbouring the double histidine 327/372 to phenylalanine mutation (H327/372F) were demonstrated to be catalytically inactive when compared to the PLCγ2 WT control (Figure 1.6)[232]. Furthermore, Walliser et al., generated a PLCγ2 cDNA construct that replaced the four tyrosine residues (Y753, Y759, Y1197, Y1217) known to be phosphorylated during PLCγ2 activation with phenylalanines, in addition to a PLCγ2 mutation that prevents Rac activation, F897Q. The construct was characterised as lipase dead in COS-7 cells and is abbreviated to '4F + F897Q'[171,176].

1.6.5 Summary

A summary of the reported germline/non-somatic PLCγ2 disease-linked variants is presented in Table 1.2. The observed clinical phenotype is likely due to the PLCγ2 variant affecting either the autoinhibitory interface, allosteric networks, membrane interactions, domain stability or interactions with regulatory proteins[147]. Somatic PLCγ2 mutations that are causative of cancer drug resistance are not being covered in this thesis as they do not fit within the scope of inflammation. However, all APLAID mutations are associated with cancer resistance.

Species	**PLCγ2 Mutation**	**Association**	**Domain**	**IP Production vs. WT**	**Intracellular Calcium Flux vs. WT**	**References**
Mouse	D933G	Ali5	Y-Box	↑	↑	205,207
	Y495C	Ali14	spPH	↑	↑	205,206
Human	Δ646-685	PLAID	cSH2	↑	↓	211
	Δ686-806		cSH2 & SH3	↑	↓	211
	S707Y	APLAID	cSH2	↑	↑	215,216
	A708P		cSH2	↑	N/A	171,222
	L848P		spPH	↑	N/A	216
	M1141K		C2	N/A	↑	223,224

	Δ845-848		spPH	↑	N/A	[222]
	H244R	IBD	EF	N/A	N/A	[138]
	R268W		EF	N/A	↑	[138]
	P522R	AD	spPH-nSH2 Linker	↑	↑	[139,226]
	M28L		PH	-	N/A	[176]

Table 1.2 Summary of literature PLCγ2 disease-linked variants. Abbreviations: (↑) increase, (↓) decrease, (-) no change, (N/A) not available, (APLAID) autoinflammation and PLCγ2-associated antibody deficiency and immune dysregulation, (PLAID) PLCγ2-associated antibody deficiency and immune dysregulation, (IBD) inflammatory bowel disease, (AD) Alzheimer's disease, (PH) pleckstrin homology, (EF) EF-hands, (X and Y box) TIM barrel, (C2) C2 domain, (spPH) split PH, (nSH2 and cSH2) n and c terminus src-homology 2 and (SH3) src-homolgy 3.

1.7 Cell Models

1.7.1 Human induced pluripotent stem cells (hiPSCs) and embryonic stem cells (hESCs)

Over recent years, hESCs and hiPSCs have been increasingly used as a model system in biomedical research because of their ability to be differentiated into many different cell types that can be used to model diseases and disorders at a cellular level[233]. As hESC are derived from the inner cell mass of developing embryos, they serve as good *in vitro* models of embryonic development[234]. Whereas, hiPSCs are not derived from embryos and are designed to mimic hECS[234]. However, hiPSCs do offer their own unique advantages. Firstly, they eliminate the ethical issues presented by hESCs due to their embryonic origins. Secondly, they allow for the production of patient-specific pluripotent stem cells[235]. This is achieved by overexpressing four defined transcription factors: octamer-binding transcription factor 4 (Oct4), Krüppel-like factor 4 (Klf-4), c-myc and sex determining region Y-box 2 (Sox-2) in human somatic cells[236,237]. Global gene expression profiles of hESCs and hiPSCs are mostly similar with subtle differences in messenger RNAs and microRNAs reported[234,238,239]. However, no unique epigenetic or transcriptional deviation is found to be shared by all hiPSC lines[240].

1.7.1 Stem cell-derived macrophage precursors (preMac) and macrophages

Myeloid cells are a vital component of the human innate immune system and their dysregulation has been implicated in several diseases[241]. Within in the field, challenges regarding donor variability of primary blood-derived cells, as well as isolation of tissue-resident macrophages compromise experimentation[241]. To combat these issues, several protocols to generate hiPSC-derived macrophage cells have been published. Spontaneous mesoderm differentiation of stem cells via embryoid bodies (EBs), followed by timed exposure to macrophage colony stimulating factor (M-CSF) and interleukin-3 (IL-3) induces myeloid differentiation for the production of macrophage precursors (preMacs)[242]. This method offers a virtually unlimited supply of *in vitro* generated preMac cells, with consistent genotype and function, eliminating the risk of donor variability where needed[243]. preMac cells generated via this protocol have demonstrated good expression of the myeloid markers CD11b (integrin subunit alpha M), CD14 (cluster of differentiation 14) and CD68 (cluster of differentiation 68) over the lifespan on the cells[243]. Harvested preMacs exposed to XVIVO15 media supplemented with M-CSF for 7 days results in the generation of macrophage cells[243]. Compared to primary blood-derived macrophages, these stem cell-derived macrophages exhibit similar polarisation, as well as a higher rate of engulfment of dead and dying cells (efferocytosis)[243].

1.7.2 Stem cell-derived microglia

Over recent years it has become more evident that rodent biology does not always recapitulate human biology, especially in the context of AD[244,245]. Comparing the homology of human and mouse proteins enriched in microglia, shows that over half of the proteins display less than 70% homology[246]. Furthermore, significant gene expression differences between human and mouse microglia have been documented especially in the context of the complement system, several inflammatory cytokines, as well as genes related to neurodegenerative diseases, such as AD[53,247,248].

In order to solve this issue, some labs have established procedures to obtain primary human microglia[249]. However, the process is not straightforward. Firstly, very few labs have the access and the expertise to process human brain tissue, and those that do harvest a low number of microglia, making it very challenging to perform multiple experiments. Secondly, primary samples are often obtained from post-mortem patients that have different ages and disease progression, that can potentially confound the

interpretation of experimental results. Finally, it has been demonstrated that once microglia are removed from the brain, they undergo rapid transcriptomic and phenotypic changes that diminish the accuracy of these cells as a model for *in vivo* microglia[27,53,250].

In order to circumvent the issues associated with primary human and mouse microglia, multiple protocols have been developed to generate large numbers of human 'like' microglia, derived from preMacs[251]. These protocols aim to mimic microglia development by timely exposing the preMacs to growth factors and small molecules. Stem cell-derived microglia are defined as microglia 'like' because they have not been generated from the native yolk sac erythromyeloid progenitors. The ability to mass-produce human microglia 'like' cells allows researchers to perform multiple high-throughput experiments for applications such as drug screening, as well as disease modelling. Furthermore, the abundance of cells means multiple control groups and experimental replicates can be run, adding further validity to studies. A detailed summary of the molecular markers and functional assays used to characterise human pluripotent stem cell derived microglia 'like' cells from multiple protocols is listed in Table 1.3.

Protocol	**Pluripotent stem cell derived microglia cell characterisation**
Muffat et al.[252]	**Morphology:** multiple thin first-order branches **ICC:** TMEM119, P2RY12, IBA1, CD45 **RNASeq:** TMEM119, MERTK, C1QA, P2Y12, P2Y13
Haenseler et al.[242]	**Morphology:** ramified (secondary branches) **Flow cytometry:** CD11b, CD11c, CD14, CD45 **qPCR:** C1QA, GAS6, GPR34, MERTK, P2Y12, TREM2, TMEM119
Abud et al.[253]	**Morphology:** high nucleus to cytoplasm ratio **ICC:** PU.1, CX3CR1, TREM2, P2Y12, TGFBR1, PROS1, MERTK, ITGB5 **qPCR:** P2RY12, GPR34, C1Q, TREM2, APOE **Phagocytosis:** pHrodo-E.coli **Calcium Signalling:** ADP-response

Table 1.3 Summary of the morphology, molecular markers and functional tests used to characterise human pluripotent stem cell derived microglia 'like' cells. Abbreviations:

(ICC) immunocytochemistry, (RNASeq) RNA sequencing and (qPCR) quantitative polymerase chain reaction.

Stem cell-derived microglia have a similar transcriptomic and functional profile to that of cultured human adult and foetal microglia[253]. However, as microglia do not exist in isolation, questions have been raised over whether data generated using monocultured microglia *in vitro* could be translated to the function of microglia *in vivo*[246]. Thus, while monoculture experiments would likely provide an initial assessment of microglial function, additional application of co-culture or organoid methods that combine microglia with stem cell-derived neurons, astrocytes, endothelial cells, or other cell types would likely provide important additional information. Furthermore, stem cell-derived microglia transplanted into mouse brain can also provide a more physiologically relevant model to address microglia's role in AD pathophysiology.

1.8 Aims

PLCγ2 hypermorphic variants e.g. S707Y, have been demonstrated to increase enzymatic activity resulting in alterations to downstream signalling. Recent GWAS and clinical studies have identified multiple PLCγ2 disease-linked variants that are still yet to be fully characterised to understand what effect, if any, they have on disease initiation or progression. The identification of the LOAD protective PLCγ2 P522R variant suggests that PLCγ2 plays a crucial in microglial function. However, PLCγ2 P522R models have yet to fully decipher what role this variant has on microglia function, especially given its mild GOF activity. Therefore, in order to better clarify the role that PLCγ2 has on microglial functionality, genetically manipulated hypermorphic variants of PLCγ2, such as the S707Y variant, can be used in stem cell-derived microglia to characterise what effect strong hypermorphic PLCγ2 variants have on microglia function. More specifically, I will address the following aims:

1. Characterise and rank the enzymatic activity of rare and novel PLCγ2 disease-linked variants.
2. Explore the role that PLCγ2 has in microglial functionality using PLCγ2 WT and S707Y hiPSC-derived microglia.
3. Characterise the impact the disease-linked PLCγ2 S707Y variant has on microglial gene expression to understand disease mechanisms.

Chapter 2 - Materials and Methods

2.1 Materials

Table 2.1 General reagents used for various techniques

Item	Catalogue Number	Manufacturer
Ethanol Absolute	10342652	VWR Chemicals
Distilled Water (MilliQ)	-	-
UltraPure DNase/RNase-Free Distilled Water	10977035	Invitrogen
1x Dulbecco's Phosphate-Buffered Saline (PBS): No Calcium, No Magnesium	14190094	Gibco
Chloroform	22711.290	VWR Chemicals
Isopropanol	P/7500/21	Fisher Chemical

Table 2.2 Bacterial culture reagents

Item	Catalogue Number	Manufacturer
Miller LB Broth	L3522	Sigma
Miller LB Agar	L3027	Sigma
Kanamycin	15160054	Gibco
Ampicillin	A5354	Sigma
S.O.C. Medium	15544034	Invitrogen
Glycerol	G5516	Sigma
XL1-Blue MR Supercompetent Cells	200229	Agilent Technologies

Table 2.3 Site-directed mutagenesis kits and DNA extraction kits used to isolate DNA from bacterial and human cultures

Item	Catalogue Number	Manufacturer
QuikChange Lightning Site-Directed Mutagenesis Kit	210518	Agilent Technologies
QIAprep Spin Miniprep Kit	27106	Qiagen
QIAGEN Plasmid Plus Maxi Kit	12963	Qiagen
DNeasy Blood & Tissue Kit	69504	Qiagen

Table 2.4 Agarose gel electrophoresis reagents

Item	Catalogue Number	Manufacturer
Agarose Powder	A9539	Sigma
UltraPure DNA Typing Grade 50x TAE Buffer	24710030	Invitrogen
1kb Plus DNA ladder	10787018	Invitrogen
SYBR Safe DNA Gel Stain	S33102	Invitrogen
NE Buffer 3.1 (10x)	B7203S	New England Biolabs
DNA Gel Loading Dye (6x)	R0611	Thermo Scientific
SalI Restriction Enzyme	R0138S	New England Biolabs

Table 2.5 Commercial plasmids

Item	Catalogue Number	Manufacturer
EGFR WT	11011	Addgene

Table 2.6 Commercial cell lines

Item	Catalogue Number	Manufacturer
HeLa	CCL-2	ATCC
COS-7	CRL-1651	ATCC
SH-SY5Y	CRL-2266	ATCC

Table 2.7 Cell culture reagents

Item	Catalogue Number	Manufacturer
DMEM (High Glucose, GlutaMAX Supplement, Pyruvate)	31966021	Gibco
DMEM/F-12, GlutaMAX Supplemented	31331028	Gibco
RPMI-1640 Medium	11875093	Gibco
Fetal Bovine Serum (FBS)	F9665	Sigma
Penicillin-Streptomycin Solution	15140148	Gibco
Opti-MEM	31985062	Invitrogen
Trypsin	25200056	Gibco

Accutase	AT104	Innovative Cell Technology
β-Mercaptoethanol (55mM)	21985-023	Gibco
Geltrex LDEV-Free Reduced Growth Factor Basement Membrane Matrix	A1413201	Gibco
RevitaCell Supplement (100x)	A2644501	Gibco
UltraPure 0.5M EDTA	15575020	Invitrogen
mTeSR1 Plus	100-0276	StemCell Technologies
Vitronectin XF	07180	StemCell Technologies
Gentle Cell Dissociation Reagent	100-0485	StemCell Technologies
Anti-Adherence Rinsing Solution	07010	StemCell Technologies
37uM Cell Strainers	27250	StemCell Technologies
Recombinant Human BMP-4 (HeLa Derived)	120-05	Peprotech
Recombinant Human VEGF165	100-20	Peprotech
Recombinant Human SCF	300-07	Peprotech
X-VIVO 15 Serum-free Hematopoietic Cell Medium	BE02-060F	Lonza
GlutaMAX Supplement	35050061	Gibco
Recombinant Human M-CSF	300-25	Peprotech
Recombinant Human IL-3	200-03	Peprotech
Recombinant Human IL-34	200-34	Peprotech
Recombinant Human TGF-β1 (HEK293 derived)	100-21	Peprotech
Cholesterol-Water Soluble	C4951	Sigma Aldrich
Advanced DMEM/F-12	12634010	Gibco
N2 Supplement (100x)	17502001	Gibco

Y-27632 dihydrochloride	SC-281642A	Santa Cruiz Biotechnology
Neubauer Improved C-Chip Disposable Haemocytometer	DHC-N01-50	NanoEnTek
DMSO	D8418	Sigma Aldrich
KnockOut Serum Replacement	10828028	Gibco
Countess Cell Counting Chamber Slides	C10228	Invitrogen
Trypan Blue Stain (0.4%)	T10282	Invitrogen
Nalgene Mr. Frosty Freezing Container	5100-0001	Thermo Scientific
Human Plasma Fibronectin	F2006	Sigma Aldrich

Table 2.8 Mycoplasma detection reagents

Item	Catalogue Number	Manufacturer
MycoAlert Mycoplasma Detection Kit	LT07-318	Lonza

Table 2.9 Transfection reagents for adherent cells

Item	Catalogue Number	Manufacturer
Lipofectamine 3000	L3000015	Invitrogen
jetPEI DNA Transfection Reagent Kit	101-10N	Polyplus
Lipofectamine 2000	11668019	Invitrogen
PLUS reagent	11514015	Invitrogen
Lipofectame LTX	15338100	Invitrogen

Table 2.10 Cell lysis and protein determination reagents

Item	Catalogue Number	Manufacturer
RIPA Buffer	20-188	Millipore
cOmplete Protease Inhibitor Cocktail	4693116001	Roche
PhosSTOP	4906845001	Roche

Pierce Coomassie (Bradford) Protein Assay Kit	23200	Thermo Scientific

Table 2.11 Western blotting reagents

Item	Catalogue Number	Manufacturer
NuPAGE LDS Sample Buffer (4x)	NP0007	Thermo Fisher
NuPAGE Sample Reducing Agent (10x)	NP0009	Thermo Fisher
4–15% Mini-PROTEAN TGX Precast Protein Gels, 15-well, 15µL	4561086	Biorad
Chameleon Duo Pre-Stained Protein Ladder	928-60000	LI-COR
NuPAGE MES SDS Running buffer (20x)	NP0002	Thermo Fisher
NuPAGE Transfer Buffer (20x)	NP0006	Thermo Fisher
Amersham Hybond Western Blotting Membranes, PVDF	10600023	GE Healthcare Life Sciences
Methanol ≥99.8%	20847.307	VWR Chemicals
TWEEN 20	P1379	Sigma
Bovine Serum Albumin (BSA)	A9418	Sigma

Table 2.12 WES reagents

Item	Catalogue Number	Manufacturer
12-230 kDa Wes Separation Module, 8 x 25 capillary cartridges + EZ Standard Pack	SM-W004	Protein Simple
Anti-Rabbit Detection Module For WES	DM-001	Protein Simple
Anti-Mouse Detection Module For WES	DM-002	Protein Simple

Table 2.13 Antibodies for western blots and WES

Item	Catalogue Number	Manufacturer
Phospho-PLCγ2 (Y759) Antibody (Rabbit)	3874	Cell Signaling Technologies
Anti-PLCγ2 Antibody (Rabbit)	3872	Cell Signaling Technologies
Anti-PLCγ2 Polyclonal Antibody (Rabbit)	A2182	ABclonal
Anti-PLCγ2 Antibody (H-160) (Rabbit)	sc-9015	Santa Cruz
Anti-PLCγ2 Antibody (B-10) (Mouse)	sc-5283	Santa Cruz
Donkey anti-Rabbit IgG (H+L) Highly Cross-Adsorbed Secondary Antibody, Alexa Fluor 680	A10043	Invitrogen
Anti-GAPDH Antibody (Rabbit)	2118	Cell Signaling Technologies
Anti-PLCγ1 Antibody (Mouse)	05-163	EMD Millipore
Anti-GAPDH Antibody (Mouse)	4267	Cell Signaling Technologies
Anti-NF-κB p65 Antibody (Rabbit)	8242	Cell Signaling Technologies
Phospho-NF-κB p65 (Ser536) Antibody (Rabbit)	3033	Cell Signaling Technologies

Table 2.14 qPCR reagents

Item	Catalogue Number	Manufacturer
TRIzol Reagent	15596026	Invitrogen
RQ1 (RNAse-Free) DNAse 10x Reaction Buffer	M198A	Promega
RQ1 (RNAse-Free) DNAse (1uL/µg of RNA)	M610A	Promega
RNAse Inhibitor	4374966	Applied Biosystems

10X RT Buffer		
10X RT Random Primers		
25X dNTP Mix (100 mM)		
MultiScribe Reverse Transcriptase (50 Units/µL)		
RQ1 DNAse Stop Solution	M199A	Promega
RT-qPCR One step Master Mix	OSPLUS-XXML	Primerdesign Ltd
RT-qPCR Master Mix	PPLUS-XXML	Primerdesign Ltd
DNAse	DNASE-50	Primerdesign Ltd
LightCycler 480 SYBR Green I Master (2X)	04707516001	Roche

Table 2.15 TaqMan Primers

Item	Catalogue Number	Manufacturer
PLCg1	Hs01008225_m1	Thermo Fisher
PLCg2	Hs01101857_m1	Thermo Fisher
P2RY12	Hs00375457_m1	Thermo Fisher
AIF1 (IBA1)	Hs00610419_g1	Thermo Fisher
TREM2	Hs00219132_m1	Thermo Fisher
CD68	Hs02836816_g1	Thermo Fisher
CX3CR1	Hs01922583_s1	Thermo Fisher
BLNK	Hs00179459_m1	Thermo Fisher
SYK	Hs00895377_m1	Thermo Fisher
LYN	Hs01015816_m1	Thermo Fisher
BTK	Hs00975865_m1	Thermo Fisher
CD14	Hs00169122_g1	Thermo Fisher
MERTK	Hs00179024_m1	Thermo Fisher
ITGAM (CD11b)	Hs00167304_m1	Thermo Fisher
PTPRC (CD45)	Hs04189704_m1	Thermo Fisher
SAC2A5	Hs01086390_m1	Thermo Fisher
SPI1 (PU.1)	Hs02786711_m1	Thermo Fisher
ACTB	JN177175	Primerdesign Ltd
ATP5B	JN177176	Primerdesign Ltd

UBC	CPO-02-000007	Primerdesign Ltd

Table 2.16 Reagents for the fixing and staining of cells

Item	Catalogue Number	Manufacturer
Paraformaldehyde (PFA)	F8775	Sigma
Triton X	X100	Sigma
Bovine Serum Albumin (BSA)	A9418	Sigma

Table 2.17 Antibodies for immunocytochemistry (ICC)

Item	Catalogue Number	Manufacturer
Anti-IBA1 (Rabbit) Antibody	019-19741	Wako
DAPI (4',6-Diamidino-2-Phenylindole)	62248	Thermo Scientific
Goat anti-Rabbit IgG (H+L) Cross-Adsorbed Secondary Antibody, Alexa Fluor 488	A-11008	Invitrogen
Anti-NF-κB p65 Antibody (Rabbit)	8242	Cell Signaling Technologies

Table 2.18 Assay kits

Item	Catalogue Number	Manufacturer
IP-One Gq Kit (20,000 tests)	62IPAPEC	Cisbio
FLIPR Calcium 6 Assay Kit	R8191	Molecular Devices
CellTiter-Glo Luminescent Cell Viability Assay	G7571	Promega
MSD V-PLEX Viral Panel 2 (human) kit	K15346D	Meso Scale Discovery

Table 2.19 Reagents for cell stimulation

Item	Catalogue Number	Manufacturer
Epidermal Growth Factor (EGF) Recombinant Human Protein	PHG0311	Gibco

TREM2 Polyclonal Antibody	AF1828	Bio-Techne
Goat IgG Isotype Control	AB-108-C	Bio-Techne
Human Fc gamma RIIA/CD32a Antibody	AF1875	Bio-Techne
Ultra Pure ATP	V915B	Promega
Ionomycin calcium salt from Streptomyces conglobatus	I0634	Sigma Aldrich
Lipopolysaccharides from Escherichia coli O55:B5	L2880	Sigma Aldrich

Table 2.20 Phagocytosis assay reagents

Item	Catalogue Number	Manufacturer
Protein LoBind, 50 ml, concial tube	0030122240	Eppendorf
Protein LoBind, 15 ml, concial tube	0030122216	Eppendorf
pHrodo iFL Red STP-Ester (amine-reactive)	P36010	Invitrogen
Hanks' Balanced Salt Solution (HBSS) - No Calcium, No Magnesium, No Phenol Red	14175095	Gibco
Live Cell Imaging Solution	A14291DJ	Invitrogen
Cytochalasin D	PHZ1063	Invitrogen

Table 2.21 Cell culture and assay plates

Item	Catalogue Number	Manufacturer
96 Well Microplate (U-bottom), Clear	650970	Greiner Bio-One
AggreWell 800	34811	StemCell
CellCarrier-96 Ultra Microplates, Black	6055302	PerkinElmer
96 Well HTRF IP_1 Plate	66PL96025	Cisbio
White 96 Well Tissue Culture Plate	655083	Greiner Bio-One
6 Well	657160	Greiner Bio-One
24 Well	3524	Corning

384 Well Plate, Black	781091	Greiner Bio-One
384 Well Plate, v Bottom, Clear	781280	Greiner Bio-One
T-25 Flask	690175	Greiner Bio-One
T-75 Flask	658175	Greiner Bio-One
T175 Flask	660175	Greiner Bio-One
LightCycler 480 Multiwell Plate 384, White	04729749001	Roche
Petri Dish	632180	Greiner Bio-One

2.2 Methods

2.2.1 Luria-Bertani (LB) medium and LB agar plates

Luria-Bertani (LB) medium was made by dissolving Miller LB broth (Sigma) in distilled water at 25g/L. The resulting solution was sterilised in an autoclave at 121°C until the cycle was completed.

LB agar was made by dissolving Miller LB agar (Sigma) in distilled water at 40g/L, before being autoclaved by the same process. The LB agar was then allowed to cool to ~40°C before 100μg/mL of ampicillin (Sigma) or kanamycin (Gibco) was added. The LB agar was poured into sterile petri dishes and allowed to set, before being stored at 4°C.

2.2.2 Bacteria transformation

0.85μL of β-Mercaptoethanol (Agilent Technologies) was added to 25μL of XL1-blue MR supercompetent cells (Agilent Technologies) before incubation on ice for 10 minutes, with gentle agitation every 2 minutes. 25ng of purified plasmid DNA was then added to the cells before incubation on ice for 30 minutes, with gentle agitation every 5 minutes. The cells were then subjected to a heat shock treatment of 42°C for 45 seconds, before being plunged in ice for 2 minutes. The cell suspension was then added to 450μL of pre-warmed (37°C) S.O.C medium (Invitrogen), before being incubated at 37°C for 1h with shaking at 230 rpm, to enhance the recovery of the cells. 25μL of the cell suspension was then spread onto an LB agar plate, containing the relevant plasmid selective antibiotic. The LB agar plate was then incubated for 16h at 37°C to allow for the production of visual colonies, before being sealed and stored at 4°C.

2.2.3 Bacteria cultures

Individual bacterial colonies were inoculated in 10mL of LB medium supplemented with 100µg/mL of ampicillin or kanamycin for 16h at 37°C, with shaking at 230 rpm. Alternatively, 5mL LB medium starter cultures supplemented with 100µg/mL of ampicillin or kanamycin were incubated for 8h at 37°C, with shaking at 230 rpm. 1mL of the starter culture was added to 99mL of LB medium supplemented with 100µg/mL of ampicillin or kanamycin. Large 100mL cultures were grown for 16h at 37°C, with shaking at 230 rpm. Bacterial cultures were centrifuged at 4700 rpm for 40 minutes at 4°C, with the resulting pellets either frozen at -20°C or used immediately for plasmid DNA isolation.

2.2.4 Glycerol stocks

Glycerol stocks of bacterial cultures were made by mixing 500µL of 50% (v/v) glycerol (Sigma) in UltraPure DNase/RNase-Free distilled water (Invitrogen), with 500µL of bacterial culture prior to storing at -80°C.

2.2.5 Streaking glycerol stocks

1µL of the bacterial glycerol stock was diluted in 49µL of LB medium before being spread onto LB agar plates containing the relevant antibiotic. The LB agar plate was then incubated for 16h at 37°C to allow for the production of visual colonies, before being sealed and stored at 4°C.

2.2.6 Plasmid DNA isolation

Plasmid/mammalian DNA was isolated from bacterial/human inducible pluripotent cell pellets. For the bacterial DNA extraction, the QIAprep Spin Miniprep Kit (Qiagen) or the QIAGEN Plasmid Plus Maxi Kit (Qiagen), was used in accordance with the manufacturer's guidelines. For each kit, the Plasmid DNA was eluted into 50µL or 200µL of UltraPure DNase/RNase-Free distilled water, respectively. For the mammalian DNA extraction, the DNeasy Blood & Tissue Kit was used in accordance with the manufacturer's instruction with the DNA eluted into 200µL of Buffer AE. DNA concentrations were quantified using a SpectraMax QuickDrop Micro-Volume Spectrophotometer (Molecular Devices), before being stored at -20°C.

2.2.7 Agarose gel

A 0.7% agarose gel was made by dissolving 0.7g of agarose (Sigma) in 100mL of 1x Tris-acetate-EDTA (TAE, Invitrogen), diluted in distilled water. The resulting mixture was heated until all the agarose powder had been solubilised. The gel was then placed into a cast and allowed to set.

The recipe for the restriction enzyme digestion of PLCγ2 plasmids is shown in Table 2.22. The resulting solution was incubated at 37°C for 1h so that the restriction enzyme could cleave the DNA. 2µL of DNA gel loading dye (Thermo Scientific) was then added to the reaction mixture before 6µL (100ng of DNA) of the reaction mixture was then added to each well of the agarose gel. 7µL of the 1kb Plus DNA ladder (Invitrogen) was added as a reference for the molecular weight band. Gels were run at 60V for 110 minutes. The gel was then incubated in the dark for 16h at 4°C in 100 ml of 1x TAE buffer supplemented with 30µL of SYBR Safe DNA Gel Stain (Invitrogen). The gel was then imaged on an Amersham imager 680 (GE Healthcare Life Sciences).

Table 2.22 Restriction enzyme digestion recipe

Reagent	Volume
SalI Restriction Enzyme	0.2µL
Plasmid DNA (PLCγ2 Variants)	200ng
NE Buffer 3.1 (10x)	1µL
Pure Water	Make the total volume to 10µL

2.2.8 Plasmids

PLCγ2-pTriEx-4 (PLCγ2-HIS) and peGFP-PLCγ2 (PLCγ2-GFP) vectors which encode the full length wild-type (WT) human PLCγ2 cDNA, as well as the empty peGFP-C1 vector were kindly provided by Prof. Matilda Katan (UCL, London, England). These vectors were used as a template to create mutant PLCγ2 constructs by site-directed mutagenesis. Epidermal growth factor receptor (EGFR) plasmids were obtained from Addgene. Table 2.23 lists all the plasmids used in this study.

Table 2.23 Plasmids used in the study

Plasmid name	Key property	Vector	Antibiotic resistance	Source
EGFR WT	EGF Receptor (EGFR)	pBABE	Ampicillin	Addgene
PLCγ2-HIS WT	FL hPLCG2 wild-type cDNA	pTriEx-4	Ampicillin	Matilda Katan
PLCγ2-HIS P522R	FL hPLCG2 cDNA: c.C1565G mutant	pTriEx-4	Ampicillin	Daniel Bull
PLCγ2-HIS R268W	FL hPLCG2 cDNA: c.C802T mutant	pTriEx-4	Ampicillin	Daniel Bull
PLCγ2-HIS Δ845-848	FL hPLCG2 cDNA: c.del2533-2544 mutant	pTriEx-4	Ampicillin	Tom Bunney
PLCγ2-HIS H327/372F	FL hPLCG2 cDNA: c.C979T, A980T, C1114T & A1115T mutant	pTriEx-4	Ampicillin	Daniel Bull
PLCγ2-HIS M1141K	FL hPLCG2 cDNA: c.T3422A mutant	pTriEx-4	Ampicillin	Daniel Bull
PLCγ2-HIS A708P	FL hPLCG2 cDNA: c.G2122C mutant	pTriEx-4	Ampicillin	Tom Bunney
PLCγ2-HIS V1103I	FL hPLCG2 cDNA: c.G3307A mutant	pTriEx-4	Ampicillin	Daniel Bull
PLCγ2-HIS D993G	FL hPLCG2 cDNA: c.A2978G mutant	pTriEx-4	Ampicillin	Daniel Bull
PLCγ2-HIS S707Y	FL hPLCG2 cDNA: c.C2120A mutant	pTriEx-4	Ampicillin	Daniel Bull
PLCγ2-HIS 4F+F897Q	FL hPLCG2 cDNA: c. A2258T, C2259T, A2276T, A3590T C3591T, A3650T, T2689C, T2690A & T2691A mutant	pTriEx-4	Ampicillin	Daniel Bull
PLCγ2-HIS H244R	FL hPLCG2 cDNA: c.C730A, A731G & T732A mutant	pTriEx-4	Ampicillin	Daniel Bull
PLCγ2-HIS M28L	FL hPLCG2 cDNA: c.A82C mutant	pTriEx-4	Ampicillin	Daniel Bull

peGFP-C1	Empty Vector	peGFP-C1	Kanamycin	Matilda Katan
PLCγ2-GFP WT	FL hPLCG2 wild-type cDNA	peGFP-C1	Kanamycin	Matilda Katan
PLCγ2-GFP P522R	FL hPLCG2 cDNA: c.C1565G mutant	peGFP-C1	Kanamycin	Daniel Bull
PLCγ2-GFP D993G	FL hPLCG2 cDNA: c.A2978G mutant	peGFP-C1	Kanamycin	Daniel Bull
PLCγ2-GFP S707Y	FL hPLCG2 cDNA: c.C2120A mutant	peGFP-C1	Kanamycin	Daniel Bull
PLCγ2-GFP H327/372F	FL hPLCG2 cDNA: c.C979T, A980T, C1114T & A1115T mutant	peGFP-C1	Kanamycin	Daniel Bull

2.2.9 Site-directed mutagenesis

Site direct mutagenesis was performed in accordance with the manufactures instructions using reagents from the QuikChange Lightning site-directed mutagenesis kit (Agilent Technologies). The PCR-based mutagenesis reactions were prepared as per Table 2.24. The forward and reverse mutagenesis primers (Sigma) used to introduce the nucleotide changes are listed in Table 2.25. Reactions were subjected to the thermal cycling conditions shown in Table 2.26.

22.5µL of the transformed cells was added to 250µL of S.O.C. medium and allowed to recover for 1h at 37°C with shaking at 230 rpm. Cells were then spread onto LB-agar plates containing 100µg/mL ampicillin or kanamycin (depending on the antibiotic resistance of the plasmid) to select for successfully transformed cells. Plates were then incubated at 37°C for 16h before being stored at 4°C.

Table 2.24 Site-directed mutagenesis reaction composition, derived from the QuikChange Lightning site-directed mutagenesis kit protocol

Reagent	Volume
10× QuikChange Lightning Buffer	2.5µL
PLCγ2 WT Plasmid	100ng

Forward Primer	125ng
Reverse Primer	125ng
dNTP mix	0.5µL
QuikSolution reagent	0.75µL
UltraPure DNase/RNase-Free Distilled Water	Make 25µL total volume
QuikChange Lightning Enzyme	0.5µL

Table 2.25 Forward and reverse primers used for site-directed mutagenesis

Primer Name	Sequence (5’ to 3’)	Target Variant
PLCg2_D993G_F	CAAAGGGACAAAGAGTTGGCTCTTCAAACTACGACCC	D993G
PLCg2_D993G_R	GGGTCGTAGTTTGAAGAGCCAACTCTTTGTCCCTTTG	
PLCg2_R268W_F	CTGAACAAAGTCCGTGAGTGGATGACAAAGTTCATTGAT	R268W
PLCg2_R268W_R	ATCAATGAACTTTGTCATCCACTCACGGACTTTGTTCAG	
PLCg2_H244R_F	TGCCTCTGCTGTTTACCTGAGAGACTTCCAGAGGTTTCTCA	H244R
PLCg2_H244R_R	TGAGAAACCTCTGGAAGTCTCTCAGGTAAACAGCAGAGGCA	
PLCg2_P522R_F	GAGGAAGTGCCCCAGGATATAAGGCCTACAGAACTACATT	P522R
PLCg2_P522R_R	AATGTAGTTCTGTAGGCCTTATATCCTGGGGCACTTCCTC	
PLCg2_M1141K_F	CGCTTTGTGGTTTATGAAGAAGATAAGTTCAGCGATCCCA	M1141K

PLCg2_M1141K_R	TGGGATCGCTGAACTTATCTTCTTCATAAACCACAAAGCG	
PLCg2_S707Y_F	GCACTTTGTGCTGGGGACCTACGCCTATTTTG	S707Y
PLCg2_S707Y_R	CAAAATAGGCGTAGGTCCCCAGCACAAAGTGC	
PLCg2_H327F_F	TTACTGGATCTCCTCGTCATTTAACACGTACCTTACAGGT	H327F
PLCg2_H327F_R	ACCTGTAAGGTACGTGTTAAATGACGAGGAGATCCAGTAA	
PLCg2_H372F_F	AAGCCGGTCATCTACTTTGGCTGGACGCGGAC	H372F
PLCg2_H372F_R	GTCCGCGTCCAGCCAAAGTAGATGACCGGCTT	
PLCg2_F897Q_F	GACAGGGTGGAGGAGCTCCAAGAGTGGTTTCAGAGCATC	F897Q
PLCg2_F897Q_R	GATGCTCTGAAACCACTCTTGGAGCTCCTCCACCCTGTC	
PLCg2_M28L_F	AGCTGGGGACGGTGCTGACTGTGTTCAGCTT	M28L
PLCg2_M28L_R	AAGCTGAACACAGTCAGCACCGTCCCCAGCT	
PLCg2_Y753F_F	AGAGATATAAACTCCCTCTTTGACGTCAGCAGAATGTATG	Y753F
PLCg2_Y753F_R	CATACATTCTGCTGACGTCAAAGAGGGAGTTTATATCTCT	
PLCg2_Y759F_F	CCTCTTTGACGTCAGCAGAATGTTTGTGGATCCCAG	Y759F

PLCg2_Y759F_R	CTGGGATCCACAAACATTCTGCTGACGTCAAAGAGG	
PLCg2_Y1197F_F	CCTGGAGAGCGAAGAGGAACTTTTTTCCTCCTGTCGC	Y1197F
PLCg2_Y1197F_R	GCGACAGGAGGAAAAAAGTTCCTCTTCGCTCTCCAGG	
PLCg2_Y1217F_F	ACTGAACAACCAGCTCTTTCTGTTTGACACACACCA	Y1217F
PLCg2_Y1217F_R	TGGTGTGTGTCAAACAGAAAGAGCTGGTTGTTCAGT	
PLCg2_V1103I_F	CAACAAGTTCAAGACGACGATTGTGAATGATAATGGCCT	V1103I
PLCg2_V1103I_R	AGGCCATTATCATTCACAATCGTCGTCTTGAACTTGTTG	

Table 2.26 Thermal cycling conditions for site-directed mutagenesis reactions

Step	Cycles	Temperature (^{o}C)	Time
Initial denaturation	1	95	2 minutes
Denaturation	18	95	20 seconds
Annealing		60	10 seconds
Extension		68	5 minutes
Final extension	1	68	5 minutes

2.2.10 Sanger sequencing

5µL of purified plasmid DNA (100ng/µL) was sent to Source Bioscience (Cambridge) for Sanger sequencing, along with 5µL of sequencing primers (3.2µM). Table 2.27 lists the primers used to sequence the vector regulatory genes. Table 2.28 lists the primers

used to sequence the full-length PLCG2 gene to confirm successful site-directed mutagenesis. Sequencing data files were analysed using Snapgene software (GSL Biotech LLC).

Table 2.27 Sanger sequencing primers used to sequence the regulatory regions of plasmids

Primer Name	Sequence (5’ to 3’)	Manufacturer
pCMV forward	GAGCTCGTTTAGTGAACCGTC	Source Bioscience

Table 2.28 Sanger sequencing primers used to sequence the full-length PLCG2 gene

Primer Name	Sequence (5’ to 3’)	Manufacturer
PLCG2-2Seq	CTGCATGACTTCCAGAGGTT	Sigma
PLCG2-3Seq	ACATTTTGGGGAGAAATGGT	Sigma
PLCG2-4Seq	AGGAGACTATGGAACCAGGA	Sigma
PLCG2-5Seq	AGCCGAGTATGACAACAACA	Sigma

2.2.11 Cell lines

HEK293T cells (provided by Prof. Matilda Katan, UCL), HeLa (ATCC), SH-SY5Y (ATCC) and COS-7 (ATCC) were cultured in complete ‘Dulbecco's Modified Eagle Medium’ (DMEM, Gibco) supplemented with 10% (v/v) foetal bovine serum (FBS, Sigma) and 1% (v/v) penicillin streptomycin (100µg/mL) solution (Gibco). Cultures were maintained at 37°C, 5% CO_2 and 95% humidity in T75 flasks (Corning). Cells were sub-cultured twice a week by washing with 5 mL phosphate-buffered saline (PBS) and dissociating with 3 mL Trypsin (Gibco).

Raji cells were provided by Dr. Clare Jolly (UCL). These cells were cultured in Roswell Park Memorial Institute (RPMI)-1640 Medium supplemented with 10% (v/v) FBS and 1% (v/v) penicillin (100 Units/mL) streptomycin (100µg/mL) solution. Cultures were maintained at 37°C, 5% CO_2 and 95% humidity in T75 flasks (Corning). Cells were sub-cultured twice a week.

H9 human embryonic stem cells (hESCs, kindly provided by Prof. Bart de Strooper, UCL) and PLCγ2 S707Y and WT human induced pluripotent stem cells (hiPSCs, provided by Dr. Rebecca McIntyre and Julie Matte, Wellcome Sanger Institute,

Cambridge, England) lines were cultured in mTeSR Plus (StemCell). Cultures were maintained at 37°C, 5% CO_2 and 95% humidity on Vitronectin XF (StemCell) coated 6 well plates. The media was replaced every two days. Cells were sub-cultured once a week, through 0.5mM EDTA (Invitrogen) dissociation.

2.2.12 Reviving cells from cryopreservation

Cell lines were thawed in a 37°C water bath for 1-2 minutes. Once thawed, the cell solution was added to 14mL of the relevant pre-warmed cell media, in a slow dropwise fashion, before being centrifuged (300g for 5 minutes). The supernatant was then removed and the cells re-suspended in 10mL of the relevant pre-warmed cell media. For the recombinant cell lines, the cell suspension was placed into a T-25/T-75 flask (Corning) until confluent. For the hESC/hiPSC lines, cells were re-suspended in 1mL of RevitaCell (Gibco) supplemented mTeSR plus media and the cell suspension was plated onto a Vitronectin XF coated 6 well plate until confluent.

2.2.13 Cryopreservation of cell lines

Cells in the log phase of growth were frozen at a density of 1-10 million cells/mL of cryopreservation medium composed of filter sterilised 90% (v/v) FBS (Sigma) supplemented with 10% (v/v) dimethyl sulfoxide (DMSO, Sigma) for the HEK293T, HeLa, COS-7, Raji and SH-SY5Y cells. The cryopreservation media for the hESC and hiPSC lines consisted of 90% (v/v) KnockOut serum replacement (Gibco) supplemented with 10% (v/v) DMSO. Cells were stored in cryogenic vials and slowly frozen inside a Mr. Frosty freezing container (Nalgene) at -80°C for 16h, before being transferred to liquid nitrogen and stored in the vapour phase (<135°C).

2.2.14 Stem cell-derived macrophage precursors (preMac)

Gentle cell dissociation reagent (StemCell) was used to dissociate the hESCs/hiPSCs. The cell suspension was diluted 1:10 in mTeSR plus supplemented with 10uM Y-27632 dihydrochloride (Rho kinase inhibitor, Santa Cruz). The cells were pelleted (300g for 5 minutes) before being re-suspended in mTeSR1 plus medium (StemCell Technologies) supplemented with 10uM Y-27632. The cells were counted and 4,000,000 cells/well were added to the AggreWell 800 (24 well, StemCell) in accordance with the manufacturer's instructions. The cells were then aggregated through centrifugation (100g for 3 minutes), before being placed into the incubator. The following three days, a

75% media change of each well was performed with mTeSR plus media supplemented with 50 ng/mL recombinant human bone morphogenetic protein 4 (BMP4, Peprotech), 50 ng/mL recombinant human vascular endothelial growth factor (VEGF, Peprotech) and 20 ng/mL recombinant human stem cell factor (SCF, Peprotech). Four days after plating, the resulting embryoid bodies (EBs) were collected in a 37µm reversable strainer and plated at a density of 1 EB/cm^2 in Geltrex LDEV-Free Growth Factor Reduced (GFR) coated T-175 flask filled with XVIVO 15 media (Lonza) supplemented with 2mM GlutaMax (Gibco), 1% (v/v) penicillin-streptomycin solution, 55µM β-mercaptoethanol (Gibco), 100ng/mL recombinant human macrophage-colony stimulating factor (M-CSF, Peprotech) and 25ng/mL recombinant human interleukin-3 (IL-3, Peprotech). Half media changes were performed every week with macrophage progenitors collected from the supernatant by centrifugation. Due to the high number of cells generated via this process, the flask of preMacs is often referred to as a 'myeloid factories.

2.2.15 Stem cell-derived macrophages

150,000 cells/cm^2 of macrophage precursors (preMacs) were plated in XVIVO15 media (Lonza) supplemented with 2mM GlutaMax, 1% (v/v) penicillin-streptomycin solution and 100ng/mL M-CSF. Half media changes were performed every 2 or 3 days. 7 days after plating the cells were ready for experiments.

2.2.16 Stem cell-derived microglia

Macrophage precursors (preMacs) were plated into a 10µg/mL human plasma fibronectin (Sigma) coated plate/flask filled with microglia differentiation media, consisting of advanced DMEM/F12 (Gibco) supplemented with 2mM GlutaMax, 1% (v/v) penicillin-streptomycin solution, 1x N2 Supplement (Gibco), 100ng/mL recombinant human interleukin-34 (IL-34, Peprotech), 1.5µg/mL cholesterol (Sigma), 100ng/mL M-CSF and 5ng/mL recombinant human transforming growth factor-beta 1 (TGF-β1, Peprotech).

Initial experiments involved plating the H9-derived microglia in the assay plate before the cells were differentiated for 7 days with a media change every 2/3 days. However, the protocol was altered to prevent cell number variability on the day of experimentation. As a result, the H9/hiPSC-derived microglia were differentiated for 4 days in T-75 flasks (4 million preMac cells/flask) with a half media change on day 2.

On day 4, the cells were lifted with Accutase (Innovative Cell Technology) and re-plated at a density of 50,000 cells/cm^2 on fibronectin coated assay plates. The cells were differentiated for a further 3 days, and on day 7 the cells were ready for experiments.

2.2.17 MyCoplasma Testing

The MycoAlert mycoplasma detection kit (Lonza) was used as per the manufacturer's guidelines. This assay takes advantage of Mycoplasmal enzymes, which react with the MycoAlert substrate and convert ADP to ATP. The difference in ATP levels before and after the addition of the substrate are detected by the following bioluminescent reaction:

$$\text{ATP} + \text{Luciferin} + O_2 \xrightarrow[Mg^{2+}]{\text{Luciferase}} \text{Oxyluciferin} + \text{AMP} + \text{PPi} + CO_2 + \textbf{LIGHT}$$

The light intensity emitted correlates linearly to the ATP concentration in the sample. Assays were performed in opaque white 96-well flat bottom plates (Sigma) and relative light units (RLU) were determined with the PHERAstar FSX (BMG Labtech) and analysed with the MARS data analysis software (BMG Labtech). Cells were routinely tested for mycoplasma with all cell lines found to be negative for it.

2.2.18 Cell transfections

50,000 COS-7 cells/well were plated into a 24 well plate in DMEM supplemented with 10% (v/v) FBS. The following day, the cell media was removed and replaced with DMEM. The cells were transfected with 100-500ng of PLCγ2 WT-HIS/GFP and 0.5-1.5uL of Lipofectamine 3000 (Invitrogen) diluted in Opti-MEM (Invitrogen) in accordance with the manufacturer's instructions. Cells were incubated for 6h before the transfection media was removed and replaced with DMEM supplemented with 10% (v/v) FBS and 1% (v/v) penicillin-streptomycin solution. Cells analysis was performed 24-48h post transfection.

60,000 HEK293T cells/well were plated into a 24 well plate in HEK293T media (recipe shown in 2.2.11 Cell line). The following day, the cell media was removed and replaced with DMEM supplemented with 10% (v/v) FBS. The cells were then transfected with 20-500ng of PLCγ2 HIS/GFP and/or 50-500ng of EGFR plasmids with 1.2uL of jetPEI DNA transfection reagent (Polyplus) diluted in sodium chloride (Polyplus) in

accordance with the manufacturer's instructions. Mock transfections consisted of an empty peGFP-C1 plasmid in place of the PLCγ2 plasmid. Furthermore, the empty peGFP-C1 plasmid was added to keep the total DNA consistent during transfection. Cells were incubated for 16h before the media was replaced with DMEM supplemented with 10% (v/v) FBS and 1% (v/v) penicillin-streptomycin solution. Cells analysis was performed 24-48h post transfection.

2.2.19 Protein extraction

1-4 million cells were washed once with ice cold PBS before an ice cold lysis/inhibitor cocktail consisting of 1x RIPA buffer (Millipore), 1x cOmplete protease inhibitor (Roche) and 1x PhosSTOP (Roche) was used to lyse the cell pellet. Adherent cells were removed with a cell scraper before being washed. Lysates were chilled on ice for 20 minutes with gentle agitation every 5 minutes, before being centrifuged (21,100g for 5 minutes at 4°C). The protein containing supernatant was extracted and stored at -80°C.

2.2.20 Protein determination

The protein concentration of the lysates was measured using the colorimetric 'Pierce Coomassie protein assay kit' (Thermo Scientific) in accordance with the manufacturer's instructions. The mean absorbance (595nm) of the bovine serum albumin (BSA) standards and the protein samples was measured using the PHERAstar FSX and analysed with the MARS data analysis software (BMG Labtech).

2.2.21 Western blotting

Protein lysates were mixed with 1x NuPAGE LDS sample buffer (Thermo Fisher) and 1x NuPAGE sample reducing agent (Thermo Fisher) to a final protein concentration of 1µg/µL. Samples were then heated at 70°C for 10 minutes. 12µg of protein sample was loaded into a 4–15% Mini-PROTEAN TGX precast protein gels (Biorad), alongside 7µL of chameleon duo pre-stained protein ladder (LI-COR). The gel was run in 1x NuPAGE MES SDS running buffer (Bio-Rad) at a constant voltage of 110V for 50 minutes. A semi-dry transfer was carried out by relocating the proteins from the gel to a polyvinylidene difluoride (PVDF) membrane (GE Healthcare), by electro-transfer (200 mA for 90 minutes at 4°C). The transfer buffer was comprised of 1x NuPAGE Transfer buffer (Bio-Rad) and 20% (v/v) methanol (VWR). The membranes were blocked in a

solution of 0.1% PBS-Tween (0.1% PBST, Sigma) supplemented with 5% (v/v) BSA (Sigma) for 1h at room temperature.

The membranes were incubated with the primary antibodies: anti-PLCγ2 rabbit antibody (1:1000, Cell Signaling Technology), anti-PLCγ2 rabbit antibody (1:1000, ABclonal), anti-PLCγ2 rabbit antibody (H-160, 1:1000, Santa Cruz) or anti-PLCγ2 rabbit antibody (1:1000, provided by our collaborator Dr. Todd Golde) for 16h at 4°C. The membranes were washed three times with 0.1% PBST, before being incubated in the dark with a donkey anti-Rabbit IgG secondary antibody, Alexa Fluor 680 (1:1000, Invitrogen) for 1h at room temperature. The membranes were washed three times with 0.1% PBST before being imaged on the Odyssey CLx (LI-COR). All antibodies were diluted in a solution consisting of 0.1% PBST supplemented with 5% BSA.

2.2.22 WES – Western blot

The WES was performed in accordance with the manufacturer's instructions (Protein Simple). Protein lysates were run at 0.3-1µg/µL. The primary antibodies: anti-PLCγ2 rabbit antibody (1:50, Cell Signaling Technology), anti-PLCγ2 mouse antibody (B-10, 1:25, Santa Cruz), anti-Y759 PLCγ2 rabbit antibody (1:25, Cell Signaling Technology), anti-PLCγ1 mouse antibody (1:75, EMD Millipore), anti-GAPDH mouse antibody (1:100, Abcam), anti-GAPDH rabbit antibody (1:300, Cell Signaling Technology), anti-EGFR rabbit antibody (1:50, Cell Signaling Technology), anti-NF-κB p65 rabbit antibody (1:40, Cell Signaling Technology) and anti-S536 NF-κB p65 rabbit antibody (1:40, Cell Signaling Technology) were used. The respective secondary antibody detection kit was used depending on the species specificity of the primary antibody. Quantification was performed by the WES (Protein Simple), with data analysis performed in the Compass software (Protein Simple).

2.2.23 RNA extraction

5 million hiPSC/hESC derived-preMacs were harvested fresh from cultures. Adherent cells (HEK293T, COS-7, HeLa, hiPSC/hESC derived-macrophages and microglia) were plated onto 6 well plates until 80-90% confluent or until they were differentiated for 7 days. RNA extraction via TRIzol (Invitrogen) was performed according to the manufacturer's instructions. The RNA was re-suspended in 30µL of UltraPure DNase/RNase-free distilled water. RNA concentrations were quantified using a SpectraMax QuickDrop micro-volume spectrophotometer and stored at -80°C.

2.2.24 Reverse transcription (RT) for two step qPCR

Extracted RNA was diluted in UltraPure DNase/RNase-free distilled water to a final concentration of 3µg/13µL. 7µL of DNAse master mix (recipe shown in Table 2.29) was added to the RNA. The resulting solution was then incubated at 37°C for 30 minutes, before 2µL of the RQ1 DNase stop solution was added. The solution was incubated at 65°C for 10 minutes to stop the reaction. 20µL of reverse transcription master mix (recipe shown in Table 2.30) was then added. The resulting solution was subjected to the thermal conditions shown in Table 2.31. The resulting cDNA was then stored at -20°C until needed.

Table 2.29 Recipe for DNAse master mix

Reagent	Final Concentration	Volume
RQ1 (RNAse-Free) DNAse 10x Reaction Buffer	1x	2µL
RQ1 (RNAse-Free) DNAse	1uL/µg of RNA	3µL
RNAse Inhibitor (20 Units/µL)	40 Units	2µL

Table 2.30 Recipe for reverse transcription master mix

Reagent	Final Concentration	Volume
10X RT Buffer	2x	4µL
10X RT Random Primers	2x	1.6µL
25X dNTP Mix (100 mM)	2x	4µL
MultiScribe Reverse Transcriptase (50 Units/µL)	5 Units/µL	2µL
RNase Inhibitor (20 Units/µL)	2 Units/µL	2µL
UltraPure DNase/RNase-Free Distilled Water	-	6.4µL

Table 2.31 Thermal cycling conditions for reverse transcription

Temperature (°C)	Duration (minutes)
25	10
37	120
85	5

2.2.25 Two-step qPCR

The qPCR detection master mix was composed according to Table 2.32. The forward and reverse primers are listed in Table 2.33. Reactions were plated onto a LightCycler multiwell 384 white plate (Roche), in triplicate, and subjected to the thermal conditions shown Table 2.34, using the LightCycler 480 System (Roche) to produce cycle threshold (C_t) values. Real-time data was analysed using the $2^{-(\Delta\Delta Ct)}$ method[254].

Table 2.32 Two Step qPCR detection master mix composition

Reagent	Concentration	Volume
Water	-	1.5µL
Forward Primer	10uM	0.5µL
Reverse Primer	10uM	0.5µL
LightCycler 480 SYBR Green I Master (2X)	1x	5µL
cDNA	-	2.5µL

Table 2.33 RT-PCR primers

Gene	Primer	Sequence
EGFR	EGFR_Fwd	GTGGATGGCATTGGAATCA
	EGFR_Rev	CAAAGGTCATCAACTCCCAAA
GAPDH	GAPDH_Fwd	ACACCCACTCCTCCACCTTT

	GAPDH_Rev	TAGCCAAATTCGTTGTCATACC

Table 2.34 Two Step qPCR thermal cycling conditions

Step	Temperature (°C)	Duration (seconds)	Cycles
Enzyme Activation	95	300	1
Denaturation	95	12	35
Annealing	58	24	
Extension	72	36	
Melting Curve	95	6	1
	65-97	12/°C	1

2.2.26 One-step qPCR

TaqMan primers (2.1Table 2.15) were validated with 2-fold diluted concentrations of RNA, with the addition of 'no reverse transcriptase' (Table 2.36) and 'no RNA' controls. 25ng of sample RNA was added to each well, in triplicate, onto a LightCycler multiwell 384 white plate (Roche). 3uL of the qPCR detection master mix (Table 2.35) was added to each well before being subjected to the thermal conditions shown in Table 2.37, using the LightCycler 480 System (Roche) to produce cycle threshold (C_t) values. Real-time data was analysed using the $2^{-(\Delta\Delta Ct)}$ method[254].

Table 2.35 One-step qPCR detection master mix composition

Reagent	Concentration	Volume
Water	-	0.125µL
FAM Primer	-	0.25µL
RT-qPCR One step Master Mix	-	2.5µL
1 in 10 DNAse	-	0.125µL

Table 2.36 No RT control master mix composition

Reagent	Concentration	Volume
Water	-	0.125µL
FAM Primer	-	0.25µL
RT-qPCR Master Mix	-	2.5µL
1 in 10 DNAse	-	0.125µL

Table 2.37 One-step qPCR thermal cycling conditions

Step	Temperature (^{o}C)	Duration (minutes)	Cycles
DNase Activation	37	25	1
RT	55	10	1
Taqman Hotstart	95	2	1
Denaturation	95	0.1	40
Annealing/Extension	60	1	

2.2.27 Immunocytochemistry (ICC)

Plated cells were fixed with 4% paraformaldehyde (PFA, Sigma) for 15-30 minutes, followed by three PBS washes. Cells were blocked with a solution consisting of PBS supplemented with 0.1% (v/v) TritonX (Sigma) and 10% (v/v) FBS for 1h at room temperature. The cells were then incubated for 24h at 4°C with either anti-IBA1 rabbit antibody (1:500, Wako) or anti-NF-κB rabbit antibody (1:400, CST). Following three PBS washes, the cells were exposed to an Alexa Fluor 488 Goat anti-Rabbit IgG secondary antibody (1:1000, Invitrogen) and DAPI (1:1000, Invitrogen), for 1h in the dark. Following three PBS washes, the plate was imaged on an Operetta/Opera Phenix Plus high-content imaging system (Perkin Elmer). The percentage of GFP positive cells/DAPI stained cells, as well as the NF-κB nuclear translocation (Nuclear:Cytoplasm ratio), was calculated through the Harmony/Columbus software

(PerkinElmer). All antibodies were diluted in a solution consisting of PBS supplemented with 0.1% (v/v) TritonX and 10% (v/v) FBS.

2.2.28 IP_1 (inositol monophosphate) HTRF accumulation assay

HEK293T cells were transfected as previously mentioned in 2.2.18. Post-transfection, the media was removed and replaced with fresh media. Later that day, the media was removed and replaced with DMEM supplemented with 1% (v/v) FBS and 0.1% (v/v) penicillin-streptomycin solution, to cause a partial serum starve for 24h. Stimulation of EGFR was achieved by the addition of 150ng/µL of epidermal growth factor (EGF, Gibco) for 1-1.5h.

The H9-derived microglia cells were differentiated for 7 days after an initial plating of 50,000-150,000 preMac cells/24 well. The hiPSC-derived microglia cells were differentiated and re-plated onto a 96 well plate on day 4 of differentiation. Both protocols are described in 2.2.16. After 7 days of differentiation, both microglia derived cells were stimulated with 12.5-50ug/mL of TREM2 or Goat-IgG (Bio-Techne) for 2h.

The IP_1 protocol was performed in accordance with the manufactures instructions (Cisbio). A homogenous time-resolved fluorescence (HTRF) ratio was obtained through the PHERAstar FSX, with data analysis performed in GraphPad Prism 7 (GraphPad). Unless stated, the IP_1 data was normalised to the PLCγ2 expression of the experimental lysates.

2.2.29 Calcium assay

The H9-derived microglia cells were differentiated for 7 days after an initial plating of 10,000 preMac cells/384 well. The hiPSC-derived microglia cells were differentiated and re-plated onto a 384 well plate on day 4 of differentiation. Both protocols are described in 2.2.16.

Calcium 6 dye was diluted in HBSS assay buffer (1.4mM $MgCl_2$, 2mM $CaCl_2$, 10mM HEPES in HBSS) to achieve a 1X solution. Media was removed from the H9/hiPSC-derived microglia cells so that only 20uL of media remains. 20uL of 1X Calcium 6 dye was added to the cells before being placed into the incubator for 2h. Baseline calcium signal was measured in FLIPR Tetra (Molecular Devices) before cells were exposed at set time points to either HBSS assay buffer, 10 µg/mL Goat IgG, 1.25/2.5/5/10 µg/mL of TREM2 or FcγRIIA/CD32a, 500 µM ATP or 5 µM Ionomycin. For the hiPSC-

derived microglia, cells were re-stimulated with 5 µM Ionomycin once the calcium signal had returned to baseline. Area under the curve (AUC) data was analysed using Screenworks (Molecular Devices). hiPSC-derived microglia stimulation values were normalised to ionomycin re-stimulation values.

2.2.30 Preparation of pHrodo labelled SH-SY5Y cells

Confluent SH-SY5Y cells were dislodged and pelleted (300g for 3 minutes) in a LoBind conical tube (Eppendorf). The pellet was washed with HBSS before being centrifuged again. The resulting pellet was re-suspended in live imaging solution (Invitrogen) supplemented with 2% paraformaldehyde (PFA) to induce apoptosis. The cells were then mixed for 10 minutes, before HBSS was added to dilute the PFA. The cells were washed twice with live cell imaging solution through centrifugation (1200g for 7 minutes). For every million cells, 2µL of 5mg/mL pHrodo (Invitrogen) was added. The cells were mixed in the dark for 30 minutes before being pelleted (1200g for 10 minutes at 4°C). The cells were diluted to a concentration of 1.6 million cells/mL in live cell imaging solution supplemented with 5% (v/v) DMSO. The pHrodo SH-SY5Y cells were stored in the dark at -20°C.

2.2.31 Phagocytosis assay

The H9-derived microglia cells were differentiated for 7 days after an initial plating of 20,000 preMac cells/96 well. The hiPSC-derived microglia cells were differentiated and re-plated onto a 96 well plate on day 4 of differentiation. Both protocols are described in 2.2.16.

Negative controls consisted of ‘cell only’, ‘substrate only (pHrodo labelled SH-SY5Y cells)’ and cytochalasin D (1uM), a known phagocytosis inhibitor. 50,000 pHrodo labelled SH-SY5Y cells/well were added to the microglia cells before being placed into a IncuCyte S3 live-cell analysis system (Sartorius) chamber, with an image captured every 10 minutes for 5h, then 1h for a further 19h. Live cell imaging solution was used for the negative controls to ensure the total volume was equal. Image analysis was performed on the IncyCyte analysis software.

2.2.32 CellTiter-Glo luminescent cell viability assay

H9 and hiPSC-derived microglia cells were differentiated and re-plated onto a white opaque 96 well plate at a density of 50,000 cells/cm^2 as described in 2.2.16. After 7

days of microglial differentiation, the assay was performed in accordance with the manufacturer's instructions. Briefly, CellTiter-Glo reagent was added to the cells in an equal volume and the cells were lysed for 2 min on a shaker in the dark. The plate was then incubated at room temperature for 10 minutes in the dark to stabilize luminescent signal before the luminescence signal was read on the PHERAstar FSX. Blank values were subtracted from the experimental measurements.

2.2.33 Cytokine assay

H9 and hiPSC-derived microglia cells were differentiated and re-plated onto a 96 well plate at a density of 50,000 cells/cm^2 as described in 2.2.16. After 7 days of microglial differentiation, cell culture supernatant was removed and immediately frozen. Cells were challenged with ± LPS (1 ng/mL) for 24h and the cell culture supernatant was removed and immediately frozen. IFN-γ, IL-1β, IL-4, IL-6, IL-8, IL-10, TNF-α cytokine concentration was quantified with the MSD V-PLEX Viral Panel 2 (human) kit (Meso Scale Discovery). Cytokine values were normalised to total cell number imaged on the IncuCyte S3 live-cell analysis system (Sartorius).

2.2.34 RNASeq

RNA was extracted from PLCγ2 S707Y and WT hiPSC-derived microglia from three separately generated preMac factories, through the process outlined in 2.2.23. Libraries were prepared using the KAPA RNA HyperPrep Kit and sequenced on an Illumina HiSeq 4000 sequencer at a minimum of 25 million paired-end reads (75 bp) per sample performed by UCL Genomics (London, England). Raw counts per million (CPM) were obtained and processed through iDEP (integrated Differential Expression and Pathway analysis, http://bioinformatics.sdstate.edu/idep/)[255] with the parameters of a minimum CPM of 25 in 3 libraries, a DESeq2 analysis with a min fold change ≥ 1.5 and a false discovery rate (FDR) ≤ 0.05. The top differential expressed genes (DEGs) were obtained and ranked by the log2 fold change. Gene Ontology (GO) enrichment and gene set enrichment analysis (GSEA) of the DEGs for biological process was performed and ranked by adj.Pval. STRING (Search Tool for the Retrieval of Interacting Genes/Proteins, https://string-db.org/)[256] analysis was performed on the top DEGs (log2 Fold Change > 2, high confidence > 0.7) to predict protein-protein interactions.

2.2.35 Statistical analysis

Results are expressed as mean ± standard deviation. All experiments were performed three times (biological replicates), with at least three experimental replicates per condition and for each biological replicate, unless stated otherwise. Statistical methods for analysing the various data sets are indicated directly in the figure legends. Data were analysed using Graphpad Prism 9 (GraphPad Software version 9.3.1, GraphPad, San Diego, CA, USA).

Chapter 3 - Development of a heterologous cell system for characterisation of PLCγ2 disease-linked variants

3.1 Introduction

Previous characterisation of PLCγ2 variant enzymatic activity has been performed in patient PBMCs[215], COS-7[139,147,216], HEK293T[139], WEHI-231[207], bone marrow-derived macrophages[227], as well as hiPSC-derived microglia[133] and macrophage[183] cells. While some of these cell models express high levels of endogenous PLCγ2, others do not (Human Protein Atlas available from www.proteinatlas.org)[139,183]. Cell models that exhibit low levels of endogenous PLCγ2 expression, as well as other PLC enzymes, offer the opportunity for overexpression assays. Taking this into account, as well as the complexity and length for the generation of some of these different cell models, COS-7 and HEK293T cell lines transfected with PLCγ2 cDNA constructs are classically used to characterise PLCγ2 variant enzymatic activity[139,147,216].

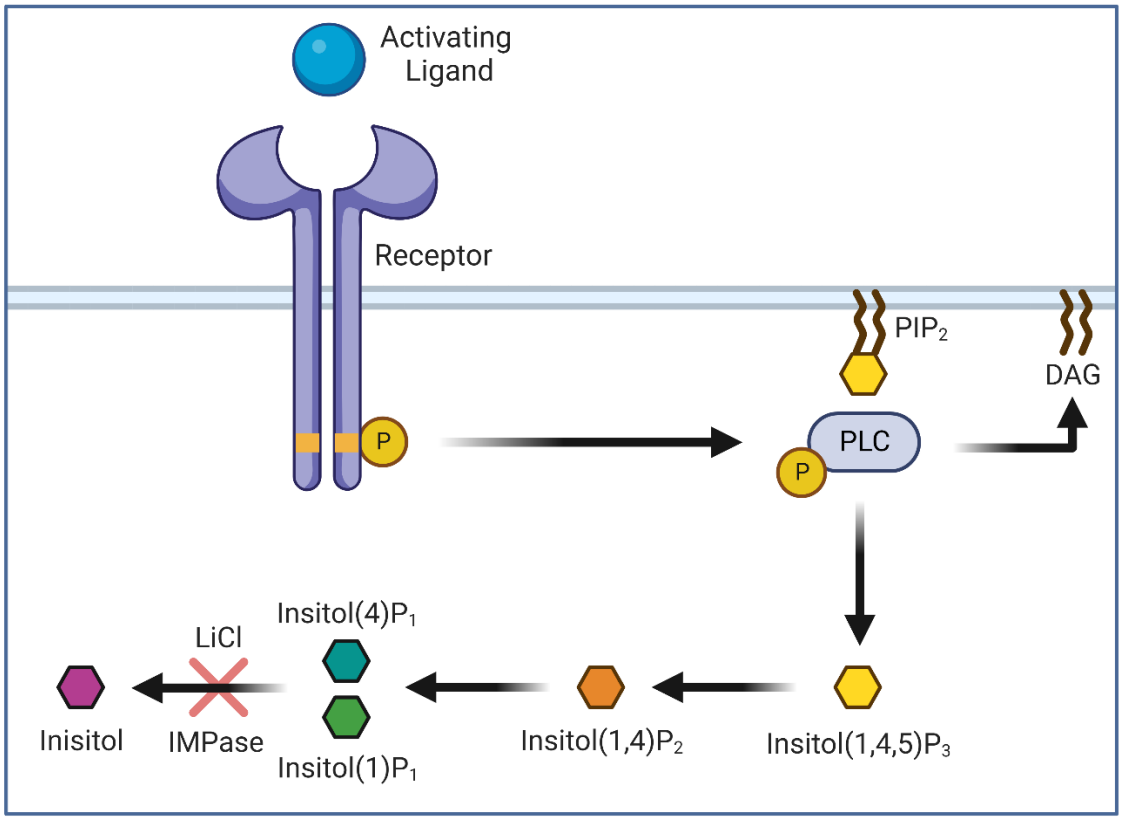

Figure 3.1 Inositol monophosphate (IP_1) assay schematic. Upon PLC activation, PIP_2 is hydrolysed into DAG and inositol (1,4,5) trisphosphate (IP_3). IP_3 is rapidly degraded into inositol (1,4) bisphosphate (IP_2), and subsequently inositol (4) monophosphate or inositol (1) monophosphate (IP_1). The addition of lithium chloride (LiCl) inhibits inositol monophosphase (IMPase) dephosphorylation of IP_1 causing it to accumulate.

PLC enzymatic quantification utilises IP_3 production, by capturing the secondary metabolite of IP_3, inositol monophosphate (IP_1). Cells are incubated in the presence of lithium chloride (LiCl) that blocks the formation of both inositol (4) monophosphate and inositol (3) monophosphate by inhibiting inositol polyphosphate 1 phosphatase, as well as blocking the degradation of IP_1, resulting in it to be the only inositol monophosphate to form and accumulate (Figure 3.1)[257]. The cells are then lysed, before IP_1 is quantified. Previous enzymatic quantification had been carried out through the use of a radioactive [^{3}H] myo-inositol assay, whereby tritium is incorporated into the inositol-lipids in the cells[205]. However, this procedure is complex to set up and has low throughput. To mitigate these issues, the Cisbio IP_1 kit uses HTRF (homogeneous time resolved fluorescence) detection to quantify IP_1 concentration, allowing for a greater throughput and safety than its radioactive counterpart. Briefly, the assay is a competitive immunoassay whereby free IP_1 competes against IP_1-d2 (acceptor) for binding to anti-IP_1 Cryptate conjugate (donor)[257]. The resulting signal is inversely proportional to the concentration of IP_1 in the sample, with a standard curve generated to convert raw data to an IP_1 concentration, as exemplified in Figure 3.2[257].

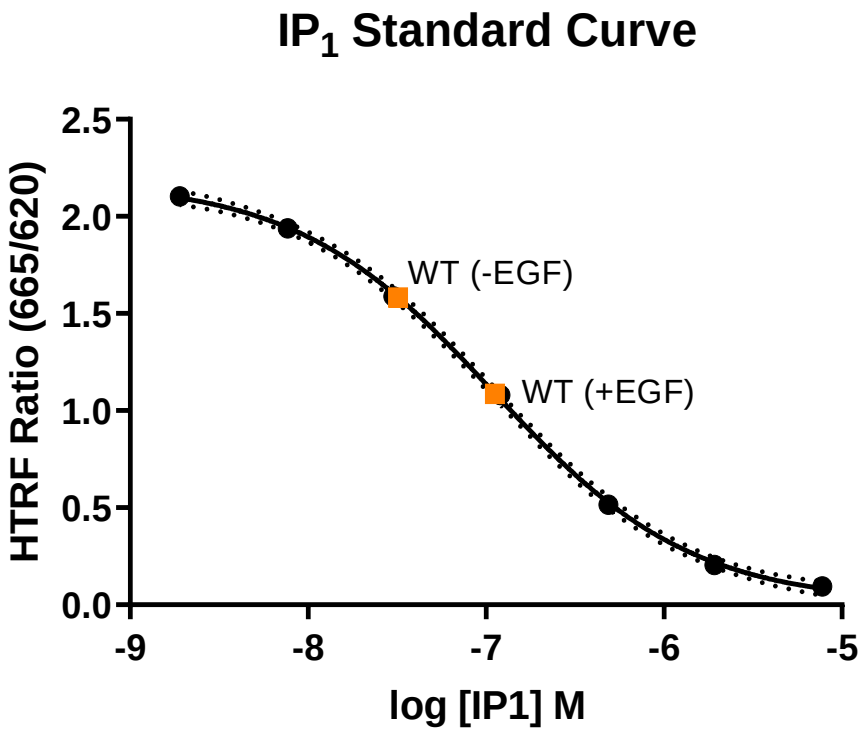

Figure 3.2 Representative standard calibration curve for the HTRF IP_1 assay. A standard curve is plotted using the 665/620 ratio vs IP_1 concentration using non-linear least squares fit (sigmoidal dose response variable slope, 4PL). Fitting of HEK293T

cells co-transfected with EGFR and PLCγ2 WT constructs (1:1 cDNA ratio) exposed to ± EGF (150 ng/ul) for 1.5h.

Epidermal growth factor receptor (EGFR) stimulation though the use of epidermal growth factor (EGF) has been demonstrated to activate PLCγ2[139]. Therefore, the IP_1 assay can be utilised to characterise PLCγ2 disease-linked variant enzymatic activity under both basal and stimulated (via EGFR) conditions. When developing any assay, negative and positive controls are essential for validation. Previously characterised PLCγ2 variants can be utilised to act as controls for the development and optimisation of the assay as PLCγ2 loss-of-function and GOF variants have been documented[139,171,232].

3.2 Results

3.2.1 Generation and validation of PLCγ2 variants expression plasmids

To understand the effect of the PLCγ2 disease-linked variants on enzyme activity, site directed mutagenesis was employed to introduce mutations into the full length PLCγ2 WT-HIS/GFP plasmids. Both plasmids contain the cytomegalovirus (CMV) promotor, which allows for strong mammalian expression. The WT PLCγ2 vector was used as a template to create the R268W, H244R, P522R, S707Y, D993G, A708P, M1141K, V1103I, M28L, Δ845-848, H327/372F and 'T753/759/1197/1217F + F897Q (4F/F897Q)' variant constructs. The A708P and Δ845-848 constructs were generated and validated by Dr. Tom Bunney (Katan Lab). Successful mutagenesis was confirmed by Sanger sequencing (Source Bioscience, Figure S1). The expected molecular weights of the plasmids and the absence of degradation was confirmed by agarose gel electrophoresis (data not shown).

3.2.2 Development, optimisation and characterisation of a model cell system to assess expression and function of PLCγ2 variants

3.2.2.1 Assessing and validating cellular models and tools

Characterisation of PLC mutant activity has been well documented in COS-7 monkey kidney fibroblast cells[139,147,216]. The main advantage of the COS-7 cell line, is that the expression of EGFR, an activator of PLCγ2, is higher than that of other widely used cell lines (Figure 3.3). EGFR expression in COS-7 cells was demonstrated by qPCR to be >6500% fold higher than that of HEK293T cells (Figure 3.3). Additionally, comparing the individual EGFR cycle threshold (C_t) values (not normalised to the GAPDH

housekeeping gene) shows the same result (Figure 3.3). Hence, upon EGFR stimulation in COS-7 cells, PLCγ2 activation should be robust enough to detect changes in enzymatic activity across the various PLCγ2 variants.

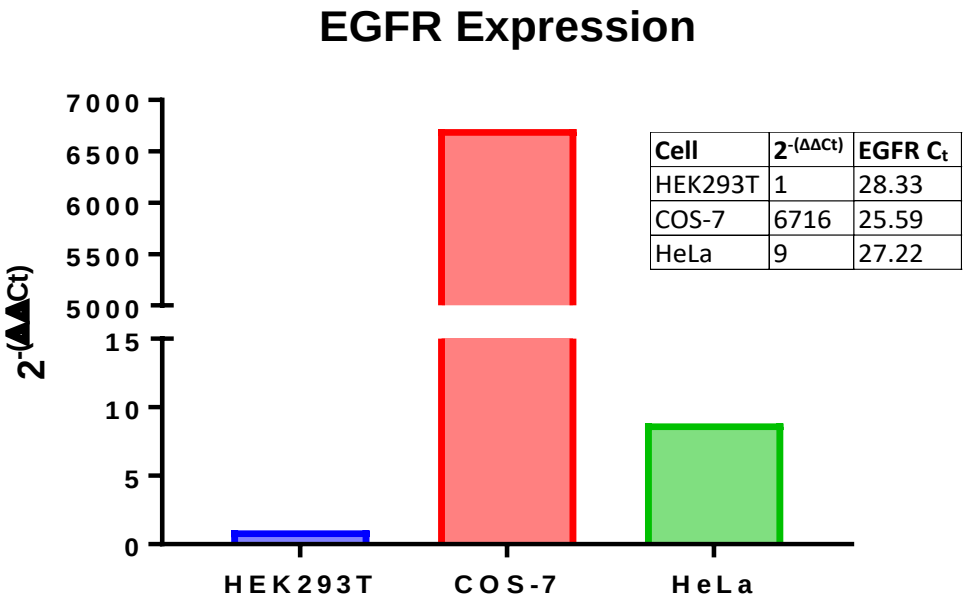

Figure 3.3 qPCR data comparing the EGFR mRNA levels of HEK293T, COS-7 and HeLa cells. EGFR cycle threshold (C_t, values displayed in the table) values were normalised to the GAPDH C_t values of each cell type before the fold ratio change for each cell type was normalised to the HEK293T cells ($2^{-(\Delta\Delta Ct)}$, values displayed in the table). Data is representative of one biological replicate with three experimental replicates (n=1).

Testing this hypothesis, a transfection protocol for the COS-7 (using Lipofectamine 3000 reagent) was developed and optimised (data not shown). Cells were transfected with the PLCγ2-GFP construct and GFP transfection efficiency assessed through the Harmony high-content imaging and analysis software (PerkinElmer). The transfection efficiency of the COS-7 cells was demonstrated to be 29 ± 4% (Figure 3.4). Other transfection reagents were also tested to try and improve the transfection efficiency. However, transfection efficiency did not sufficiently improve (data not shown). With the COS-7 cells exhibiting such a low transfection efficiency, it was hypothesised that small changes in PLCγ2 variant activity may not be detected due to low total PLCγ2 expression. Because of this, a HEK293T transfection protocol (using jetPEI reagent) was also developed and optimised (data not shown), as HEK293T cells are known to exhibit high levels of transfection efficiency[258]. The HEK293T cells displayed a transfection efficiency of 80 ± 3%, considerably higher than that of the COS-7 cells

(Figure 3.4). However, because of the low endogenous EGFR expression in the HEK293T cells (Figure 3.3), concerns regarding inadequate receptor PLCγ2 activation were highlighted. Therefore, in addition to PLCγ2, EGFR would also need to be co-transfected.

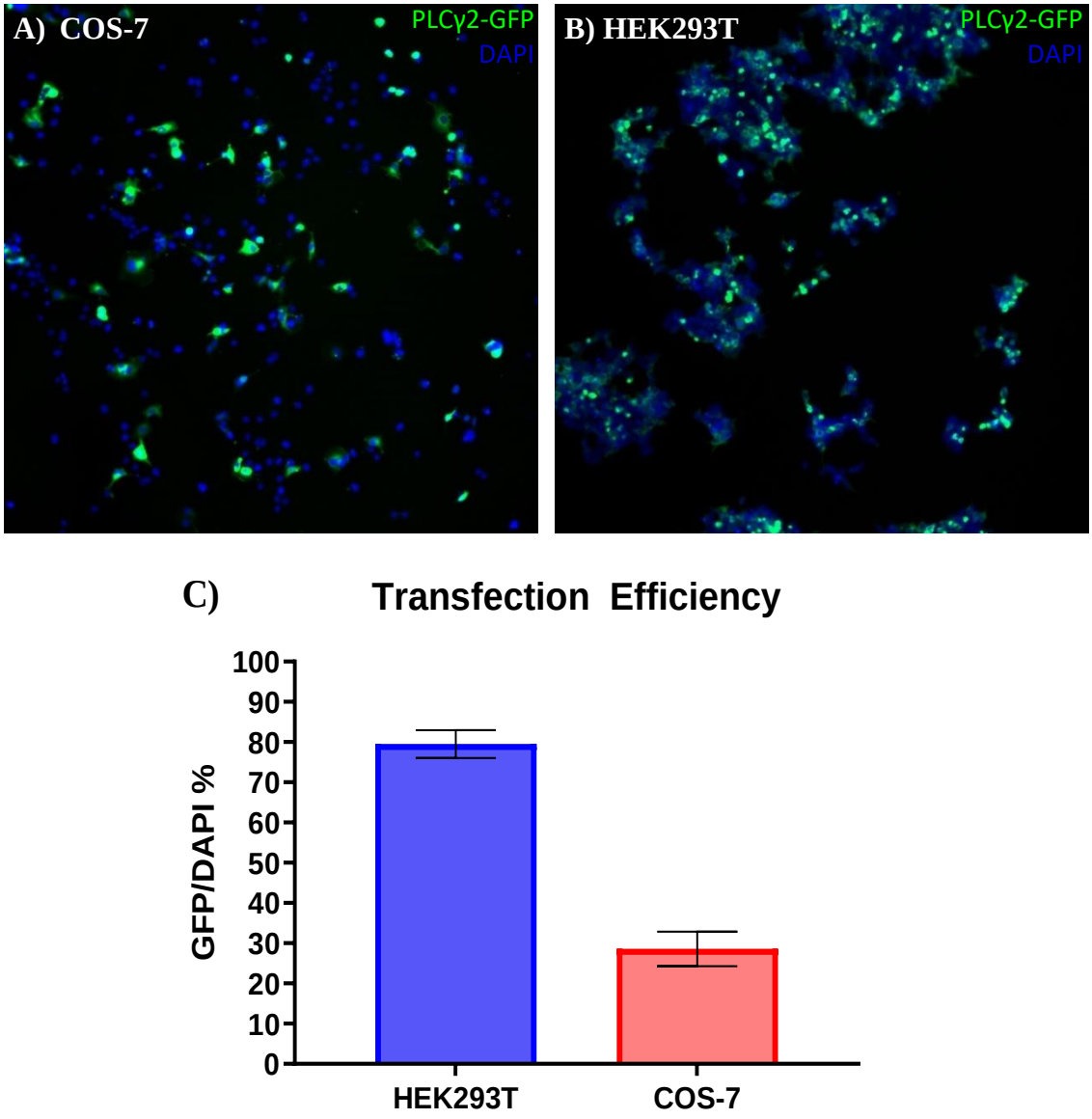

Figure 3.4 Transfection efficiency of WT PLCγ2-GFP in HEK293T cells and COS-7 cells. **A)** Representative images of transfected COS-7 cells with PLCγ2-GFP (green) and DAPI (blue) staining. **B)** Representative images of transfected HEK293T cells with PLCγ2-GFP (green) and DAPI (blue) staining. **C)** Quantitative analysis of the percentage of GFP positive cells/DAPI stained cells. Cells were imaged on the operetta high-content imaging system (Perkin Elmer) and GFP/DAPI quantified on the Harmony software (PerkinElmer). Data represents mean value ± SD. Data is representative of two biological replicates with at least three experimental replicates (n=2).

Due to lack of well validated antibodies to PLCγ2, a range were tested to determine antibody specificity to PLCγ2 to validate an antibody that could be used throughout the duration of the project. Comparing commercially available and collaborator generated (Prof. Todd Golde, University of Florida, USA) PLCγ2 antibodies on WT PLCγ2-GFP transfected HEK293T cells and PLCγ2 KO whole mouse brain lysate through western blotting, revealed some antibodies specific to PLCγ2 (Figure 3.5). The best and readily available antibody was the rabbit anti-PLCγ2 polyclonal antibody from Cell Signaling Technology (CST, Figure 3.5A). This antibody was raised against a synthetic peptide corresponding to residues surrounding the carboxy-terminus of human PLCγ2. The other antibodies were not selected as the Santa Cruz antibody had been discontinued (Figure 3.5D), the collaborator antibody was not readily available (Figure 3.5C) and the ABclonal antibody was not specific to PLCγ2 (Figure 3.5B).

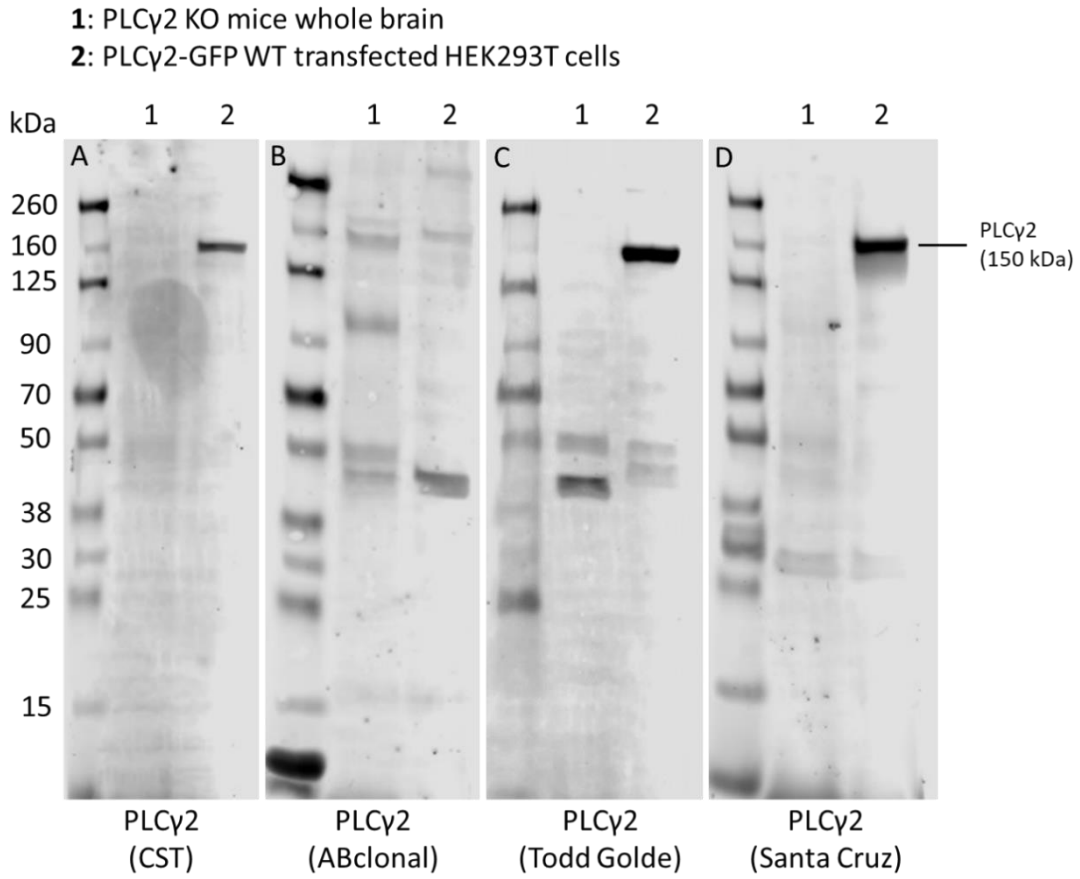

Figure 3.5 Western blot validation of PLCγ2 antibodies. Lysates of PLCγ2 KO mice whole brain (**1**) and PLCγ2-GFP WT transfected HEK293T cell lysate (**2**) were stained for PLCγ2 (150kDa). **A)** anti-PLCγ2 (Cell Signaling Technology, 3872), **B)** anti-PLCγ2 (ABclonal, A2182), **C)** anti-PLCγ2 (kindly provided by Todd Golde) and **D)** anti-

PLCγ2 (Santa Cruz, SC9015). All antibodies used at 1:1000 dilution. The experiment consists of one biological replicate (n=1).

With the validation of a PLCγ2 specific antibody, expression of EGFR and PLCγ2 in transfected HEK293T cells could be assessed. Western blot analysis shows good over-expression of both EGFR and PLCγ2 in the transfected HEK293T cells (Figure 3.6). However, the optimal expression ratio of both constructs can only be determined once activity can be measured.

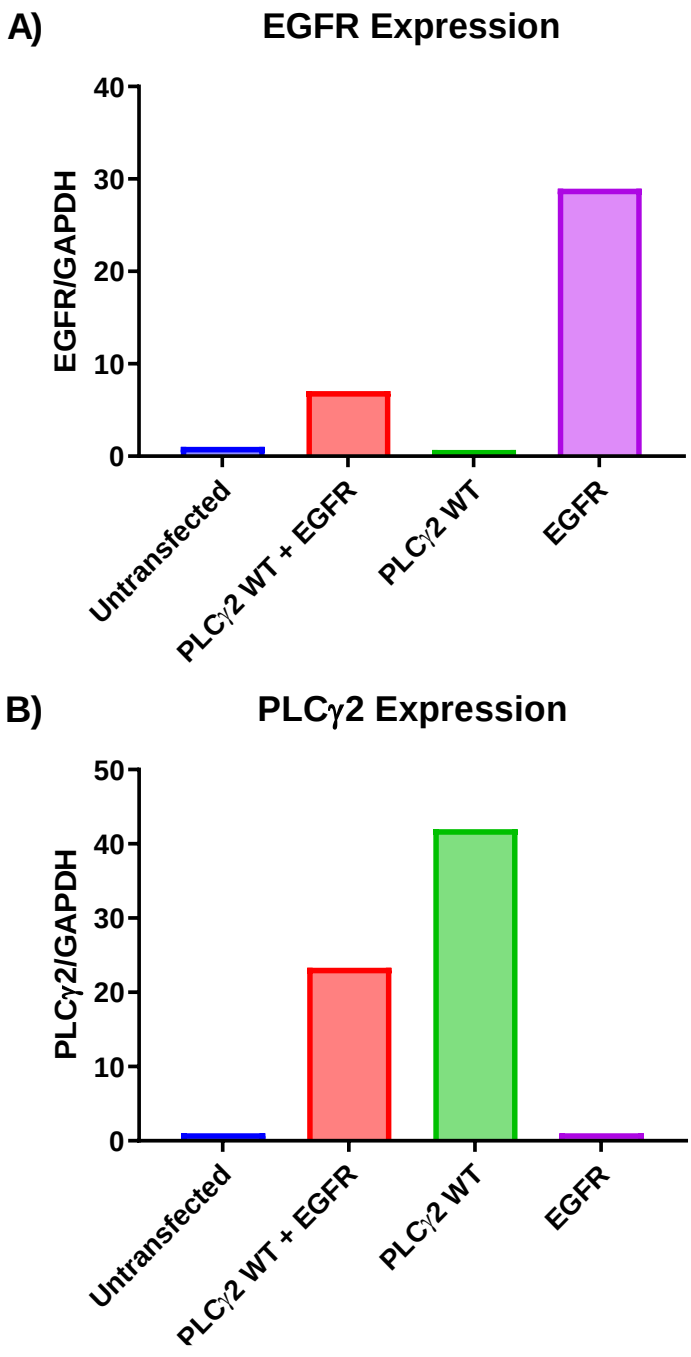

Figure 3.6 Comparison of EGFR and PLCγ2 protein expression in HEK293T cells co-transfected with EGFR and PLCγ2 (1:1 cDNA ratio). **A)** Relative EGFR protein expression normalised to GAPDH expression. **B)** Relative PLCγ2 protein expression normalised to GAPDH expression. Experimental WES Western blot is located in Figure S2. Expression analysis was performed in Compass (Protein Simple). Data is representative of one biological replicate with one experimental replicate (n=1).

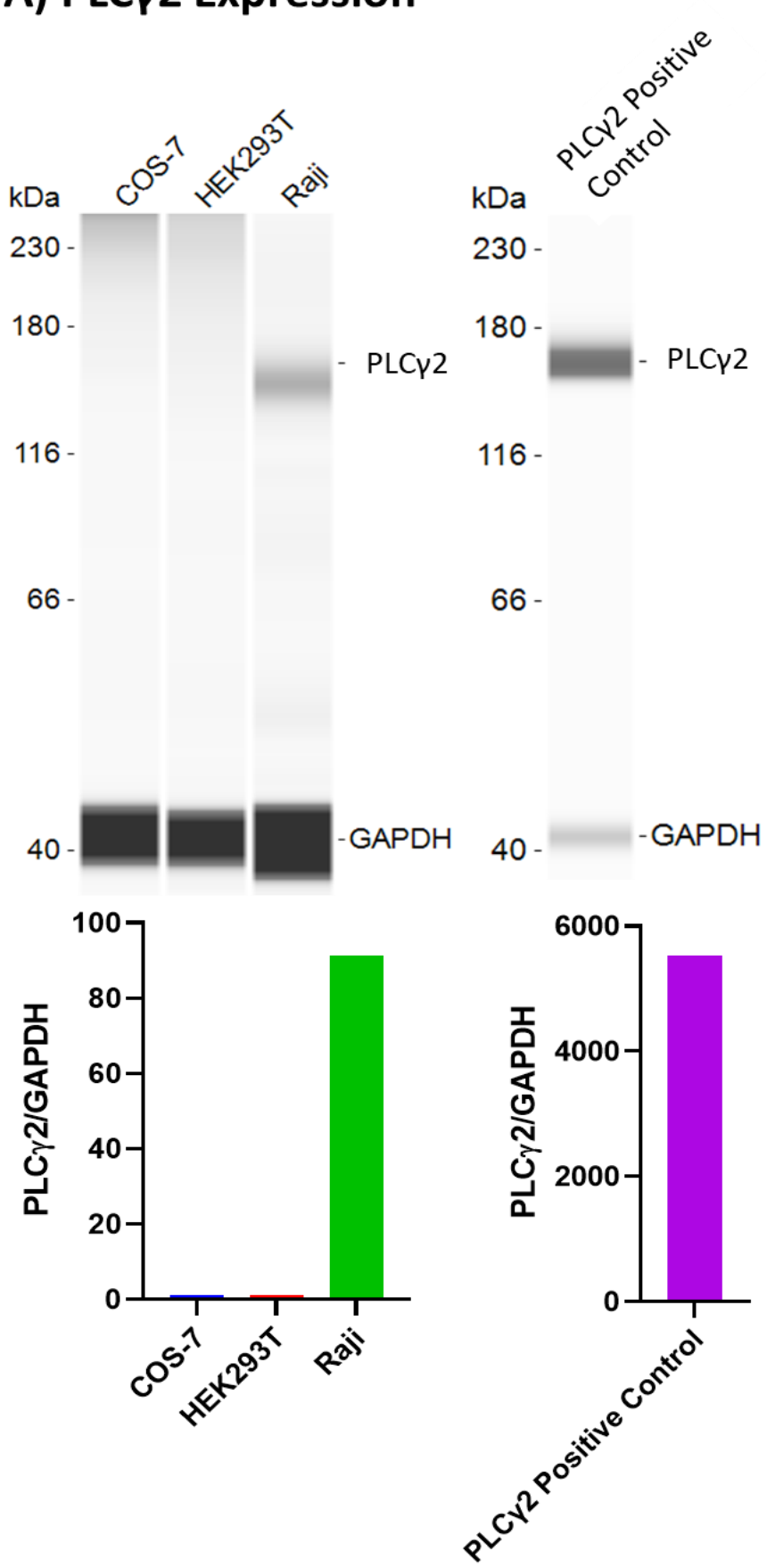
A) PLCγ2 Expression
kDa
COS-7
HEK293T
Raji
230
180
116
66
40
PLCγ2
GAPDH
PLCγ2 Positive Control
PLCγ2/GAPDH
100
80
60
40
20
0
6000
4000
2000

B) PLCγ1 Expression

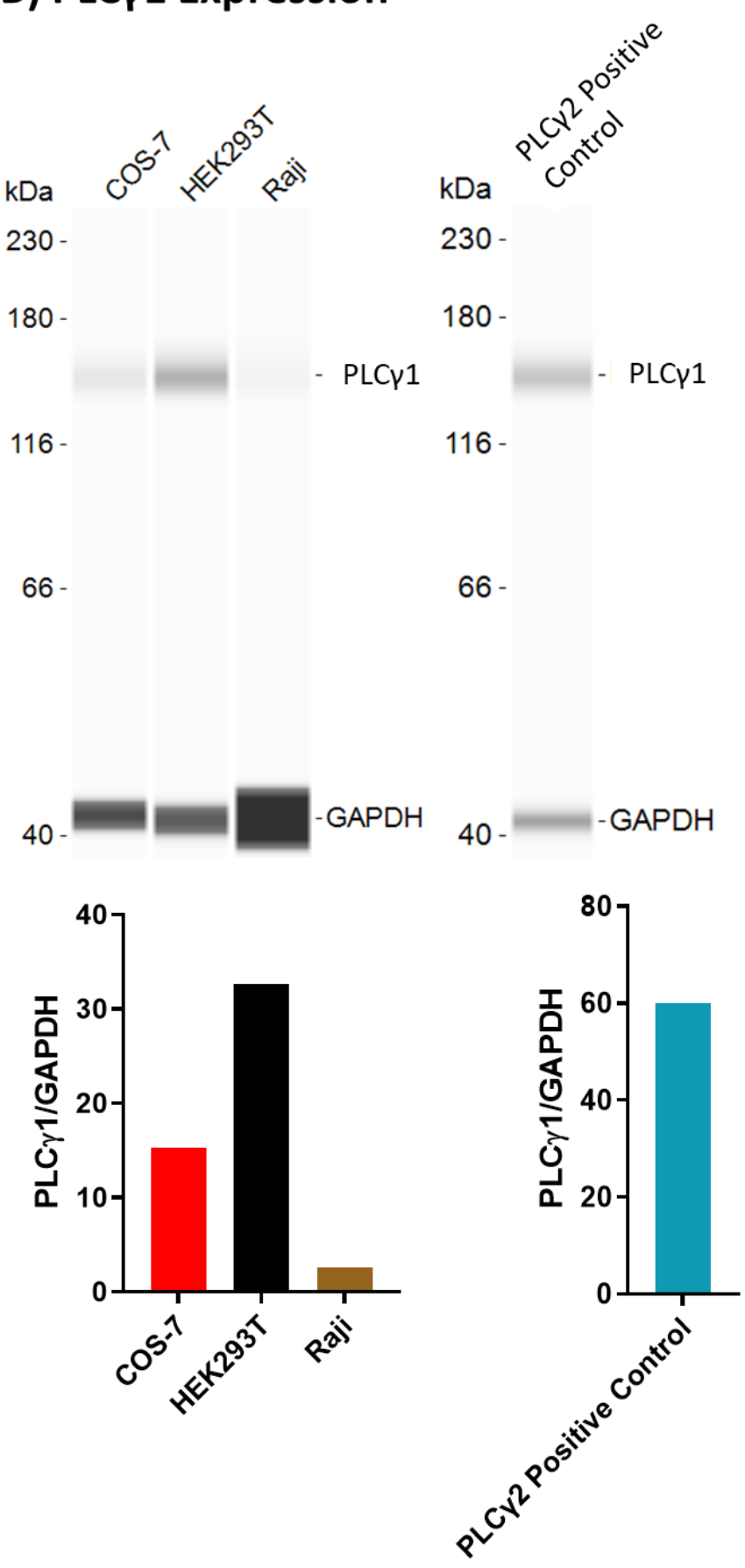

Figure 3.7 Expression of PLCγ2 and PLCγ1 in immortalised cell lines. Lysates from COS-7, HEK293T, Raji and HEK293T cells transfected with WT PLCγ2-GFP (PLCγ2 positive control) were run through the WES Western blotting with expression quantified on the Compass software (Protein Simple). **A)** Staining of PLCγ2 (Cell Signaling Technology, 3872, 1:10) and GAPDH (Cell Signaling Technology, 2118s, 1:300) expression. PLCγ2 expression data was normalised to GAPDH expression. **B)** Staining of PLCγ1 (EMD Millipore, 05-163, 1:75) and GAPDH (Cell Signaling Technology, 4267, 1:300) expression. PLCγ1 expression data was normalised to GAPDH expression. The experiment consists of one biological replicate with one experimental replicate (n=1).

Endogenous PLCγ2 and PLCγ1 expression was also assessed in the HEK293T cells to determine if endogenous PLCγ expression was high enough to influence future experimental readouts. Western blot analysis revealed endogenous HEK293T PLCγ2 expression to be low, whereas PLCγ1 expression was found to be moderate, relative to the COS-7 and Raji cells (Figure 3.7). The moderate expression of PLCγ1 could cause potential issues as EGFR stimulation also activates PLCγ1[147]. Therefore, this should be considered when interpreting experimental data.

3.2.2.2 Assessing the sensitivity of the IP_1 accumulation assay

The HTRF IP_1 accumulation assay has demonstrated to be sensitive enough to determine differences between TREM2 and PLCγ2 KO hiPSC-derived macrophages following TREM2 stimulation[183]. Although an optimised transfection protocol has been established, development and optimisation of an IP_1 accumulation assay needs to be accomplished to be confident that differences in PLCγ2 variant activity can be measured, and that these differences are due to PLCγ2 variant activity alone.

The PLCγ2 S707Y and D993G variants were selected as controls for experimental development as they are well characterised variants of PLCγ2 that increase enzymatic activity with high and moderate impact, respectively, under both basal and stimulated conditions[139,171]. The P522R variant was also selected as it has very low impact on enzymatic activity when activated[139]. Therefore if detected, provides evidence that the assay is sensitive. Finally, an empty plasmid (mock) acts as a negative control to quantify endogenous cellular IP_1 production. Regulatory inactive PLCγ2 variants were not used to validate the assay as they had yet to be generated.

Preliminary experiments showed that EGFR and PLCγ2 co-transfected HEK293T cells produced significantly more IP_1 when stimulated with EGF (Figure 3.8). Differences in IP_1 production under both basal and stimulated conditions were also detected between the well-characterised GOF PLCγ2 variants (D993G and S707Y) and WT (Figure 3.8, statistics not shown). Also, under stimulated conditions the HEK293T endogenous PLC IP_1 production was low relative to the transfected cells, as demonstrated in the Mock condition (Figure 3.8). Furthermore, Figure 3.2 demonstrates that the assay has been optimised for the 24 well plate format as the values of IP_1 generated in PLCγ2 transfected cells lie within the linear portion of the standard curve.

Overall, the data indicates that the HTRF IP_1 accumulation assay allows for the quantification of PLCγ2 variant activity under both basal and stimulated conditions when the variant exhibits a strong phenotype. However, as configured it appears that the assay is not sufficiently sensitive as the mild hypermorphic activity of the P522R variant is not observed under stimulated conditions (Figure 3.8)[139].

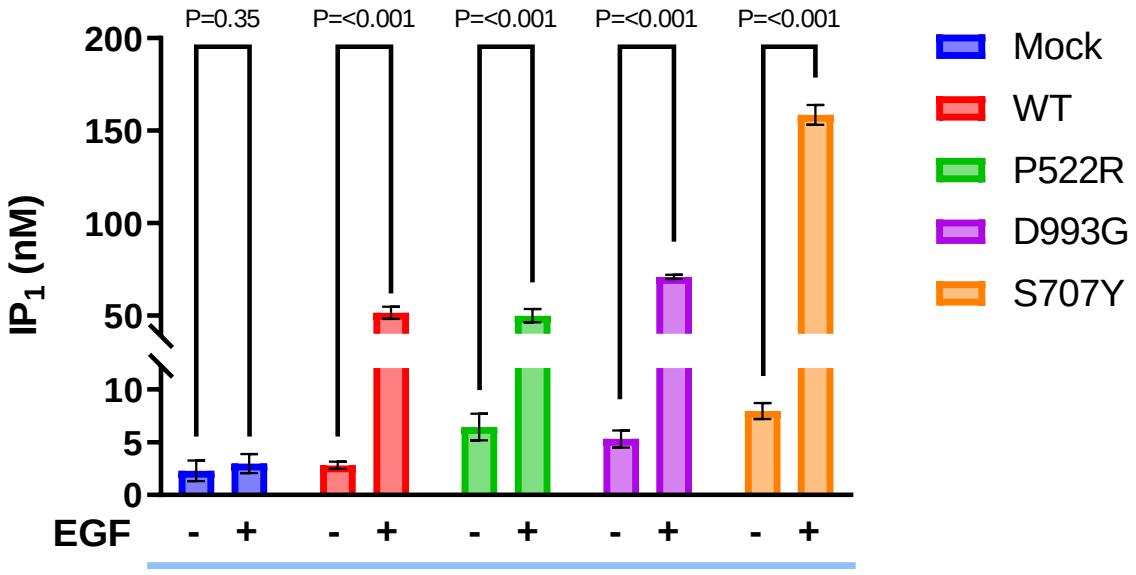

Figure 3.8 Comparison of PLCγ2 variant activity under basal and stimulated conditions. HEK293T cells were co-transfected with EGFR and PLCγ2-GFP constructs (1:1 cDNA ratio). The cells were exposed to ± EGF (150 ng/ul) for 1h. PLC variant activity was assessed using the HTRF IP_1 accumulation assay in accordance with the manufactures instructions. The mock construct consisted of an empty peGFP-N1 plasmid. The IP_1 data has not been normalised to total PLCγ2 protein expression. Data displays the mean value ± SD, and is representative of one biological replicate with

three experimental replicates (Two-tailed unpaired t-test, p-values displayed on the graph, n=1).

3.2.2.3 The effect of different protein tags on PLCγ2 activity

Initial data appeared to suggest that there may be differences in PLCγ2 activity between the different PLCγ2-HIS and PLCγ2-GFP tagged constructs (data not shown). Comparing the IP_1 activity of the HIS and GFP tagged constructs using HEK293T transfected cells revealed that the PLCγ2 HIS-tagged constructs had higher activity than that of their GFP counterparts (Figure 3.9). However, additional studies would be necessary to understand this observation. It should be noted that the plasmid peGFP-C1 does not contain a C1 signalling domain.

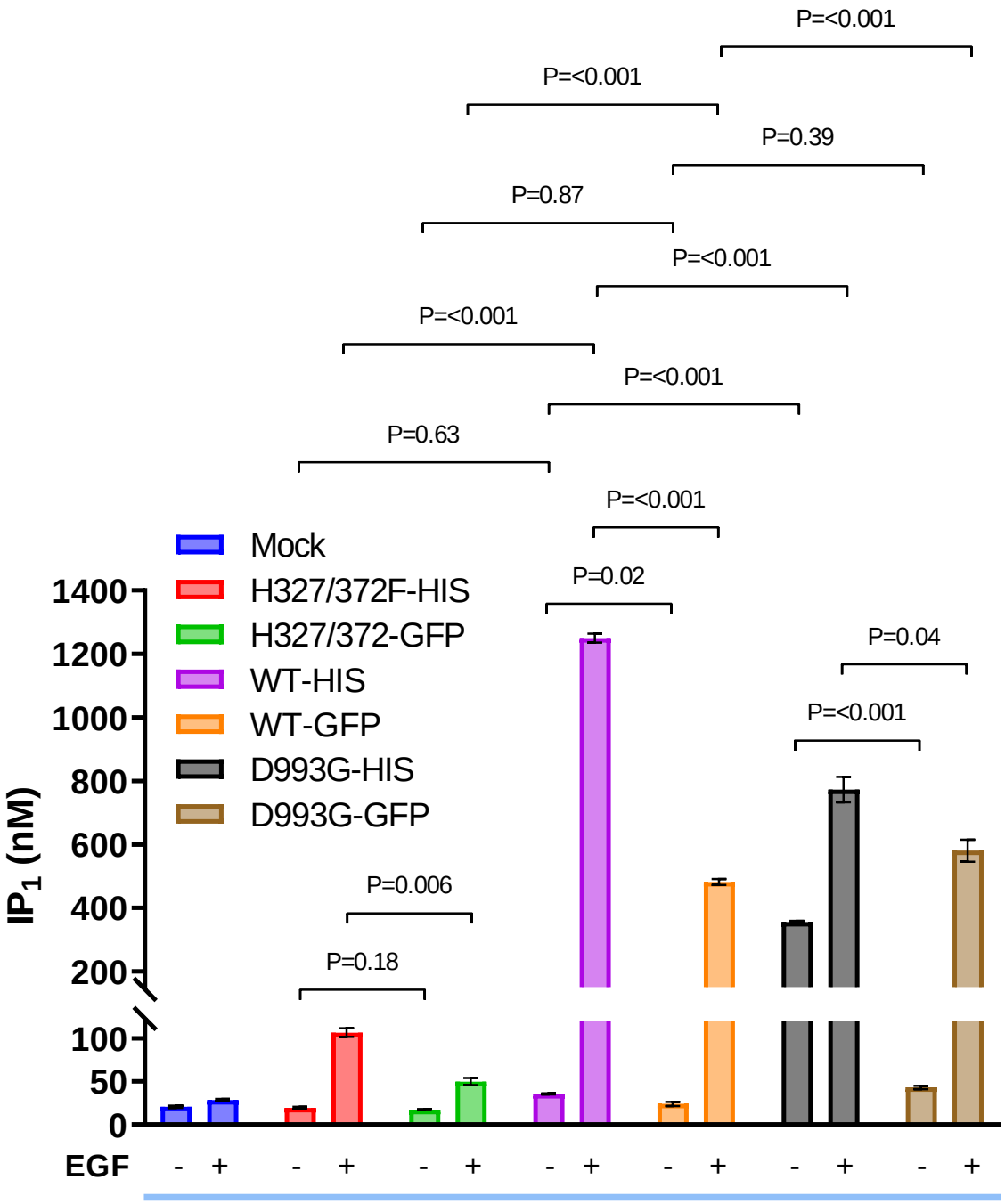

Figure 3.9 Comparison of PLC activity between PLCγ2-HIS and PLCγ2-GFP tagged constructs under basal and stimulated conditions. HEK293T cells were co-transfected with EGFR and PLCγ2-HIS/GFP constructs (1:1 cDNA ratio). The cells were exposed to ± EGF (150 ng/ul) for 1h. PLC variant activity was assessed using the HTRF IP_1 accumulation assay in accordance with the manufactures instructions. The mock construct consisted of an empty peGFP-N1 plasmid. The IP_1 data has not been normalised to total PLCγ2 protein expression. Data displays the mean value ± SD, and

is representative of one biological replicate with three experimental replicates (Two-tailed unpaired t-test, p-values displayed on the graph, n=1).

3.2.2.4 IP_1 assay normalisation

Polyacrylamide gel based western blots have low throughput, require large sample volume, lack sensitivity and reproducibility, and are semi-quantitative. To overcome these issues, the WES (Protein Simple) automates the western blot process and is sensitive enough to generate quantitative data from small sample volume. The protein sample, separation matrix, stacking matrix, antibodies and reagents are manually loaded onto a specially designed plate. The WES begins by aspirating the separation and stacking matrix into each capillary, so that the proteins will stack tightly before they separate, similar to a sodium dodecyl sulfate polyacrylamide gel electrophoresis (SDS-PAGE). Next, the protein lysate is loaded and voltage is applied to enable separation by molecular weight. Once the separation is complete, UV light immobilises the proteins to the capillary wall, followed by primary antibody immunoprobing and subsequent incubation of secondary horseradish peroxidase conjugate and chemiluminescent substrate. The chemiluminescent reaction gives off light that is recorded by a charge-coupled device camera, resulting in quantitative size-based data.

Literature states that the PLCγ2 D993G variant has higher enzymatic activity under both basal and stimulated conditions, compared to PLCγ2 WT[139]. However, experimental data from Figure 3.9 shows that under stimulated conditions, PLCγ2 D993G has reduced IP_1 production compared to PLCγ2 WT. At this point in my research, no method of normalisation existed. In order for future IP_1 data to be comparable so that disease-linked PLCγ2 variants can be characterised, every experimental condition needs to be equivalent in cell density, as well as PLCγ2 and EGFR expression.

This prompted the generation of a normalisation technique for the IP_1 assay. Firstly, PLCγ2-GFP constructs could be used to quantify total PLCγ2 expression though the use of a total GFP measurement. Secondly, experimental IP_1 lysates could be analysed by WES Western blot to normalise to not only PLCγ2 expression, but also total cell number, through the use of a GAPDH loading control. However, given that the HEK293T endogenous PLC IP_1 production is low relative to the overexpression IP_1 data (Mock condition: Figure 3.8 and Figure 3.9), small changes in cell number between experimental conditions should not drastically affect the IP_1 experimental readout.

The IP_1 assay was performed in HEK293T cells co-transfected with PLCγ2-GFP and EGFR constructs with both methods of normalisation implemented. Before experimentation, the total GFP fluorescence in each experimental well was quantified on the PHERAstar FSX (BMG Labtech). After the IP_1 assay had been performed in accordance with the manufacturer's instructions, part of the cell lysate was removed to quantify total PLCγ2 expression by Western blotting on the WES. Both normalisation techniques were implemented on the IP_1 experimental data (Figure 3.10A). The Western blot normalisation technique produced more consistent data and the small hypermorphic change in activity of the PLCγ2 P522R variant was more distinctive under stimulated conditions (Figure 3.10B). Furthermore, the PLCγ2 D993G variant exhibited lower expression (Figure S3), but higher IP_1 activity that that of PLCγ2 WT (Figure 3.10). It was encouraging to see that Western blot normalisation can differentiate between the protein expression of two different PLCγ2 constructs, so that direct comparisons in enzymatic activity can be made. Due to the IP_1 variability experienced from GFP normalisation (Figure 3.10C), as well as the fact that the presence of the GFP tag dampens PLCγ2 enzymatic activity (Figure 3.9), both PLCγ2-HIS constructs and Western blot normalisation would be implemented for future HTRF IP_1 experimentation.

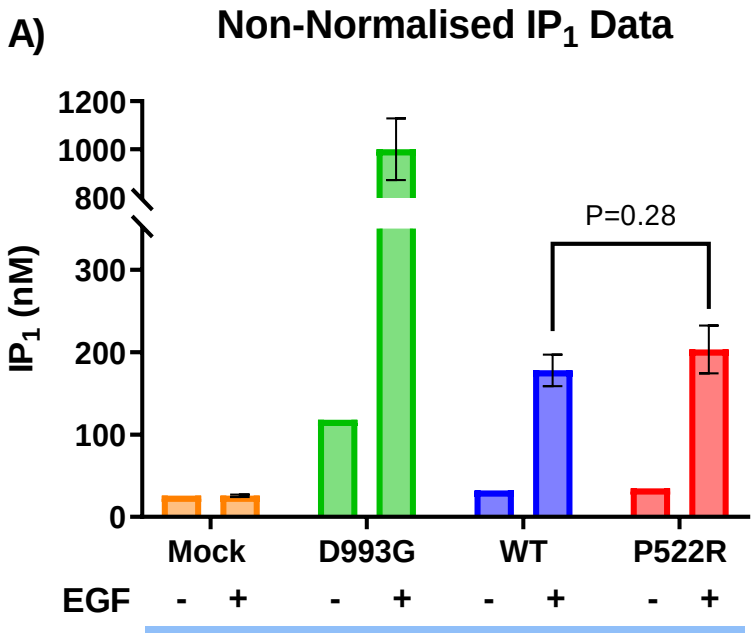

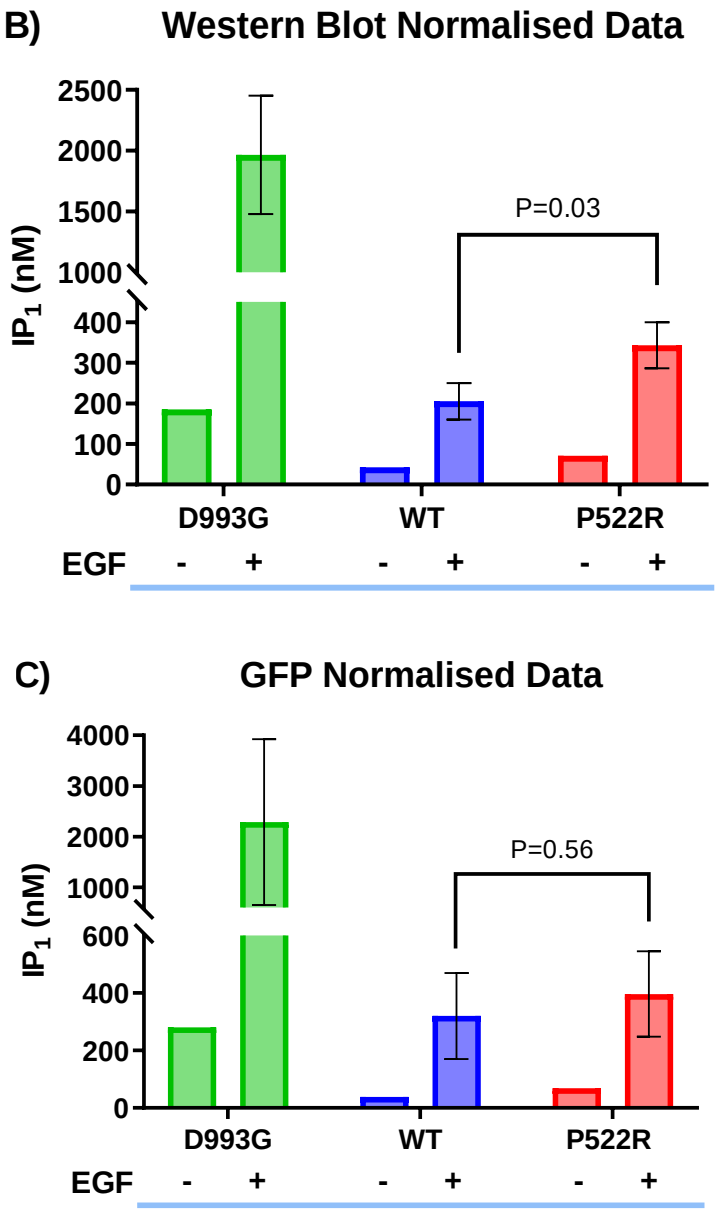

Figure 3.10 Comparison of Western blot and GFP normalisation techniques for the HTRF IP_1 assay. HEK293T cells were co-transfected with EGFR and PLCγ2-GFP constructs (1:1 cDNA ratio). The cells were exposed to ± EGF (150 ng/ul) for 1h. PLC variant activity was assessed using the IP_1 accumulation assay. **A)** Non-normalised experimental IP_1 data. **B)** Western blot normalised IP_1 data. **C)** GFP normalised IP_1 data. The mock construct consisted of an empty peGFP-N1 plasmid. Data represents mean value ± SD, and is representative of one biological replicate with at least three experimental replicates for the stimulated conditions, but only one experimental replicate for the unstimulated condition (Two-tailed unpaired t-test, p-values displayed on the graph, n=1).

3.2.2.5 The impact of relative expression of EGFR and PLCγ2 relationship on IP_1 production

With an experimental protocol established to measure PLCγ2 activity, it was imperative to understand the influence of the EGFR:PLCγ2 transfected cDNA ratio on IP_1 production, as all previous experiments had been performed using a EGFR:PLCγ2 ratio of 1:1. HEK293T cells were co-transfected with EGFR and PLCγ2-HIS constructs, with the ratio of DNA titrated (total amount of DNA fixed). Cells were exposed to ± EGF (150 ng/ul) for 1.5h to allow for more IP_1 accumulation. The experimental results show a decrease in IP_1 production when the cDNA was titrated in favour of PLCγ2 (Figure 3.11). A 1:3 (EGFR:PLCγ2) ratio appears to be optimal for quantifying the activity of mild GOF PLCγ2 variants, as differences in IP_1 production were observed for the PLCγ2 P522R variant under stimulated conditions (Figure 3.11), with comparable expression to PLCγ2 WT (Figure S4).

Due to the high IP_1 values experienced from the 'EGFR Only' and the 1:1 experimental conditions, it seems evident that high EGFR expression can cause sizable IP_1 production (Figure 3.11). It is possible that with enough EGFR expression, endogenous PLC enzymes can significantly contribute to IP_1 generation. As small changes in experimental EGFR expression could falsely be interpreted as differences in PLCγ2 activity, in addition to PLCγ2 expression, attempts were made to normalise the experimental data to EGFR expression (Figure S4). Unfortunately, western blotting for EGFR was not possible post-experimentation as the resulting bands were weak at the low EGFR ratios (Figure S4).

In order to mitigate the concern of EGFR mediated IP_1 production through endogenous PLC enzymes, a ratio of 1:3 (EGFR:PLCγ2) would be used for future PLCγ2 variant characterisation experiments. Having the transfection cDNA favoured to PLCγ2 not only limits the effect of EGFR mediated IP_1 production, but also results in more PLCγ2 mediated IP_1 production. The data from Figure 3.11 indicates that this ratio is optimal for maximising the IP_1 assay signal window as the mild hypermorphic PLCγ2 P522R variant was detectable under stimulation.

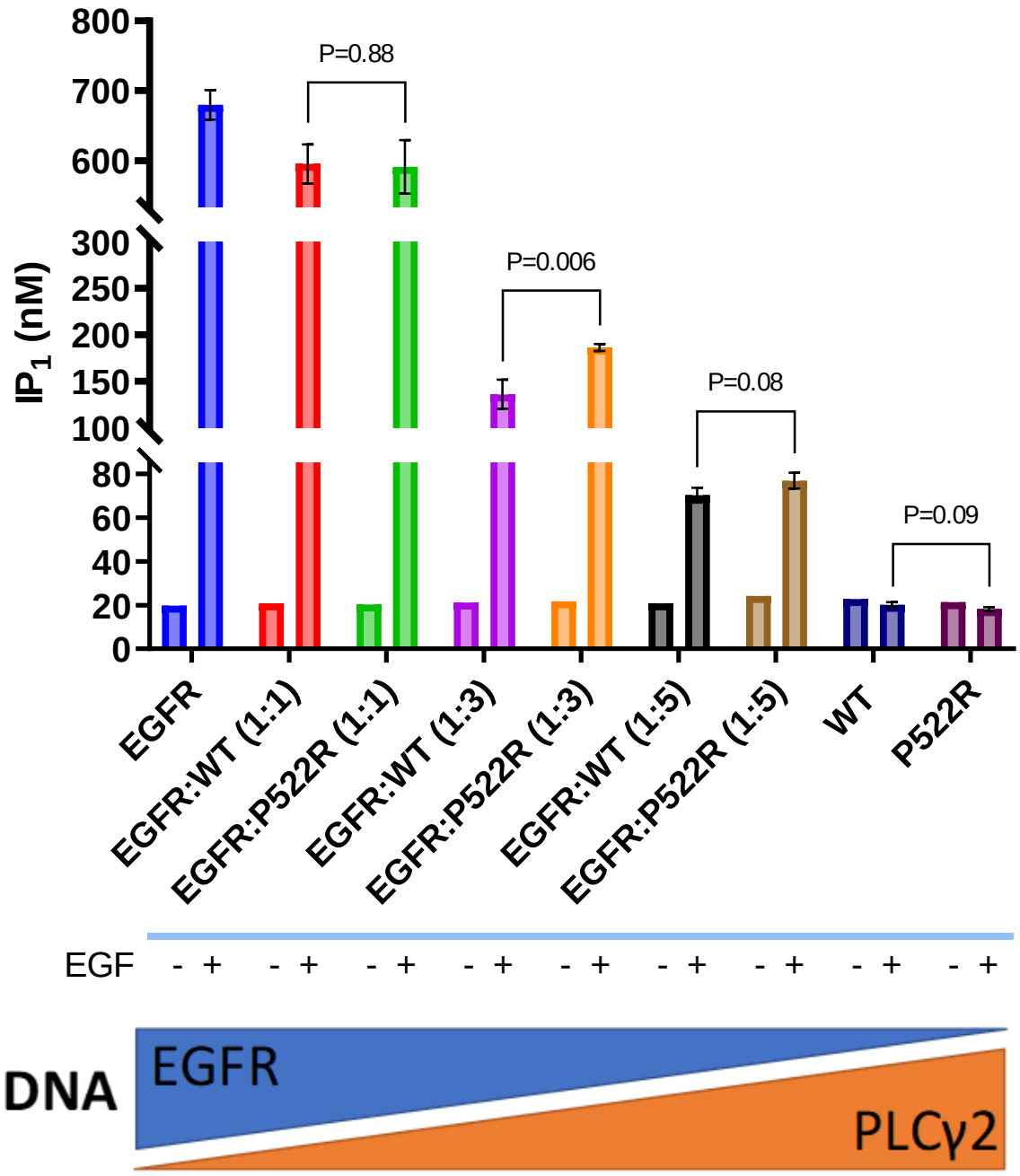

Figure 3.11 The relationship EGFR and PLCγ2 have on IP_1 production. HEK293T cells were co-transfected with EGFR and PLCγ2-HIS constructs at different EGFR:PLCγ2 DNA ratios (total DNA fixed) to compare the IP_1 activity of PLCγ2 WT and P522R. The cells were exposed to ± EGF (150 ng/ul) for 1h. PLC variant activity was assessed using the HTRF IP_1 assay. IP_1 data has not been normalised to either total PLCγ2 and/or EGFR protein expression. Data represents mean value ± SD, and is representative of one biological replicate with at least three experimental replicates for the stimulated conditions, but only one experimental replicate for the unstimulated condition (Two-tailed unpaired t-test, p-values displayed on the graph, n=1). PLCγ2 and EGFR protein expression complements these observations (Figure S4).

3.3 Discussion

The COS-7 cells would have been the ideal cell model for experimentation due to the high endogenous EGFR expression and low endogenous PLCγ1 and PLCγ2 expression, relative to HEK293T cells (Figure 3.3 and Figure 3.7). Although a good transfection efficiency was achieved for the HEK293T cells (Figure 3.4), the dual transfection of both EGFR and PLCγ2 results in two experimental variables, that both influence IP_1 production, but could not both be normalised. Furthermore, as EGFR is endogenously expressed at a low level within HEK293T cells (Figure 3.3, Figure 3.6 and Figure S4) this could have implications for levels of co-transfection achieved simultaneously with PLCγ2 and EGFR. Perhaps the generation of a EGFR HEK293T stable cell line could have been used to keep EGFR expression consistent, removing this experimental variable. However as previously mentioned, IP_1 production at a 1:3 ratio (EGFR:PLCγ2) would predominantly be generated from the transfected PLCγ2 construct.

Although PLCy2 can be directly activated by tyrosine phosphorylation, PLCy2 can also be activated through other mechanisms e.g. through Rac2[150,174,175]. Therefore, perhaps PLCy2 variants may influence different modes of activation resulting in their clinical phenotype. As a result, although EGF/EGFR activation provides an initial assessment of PLCy2 variant activity, other activation methods should also be explored.

GFP-tagged proteins are a good method of visualising/quantifying protein expression, as well as observing the movement of proteins. However, the GFP motif (located on the C-terminal) is relatively large (26.9 kDa) and therefore has the potential to influence various factors including protein expression, protein function, as well as the ability of PLCγ2 to bind to the membrane to carry out its catalytic function. However, additional studies would be necessary to understand this observation.

Only a 1 hour time point of was considered for experimentation as that is what has been previously reported in literature[139]. However, a time course experiment should have been implemented to potentially extended the assay signal window resulting in better characterisation of the PLCγ2 disease-linked variants.

Furthermore, although JETpie transfection can be cytotoxic towards cells, this experimental design resulted in minimal transfection mediated cell death.

3.4 Conclusion

The development and optimisation of an artificial HTRF IP_1 accumulation assay to characterise PLCγ2 variant enzymatic activity has been established. During the process, it was determined that EGF stimulated HEK293T cells co-transfected with EGFR and PLCγ2 constructs elicit a robust IP_1 response (Figure 3.8), PLCγ2-GFP-tagged constructs could not be used as they diminish IP_1 production compared to their HIS-tagged counterparts (Figure 3.9), a 1:3 (EGFR:PLCγ2) ratio of DNA is crucial for the quantification of mild GOF PLCγ2 variants e.g. P522R (Figure 3.11) and that an experimental PLCγ2 total protein normalisation technique, through the use of a PLCγ2 selective antibody from CST (Figure 3.5), is essential for the correct interpretation of PLCγ2 variant enzymatic activity (Figure 3.10).

Chapter 4 - Comparative assessment of PLC activity for PLCγ2 disease-linked variants

4.1 Introduction

The HRTF IP_1 assay allows for each PLCγ2 variant to be functionally compared and ranked accordingly. As mentioned previously in 1.6, literature has already identified and characterised various PLCγ2 engineered and disease-linked variants (Table 1.2). If the PLCγ2 variants exhibit the same phenotype within the HEK293T HTRF IP_1 assay, as stated in literature, it will not only validate the assay but also provide confidence that the IP_1 assay is sensitive and robust enough to characterise rare and novel disease-liked variants of PLCγ2.

As previously mentioned in 1.6.2, an IBD GWAS identified novel PLCγ2 non-synonymous SNPs, R268W and H244R[138]. However, to what effect each variant has on the properties of PLCγ2, if any, is yet to be fully characterised. Furthermore, collaborators Juan I. Arostegui (August Pi i Sunyer Biomedical Research Institute, Barcelona, Spain) and João Farela Neves (Primary Immunodeficiencies Unit, Hospital Dona Estefânia, Lisbon, Portugal) identified patients experiencing APLAID-like symptoms. Genotyping of these patients resulted in the identification of the PLCγ2 A708P, Δ845-848 and V1103I variants (Figure 1.6), with the latter two being novel. Additionally, the PLCγ2 M1141K variant within the C2 domain has been demonstrated to cause an influx of external calcium in B cells when stimulated with IgM. However, to what effect PLCγ2 M1141K has on enzymatic activity has yet to be determined. It will be important to characterise each variants effect on PLCγ2 enzymatic activity to understand what impact each variant may have on disease initiation or progression.

4.2 Results

4.2.1 PLC activity of characterised PLCγ2 variants

Initial experiments using the 1:3 (EGFR:PLCγ2) ratio to characterise PLCγ2 variants resulted in considerable variability amongst the biological replicates (example shown in Figure S5) due to the protein expression between PLCγ2 WT and PLCγ2 variants being noncomparable. The PLCγ2 expression normalisation technique failed to mitigate this issue, as the assay was heavily reliant on WES Western blotting. As in Figure 3.11, the previous experimental design involved transfecting HEK293T cells with 100ng of EGFR and 300ng of PLCγ2 DNA (400ng total DNA) at a 1:3 (EGFR:PLCγ2) ratio. In order to combat the normalisation issue, EGFR DNA was fixed at 100ng and PLCγ2

DNA titrated so that the experimental IP_1 production would be PLCγ2 dependent. Therefore, IP_1 values that have comparable PLCγ2 expression would be matched, instead of normalised to expression. Protein matching would always be performed by comparing the two most similar protein band areas (as quantified by WES) between the PLCγ2 variant and PLCγ2 WT, regardless of where expression was similar from the cDNA titration. As a result, the experimental IP_1 quantification would be true reflection of PLCγ2 variant activity as well as be non-subjective.

Therefore, HEK293T cells were co-transfected with EGFR (100ng, fixed), as well as PLCγ2 (20-300ng, titrated) and/or a eGFP-C1 construct (0-300ng, titrated) to keep total cDNA fixed at 400ng. Cells were subjected to ± EGF stimulation for 1.5h before the HTRF IP_1 assay was performed in accordance with manufactures instructions. Cell lysate from each well was run through the WES Western blotting to quantify PLCγ2 expression for each experimental condition. As some PLCγ2 variants have differences in expression relative to WT, IP_1 values that had comparable PLCγ2 expression were matched, with basal and stimulated conditions matched separately. These matched datasets allowed for the direct comparison of PLCγ2 WT and its variants in both basal and stimulated environments. Finally, the fold difference in IP_1 production for each variant under basal and stimulated conditions would also be calculated.

4.2.1.1 PLCγ2 regulatory inactive variants: H327/372F and 4F+F847Q

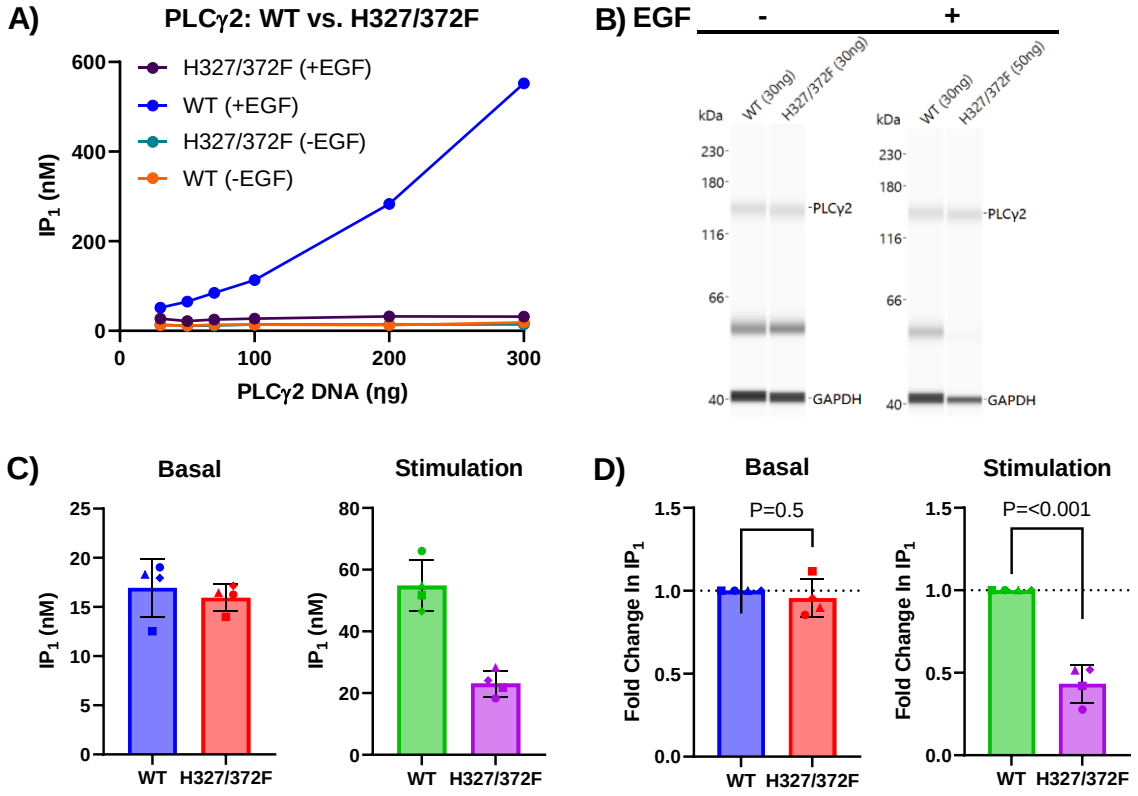

Figure 4.1 PLCγ2 H327/372F variant has decreased PLC activity. **A)** Representative data comparing PLC activity of PLCγ2 WT and PLCγ2 H327/372F (titrated DNA) in transfected HEK293T cells under basal (-EGF) and stimulated (+EGF, 150 ng/ul for 1.5h) conditions. PLC activity was assessed using the HTRF IP_1 assay. The data is representative from one biological replicate. **B)** PLCγ2 (150kDa) expression for each IP_1 datapoint (basal (-EGF) and stimulated (+EGF) conditions) was measured by WES Western blotting. PLCγ2 expression (arbitrary units) was: WT/-EGF = 360645, WT/+EGF = 362190, H327/372F/-EGF = 353281 and H327/372F/+EGF = 326073. The data is representative from one biological replicate. PLCγ2 protein expression levels were comparable. **C)** IP_1 values that had comparable PLCγ2 expression were matched. Basal and stimulated conditions were matched separately. The graph represents the matched IP_1 data from all biological replicates. Each graphical symbol shape (square, triangle, circle and diamond) represents each set of biological replicates (n=4). Data represents mean value ± SD. **D)** The PLCγ2 H327/372F IP_1 values were normalised to the PLCγ2 WT IP_1 values to represent the fold-change in PLCγ2 H327/372F IP_1 production under basal (-EGF) and stimulated (+EGF) conditions relative to PLCγ2 WT. Each graphical symbol shape (square, triangle, circle and diamond) represents the

fold change in IP_1 for each set of biological replicates (Two-tailed unpaired t-test, p-values displayed on the graph, n=4). Data represents mean value ± SD.

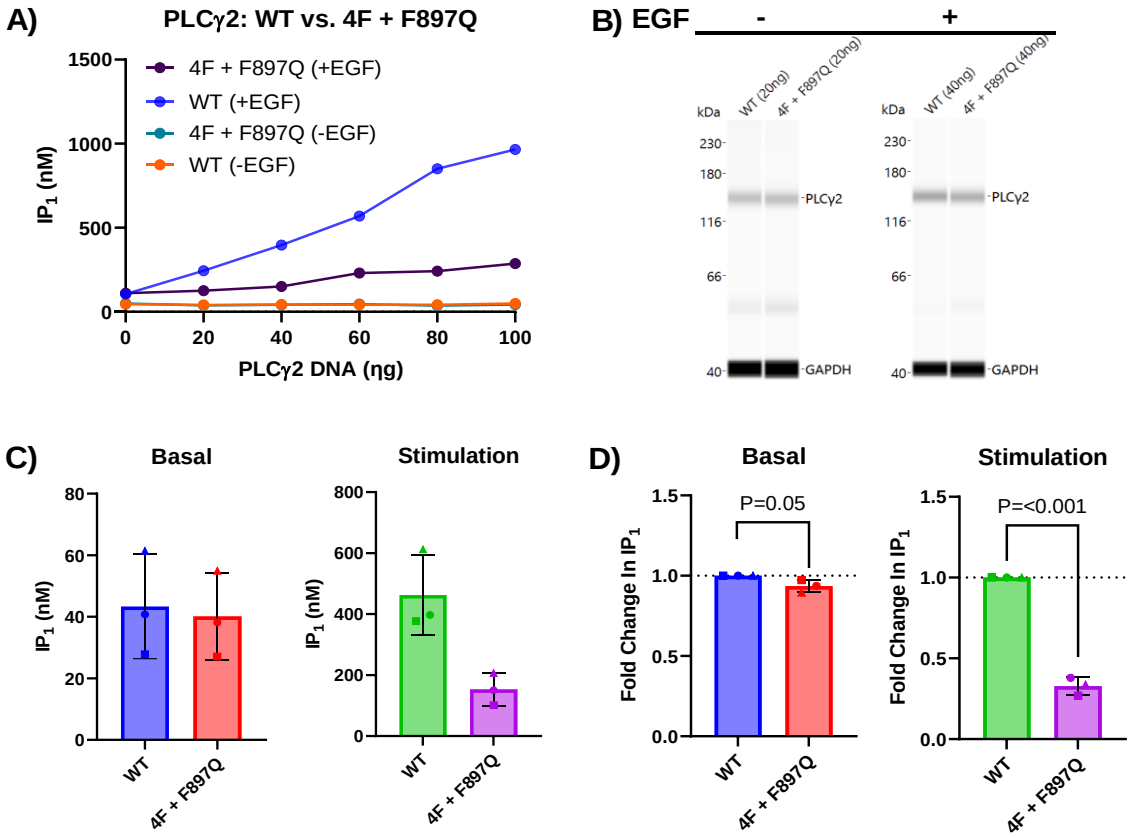

Figure 4.2 PLCγ2 '4F + F897Q' variant has decreased PLC activity. **A)** Representative data comparing PLC activity of PLCγ2 WT and PLCγ2 '4F + F897Q' (titrated DNA) in transfected HEK293T cells under basal (-EGF) and stimulated (+EGF, 150 ng/ul for 1.5h) conditions. PLC activity was assessed using the HTRF IP_1 assay. The data is representative from one biological replicate. **B)** PLCγ2 (150kDa) expression for each IP_1 datapoint (basal (-EGF) and stimulated (+EGF) conditions) was measured by WES Western blotting. PLCγ2 expression (arbitrary units) was: WT/-EGF = 434246, WT/+EGF = 625254, '4F + F897Q'/-EGF = 427544 and '4F + F897Q'/+EGF = 626594. The data is representative from one biological replicate. PLCγ2 protein expression levels were comparable. **C)** IP_1 values that had comparable PLCγ2 expression were matched. Basal and stimulated conditions were matched separately. The graph represents the matched IP_1 data from all biological replicates. Each graphical symbol shape (square, triangle and circle) represents each set of biological replicates (n=3). Data represents mean value ± SD. **D)** The PLCγ2 '4F + F897Q' IP_1 values were normalised to the PLCγ2 WT IP_1 values to represent the fold-change in PLCγ2 '4F + F897Q' IP_1 production under basal (-EGF) and stimulated (+EGF) conditions relative to

PLCγ2 WT. Each graphical symbol shape (square, triangle and circle) represents the fold change in IP_1 for each set of biological replicates (Two-tailed unpaired t-test, p-values displayed on the graph, n=3). Data represents mean value ± SD.

4.2.1.2 PLCγ2 hypermorphic variants: D993G, S707Y and P522R

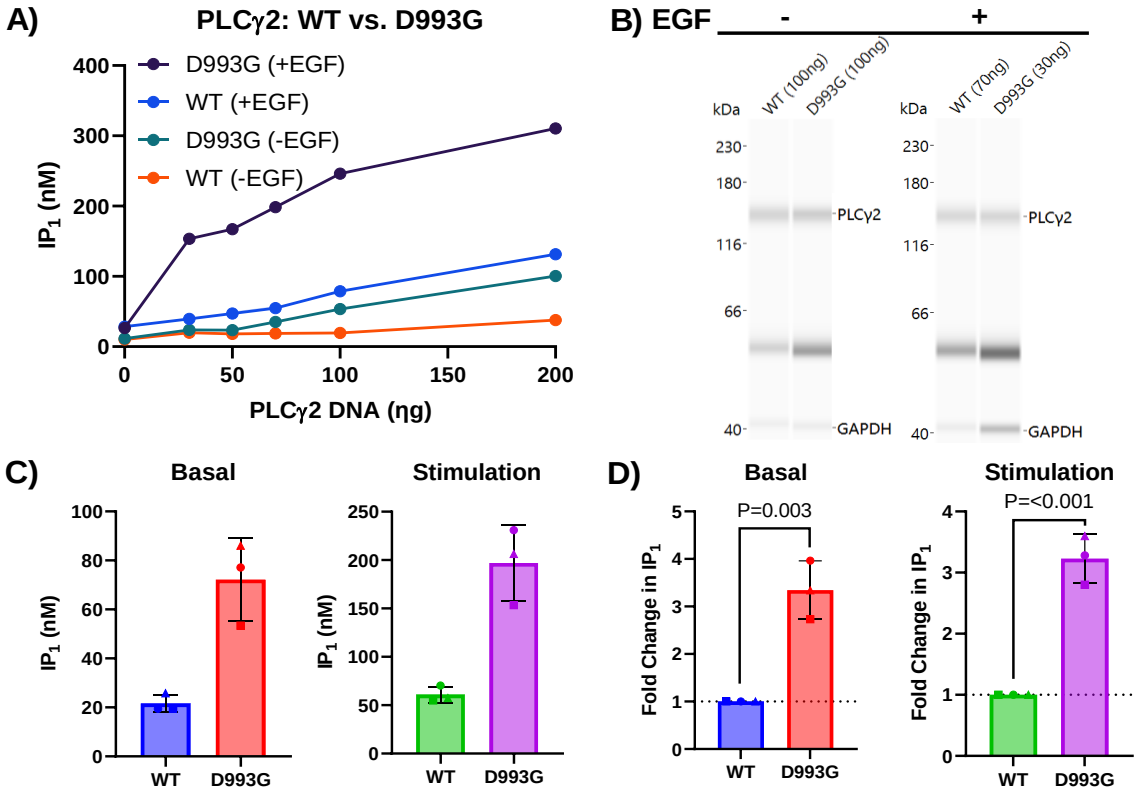

Figure 4.3 PLCγ2 D993G variant has increased PLC activity. **A)** Representative data comparing PLC activity of PLCγ2 WT and PLCγ2 D993G (titrated DNA) in transfected HEK293T cells under basal (-EGF) and stimulated (+EGF, 150 ng/ul for 1.5h) conditions. PLC activity was assessed using the HTRF IP_1 assay. The data is representative from one biological replicate. **B)** PLCγ2 (150kDa) expression for each IP_1 datapoint (basal (-EGF) and stimulated (+EGF) conditions) was measured by WES Western blotting. PLCγ2 expression (arbitrary units) was: WT/-EGF = 447928, WT/+EGF = 270557, D993G/-EGF = 477621 and D993G/+EGF = 278755. The data is representative from one biological replicate. PLCγ2 protein expression levels were comparable. **C)** IP_1 values that had comparable PLCγ2 expression were matched. Basal and stimulated conditions were matched separately. The graph represents the matched IP_1 data from all biological replicates. Each graphical symbol shape (square, triangle and circle) represents each set of biological replicates (n=3). Data represents mean value ± SD. **D)** The PLCγ2 D993G IP_1 values were normalised to the PLCγ2 WT IP_1 values to represent the fold-change in PLCγ2 D993G IP_1 production under basal (-EGF)

and stimulated (+EGF) conditions relative to PLCγ2 WT. Each graphical symbol shape (square, triangle and circle) represents the fold change in IP_1 for each set of biological replicates (Two-tailed unpaired t-test, p-values displayed on the graph, n=3). Data represents mean value ± SD.

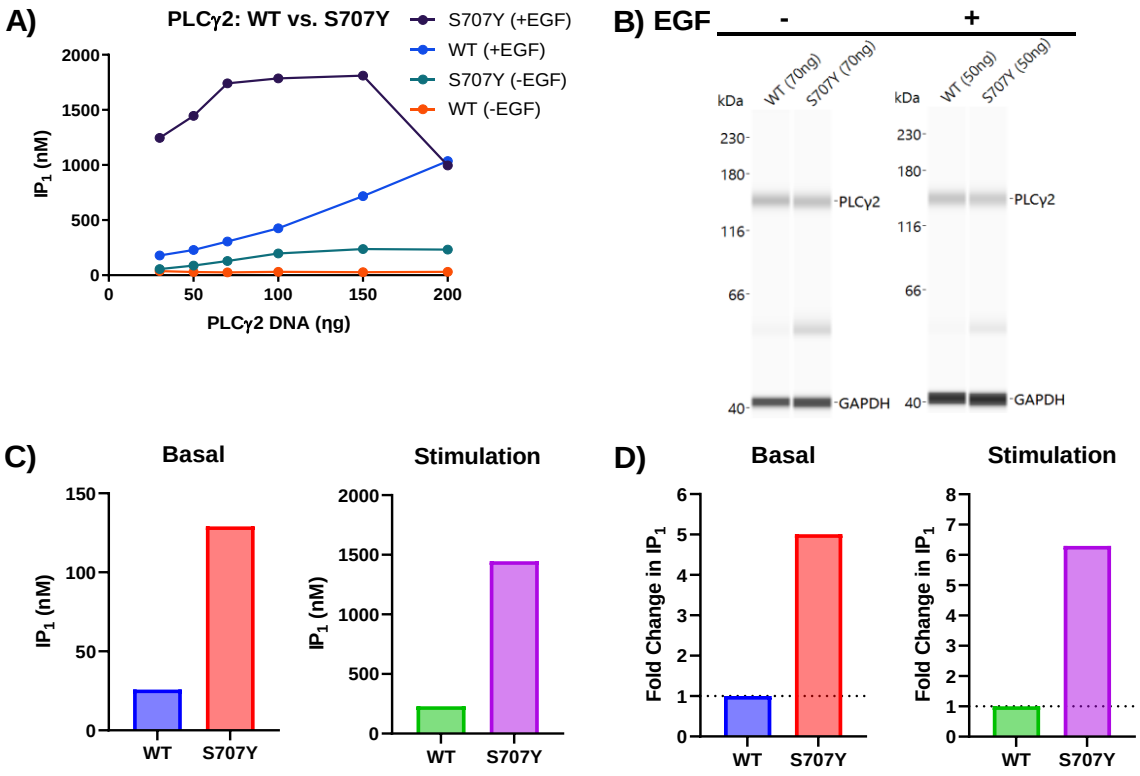

Figure 4.4 PLCγ2 S707Y variant has increased PLC activity. **A)** Representative data comparing PLC activity of PLCγ2 WT and PLCγ2 S707Y (titrated DNA) in transfected HEK293T cells under basal (-EGF) and stimulated (+EGF, 150 ng/ul for 1.5h) conditions. PLC activity was assessed using the HTRF IP_1 assay. The data is representative from one biological replicate. **B)** PLCγ2 (150kDa) expression for each IP_1 datapoint (basal (-EGF) and stimulated (+EGF) conditions) was measured by WES Western blotting. PLCγ2 expression (arbitrary units) was: WT/-EGF = 622294, WT/+EGF = 884058, S707Y/-EGF = 604343 and S707Y/+EGF = 851419. The data is representative from one biological replicate. PLCγ2 protein expression levels were comparable. **C)** IP_1 values that had comparable PLCγ2 expression were matched. Basal and stimulated conditions were matched separately. The graph represents the matched IP_1 data from one experiment (n=1). Data represents mean value. **D)** The PLCγ2 S707Y IP_1 values were normalised to the PLCγ2 WT IP_1 values to represent the fold-change in PLCγ2 S707Y IP_1 production under basal (-EGF) and stimulated (+EGF) conditions

relative to PLCγ2 WT. The data is representative of one experiment. Data represents mean value.

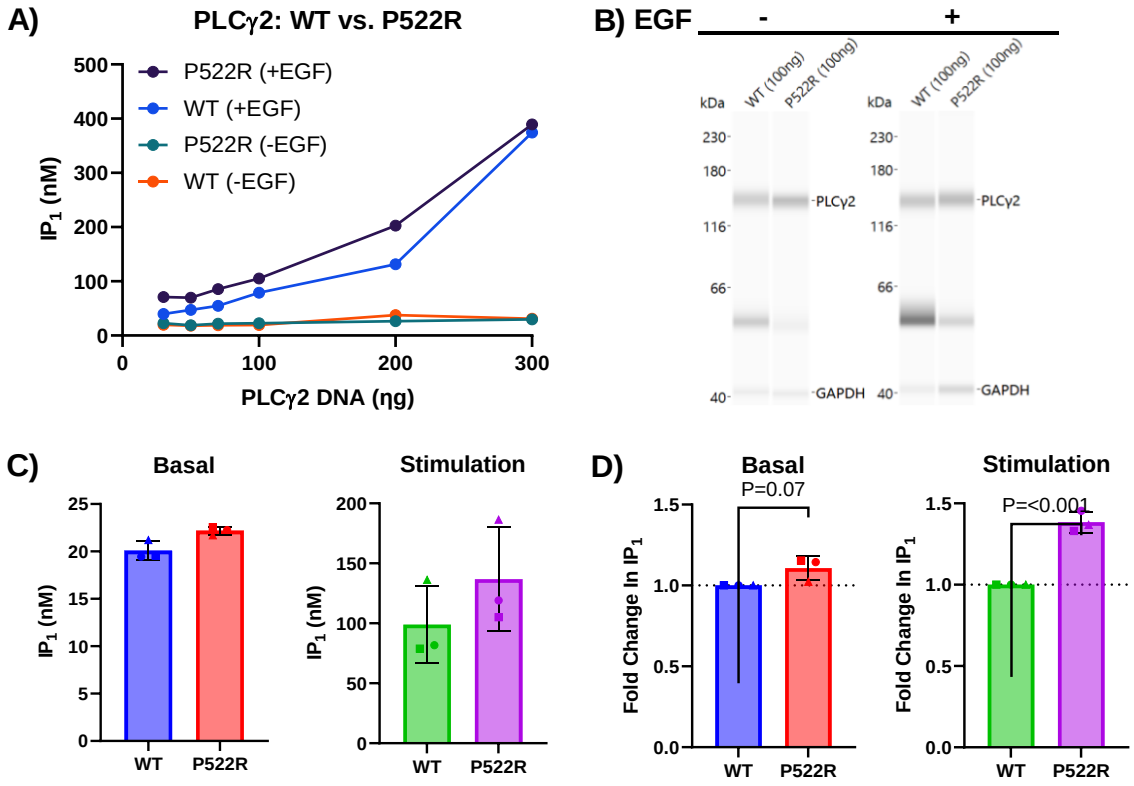

Figure 4.5 PLCγ2 P522R variant has increased PLC activity. **A)** Representative data comparing PLC activity of PLCγ2 WT and PLCγ2 P522R (titrated DNA) in transfected HEK293T cells under basal (-EGF) and stimulated (+EGF, 150 ng/ul for 1.5h) conditions. PLC activity was assessed using the HTRF IP_1 assay. The data is representative from one biological replicate. **B)** PLCγ2 (150kDa) expression for each IP_1 datapoint (basal (-EGF) and stimulated (+EGF) conditions) was measured by WES Western blotting. PLCγ2 expression (arbitrary units) was: WT/-EGF = 447928, WT/+EGF = 460299, P522R/-EGF = 446215 and P522R/+EGF = 477993. The data is representative from one biological replicate. PLCγ2 protein expression levels were comparable. **C)** IP_1 values that had comparable PLCγ2 expression were matched. Basal and stimulated conditions were matched separately. The graph represents the matched IP_1 data from all biological replicates. Each graphical symbol shape (square, triangle and circle) represents each set of biological replicates (n=3). Data represents mean value ± SD. **D)** The PLCγ2 P522R IP_1 values were normalised to the PLCγ2 WT IP_1 values to represent the fold-change in PLCγ2 P522R IP_1 production under basal (-EGF) and stimulated (+EGF) conditions relative to PLCγ2 WT. Each graphical symbol shape (square, triangle and circle) represents the fold change in IP_1 for each set of biological

replicates (Two-tailed unpaired t-test, p-values displayed on the graph, n=3). Data represents mean value ± SD.

4.2.1.3 PLCγ2 silent variants: M28L

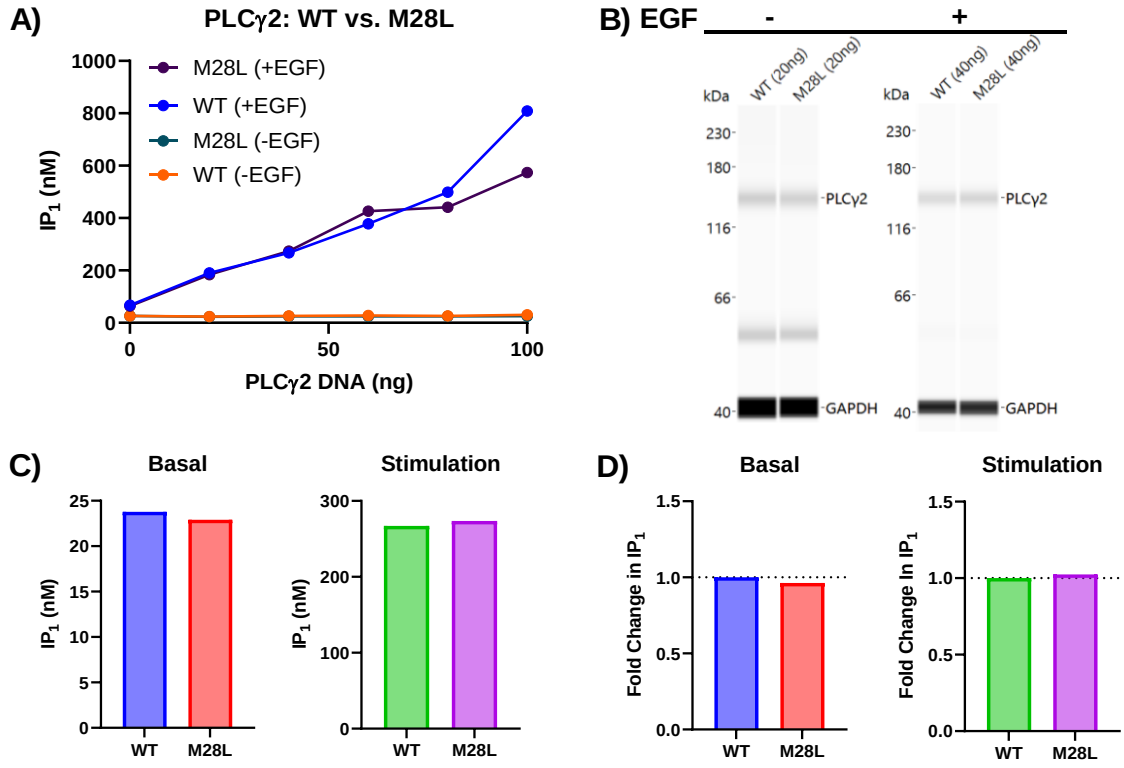

Figure 4.6 PLCγ2 M28L variant causes no change in PLC activity. **A)** Representative data comparing PLC activity of PLCγ2 WT and PLCγ2 M28L (titrated DNA) in transfected HEK293T cells under basal (-EGF) and stimulated (+EGF, 150 ng/ul for 1.5h) conditions. PLC activity was assessed using the HTRF IP_1 assay. The data is representative from one biological replicate. **B)** PLCγ2 (150kDa) expression for each IP_1 datapoint (basal (-EGF) and stimulated (+EGF) conditions) was measured by WES Western blotting. PLCγ2 expression (arbitrary units) was: WT/-EGF = 426187, WT/+EGF = 639772, M28L/-EGF = 413992 and M28L/+EGF = 672770. The data is representative from one biological replicate. PLCγ2 protein expression levels were comparable. **C)** IP_1 values that had comparable PLCγ2 expression were matched. Basal and stimulated conditions were matched separately. The graph represents the matched IP_1 data from one experiment (n=1). Data represents mean value. **D)** The PLCγ2 M28L IP_1 values were normalised to the PLCγ2 WT IP_1 values to represent the fold-change in PLCγ2 M28L IP_1 production under basal (-EGF) and stimulated (+EGF) conditions relative to PLCγ2 WT. The data is representative of one experiment. Data represents mean value.

4.2.2 Characterisation of novel and rare PLCγ2 disease-linked variants

4.2.2.1 Δ845-848

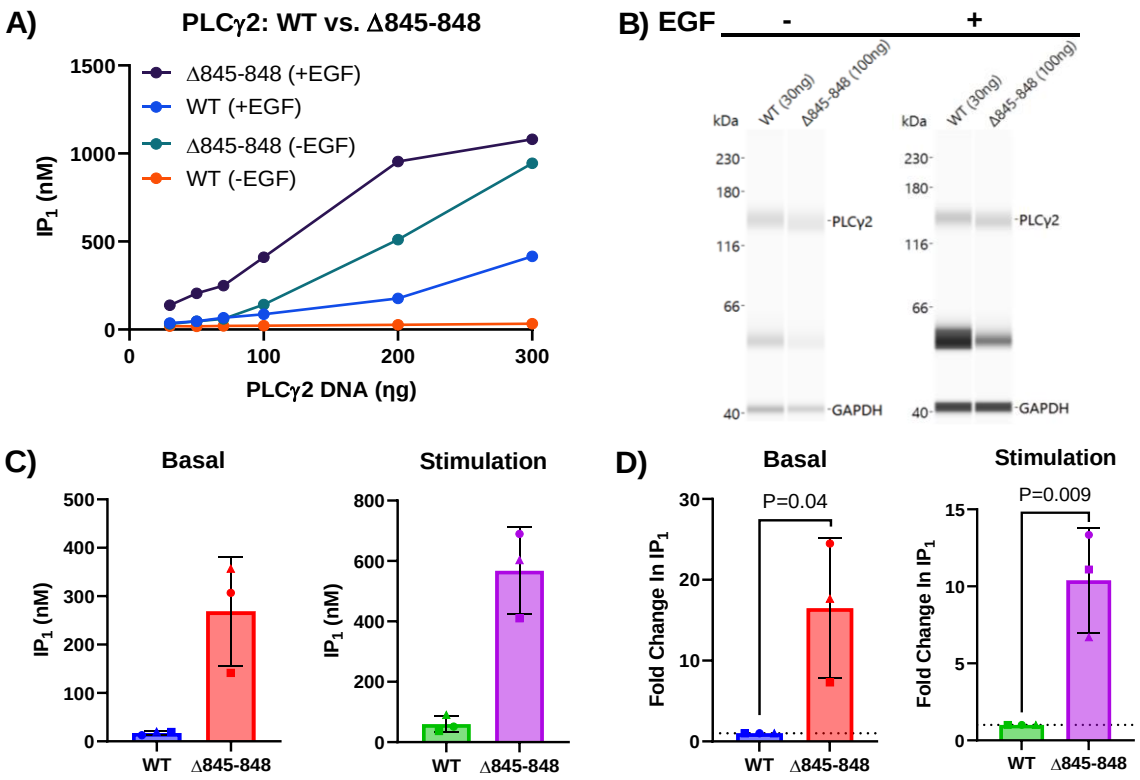

Figure 4.7 PLCγ2 Δ845-848 variant has increased PLC activity. **A)** Representative data comparing PLC activity of PLCγ2 WT and PLCγ2 Δ845-848 (titrated DNA) in transfected HEK293T cells under basal (-EGF) and stimulated (+EGF, 150 ng/ul for 1.5h) conditions. PLC activity was assessed using the HTRF IP_1 assay. The data is representative from one biological replicate. **B)** PLCγ2 (150kDa) expression for each IP_1 datapoint (basal (-EGF) and stimulated (+EGF) conditions) was measured by WES Western blotting. PLCγ2 expression (arbitrary units) was: WT/-EGF = 168750, WT/+EGF = 223020, Δ845-848/-EGF = 139830 and Δ845-848/+EGF = 204983. The data is representative from one biological replicate. PLCγ2 protein expression levels were comparable. **C)** IP_1 values that had comparable PLCγ2 expression were matched. Basal and stimulated conditions were matched separately. The graph represents the matched IP_1 data from all biological replicates. Each graphical symbol shape (square, triangle and circle) represents each set of biological replicates (n=3). Data represents mean value ± SD. **D)** The PLCγ2 Δ845-848 IP_1 values were normalised to the PLCγ2 WT IP_1 values to represent the fold-change in PLCγ2 P522R IP_1 production under basal (-EGF) and stimulated (+EGF) conditions relative to PLCγ2 WT. Each graphical symbol shape (square, triangle and circle) represents the fold change in IP_1 for each set

of biological replicates (Two-tailed unpaired t-test, p-values displayed on the graph, n=3). Data represents mean value ± SD.

4.2.2.2 M1141K

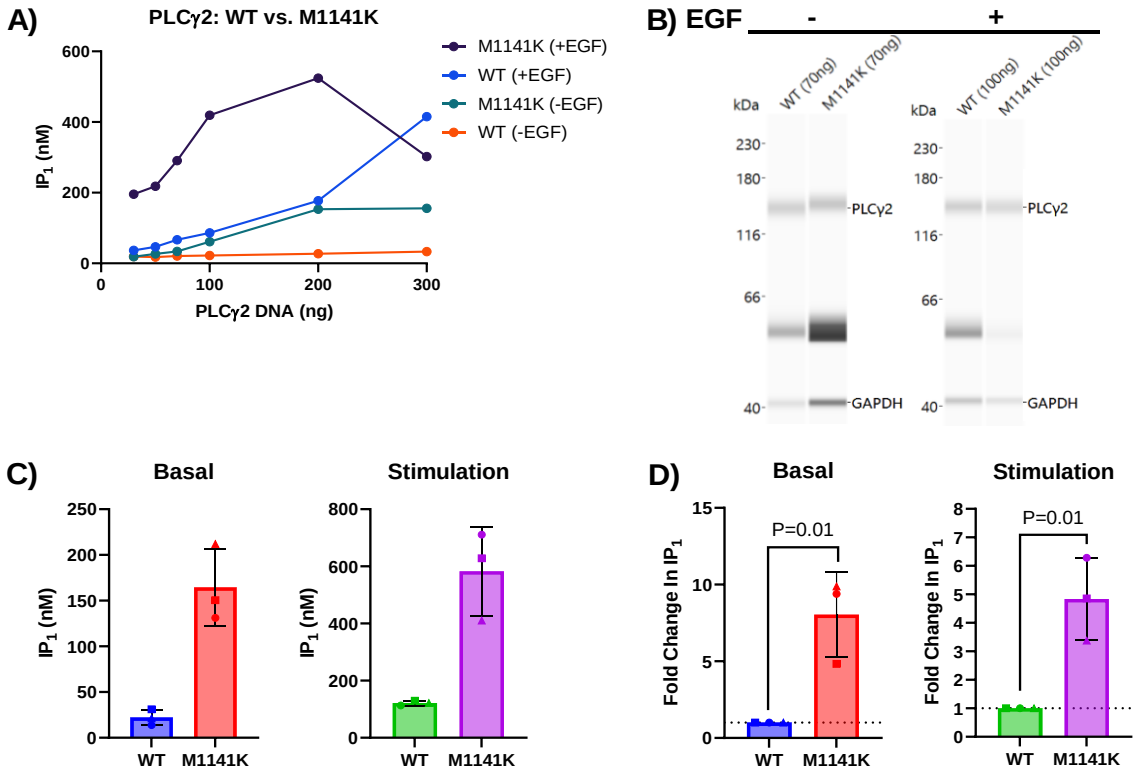

Figure 4.8 PLCγ2 M1141K variant has increased PLC activity. **A)** Representative data comparing PLC activity of PLCγ2 WT and PLCγ2 M1141K (titrated DNA) in transfected HEK293T cells under basal (-EGF) and stimulated (+EGF, 150 ng/ul for 1.5h) conditions. PLC activity was assessed using the HTRF IP_1 assay. The data is representative from one biological replicate. **B)** PLCγ2 (150kDa) expression for each IP_1 datapoint (basal (-EGF) and stimulated (+EGF) conditions) was measured by WES Western blotting. PLCγ2 expression (arbitrary units) was: WT/-EGF = 372094, WT/+EGF = 649967, M1141K/-EGF = 426182 and M1141K/+EGF = 626735. The data is representative from one biological replicate. PLCγ2 protein expression levels were comparable. **C)** IP_1 values that had comparable PLCγ2 expression were matched. Basal and stimulated conditions were matched separately. The graph represents the matched IP_1 data from all biological replicates. Each graphical symbol shape (square, triangle and circle) represents each set of biological replicates (n=3). Data represents mean value ± SD. **D)** The PLCγ2 M1141K IP_1 values were normalised to the PLCγ2 WT IP_1 values to represent the fold-change in PLCγ2 M1141K IP_1 production under basal (-EGF) and stimulated (+EGF) conditions relative to PLCγ2 WT. Each graphical symbol

shape (square, triangle and circle) represents the fold change in IP_1 for each set of biological replicates (Two-tailed unpaired t-test, pvalues displayed on the graph, n=3). Data represents mean value ± SD.

4.2.2.3 A708P

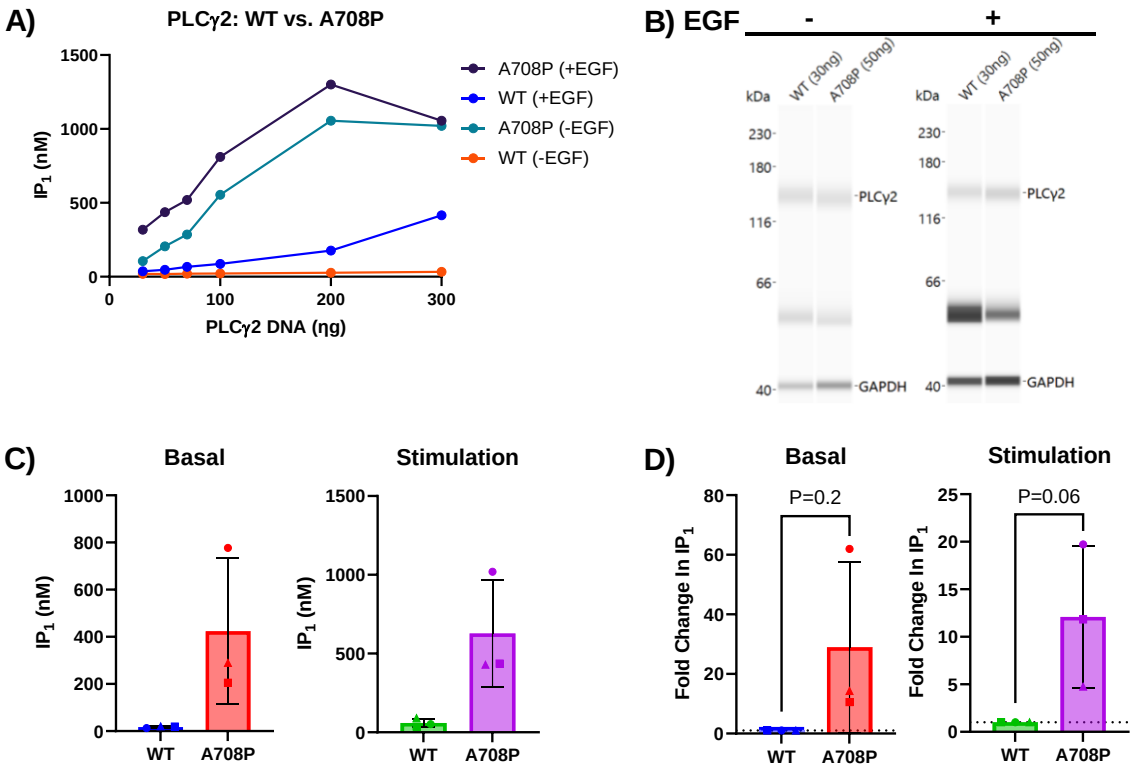

Figure 4.9 PLCγ2 A708P variant has increased PLC activity. **A)** Representative data comparing PLC activity of PLCγ2 WT and PLCγ2 A708P (titrated DNA) in transfected HEK293T cells under basal (-EGF) and stimulated (+EGF, 150 ng/ul for 1.5h) conditions. PLC activity was assessed using the HTRF IP_1 assay. The data is representative from one biological replicate. **B)** PLCγ2 (150kDa) expression for each IP_1 datapoint (basal (-EGF) and stimulated (+EGF) conditions) was measured by WES Western blotting. PLCγ2 expression (arbitrary units) was: WT/-EGF = 168750, WT/+EGF = 223020, A708P/-EGF = 168292 and A708P/+EGF = 240725. The data is representative from one biological replicate. PLCγ2 protein expression levels were comparable. **C)** IP_1 values that had comparable PLCγ2 expression were matched. Basal and stimulated conditions were matched separately. The graph represents the matched IP_1 data from all biological replicates. Each graphical symbol shape (square, triangle and circle) represents each set of biological replicates (n=3). Data represents mean value ± SD. **D)** The PLCγ2 A708P IP_1 values were normalised to the PLCγ2 WT IP_1 values to represent the fold-change in PLCγ2 A708P IP_1 production under basal (-EGF)

and stimulated (+EGF) conditions relative to PLCγ2 WT. Each graphical symbol shape (square, triangle and circle) represents the fold change in IP_1 for each set of biological replicates (Two-tailed unpaired t-test, p-values displayed on the graph, n=3). Data represents mean value ± SD.

4.2.2.4 V1103I

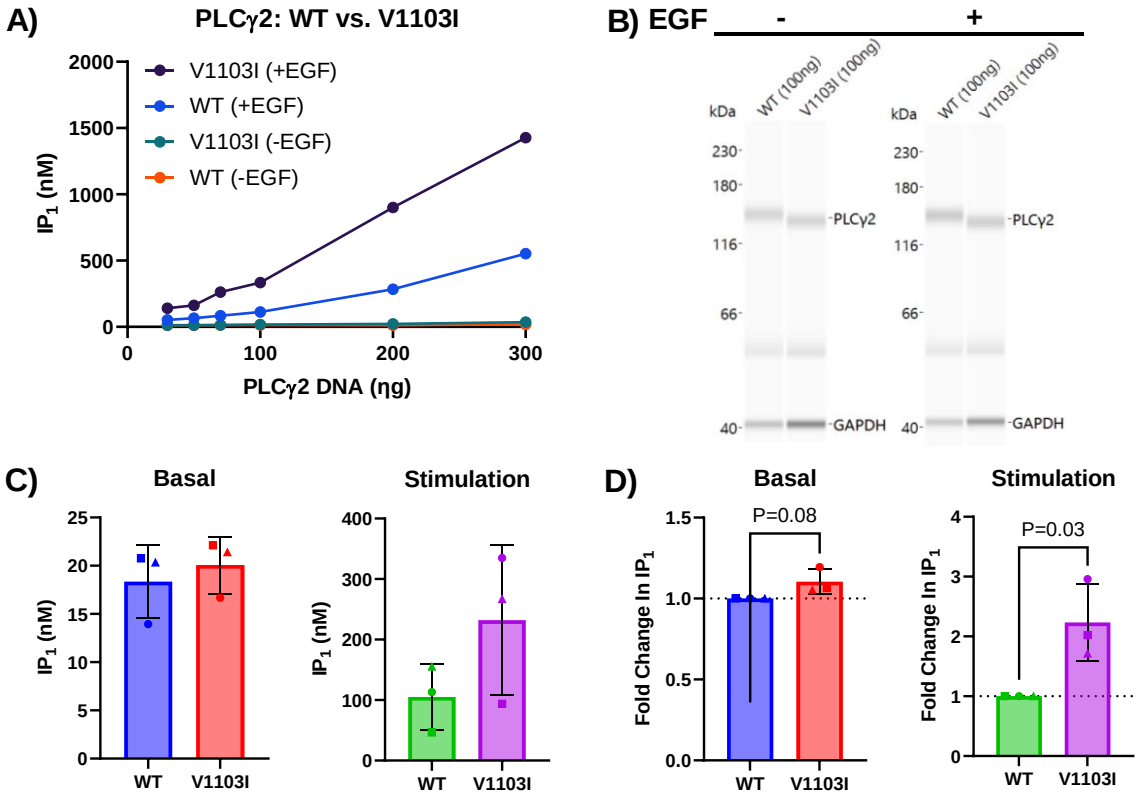

Figure 4.10 PLCγ2 V1103I variant has increased PLC activity. **A)** Representative data comparing PLC activity of PLCγ2 WT and PLCγ2 V1103I (titrated DNA) in transfected HEK293T cells under basal (-EGF) and stimulated (+EGF, 150 ng/ul for 1.5h) conditions. PLC activity was assessed using the HTRF IP_1 assay. The data is representative from one biological replicate. **B)** PLCγ2 (150kDa) expression for each IP_1 datapoint (basal (-EGF) and stimulated (+EGF) conditions) was measured by WES Western blotting. PLCγ2 expression (arbitrary units) was: WT/-EGF = 168750, WT/+EGF = 223020, A708P/-EGF = 168292 and A708P/+EGF = 240725. The data is representative from one biological replicate. PLCγ2 protein expression levels were comparable. **C)** IP_1 values that had comparable PLCγ2 expression were matched. Basal and stimulated conditions were matched separately. The graph represents the matched IP_1 data from all biological replicates. Each graphical symbol shape (square, triangle and circle) represents each set of biological replicates (n=3). Data represents mean

value ± SD. **D)** The PLCγ2 V1103I IP_1 values were normalised to the PLCγ2 WT IP_1 values to represent the fold-change in PLCγ2 V1103I IP_1 production under basal (-EGF) and stimulated (+EGF) conditions relative to PLCγ2 WT. Each graphical symbol shape (square, triangle and circle) represents the fold change in IP_1 for each set of biological replicates (Two-tailed unpaired t-test, p-values displayed on the graph, n=3). Data represents mean value ± SD.

4.2.2.5 R268W

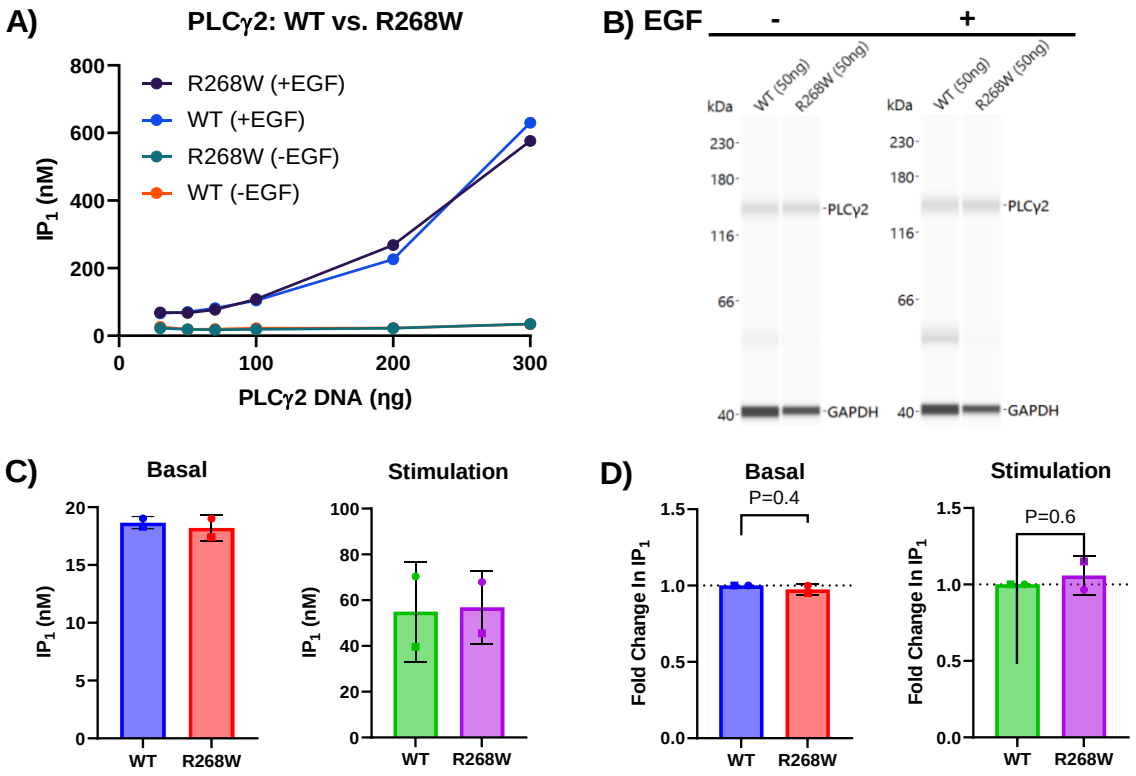

Figure 4.11 PLCγ2 R268W variant causes no change in PLC activity. **A)** Representative data comparing PLC activity of PLCγ2 WT and PLCγ2 R268W (titrated DNA) in transfected HEK293T cells under basal (-EGF) and stimulated (+EGF, 150 ng/ul for 1.5h) conditions. PLC activity was assessed using the HTRF IP_1 assay. The data is representative from one biological replicate. **B)** PLCγ2 (150kDa) expression for each IP_1 datapoint (basal (-EGF) and stimulated (+EGF) conditions) was measured by WES Western blotting. PLCγ2 expression (arbitrary units) was: WT/-EGF = 552980, WT/+EGF = 709258, R268W/-EGF = 539701 and R268W/+EGF = 685965. The data is representative from one biological replicate. PLCγ2 protein expression levels were comparable. **C)** IP_1 values that had comparable PLCγ2 expression were matched. Basal and stimulated conditions were matched separately. The graph represents the matched IP_1 data from all biological replicates. Each graphical symbol shape (square and circle)

represents each set of biological replicates (n=2). Data represents mean value ± SD. **D)** The PLCγ2 R268W IP_1 values were normalised to the PLCγ2 WT IP_1 values to represent the fold-change in PLCγ2 R268W IP_1 production under basal (-EGF) and stimulated (+EGF) conditions relative to PLCγ2 WT. Each graphical symbol shape (square and circle) represents the fold change in IP_1 for each set of biological replicates (Two-tailed unpaired t-test, p-values displayed on the graph, n=2). Data represents mean value ± SD.

4.2.2.6 H244R

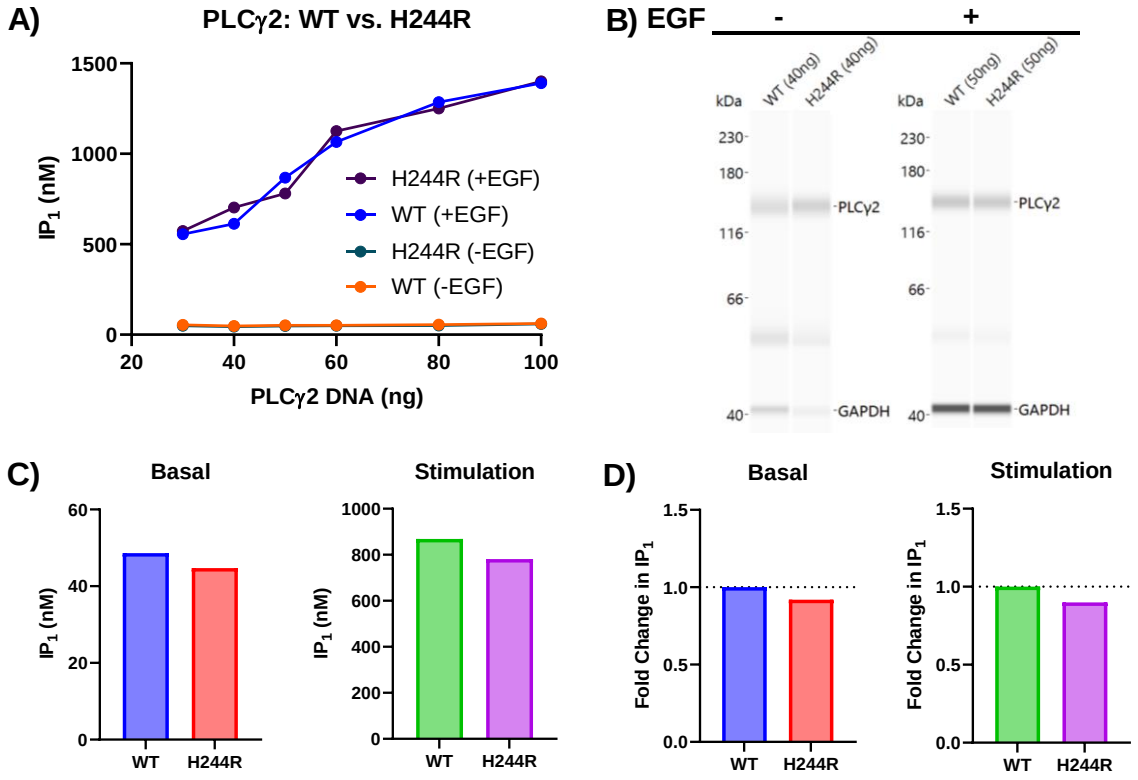

Figure 4.12 PLCγ2 H244R variant causes no change in PLC activity. **A)** Representative data comparing PLC activity of PLCγ2 WT and PLCγ2 H244R (titrated DNA) in transfected HEK293T cells under basal (-EGF) and stimulated (+EGF, 150 ng/ul for 1.5h) conditions. PLC activity was assessed using the HTRF IP_1 assay. The data is representative from one biological replicate. **B)** PLCγ2 (150kDa) expression for each IP_1 datapoint (basal (-EGF) and stimulated (+EGF) conditions) was measured by WES Western blotting. PLCγ2 expression (arbitrary units) was: WT/-EGF = 219722, WT/+EGF = 1363069, H244R/-EGF = 227290 and H244R/+EGF = 1335457. The data is representative from one biological replicate. PLCγ2 protein expression levels were comparable. **C)** IP_1 values that had comparable PLCγ2 expression were matched. Basal and stimulated conditions were matched separately. The graph represents the matched

IP_1 data from one experiment. Data represents mean value. **D)** The PLCγ2 H244R IP_1 values were normalised to the PLCγ2 WT IP_1 values to represent the fold-change in PLCγ2 H244R IP_1 production under basal (-EGF) and stimulated (+EGF) conditions relative to PLCγ2 WT. The data is representative of one biological replicate. Data represents mean value.

4.3 Discussion

PLCγ2 Variant	Basal IP_1 Fold Difference Variant vs. WT (mean ± SD)	Basal Significant Difference (p-value)	Stimulation IP_1 Fold Difference Variant vs. WT (mean ± SD)	Stimulation Significant Difference (p-value)	Biological Replicates (N)
4F + F897Q	0.94 ± 0.04	0.05	0.33 ± 0.06	<0.001	3
H327/372F	0.96 ± 0.12	0.5	0.43 ± 0.11	<0.001	4
H244R	0.92	-	0.90	-	1
M28L	0.96	-	1.02	-	1
R268W	0.98 ± 0.03	0.4	1.06 ± 0.13	0.6	2
P522R	1.11 ± 0.07	0.07	1.39 ± 0.06	<0.001	3
V1103I	1.10 ± 0.08	0.08	2.23 ± 0.65	0.03	3
D993G	3.35 ± 0.62	0.003	3.23 ± 0.40	<0.001	3
M1141K	8.04 ± 2.79	0.01	4.84 ± 1.45	0.01	3
S707Y	5.00	-	6.30	-	1
Δ845-848	16.49 ± 8.65	0.04	10.38 ± 3.38	0.009	3
A708P	28.97 ± 28.65	0.2	12.10 ± 7.48	0.06	3

Table 4.1 PLCγ2 variant ranking of IP_1 activity. Values represent the mean ± SD fold difference in IP_1 production for each PLCγ2 variant under basal and stimulated conditions. PLCγ2 variants are ranked in order of the IP_1 fold difference observed under stimulated conditions. A two-tailed unpaired t-test was performed for each PLCγ2 variant with two or more biological replicates (p-values displayed in the table). (-) symbol represents an inability to perform a statistical test due to lack of biological replicates. Orange boxes represent conditions where PLC activity was lower than WT.

Green boxes represent conditions where PLC activity was the same as WT. Blue boxes represent conditions where PLC activity was higher than WT.

The experimental design worked well for the characterisation of the PLCγ2 variants. The titration of PLCγ2 cDNA vs. IP_1 production made it relatively straightforward to determine if a PLCγ2 variant had altered enzymatic activity under basal or stimulated conditions. Matching the expression levels of the PLCγ2 variant and PLCγ2 WT resulted in reproducible data amongst the biological replicates, making it a superior normalisation technique than normalising the IP_1 data to the expression of PLCγ2.

Throughout the enzymatic characterisation of each variant, different amounts of PLCγ2 cDNA were transfected, ranging from 0-300ng. During the assay validation of the well characterised PLCγ2 variants, 0ng was used as a negative control for the assay, but it provided no insight into PLCγ2 activity. Therefore, it was substituted with larger amounts of cDNA when the rare and novel PLCγ2 variants were investigated, as some PLCγ2 variants did not achieve expression comparable to PLCγ2 WT. However, for some of the variants 200ng and 300ng of PLCγ2 DNA resulted in a reduction of IP_1 production, also known as the 'Hook effect'[259]. This was mostly due to cell death induced by strong hypermorphic IP_1 production (data not shown). Furthermore, the PLCγ2 variants that exhibited a strong phenotype under both basal and stimulated conditions such as Δ845-848 and A708P, displayed a lot of variation between biological replicates. Due to the very strong GOF these variants possess, small changes in experimental design could result in significant changes to IP_1 production, perhaps explaining the observed variability. Variants of PLCγ2 could influence protein stability, resulting in differences in protein expression relative to PLCγ2 WT. Therefore, the amount of cDNA needed to be increased for some variants to achieve comparable expression to the WT. Additionally, experimental differences e.g. plasmid purity, could also influence transfection efficiency, which is why the matching of protein expression between PLCγ2 variants and PLCγ2 WT was crucial to have comparable data.

The IP_1 fold changes for each PLCγ2 variant under basal and stimulated conditions between all biological replicates is summarised in Table 4.1. Variants were ranked in order of the IP_1 fold difference observed under stimulated conditions. The experimental IP_1 assay confirms that the PLCγ2 H327/372F and '4F+F847Q' variants are regulatory inactive forms of PLCγ2, as under stimulated conditions an IP_1 fold difference of 0.43 ± 0.11 and 0.33 ± 0.06 was observed, respectively (Table 4.1). The D993G and S707Y

PLCγ2 variants were hypermorphic in both a basal and stimulated environment, displaying an IP_1 fold difference of 3.35 ± 0.62 (D993G) and 5.00 (S707Y) under basal conditions, and 3.23 ± 0.40 (D993G) and 6.30 (S707Y) under stimulated conditions, respectively (Table 4.1). The IP_1 assay was also able to differentiate between the mild GOF P522R PLCγ2 variant, as under stimulated conditions an IP_1 fold difference of 1.39 ± 0.06 observed (Table 4.1). So far, the assay has been able to differentiate between variants that have had notable changes in PLCγ2 enzymatic activity. As mentioned previously, the PLCγ2 M28L variant has been characterised in literature before as a variant that has no effect on enzymatic activity[176]. When assessed in the IP_1 assay the same trend was observed (Table 4.1). This result provides confidence that not every variant tested in the IP_1 assay will display an effect on enzymatic activity. Therefore, as the assay has demonstrated to be sensitive and robust enough to correctly characterise the enzymatic activity of documented PLCγ2 variants, the same experimental design can also be used for the characterisation of novel and rare disease-linked variants of PLCγ2.

Characterisation of the Δ845-848 variant demonstrated it to be hypermorphic under both basal (IP_1 Fold difference: 16.49 ± 8.65) and stimulated (IP_1 Fold difference: 10.38 ± 3.38) conditions (Table 4.1). Additionally, the A708P variant was also hypermorphic under both basal (IP_1 Fold difference: 28.97 ± 28.65) and stimulated (IP_1 Fold difference: 12.10 ± 7.48) conditions (Table 4.1). These two PLCγ2 variants were the strongest GOF variants characterised. Given that the Δ845-848 and A708P variants reside respectively at the spPH and cSH2 domains, both variants are likely disrupting the PLCγ2 autoinhibitory intramolecular interactions, resulting in the observed GOF phenotype[147]. Through the use of PLCγ2 deficient mice, PLCγ2 has been shown to play a key role in healthy B cell function[209], as well as NK cell cytotoxicity and innate immunity[260]. Both patients exhibiting these PLCγ2 variants demonstrated reduced B cell numbers, as GOF PLCγ2 variants influence B cell development, resulting in agammaglobulinemia and immune deficits relative to healthy controls[222]. In contrast, Δ845-848 and A708P patient PBMCs stimulated with lipopolysaccharide (LPS) showed an increase in pro-inflammatory cytokine release, relative to healthy controls, suggesting that GOF PLCγ2 variants are causative of the APLAID phenotype. The experimental methodology and results described in section 4.2 contributed to a publication[222].

The M1141K PLCγ2 variant was also demonstrated to be hypermorphic under basal (IP_1 Fold difference: 8.04 ± 2.79) and stimulated (IP_1 Fold difference: 4.84 ± 1.45) conditions (Table 4.1). Enzymatic characterisation of the M1141K PLCγ2 variant had not been performed until now (Table 1.1). This experimental data is consistent with the enhanced intracellular calcium influx and ERK phosphorylation reported in literature[224]. Furthermore, B cells numbers were also decreased in patients exhibiting the M1141K PLCγ2 variant, providing further evidence that PLCγ2 has a key role in B cell survival. The V1103I PLCγ2 variant is a novel variant of PLCγ2 that has only been identified in the clinic and is yet to be characterised (Genome Aggregation Database available from www.gnomad.broadinstitute.org). This thesis demonstrates that the V1103I PLCγ2 variant was hypermorphic under stimulated (IP_1 Fold difference: 2.23 ± 0.65) conditions only (Table 4.1). Both the M1141K and V1103I PLCγ2 are located within the PLCγ2 C2 domain. Perhaps both variants also disrupt the autoinhibitory intramolecular interactions between the C2-cSH2 PLCγ2 domains. However, further studies would need to be performed to support this hypothesis.

Interestingly, the V1103I PLCγ2 variant displays a similar phenotype to the P522R PLCγ2 variant in that an increase in enzymatic activity is only exhibited when PLCγ2 is activated (Table 4.1). Given the V1103I variant has been associated with APLAID, but the P522R variant has been demonstrated to protect against LOAD, as well as increased longevity, it is interesting to see how small changes in PLCγ2 enzymatic activity can have such drastic effects on clinical phenotypes. However, PLCγ2 variants may be also affecting different mechanisms such as allosteric networks, membrane interactions, domain stability or interactions with regulatory proteins, not only the level of PLC activity, which can also influence the phenotype.

Some of the PLCγ2 variants tested had less than three biological replicates. The IP_1 DNA titration showed the R268W and H244R PLCγ2 variants to have equivalent IP_1 production to that of the WT control (Figure 4.11A and Figure 4.12A). Furthermore, when PLCγ2 expression was matched no fold-change in IP_1 production was observed. Because of these two factors, biological replicates were not deemed necessary. The M28L and S707Y PLCγ2 variants were only assayed once to validate the IP_1 assay, as the enzymatic activity of each variant had already been well characterised in literature.

Throughout each western blot a band of ~50kDa is present. Due to the PLCγ2 antibody being polyclonal perhaps the antibody is cross-reacting with other proteins with similar

epitopes or even a fragment of PLCγ2. This band is also apparent in the other polyclonal antibodies tested in Figure 3.5. However, this does not influence experimental interpretation as cDNA titrations support the FL PLCγ2 matching normalisation. Furthermore, perhaps a FL PLCγ2 expression to cDNA ratio matching could have been implemented to normalise the data. However, similar to before (3.2.2.4) normalising the raw IP_1 data to this ratio would result in less reproducible data amongst the biological replicates as the raw data is being manipulated.

4.4 Conclusion

Through the use of characterised PLCγ2 variants, the HTRF IP_1 assay was demonstrated to be sensitive enough to detect PLCγ2 variants that influence enzymatic activity, as well as differentiate between variants that had no effect on enzymatic activity. With confidence in the assay established, rare and novel disease-linked PLCγ2 variants were introduced into the assay and characterised. The Δ845-848, A708P and M1141K PLCγ2 variants exhibited hypermorphic activity under basal and stimulated conditions, whereas the V1103I variant was only hypermorphic under stimulated conditions. Additionally, the H224R and R268W PLCγ2 variants exhibited no impact on enzymatic activity.

This thesis provides a foundation to bridge the gap between the genotyping of disease-linked PLCγ2 variants and their associated clinical phenotype. However, further work is still needed to understand each variants effect on cell signalling and how this ultimately leads to clinical observations such as depleted B cell numbers, agammaglobulinemia and pro-inflammatory cytokine release.

5.1.1 Modelling neuroinflammation with stem cell-derived microglia

As mentioned previously in 1.7.2, rodent models cannot always recapitulate human genetics. Therefore, doubt has been cast into whether rodent models are able to accurately model human disease[261]. Primary human microglia are hard to obtain, especially in ample numbers for statistical power[246]. Additionally, the moment microglia leave the brain and are cultured *in vitro*, they undergo rapid transcriptomic and phenotypic changes that transition the microglia away from the *in vivo* state[27,53,250]. In order to combat this issue, researchers have begun to use microglia cells derived from hiPSCs and hESCs, resulting in the development of numerous protocols[262]. As microglia have been implicated in the neuroinflammatory component of AD aetiology, this cell model could enable insight into the role of microglia in neurodegeneration as these cells have demonstrated to be functionally active, with many key microglial processes such as phagocytosis and cytokine/chemokine secretion, able to be characterised[242,253].

Microglia are shaped from the microenvironment in the CNS. Once removed, they no longer have astrocyte, neuronal and oligodendrocytes interactions, causing them to display a more activated phenotype and progressively die. In order to combat this issue, serum is often used to supplement microglial cultures as it is rich in growth factors and metabolites. Although serum has been shown to increase microglial proliferation, it contains blood-borne molecules that microglia are not normally exposed to in the CNS. As a result, microglia cultured in serum display an activated phenotype[250,263]. In order to investigate microglial biology, cells need to display a more homeostatic phenotype, in a serum free setting. As a result, Bohlen et al., defined the main cytokines secreted by astrocytes, that promote microglia survival while maintaining their homeostatic state[250]. These are M-CSF, interleukin-34 (IL-34), transforming growth factor beta (TGF-β) and cholesterol.

In the brain, M-CSF is primarily secreted by astrocytes, oligodendrocytes and microglia, while IL-34 is predominantly secreted by neurons[264,265]. Although both M-CSF and IL-34 have very low sequence similarity, they have very similar tertiary structures that overlap[266,267]. It is thought that both ligands have complimentary roles in the activation of the M-CSF receptor[268]. As a result, M-CSF and IL-34, as well as TGF-β1, supplementation *in vitro* have all been demonstrated to be key for microglia

survival, proliferation and maturation[27,250,269–272]. Bohlen et al., also found that microglia express lower levels of cholesterol biosynthesis genes than astrocytes and mature oligodendrocytes[250]. Therefore, they proposed that microglia are deficient at producing cholesterol autonomously, but instead rely on other CNS cells *in vivo* or require cholesterol supplementation *in vitro*[250]. The addition of cholesterol to their *in vitro* murine microglia cultures aided in restoring the expression of the microglial specific gene, TMEM119, while also reducing the activated phenotype[250].

5.1.2 The role of PLCγ2 in microglial cell function

As mentioned in 1.6.3, several genes linked to LOAD, such as PLCG2, are highly expressed within microglia[99,116]. H9-derived preMacs exposed to M-CSF, IL-34, TGF-β and cholesterol have been demonstrated to differentiate into microglia 'like' cells[250,273]. Through the use of the H9-derived microglia, assays can be developed and optimised to characterise the role that PLCγ2 has in enzymatic activity, cell signalling and functionality, to better understand its overall role within microglial function.

5.2 Results

5.2.1 Generation and characterisation of H9-derived microglia

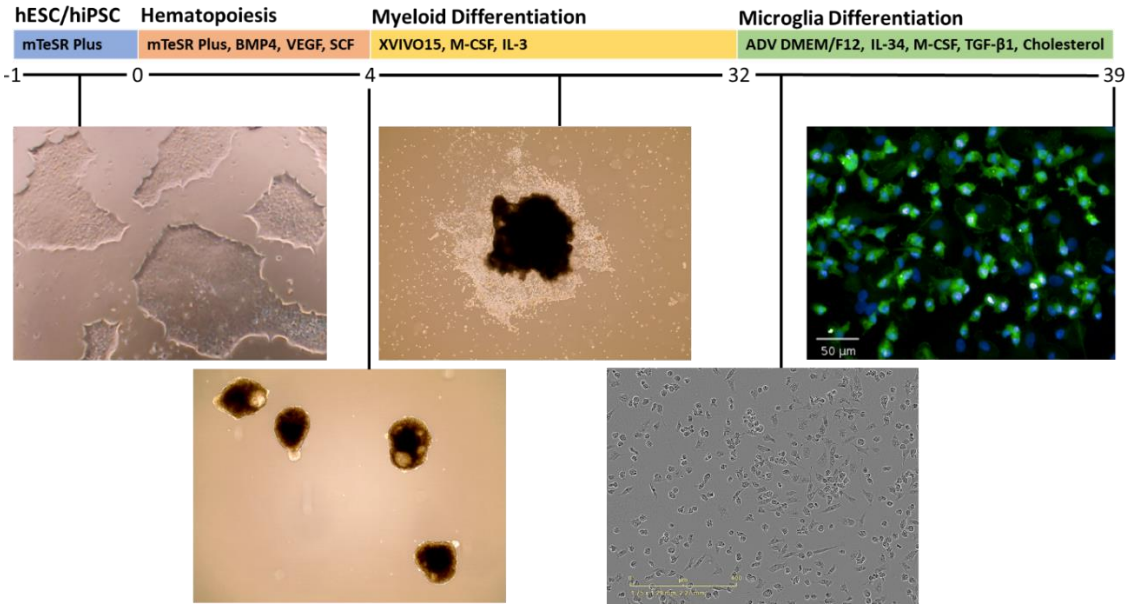

Figure 5.1 Timeline of the H9-derived microglia protocol. Schematic showing the process of differentiation from stem cells, through the mesoderm lineage (days 0-3), as well as promotion of hematopoiesis (days 4-31). Primitive hematopoietic progenitor cells begin to be appear and are collected before being resuspended into new medium to induce microglial differentiation. Day 39 immunofluorescence image of H9-derived

microglia with ionized calcium-binding adaptor molecule 1 (IBA1, green) and DAPI (blue) staining.

The protocol used to generate H9-derived microglia is based on the Haenseler et al., protocol and is outlined in Figure 5.1[242]. Briefly, H9 hESCs are cultured before being aggregated to induce spontaneous mesoderm differentiation via EBs. The EBs are subjected to bone morphogenetic protein 4 (BMP4), vascular endothelial growth factor (VEGF) and stem cell factor (SCF) to induce the hematopoietic transition of the EBs. Subsequently, the EBs are exposed to X-VIVO15 media supplemented with interleukin-3 (IL-3) and M-CSF to promote myeloid differentiation. Most EBs adhere, developing cystic, yolk-sac-like structures with surrounding adherent stromal cells. After a few weeks, macrophage progenitors (preMacs) emerge into the supernatant as a population of large round cells. These cells are collected and subjected to DMEM/F-12 media supplemented with cholesterol, M-CSF, IL-34 and TGF-β1 that together promote microglial differentiation and maturation, with a half media change every 2/3 days. After 7 days of differentiation, the microglia 'like' cells express ionized calcium-binding adaptor molecule 1 (IBA1) and display ramified morphology (Figure 5.1). For the differentiation of H9-derived macrophage cells, H9-derived preMacs were collected and cultured in X-VIVO15 media supplemented with M-CSF for 7 days.

Although multiple protocols exist for the generation of stem cell-derived microglia, microglial gene expression has been shown to vary depending on the protocol used[251,273]. Therefore, it is crucial to characterise the H9-derived microglia cellular system in order to make sure that the microglia exhibit the relevant morphology, express the relevant microglia specific markers and are functionally active.

5.2.1.1 Gene expression of the H9-derived microglia

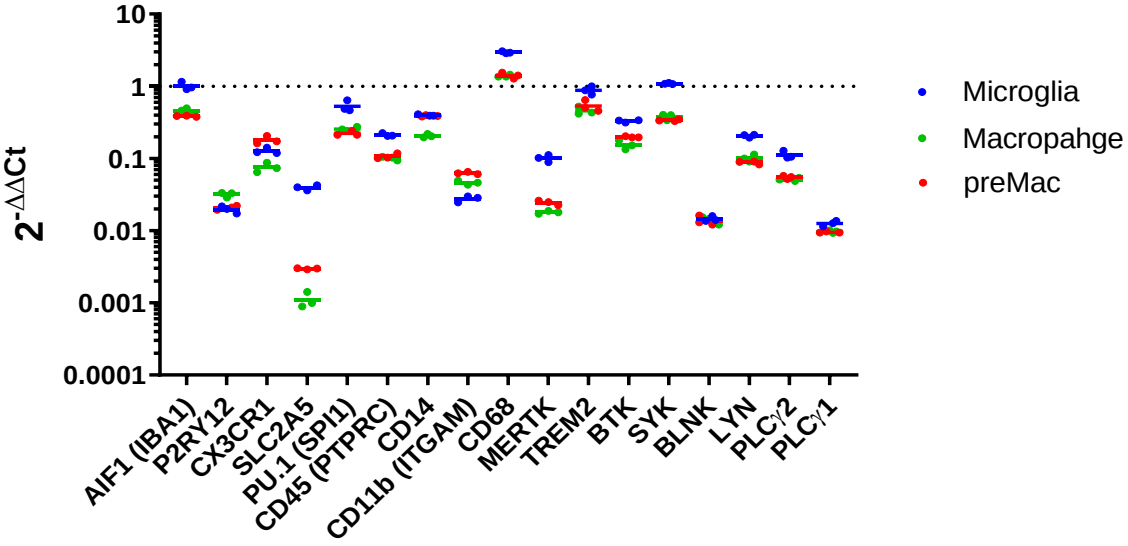

Figure 5.2 qPCR comparison of the difference in gene expression between the H9 derived-microglia (blue), macrophage (green) and preMac (red) cells. Ct values were normalised to the average expression of the Ubiquitin C (UBC), Actin Beta (ACTB) and ATP Synthase F1 Subunit Beta (ATP5B) housekeeping genes as these were most equal amongst the derived cell types. Values displayed were normalised to H9-derived microglia AIF1 (IBA1). The experiment consists of one biological replicate with three experimental replicates (n=1). Mean values are represented as a coloured bar.

RNA was extracted from the H9 derived-microglia, macrophage and preMac cells, and gene expression characterised through a one-step RT qPCR. Relative to the H9-derived preMac and macrophage cells, the H9-derived microglia cells displayed an upregulation in microglia differentially expressed genes (allograft inflammatory factor 1 (AIF1 or IBA1), solute carrier family 2 member 5 (SLC2A5, or glucose transporter type 5 (GLUT-5)), purine-rich box-1 (PU.1, or Spi-1 proto-oncogene (SPI1)), cluster of differentiation 45 (CD45, or protein tyrosine phosphatase receptor type C (PTPRC)), cluster of differentiation 68 (CD68) and MER proto-oncogene tyrosine kinase (MERTK)) and genes associated with the TREM2 signalling pathway (TREM2, BTK, SYK, LYN and PLCγ2) as shown from the qPCR analysis (Figure 5.2)[110,274,275] . However, no observable difference in gene expression of purinergic receptor P2Y12 (P2RY12), CX3C chemokine receptor 1 (CX3CR1), cluster of differentiation 14 (CD14), cluster of differentiation molecule 11b (CD11b, or Integrin alpha M (ITGAM)), BLNK and PLCγ1 was found between the different cell types (Figure 5.2). All taqman primers used were validated and had amplification efficiencies ranging from

90-110% (data not shown). The upregulation of IBA1/AIF1, TREM2, CD68 and MERTK, known markers of phagocytosis, suggests that the H9-microglia possess phagocytic capability[276–279]. SLC2A5 is known to be highly expressed within microglia cells[274]. The high SLC2A5 upregulation observed for the H9-derived microglia, relative to the macrophage and preMac cells, suggests that the differentiated cells can be considered microglial 'like' (Figure 5.2).

TMEM119 transcript was also quantified for each derived cell type but the primers failed the amplification efficiency validation (data not shown). Furthermore, several housekeeping genes were tested for qPCR normalisation (data not shown). Ubiquitin C (UBC), Actin Beta (ACTB) and ATP Synthase F1 Subunit Beta (ATP5B) were selected as the main housekeeping genes as the C_t values were most equal between each of the different cell types (microglia, macrophage and preMacs). Therefore, differences in microglial and TREM2 signalling gene expression between the different cell types was not due to housekeeping normalisation differences.

5.2.1.2 TREM2 activated PLCγ2 phosphorylation

PLCγ2 has been demonstrated to mediate TREM2 signalling in hiPSC-derived macrophages when stimulated with a commercial TREM2 antibody[183]. Using the same approach, H9-derived microglia were stimulated with the same TREM2 antibody resulting in elevated PLCγ2 Y759 phosphorylation (~20%), relative to the IgG control (Figure 5.3). The data demonstrates that in H9-derived microglia activation of PLCγ2 can be achieved by TREM2 pathway stimulation, correlating with what is known in the literature[183].

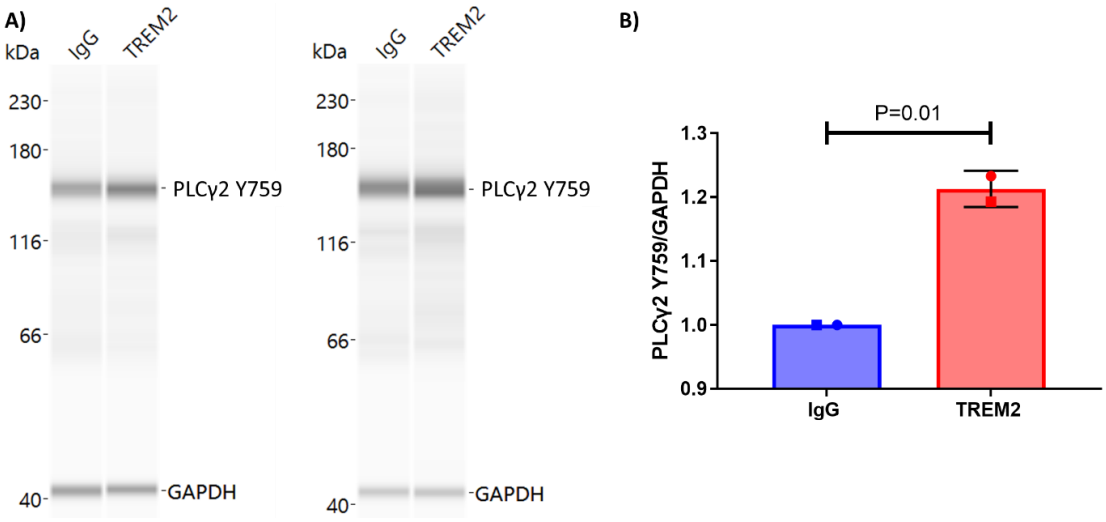

Figure 5.3 TREM2 stimulated H9-derived microglia causes PLCγ2 phosphorylation. H9-dervied microglia were treated with 100μM of Pervanadate for 50 min before being stimulated for 10 min with 5ug/mL of either IgG or TREM2 antibody. **A)** WES Western blots of phosphorylated PLCγ2 Y759 (150 kDa) and GAPDH (42 kDa) from control IgG and TREM2 antibody stimulation. WES Western blots shown are representative of two independent biological experiments. **B)** Quantification of the relative expression of PLCγ2 Y759 normalised to GAPDH expression from each biological replicate. Values displayed were normalised to the control IgG condition. Data represents mean value ± SD, with each graphical symbol shape (square and circle) representing each set of biological replicates (unpaired t-test, p-value displayed on the graph, n=2).

5.2.2 PLCγ2 enzymatic activity

5.2.2.1 HTRF IP_1 Assay

Having established a protocol for the generation of H9-derived microglia, as well as validating that the H9-derived microglia display the relevant morphology, express the correct microglia markers and that activation of PLCγ2 can be achieved by TREM2 stimulation, the development and optimisation of functional assays to characterise the role of PLCγ2 within microglia function was initiated.

The first aim was to characterise PLCγ2 enzymatic activity in H9-derived microglia. We know that PLCγ2 is the main isoform of PLCγ expressed within H9-derived microglia (Figure 5.2). However, other PLC isoforms are likely expressed within H9-derived microglia. RNAseq of hiPSC-derived microglia shows PLCγ2 to be the most highly expressed PLC isotype, with PLCβ2 second displaying 2-fold lower expression[242]. Therefore, perhaps other endogenous PLC isoforms can also contribute to IP_1 production in microglia. However, TREM2 activation has been demonstrated to be PLCγ2 specific, as PLCγ2 deficient hiPSC-derived macrophages demonstrate no IP_1 and no calcium response upon TREM2 stimulation[183].

Based upon experience gained from the HEK293T IP_1 accumulation assay, it was important to establish the correct cell density of H9-derived microglia needed to generate the best signal-window possible. 50,000, 100,000 and 150,000 H9-derived preMacs/well were plated in microglia differentiation media for 7 days, before being stimulated with a TREM2 antibody and the IP_1 production quantified in accordance with the manufacturer's instructions. A cell density dependent effect on IP_1 production

was observed, plateauing at 100,000 cells/well (Figure 5.4A). An approximate 2-fold increase in IP_1 production was observed for all cell densities through TREM2 simulation, relative to the IgG control (Figure 5.4A).

Having determined the optimum cell number of 100,000 cells/well for the IP_1 assay, it was important to determine if a concentration dependent response for TREM2 stimulation could also be established. Using the same experimental design as described previously, a TREM2 antibody dose dependent response in IP_1 production was observed (Figure 5.4B), providing further evidence that PLCγ2 IP_1 production is TREM2 dependent.

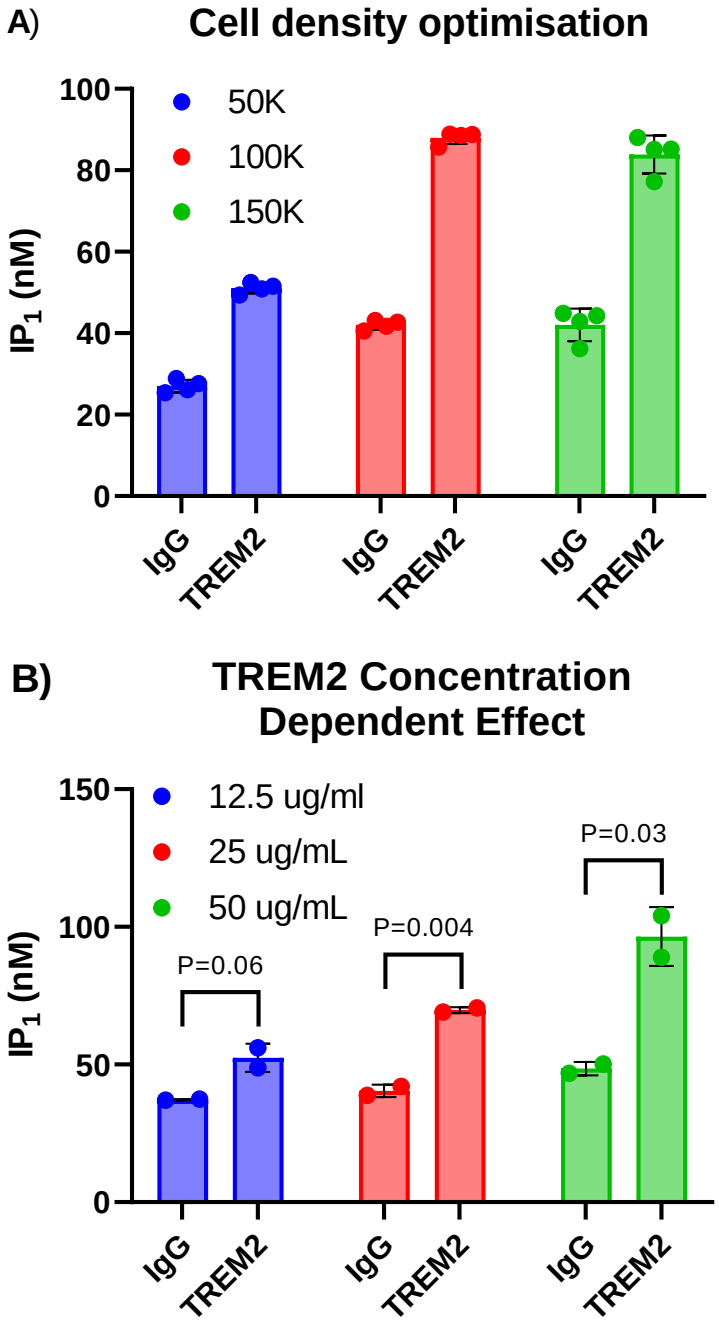

Figure 5.4 TREM2 antibody stimulated H9-derived microglia results in increased IP_1 production. **A**) Within a 24 well plate 50,000 (50k, blue), 100,000 (100K, red) and 150,000 (150K, green) H9-derived preMacs were plated in microglia differentiation media for 7 days before being stimulated with 50µg/mL of control IgG or TREM2 antibody for 2h before IP_1 production was quantified in accordance with the manufacturer's instructions. Data represents mean value ± SD (one biological replicate with four experimental replicates per condition, unpaired t-test (IgG vs. TREM2) for each cell density, $p<0.001$, n=1), **B**) 100,000 H9-derived preMacs/24 well were plated in microglia differentiation media for 7 days before being stimulated with 12.5/25/50µg/mL of control IgG or TREM2 antibody for 2h before IP_1 was quantified in accordance with the manufacturer's instructions. Data represents mean value ± SD (one biological replicate with two experimental replicates per condition, unpaired t-test (IgG vs. TREM2), p values on graph, n=1).

5.2.3 PLCγ2 mediated intracellular signalling

5.2.3.1 Calcium Assay

It is well documented that IP_3 produced from PLCγ2 enzymatic function binds to the IP_3R on the endoplasmic reticulum contributing to intracellular calcium flux[189]. Furthermore, as mentioned previously TREM2 stimulated PLCγ2 deficient hiPSC-derived macrophages exhibit no calcium flux, suggesting that calcium release via the TREM2 pathway is PLCγ2 dependent[183]. As the magnitude of PLCγ2 mediated calcium flux is dependent on enzymatic activity, a calcium assay could be utilised to further characterise the role that PLCγ2 has in microglial function.

FLIPR Calcium 6 dye has a similar binding affinity to calcium (Kd = ~320nM) compared to the ratiometric Fluo-3 (Kd = ~325nM) and Fluo-4 (Kd = ~345nM) dyes, but has a higher fluroscence quantum yield, increased signal window and is better retained inside the cell[280]. Therefore, compared to ratiometric calcium dyes, use of the calcium 6 dye results in a more sensitive quantification of intracellular calcium release.

Similar to the IP_1 assay, the optimum cellular density would need to be established in order to generate the greatest signal window possible. From the IP_1 experimental design it was concluded that a confluent well was essential for generating a good signal window. Therefore, applying the same IP_1 assay cell density of 50,000 cells/cm^2 equates to a cell density of approximately 5,000 cells/384 well for the calcium assay. However,

due to the miniature size of the wells in a 384 well plate, media changes are likely to lift cells over the 7 day differentiation timeline. Therefore, 10,000 cells/384 well was also included in the experimental comparison. An initial plating of 10,000 cells/384 well resulted in a confluent well on the day of experimentation (Figure S6). Therefore, this cell density would be used for future calcium flux experiments.

In addition to TREM2, Fc gamma receptor IIa (FcγRIIa) stimulation has also been demonstrated to produce a PLCγ2 mediated calcium response[183,226]. For microglial calcium assays, ATP and ionomycin are classically used as positive controls as they promote robust calcium release[226,281,282]. Thus for the calcium assay, 10,000 preMacs/384 well were plated in microglia differentiation media for 7 days. The cells were incubated for 2h in calcium dye before being stimulated with either HBSS, 10 µg/mL control IgG, 1.25/2.5/5/10µg/mL of TREM2 antibody or FCγRIIa antibody, 500 µM ATP or 5 µM Ionomycin, before calcium fluorescence was measured by the FLIPR Tetra (Molecular Devices).

TREM2 and FcγRIIa stimulated H9-derived microglia both elicited a strong calcium response relative to the control IgG and HBSS negative controls (Figure 5.5), suggesting that the calcium assay is suitable for characterising PLCγ2 mediated calcium flux for future experimentation. Variation between the stimulated TREM2 and ionomycin biological replicates was observed for the calcium assay (Figure 5.5). Due to the high sensitivity of the calcium assay, as well as the strong response both stimuli produced, perhaps small changes in the experimental set up e.g. cell density differences in each well, could explain such variation. To mitigate against this issue, the IncuCyte S3 platform offers a way to quantify the cell number/well that can be utilised to normalise experimental data. Perhaps this technique could be implemented for future experiments.

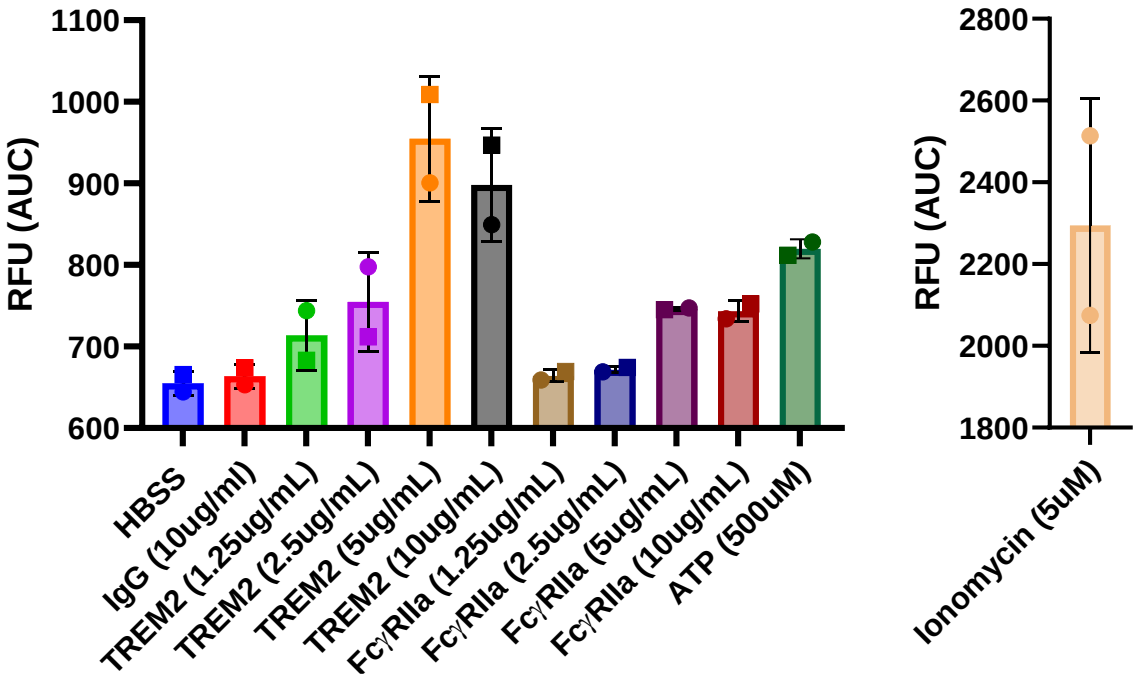

Figure 5.5 TREM2 and FcγRIIa antibody stimulated H9-derived microglia results in elevated calcium flux. 10,000 preMacs/384 well were plated in microglia differentiation media for 7 days before calcium 6 dye was added to the cells. The cells were stimulated with either HBSS, 10 µg/mL control IgG, 1.25/2.5/5/10µg/mL of TREM2 or FCγRIIa antibody, 500µM ATP or 5µM Ionomycin before the relative fluorescence units (RFU) were measured on a FLIPR Tetra (Molecular Devices). Area Under Curve (AUC) data was generated for each condition. Data represents mean value ± SD, with each graphical symbol shape (square and circle) representing each set of biological replicates (Two biological replicates with four experimental repeats per condition, n=2). Figure S7 displays the mean AUC traces for each stimulus, representative of one biological replicate.

5.2.4 Microglia functionality

5.2.4.1 Phagocytosis assay

Microglia cells use phagocytosis as a way of maintaining CNS homeostasis through the clearance of debris, microbes, apoptotic or necrotic cells[283]. PLCγ2 signalling, mediated by TREM2 activation, has been demonstrated to be pivotal for phagocytosis[133,183]. pH-sensitive pHrodo dyes can be linked to different particles to enable a kinetic measurement of phagocytosis. Dead human neuroblastoma SH-SY5Y cells stained with pHrodo have been shown to fluoresce weakly at neutral pH and more strongly inside the acidic environment of phagolysosomes of hiPSC-macrophages during phagocytosis[284].

Therefore, a phagocytosis assay can be established for the H9-derived microglia to characterise the effect PLCγ2 disease-linked variants have on phagocytosis in future experiments.

For the phagocytosis assay, 20,000 H9-derived preMacs/96 well (50,000 cells/cm^2) were plated and differentiated into microglia. After 7 days, H9-derived microglia were challenged with pHrodo labelled apoptotic SH-SY5Y cells, with phagocytosis (fluorescence) measured in real time using a IncuCyte S3 live-cell analysis system (Sartorius, Figure 5.6). Peak phagocytosis was observed at around 1.5h, with the well-known phagocytosis inhibitor Cytochalasin D acting as a negative control for analysis (Figure 5.6)[284]. The experimental results show that phagocytosis can be recorded in real time, and thus the assay can be utilised to measure the effect PLCγ2 disease-linked variants have on microglia phagocytosis.

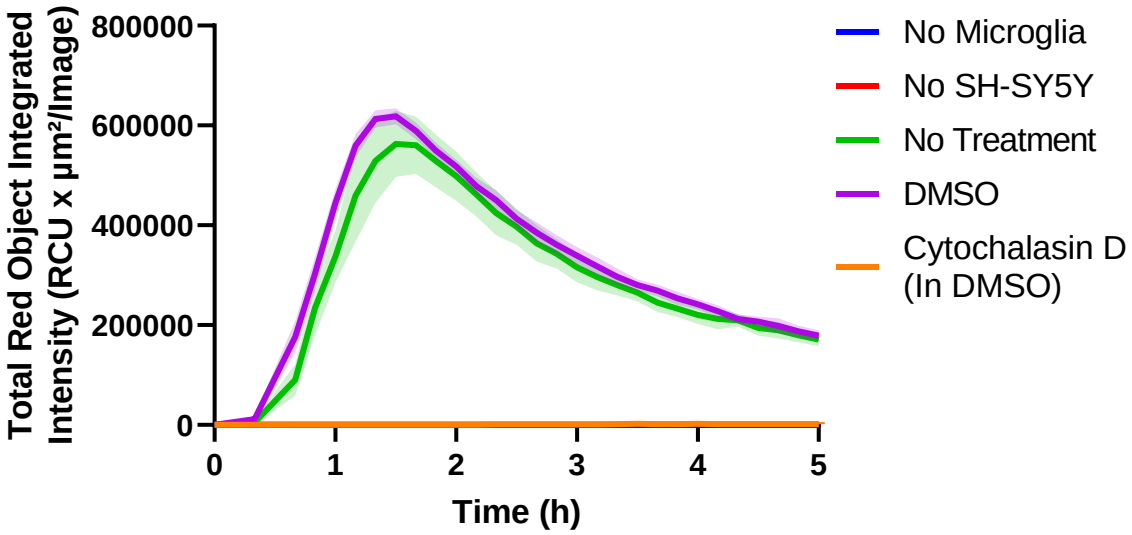

Figure 5.6 H9-derived microglia phagocytose pHrodo-labelled apoptotic SH-SY5Y cells. 1µM Cytochalasin D (0.01% DMSO (v/v)) pre-incubation prevents phagocytic uptake. 0.01% (v/v) DMSO was used as a control for the Cytochalasin D. 'No SH-SY5Y' condition acted as a no substrate control. Images were captured on the IncuCyte S3 live-cell analysis system (Sartorius) for 5h with the total red object integrated intensity (RCU x µm^2/Image) analysed on the IncuCyte analysis software. Data represents mean value ± SD (Area fill). Data represents one biological replicate with three experimental replicates per condition, n=1. Representative experimental images of phagocytosis located in Figure S8.

5.2.4.2 Cytokine secretion

Microglia have been touted as key mediators of neuroinflammation[63,72]. LPS is commonly used to induce microglia into a neuroinflammatory state by activating the toll-like receptor 4 (TLR4) pathway, initiating the innate immune response by releasing a battery of pro-inflammatory and anti-inflammatory cytokines and chemokines[285]. With the exception of interferon gamma (INF-γ), secretion of interleukin-1 beta (IL-1β), interleukin-6 (IL-6), interleukin-8 (IL-8), interleukin-10 (IL-10) and tumour necrosis factor alpha (TNF-α) have all been shown to be dependent on either NF-κB, NFAT or ERK activation[286–289]. Given the association that PLCγ2 has within these signalling pathways (Figure 1.4 and Figure 1.5), as well as the fact that PLCγ2 APLAID variants upregulate pro-inflammatory cytokine production upon LPS stimualtion[222], cytokine quantification may provide further insight into the role that PLCγ2 has within microglial function.

As a result, 20,000 H9-derived preMacs/96 well (50,000 cells/cm^2) were plated and differentiated into microglia. After 7 days, H9-derived microglia were stimulated with 1ng/mL LPS for 24h, before cytokine concentration was quantified with the MSD V-PLEX assay platform in accordance with the manufacturer's instructions. Apart from INF-γ, the cytokines IL-1β, IL-6, IL-8, IL-10 and TNF-α levels were all elevated following LPS stimulation (Figure 5.7).

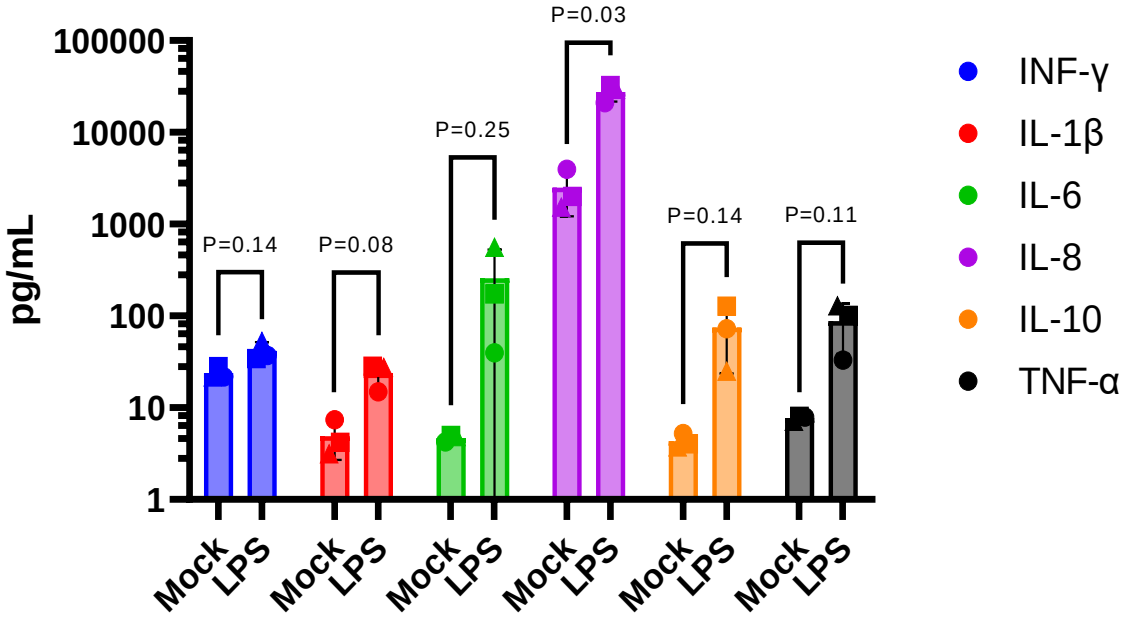

Figure 5.7 H9-derived microglia secrete elevated levels of cytokines upon LPS challenge. H9-derived microglia were challenged with ± LPS (1 ng/mL) for 24h, before

cell culture supernatant was removed and cytokine concentration quantified with the MSD V-PLEX Viral Panel 2 (human) kit in accordance with the manufacturer's instructions. Data represents mean value ± SD, with each graphical symbol shape (square, triangle and circle) representing each set of biological replicates (three biological replicates with three experimental repeats per condition, unpaired t-test, p-values displayed on the graph, n=3).

5.3 Discussion

qPCR analysis shows that the H9-derived microglia display an upregulation in microglia differentially expressed genes (AIF1 (IBA1), SLC2A5, PU.1 (SPI1), CD45 (PTPRC), CD68, MERTK and TREM2 (Figure 5.2)[110,274,275]. However, for the H9-derived cells no observable difference in P2RY12 and CX3CR1 gene expression was observed, perhaps highlighting some potential issues with the cell model. Stem cell-derived microglia have been reported to best resemble foetal or early postnatal human microglia[290]. During foetal brain development, microglia exhibit an more ameboid morphology[291]. Within the brain, P2RY12 is expressed on the ramified processes of microglia[292]. Due to their foetal nature, perhaps the lack of difference in P2RY12 expression is due to the H9-derived microglia exhibiting smaller ramifications compared to their *in vivo* counterparts, as shown from the ICC staining (Figure 5.1). However, data presented here shows that the macrophage and preMacs also express P2RY12. There is conflicting reports on whether P2RY12 is expressed in macrophages[293]. However, a meta-analysis of murine transcriptional datasets shows P2RY12 to be a robust microglia marker, suggesting that expression of P2RY12 should be higher in the H9-derived microglia[274].

CX3CR1 is prominently expressed by monocytes, subsets of natural killer and dendritic cells, as well as brain microglia[294]. Banerjee et al., performed transcriptional analysis of hiPSC-derived macrophages and microglia to characterise relevant markers[295]. They found that hiPSC-derived microglia express more CX3CR1, MERTK, P2RY12 and TREM2 than hiPSC-derived macrophages, but express less CD11b. Their data is broadly consistent with data presented in Figure 5.2. However, they do not compare the levels of expression to hiPSC-derived preMacs. CX3CR1 has been demonstrated to not be exclusively expressed by either microglia or macrophages[274]. Therefore, the lack of upregulation displayed in the H9-derived microglia is most likely not a concern.

Taking everything into account, the fact that the H9-derived microglia display an upregulation of known microglia markers such as TREM2 and SLC2A5, suggests that the model is physiologically relevant, with the lack of P2RY12 upregulation likely due to the foetal nature of the microglia. Longer differentiation times of 14 days have been shown to further mature hiPSC-derived microglia and even increase P2RY12 expression[296]. However, an extra 7-day differentiation would be costly and more time consuming for little benefit. It has also been demonstrated that the differentiation age of the preMacs harvested contributes to significant gene variation[136]. Therefore, additional biological replicates for qPCR analysis would also provide additional insight.

A limitation of the phagocytosis assay is the use of PFA fixation to prepare the phagocytic cargo as it does not fully recapitulate the process of apoptosis, since fixation prevents the cells from splitting into apoptotic bodies, which are likely to be phagocytosed more rapidly due to their smaller size[284]. It is not known what effect fixation has upon the secretion of nucleotide "find me" signals from the target cell that attract phagocytes.

Although LPS exposure elicited a mild (non-significant) neuroinflammatory response in the H9-derived microglia (Figure 5.7), given that bacterial infection is highly unlikely within the brain, other pro-inflammatory stimuli will likely be more relevant. Perhaps stimuli such as IFNγ and TNF-α could be used in order to address questions related to neuropathological changes observed in neurodegenerative disease disorders as both cytokines are elevated within the CNS in numerous pathologies and damage models[297].

5.4 Conclusion

Development and optimisation of a H9-derived microglia differentiation protocol and functional assays showed that the microglia display the relevant morphology, express microglia specific markers and are functionally active via TREM2, FCγRIIA, ATP, Ionomycin, apoptotic SH-SY5Y cell and LPS stimulation. To characterise the role of PLCγ2 within microglia, four assays: IP_1, calcium, phagocytosis and cytokine secretion, have been developed and optimised. The IP_1 assay can be used to directly assess PLCγ2 enzymatic functionality, and the calcium assay utilised to assess PLCγ2 mediated calcium release. Additionally, the phagocytosis and cytokine secretion assays can be applied to measure the role that PLCγ2 has on a key microglial functions.

Chapter 6 - PLCγ2 S707Y hiPSC-derived microglia

6.1 Introduction

Literature and data presented here (Figure 4.4) show the PLCγ2 S707Y disease-linked variant to be hypermorphic under both basal and stimulated conditions[171]. Patient PBMCs harbouring the PLCγ2 S707Y variant have also demonstrated increased calcium flux and LPS mediated pro-inflammatory cytokine secretion[217]. However, this PLCγ2 variant has never been characterised within the context of microglia. Given that the role of PLCγ2 within microglia function still requires further quantification, especially that of the LOAD protective P522R variant, the use of a strong hypermorphic variant could be used to push the cellular system to a phenotype that may be easier to observe, and therefore provide novel insight into the role of PLCγ2 in microglial function.

hiPSC lines containing a CRISPR/Cas9 edited heterozygous and homozygous form of the PLCγ2 S707Y variant, as well as the unedited WT line, were obtained via Dr. Rebecca McIntyre and Julie Matte at the Wellcome Sanger Institute (Cambridge, England). Having already established a protocol for the differentiation of H9-derived microglia, in addition to assays that characterise PLCγ2 mediated microglia functionality, the same protocols and assays could be applied to the hiPSC PLCγ2 WT and S707Y lines.

Due to the experimental variability observed between the biological replicates for the H9-derived microglia calcium assay (Figure 5.5), changes to the experimental protocol would need to be implemented to reduce such variability. Previously, preMacs were differentiated for 7 days in the assay plate to form microglia ‘like’ cells. However, this protocol would require media changes every 2/3 days, which could result in the cells progressively lifting, and thus the total cell number being variable come the day of experimentation. To mitigate against this issue, preMacs were plated into a flask for the first 4 days of differentiation, before being lifted into suspension by Accutase treatment and replated onto the assay plate at 50,000 cells/cm^2. The cells were then further differentiated for another 3 days (7 days total) before experimentation. Due to the cells being plated later in the differentiation protocol and post-replating not requiring any media changes, less variability in the total cell count on the day of the experiment would be predicted. Furthermore, prior to experimentation the cells would also be

placed into the IncuCyte S3 live-cell analysis system for quantification of cell numbers so that experimental data generated could be normalised to total cell number.

6.2 Cell line characterisation

6.2.1 Genotyping

hiPSC lines were SNP genotyped to confirm the presence of the heterozygous and homozygous PLCγ2 S707Y (rs397514562) variant. DNA was extracted from the PLCγ2 WT and S707Y hiPSC-derived microglia and sent to GVG Genetic Monitoring GmbH (Leipzig, Germany) for genotyping. SNP genotyping successfully confirmed the correct homozygous PLCγ2 S707Y (forward nucleotide: A, reverse nucleotide: T) and PLCγ2 WT (forward nucleotide: C, reverse nucleotide: G) nucleotides (Figure 6.1). Furthermore, the genotyping also established that the heterozygous line contains both WT and mutant alleles (Figure 6.1).

Additionally, the parental hiPSC kolf2 line from which the PLCγ2 WT and S707Y mutants were generated in, exhibit an heterozygous 19-bp deletion in the AT-Rich Interactive Domain-Containing Protein 2 (ARID2) gene[298]. ARID2 is one subunit of the chromatin remodelling complex and is involved in various biological processes including transcriptional regulation, cell cycle modulation, embryonic development and DNA damage repair[299]. However, it is unclear what effect, if any, this deletion in one allele of ARID2 has on the generation and functionality of hiPSC-derived microglia.

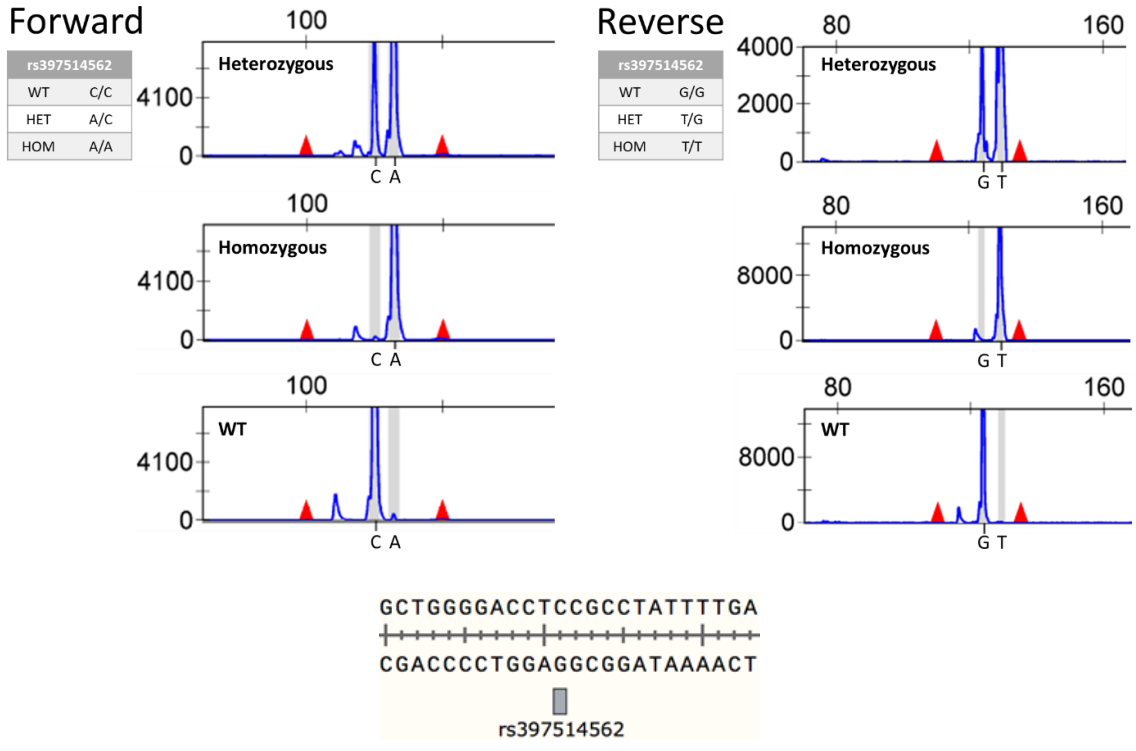

Figure 6.1 SNP genotyping of the PLCγ2 WT and S707Y hiPSC lines confirms the correct PLCγ2 WT and S707Y (rs397514562) nucleotides. Forward genotyping (TCC) characterises between the C (WT) and A (mut) nucleotides, while the reverse genotyping characterises between the G (WT) and T (mut) nucleotides.

6.2.2 PLCγ2 expression

Prior to phenotypic characterisation, PLCγ2 expression of the PLCγ2 WT and S707Y hiPSC-derived microglia needs to be quantified, as expression differences could influence future experimental interpretation. PLCγ2 WT and S707Y hiPSC-derived microglia were differentiated, lysed and PLCγ2 expression quantified through WES Western blotting. Compared to WT, the homozygous line appears to have a decrease (15 ± 7%) in PLCγ2 expression, whereas the heterozygous line has an increase (46 ± 13%) in PLCγ2 expression (Figure 6.2).

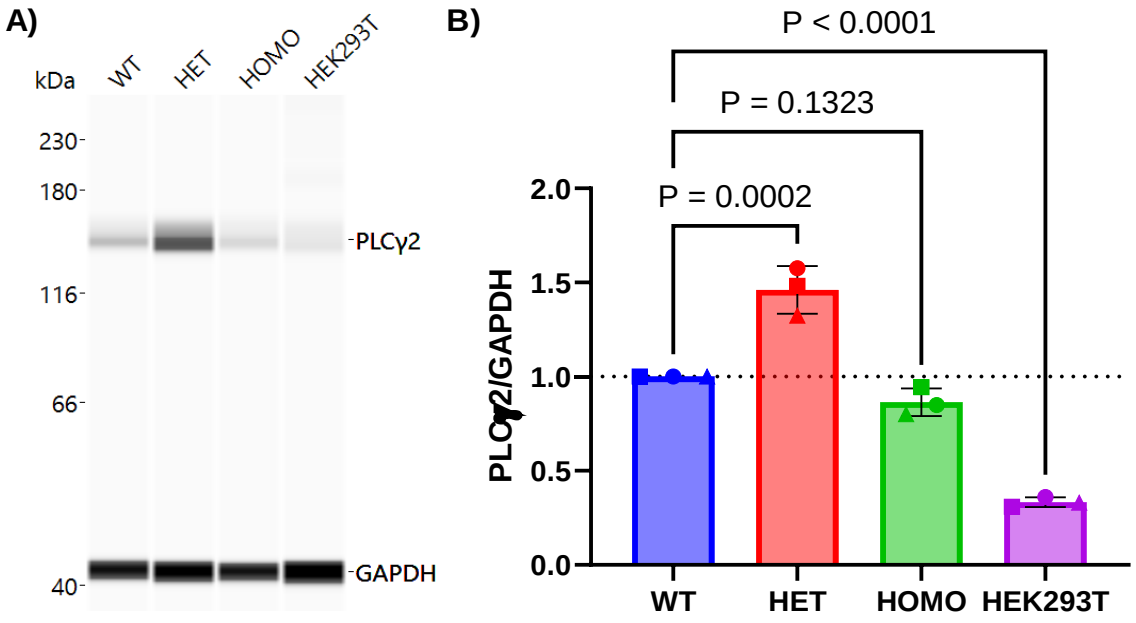

Figure 6.2 PLCγ2 expression of PLCγ2 WT, S707Y heterozygous (HET) and homozygous (HOMO) hiPSC-derived microglia. **A)** Representative WES Western blot of the PLCγ2 (150 kDa) and GAPDH (42 kDa) expression in each microglial derived line (WT, heterozygous (HET) and homozygous (HOMO)), as well as HEK293T cells (negative control). **B)** Quantification of the relative PLCγ2 expression normalised to a GAPDH loading control. Graphical values displayed are normalised to the WT hiPSC-derived microglia expression from each biological replicate. Data represents mean value ± SD, with each graphical symbol shape (square, circle and triangle) representing

each set of biological replicates (Multiple comparisons one way ANOVA, p-value displayed on the graph, n=3).

6.2.3 Metabolic Activity

CellTiter-Glo assay can directly measure the amount of ATP present in the culture. As ATP is an indicator of metabolically active cells, this assay can provide insight into the overall health of each cell line. Given that the kolf2 hiPSC PLCγ2 WT and S707Y lines were generated externally, it was important to compare if the microglia metabolic activity differed to the H9-derived microglia, as that is the cell line that the assays had been developed and optimised for. Stem cell-derived microglia were differentiated for 7 days before the CellTiter-Glo assay was performed in accordance with the manufacturer's instructions. Relative light units (RLU) were normalised to the total cell number (on the day of the assay) from a sister plate. The PLCγ2 WT and S707Y-derived microglia display a reduction in metabolic activity compared to the H9-derived microglia (Figure 6.3).

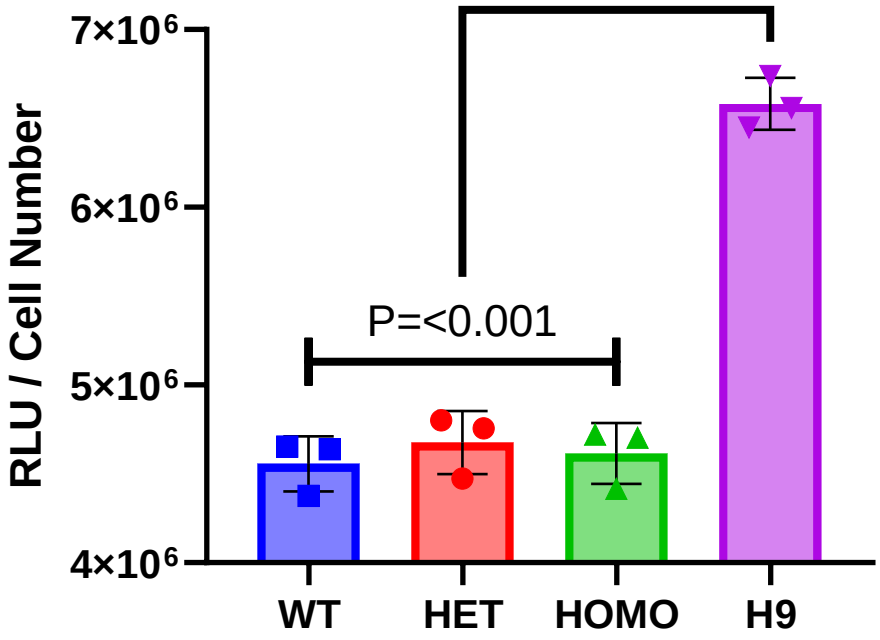

Figure 6.3 PLCγ2 WT, S707Y heterozygous (HET) and homozygous (HOMO) hiPSC-derived microglia display deficits in ATP production compared to their H9-derived microglia counterparts. Microglia were differentiated for 7 days before the CellTiter-Glo assay was performed in accordance with the manufacturer's instructions. Relative light units (RLU) were normalised to total cell number from a sister plate, captured on the IncuCyte S3 live-cell analysis system. Data represents mean value ± SD of three

experimental replates for one biological replicate (Multiple comparisons one way ANOVA, p-value displayed on the graph, n=1).

6.3 IP_1 Assay

As TREM2 stimulation of the H9-derived microglia has been demonstrated to elicit a strong IP_1 response (Figure 5.4), the same protocol could be applied to the PLCγ2 WT and S707Y hiPSC-derived microglia. IP_1 production of both the S707Y heterozygous and homozygous hiPSC-derived microglia under basal (control IgG) and stimulated (TREM2 antibody) conditions was significantly elevated compared to PLCγ2 WT hiPSC-derived microglia (Figure 6.4). This experimental result confirms the PLCγ2 S707Y hypermorphic phenotype within microglia[215].

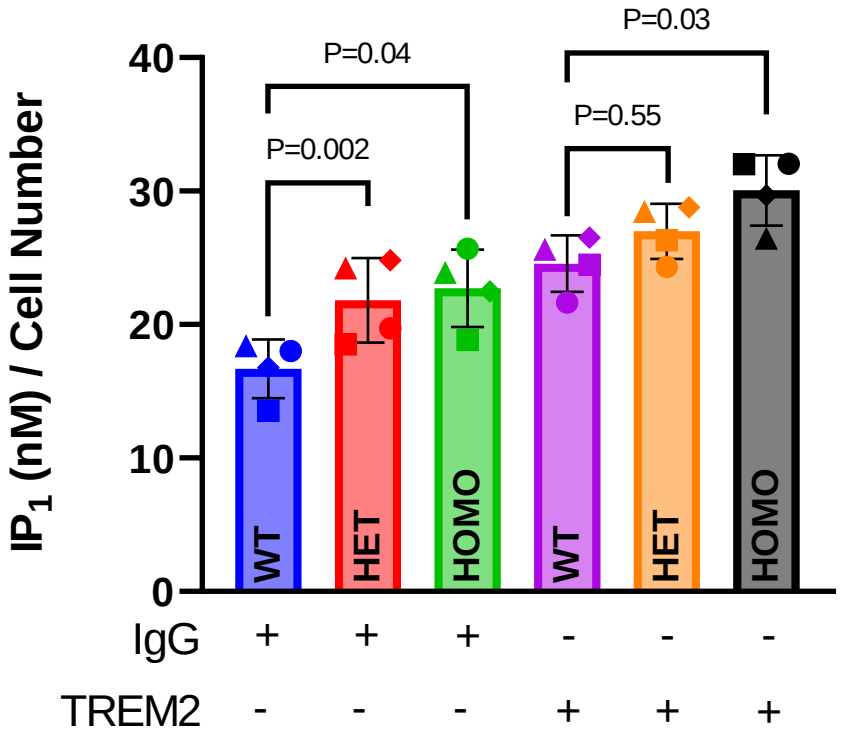

Figure 6.4 PLCγ2 S707Y heterozygous (HET) and homozygous (HOMO) hiPSC-derived microglia display heightened IP_1 production. Microglia were differentiated for 7 days before being stimulated with 25µg/mL of IgG or TREM2 for 2h before IP_1 accumulation was quantified in accordance with the manufacturer's instructions. IP_1 values were normalised to the total cell number captured on the IncuCyte S3 live-cell analysis system. Data represents mean value ± SD, with each graphical symbol shape (square, triangle, circle and diamond) representing each set of biological replicates with each biological replicate having at least three experimental replicates (Dunnett multiple comparisons one-way ANOVA, p-value displayed on the graph, n=4).

6.4 Calcium assay

Given the PLCγ2 S707Y hypermorphic phenotype observed in the IP_1 assay, the increase in enzymatic activity should directly correlate with an increase in intracellular calcium flux under both basal and stimulated conditions, as reported in literature[217]. Stimulation of the H9-derived microglia with TREM2 and FcγRIIa antibodies, as well as ionomycin resulted in a robust calcium response (Figure 5.5). From this experiment, considerable variation was observed between the AUC values from each biological replicate. In order to mitigate this issue, PLCγ2 WT and S707Y hiPSC-derived microglia were first activated with the experimental stimulus e.g. TREM2 antibody, before being re-stimulated with ionomycin once the calcium signal had returned to baseline. Experimental stimulated area under curve (AUC) data generated was then normalised to the ionomycin AUC data, providing a normalisation technique for cell number and cell health. This normalisation technique is commonly used in the analysis of calcium flux assay data[300]. Under basal and stimulated conditions, the PLCγ2 S707Y heterozygous and homozygous microglia have elevated calcium release compared to PLCγ2 WT (Figure 6.5), consistent with patient PBMCs harbouring the PLCγ2 S707Y variant, as documented in literature[215,217]. Additionally, H9-derived microglia were run in parallel to validate the normalisation technique (Figure S9).

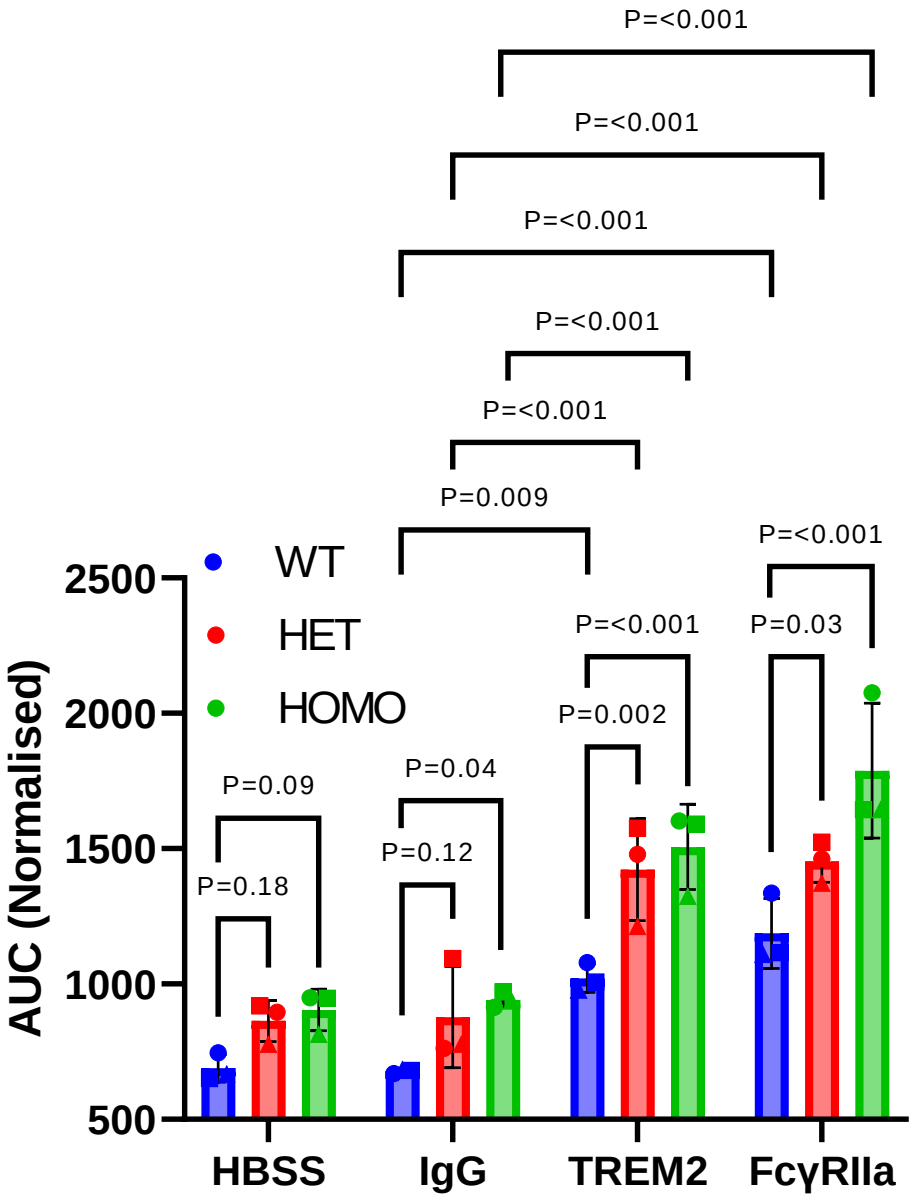

Figure 6.5 PLCγ2 S707Y heterozygous (HET) and homozygous (HOMO) microglia display increased calcium flux. Microglia were differentiated for 7 days before calcium 6 dye was added to the cells. Microglia were stimulated with either HBSS, 10 µg/mL Goat IgG, 10 µg/mL of TREM2 or FCγRIIa before the relative fluorescence units (RFU) were measured on a FLIPR Tetra (Molecular Devices). After the calcium traces had returned to baseline, each well was re-stimulated with 5uM Ionomycin and RFU measured. Experimental area under curve (AUC) calcium data was generated for each condition and normalised to the AUC of the ionomycin re-stimulation. Data represents mean value ± SD, with the graphical symbol shape (triangle, square and circle) representing each set of biological replicates with each biological replicate having at

least three experimental replicates (Dunnett multiple comparisons two-way ANOVA, p-value displayed on the graph, n=3).

6.5 Phagocytosis

Intracellular calcium signalling is important for microglial functions including ramification, migration, phagocytosis and release of cytokines[301]. It is currently unclear to what effect chronic GOF PLCγ2 enzymatic activity, and subsequent calcium flux, has on key microglia functions such as phagocytosis. To explore this, PLCγ2 WT and S707Y hiPSC-derived microglia were challenged with pHrodo labelled apoptotic SH-SY5Y cells (mimicking apoptotic neurons) for 24h, with the experimental data normalised to the total cell number before experimentation (Figure 6.6A). Compared to the initial H9-derived microglia phagocytosis experiment (Figure 5.6), the duration of the assay was increased to 24h so that a greater difference in phagocytosis could be captured. The 24h total red object integrated intensity from the PLCγ2 S707Y heterozygous and homozygous hiPSC-derived microglia was normalised to the WT hiPSC-derived microglia as a percentage change in phagocytosis (Figure 6.6B). The PLCγ2 S707Y derived-microglia showed reduced phagocytosis activity, compared to PLCγ2 WT (Figure 6.6).

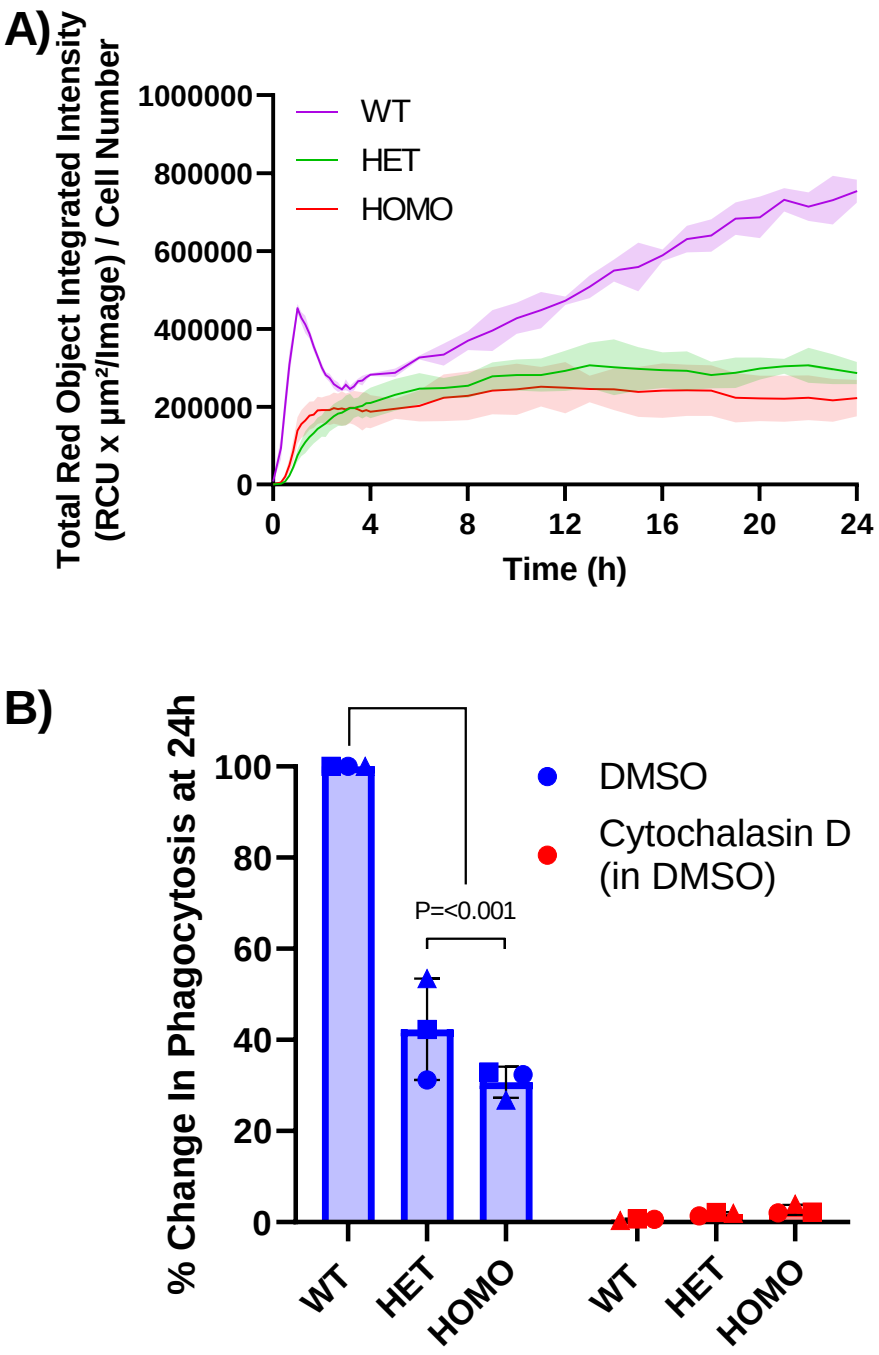

Figure 6.6 PLCγ2 S707Y heterozygous (HET) and homozygous (HOMO) hiPSC-derived microglia exhibit diminished phagocytic activity. **A**) Representative kinetic phagocytosis data of the PLCγ2 S707Y and WT hiPSC-derived microglia from one biological replicate. 1µM Cytochalasin D (0.01% DMSO (v/v)) pre-incubation prevents phagocytic uptake. 0.01% (v/v) DMSO was used as a control for the Cytochalasin D. 'No SH-SY5Y' and 'No microglia cell' experimental conditions were also included (data not shown). Images were captured on the IncuCyte S3 live-cell analysis system (Sartorius) for 24h with the total red object integrated intensity (RCU x µm^2/Image) analysed on the IncuCyte analysis software. Kinetic data was normalised to total cell

number. Data represents mean value ± SD (Area fill). **B**) Quantification of the RCU x μm^2/Image for the PLCγ2 S707Y and WT hiPSC-derived microglia at 24h. Values were normalised to the PLCγ2 WT hiPSC-derived microglia RCU x μm^2/Image. Data represents mean value ± SD, with each graphical symbol shape (triangle, square and circle) representing each set of biological replicates, with each biological replicate having at least three experimental replicates (Dunnett multiple comparisons one-way ANOVA, p-value displayed on the graph, n=3). Representative experimental images of microglia phagocytosis is located in Figure S10.

6.6 Cytokine Secretion

Similar to Figure 5.7, PLCγ2 WT and S707Y hiPSC-derived microglia were stimulated with 1ng/mL LPS for 24h, before cytokine concentration was quantified with the MSD V-PLEX assay platform in accordance with the manufacturer's instructions. Comparing the secreted amounts of INF-γ, IL-1β, IL-6, IL-8, IL-10 and TNF-α from basal (unstimulated) PLCγ2 WT and S707Y hiPSC-derived microglia before LPS stimulation, revealed a subtle increase in IL-1β and TNF-α secretion, as well as a substantial increase in IL-8, for the homozygous variant (Figure 6.7). However, when the cells were challenged with 1ng/mL of LPS for 24h, a reduction in IL-10, IL-6 and TNF-α secretion was observed for the PLCγ2 S707Y hiPSC-derived microglia, compared to PLCγ2 WT (Figure 6.8).

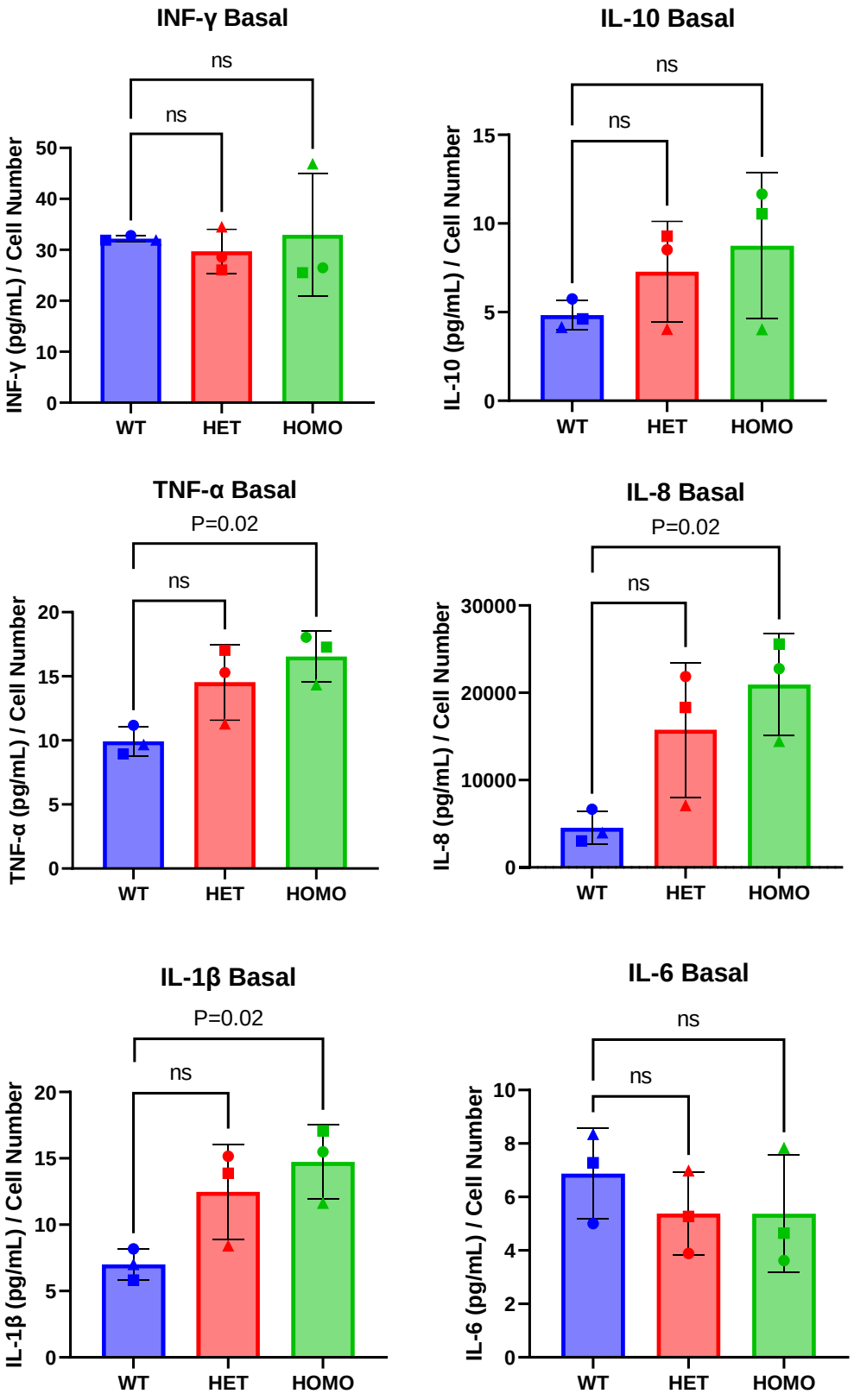

Figure 6.7 Homozygous (HOMO) PLCγ2 S707Y hiPSC-derived microglia secrete elevated levels of basal IL-1β, IL-8 and TNF-α. After 7 days of differentiation, cell supernatant was removed from the PLCγ2 S707Y heterozygous (HET), homozygous (HOMO) and WT hiPSC-derived microglia, before INF-γ, IL-1β, IL-6, IL-8, IL-10 and

TNF-α cytokine concentration was quantified with the MSD V-PLEX Viral Panel 2 (human) kit in accordance with the manufacturer's instructions. Cytokine values were normalised to total cell number captured on the IncuCyte S3 live-cell analysis system. Data represents mean value ± SD, with each graphical symbol shape (square, triangle and circle) representing each set of biological replicates with at least three experimental replicates (Dunnett multiple comparisons one-way ANOVA, p-value displayed on the graph, n=3).

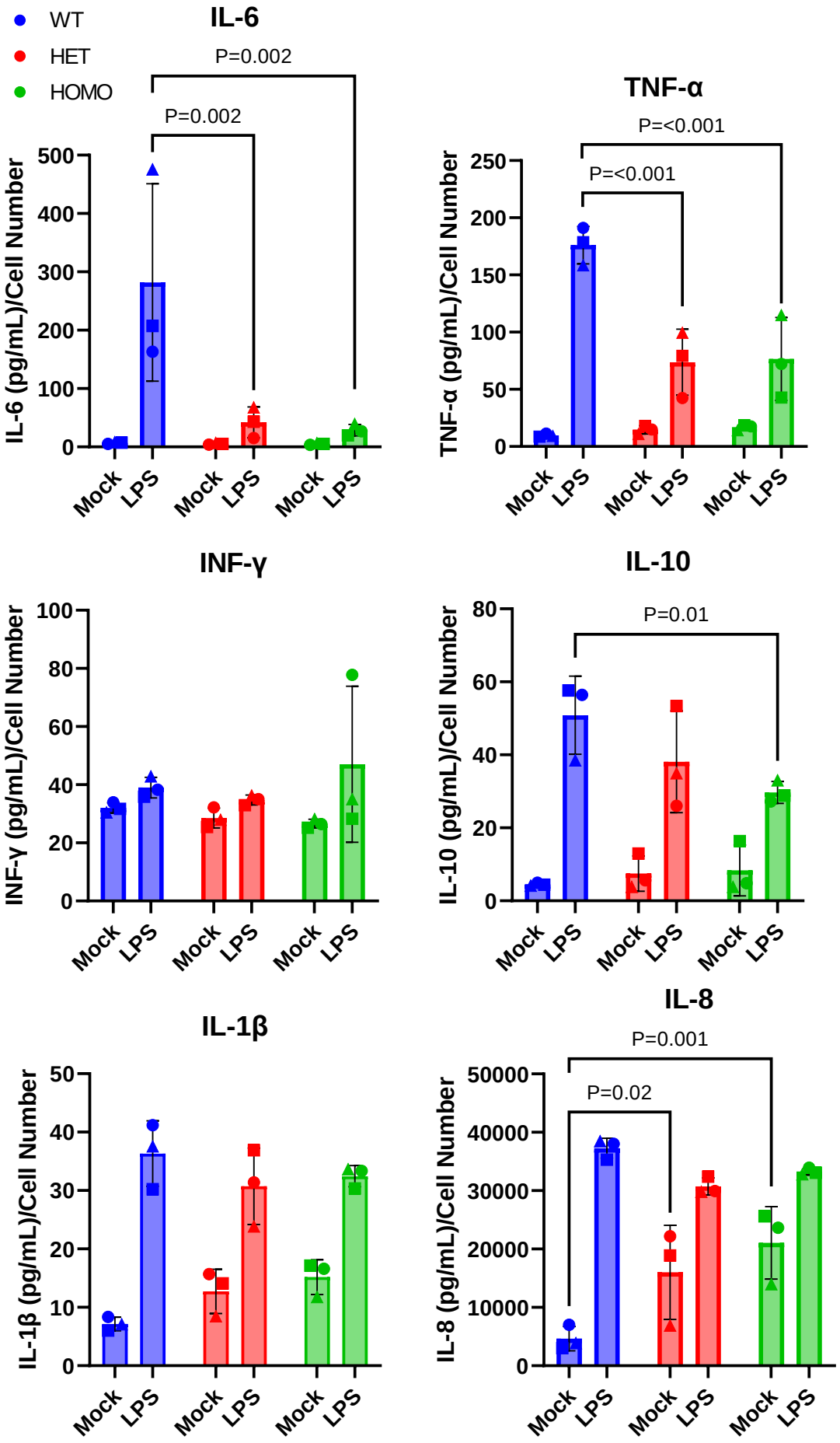
WT
HET
HOMO
IL-6
P=0.002
P=0.002
IL-6 (pg/mL)/Cell Number
500
400
300
200
100
0
Mock
LPS
Mock
LPS
Mock
LPS
TNF-α
P=<0.001
P=<0.001
TNF-α (pg/mL)/Cell Number
250
200
150
100
50
0
Mock
LPS
Mock
LPS
Mock
LPS
INF-γ
INF-γ (pg/mL)/Cell Number
100
80
60
40
20
0
Mock
LPS
Mock
LPS
Mock
LPS
IL-10
P=0.01
IL-10 (pg/mL)/Cell Number
80
60
40
20
0
Mock
LPS
Mock
LPS
Mock
LPS
IL-1β
IL-1β (pg/mL)/Cell Number
50
40
30
20
10
0
Mock
LPS
Mock
LPS
Mock
LPS
IL-8
P=0.001
P=0.02
IL-8 (pg/mL)/Cell Number
50000
40000
30000
20000
10000
0
Mock
LPS
Mock
LPS
Mock
LPS

Figure 6.8 LPS challenged PLCγ2 S707Y heterozygous (HET) and homozygous (HOMO) hiPSC-derived microglia secrete lower levels of IL-10, IL-6 and TNF-α. After 7 days of differentiation, cells were stimulated with ± LPS (1 ng/mL) for 24h. Cell supernatant was removed from the PLCγ2 S707Y heterozygous (HET), homozygous (HOMO) and WT hiPSC-derived microglia, before INF-γ, IL-1β, IL-6, IL-8, IL-10 and TNF-α cytokine concentration was quantified with the MSD V-PLEX Viral Panel 2 (human) kit in accordance with the manufacturer's instructions. Cytokine values were normalised to total cell number captured on the IncuCyte S3 live-cell analysis system. Data represents mean value ± SD, with each graphical symbol shape (square, triangle and circle) representing each set of biological replicates with at least three experimental replicates (Dunnett multiple comparisons two-way ANOVA, only statistically relevant p-values are displayed on the graph, n=3).

6.7 Nuclear factor-kappa B (NF-κB) activation

It has been well documented that microglia exposed to LPS induces IL-6 and TNF-α cytokine production[302]. Although it is not clear which specific pathways mediate the production of these cytokines, the activation of the TLR4-NF-κB classical pathway almost always appears to be implicated[287]. The NF-κB complex (p50 and p65 heterodimer) is sequestered in the cytoplasm by IkappaB (IκB) inhibitory proteins[303]. Phosphorylation and subsequent degradation of IκB proteins, releases the NF-κB complex resulting in phosphorylation of the p65 subunit, allowing the NF-κB complex to be translocated to the nucleus where it regulates gene expression[303]. Given the reduction in LPS mediated cytokine production observed for the PLCγ2 S707Y hiPSC-derived microglia in Figure 6.8, perhaps these phenotypic differences could be explained by differences in NF-κB activation and translocation. WES Western blot analysis displays a reduction in p-NF-κB activation for the PLCγ2 S707Y hiPSC-derived microglia under LPS stimulated conditions (Figure 6.9), with nuclear translocation quantification of NF-κB also displaying a similar pattern (Figure 6.10)

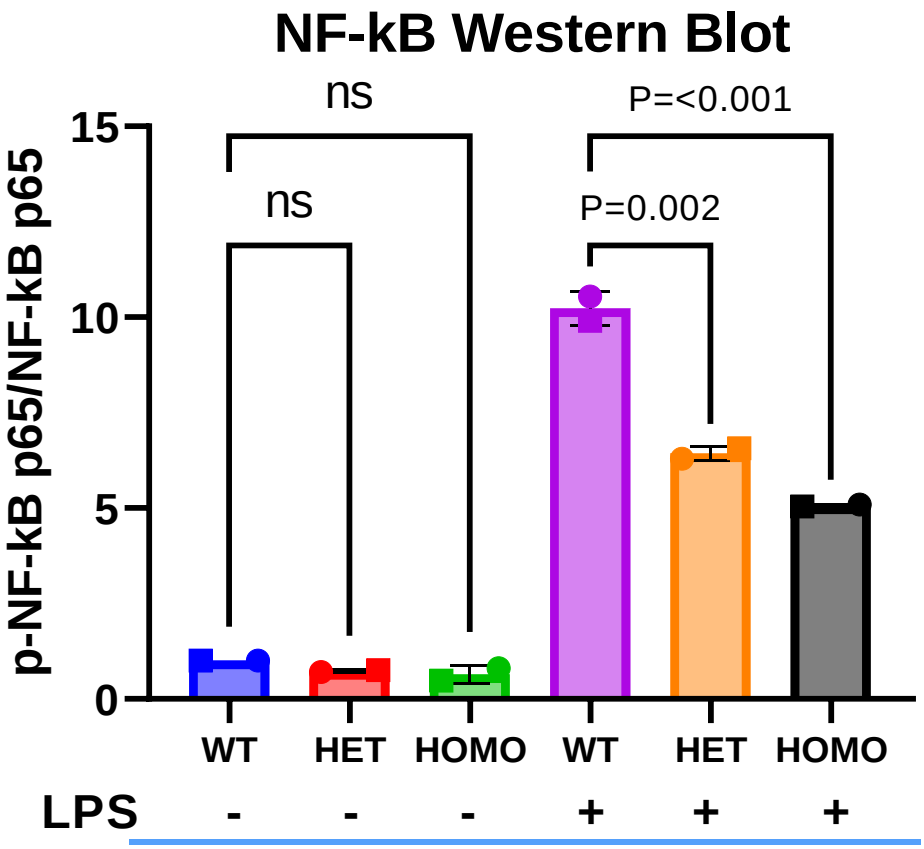

Figure 6.9 NF-κB activation is diminished in the PLCγ2 S707Y hiPSC-derived microglia under stimulated conditions, compared to the PLCγ2 WT hiPSC-derived microglia. Quantification of the relative expression of p-NF-κB p65 normalised to the total NF-κB p65 expression. Cells were stimulated with ± LPS (100ng/mL, 20 min) before being lysed and quantified on the WES Western blot. Expression values were normalised to the PLCγ2 WT hiPSC-derived microglia, without LPS exposure. Data represents mean value ± SD, with each graphical symbol shape (square and circle) representing each set of biological replicates (Dunnett multiple comparisons one-way ANOVA, p-value displayed on the graph, n=2). Representative western blot used for quantification is located in Figure S11.

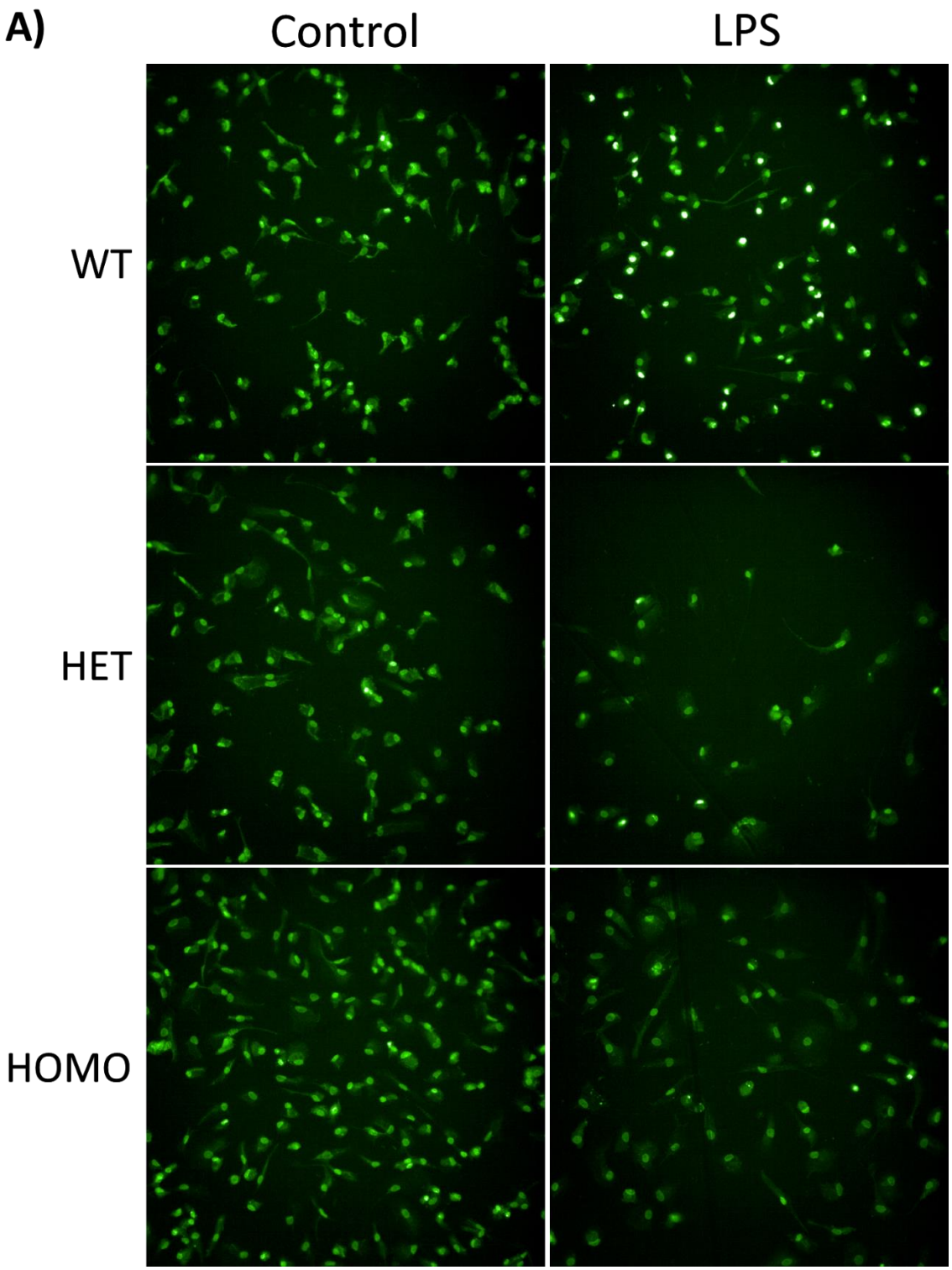
A)
Control
LPS
WT
HET
HOMO

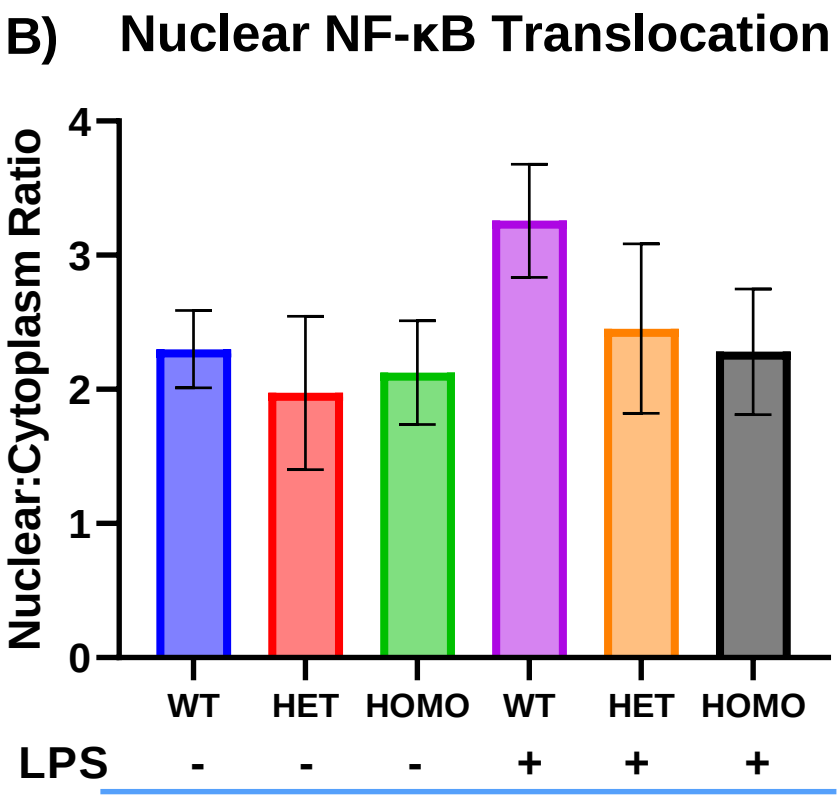

Figure 6.10 NF-κB translocation is diminished in the PLCγ2 S707Y hiPSC-derived microglia under stimulated conditions, compared to the PLCγ2 WT hiPSC-derived microglia. **A)** Representative images of NF-κB (1:400, CST) nuclear translocation of the PLCγ2 S707Y and WT hiPSC-derived microglia, following ± LPS (100ng/mL, 20min) exposure. **B)** Quantification of NF-κB nuclear translocation after ± LPS (100ng/mL, 20min) exposure. Cells were stained for NF-κB before being imaged on the Opera Phenix plus high-content imaging system (Perkin Elmer). NF-κB nuclear and cytoplasm intensity, as well as the NF-κB nuclear/cytoplasm ratio, was measured and calculated through the Columbus software (PerkinElmer). Data represents mean value ± SD, performed from one biological replicate with three experimental replicates (n=1).

6.8 Discussion

When PLCγ2 expression was evaluated in transfected HEK293T cells, the PLCγ2 S707Y variant displayed a reduction in expression relative the PLCγ2 WT (Figure S12). This pattern was also the case for the homozygous PLCγ2 S707Y hiPSC-derived microglia (Figure 6.2). Perhaps the PLCγ2 S707Y variant is influencing the stability of the PLCγ2 cSH2 domain, resulting in a reduction of expression. However, a thermal

shift assay (used to study thermal stabilisation of proteins) would need to be performed in order to confirm this[147]. It was anticipated that the heterozygous PLCγ2 S707Y-derived microglia would also display a similar PLCγ2 expression deficit. However, this was not the case as PLCγ2 expression was significantly increased (Figure 6.2). This result was unexpected and cannot be explained at this time. However, throughout the phenotypic analysis of the hiPSC-derived microglia, this increase in expression did not seem to influence the experimental outcome as mutant-dependent effects were observed.

The PLCγ2 S707Y variant, as well as other PLCγ2 APLIAD variants, have demonstrated elevated inositol phosphate and intercellular calcium release after stimulation due to activation of IP_3R on the endoplasmic reticulum through PLCγ2 mediated IP_3 production[215,224]. The IP_1 and calcium assays show that under basal (HBSS and/or IgG) and stimulated conditions (TREM2 and/or FcγRIIa antibodies) the heterozygous and homozygous PLCγ2 S707Y hiPSC-derived microglia have elevated IP_1 production and intracellular calcium flux relative to PLCγ2 WT (Figure 6.4 and Figure 6.5). Previous IP_1 and calcium experiments with the H9-derived microglia showed TREM2 stimulation to elicit a strong response (Figure 5.4 and Figure 5.5). However, when these experiments were repeated for the H9-derived microglia, as well as the PLCγ2 WT and S707Y hiPSC-derived microglia, TREM2 stimulation elicited a weaker response (Figure 6.4, Figure 6.5 and Figure S9), and as a result dampened the assay signal-window. The manufacturer confirmed that recent batches of TREM2 antibody had insufficient sensitivity in some validated applications. Perhaps with a previous batch of TREM2 antibody, greater simulation differences in the IP_1 and calcium assay would have been observed between the PLCγ2 WT and S707Y hiPSC-derived microglia (Figure 6.4 and Figure 6.5).

The key events in recognition and clearance of dying cells is broadly classified into four steps: recruitment, recognition, engulfment and processing[304]. Perhaps the initial spike of 0-4h in Figure 6.6 is more indicative of the responsive nature (recruitment, recognition, engulfment) of the hiPSC-derived microglia in their ability to "react". However, the 4-24h timepoints may be more characteristic of the processing (degradation) of the substrate and induced gene expression changes. Therefore, perhaps there are multiple interpretations from the experimental data. As a result, the data in Figure 6.6 suggests that the PLCγ2 S707Y hiPSC-derived microglia may lack the ability to recruit, recognise, engulf and process the SH-SY5Y substrate. Furthermore, a 24h

time point was chosen as this is when the greatest differences were observed between the PLCγ2 WT and S707Y hiPSC-derived microglia.

Although apoptotic neurons are one hallmark of AD, Aβ plaques and tau tangles also play significant roles towards neuronal death[284]. As a result, other physiologically relevant substrates such as pHrodo labelled Aβ and tau should also be tested to determine is the same conclusion is reached with different substrates. However, different substrates might activate different pathways. Therefore, it may not be possible to extrapolate conclusions from one substrate to another.

PLCγ2 deficient hiPSC-derived macrophages and hiPSC-derived microglia have demonstrated reduced phagocytic activity when challenged with myelin and apoptotic SH-SY5Y cells[133,183]. Given the hypermorphic nature of the PLCγ2 S707Y variant, it may be expected that an increase in enzymatic activity would result in increased phagocytosis. However, similar to the PLCγ2 KO lines, both the heterozygous and homozygous PLCγ2 S707Y hiPSC-derived microglia displayed deficits in phagocytosis. PIP_2, the substrate of PLCγ2, plays a crucial role in regulating a number of cellular processes or molecules, such as endocytosis, exocytosis, ion channel regulation, actin polymerisation, and more importantly phagocytosis[305–307]. Overexpression of PLCδ-PH domain in RAW macrophage cells resulted in a reduction of phagocytic activity due to the reduced availability of PIP_2[307]. Due to the hypermorphic nature of PLCγ2 S707Y variant under basal conditions, PIP_2 may be depleted in the hiPSC-derived microglia cells, so much so that the cells cannot effectively form phagocytic cups and clear debris[306]. However, further experiments would need to be performed to confirm this.

Before the PLCγ2 WT and S707Y hiPSC-derived microglia were exposed to LPS, cell media was removed, and cytokines quantified. IL-1β and TNF-α were shown to be mildly elevated in the homozygous PLCγ2 S707Y hiPSC-derived microglia, whereas a large increase in IL-8 production was observed for the variant line (Figure 6.7). TNF-α functions to restore brain homeostasis during acute inflammation, acting as a defensive guard to protect against CNS injury, infection, neurodegeneration, and neurotoxicity[308]. However, if secretion of TNF-α becomes chronic, it causes glutamatergic toxicity, excessive gliosis and synaptic loss[308]. Chronic TNF-α secretion has been observed within many degenerative disorders such as AD and Multiple Sclerosis (MS). IL-8 is produced in CNS by neurons, microglia, and astrocytes in response to pro-inflammatory signals. It has been found to be increased in the CSF and brains of AD patients[309].

Furthermore, IL-1β is a master regulator of inflammatory reactions in the immune system, capable of activating innate immunity by inducing the expression of numerous inflammatory cytokines and chemokines[310]. Therefore, given the basal increase in the secretion of IL-8, IL-1β and TNF-α (Figure 6.7), perhaps PLCγ2 APLAID patients are more susceptible to neurodegenerative disorders due to the upregulation of these pro-inflammatory cytokines evoking neuroinflammation. Within microglia and B cells, PLCγ2 has been implicated as a key mediator of NF-κB signalling (Figure 1.4 and Figure 1.5)[286,287]. In fact, PLCγ2 co-expression network analysis of LOAD human microglia identified pathways related to the inflammatory response including regulation of IκB/NF-κB signalling[311]. However, p-NF-κB protein expression and NF-κB nuclear staining confirm that NF-κB activation is unchanged under basal conditions for the PLCγ2 S707Y hiPSC-derived microglia (Figure 6.9 and Figure 6.10), suggesting that perhaps the basal increase in IL-8, IL-1β and TNF-α secretion is mediated through other PLCγ2 cell signalling pathways.

When the PLCγ2 WT and S707Y hiPSC-derived microglia were challenged with LPS, significant decreases in IL-6, IL-10 and TNF-α secretion were observed for the PLCγ2 S707Y hiPSC-derived microglia, compared to PLCγ2 WT (Figure 6.8). LPS activates the TLR4-NF-κB signalling cascade, responsible for the production of the TNF-α and IL-6 pro-inflammatory cytokines, as well as the immunomodulatory cytokine, IL-10[287]. PLCγ2 has been implicated as a key mediator of LPS-TLR4-NF-κB signalling[286]. It is clear from the p-NF-κB protein expression and NF-κB nuclear staining that NF-κB activation and translocation is severely reduced in the S707Y hiPSC-derived microglia upon LPS exposure, compared to the PLCγ2 WT control (Figure 6.9 and Figure 6.10). This reduction in NF-κB activity is likely causative of the decrease in IL-6, IL-10 and TNF-α secretion exhibited in Figure 6.8, demonstrating that perhaps the LPS-TLR4-NF-κB signalling cascade is responsible for IL-6, IL-10 and TNF-α secretion within microglia, and is mediated by PLCγ2. Furthermore, literature has shown TREM2 to regulate TLR4 inflammatory signalling in BV2 cells[312,313]. Perhaps the hypermorphic PLCγ2 S707Y variant facilitates chronic TREM2 signalling, irrespective of TREM2 activation, resulting in the downregulation of TLR4 signalling and subsequent cytokine production.

Upon LPS stimulation, IL-10 secretion was also demonstrated to be diminished from patient PBMCs harbouring the PLCγ2 S707Y variant[216]. Perhaps the lack of secreted IL-10 is causative of the chronic pro-inflammatory state responsible for the APLAID

clinical phenotype, as IL-10 is an anti-inflammatory cytokine responsible for the resolution of inflammation[314]. Furthermore, increased IL-1β secretion was reported in LPS stimulated human PBMCs harbouring the PLCγ2 S707Y variant[217,222]. However, data shown in Figure 6.8 does not correlate with these results. Perhaps this discrepancy could be explained by differences that might exist in PLCγ2 signalling in different cell types.

A limitation of this study is the heterozygous loss of ARID2 has been demonstrated to impair hematopoietic stem and progenitor cell differentiation, as well as upregulate genes associated with inflammatory pathways[315]. Therefore, this heterozygous deletion may have some effect on microglia generation and functionality. Additionally, genomic alteration analysis e.g. g-banding or copy number variation, should also have been performed on the hiPSC lines to confirm that each line is comparable and that any experimental phenotypes are due to the PLCγ2 S707Y variant and not genomic alteration of the hiPSC lines.

6.9 Conclusion

Overall, this chapter demonstrates that the PLCγ2 S707Y variant has hypermorphic enzymatic activity within hiPSC-derived microglia under both basal and stimulation conditions (Figure 6.4), resulting in increased calcium flux (Figure 6.5). However, when then PLCγ2 S707Y hiPSC-derived microglia were challenged with pHrodo labelled apoptotic SH-SY5Y cells, a reduction in phagocytosis was observed (Figure 6.6). Additionally, cytokine secretion of IL-1β, IL-8 and TNF-α was demonstrated to be elevated under basal conditions (Figure 6.7). However, when challenged with LPS PLCγ2 S707Y hiPSC-derived microglia exhibit a reduction in IL-10, IL-6 and TNF-α secretion (Figure 6.8), likely due to decreased NF-κB activation (Figure 6.9). Therefore, this chapter demonstrates that PLCγ2 is a key signalling node for microglial functionality.

Chapter 7 - PLCγ2 influence on microglial gene expression

7.1 Introduction

RNASeq uses next generation sequencing (NGS) to measure the levels of mRNAs in a biological sample to provide insight into the transcriptome of a cell type[316]. Bulk RNASeq of AD human and mouse models has identified transcriptional differences in microglial specific genes, relative to WT controls[317,318]. In fact single cell RNASeq of AD human microglia has identified many subsets of microglia, with each cluster experiencing unique differences in gene expression[110]. Bulk RNASeq of TREM2 and PLCγ2 deficient hiPSC-derived microglia has revealed differences in gene expression related to chemotaxis, specific immune response families, lipid processing and cell survival pathways[133,319]. Moreover, RNASeq has also demonstrated the protective PLCγ2 P522R variant to influence antigen presentation, chemokine signalling and T cell proliferation pathways[320].

RNASeq is clearly a valuable tool for providing insight into a protein, or protein variants role within cellular function. Given that the hypermorphic PLCγ2 S707Y variant influences microglial functionality (Chapter 6), it will be beneficial to characterise what influence the variant has on the microglial transcriptome to support the functional data generated, as well as potentially provide additional insight into the role PLCγ2 has within microglial function.

7.2 Results

7.2.1 Data Analysis

RNA was extracted from PLCγ2 WT and S707Y hiPSC-derived microglia from three separate hematopoietic inductions, at different preMac differentiation ages (early, middle and late). RNA samples were processed by UCL Genomics (UCL, London, England) with RNA integrity number of all samples established to be ≥ 7.8, suitable for NGS. Differentially expressed genes (DEGs) between the PLCγ2 WT and homozygous S707Y samples were analysed through iDEP.951 (integrated Differential Expression and Pathway analysis)[255], as the homozygous variant exhibits the strongest phenotype. A total of 780 DEGs were identified (Figure 7.1A, upregulated in HOMO vs WT: 401 and downregulated in in HOMO vs WT: 379) that crossed the threshold of adjusted p-values (Adj.Pval) ≤ 0.05 and log2 fold change ≥ 0.5, represented in a volcano plot (Figure 7.1B).

Additionally, RNASeq data from Andreone et al., comparing PLCγ2 WT and KO hiPSC-derived microglia was also analysed through the same methodology[133]. A total of 927 DEGs were identified (Figure S13A, upregulated in KO vs WT: 473 and downregulated in KO vs WT: 454), with the DEGs visualised in a volcano plot (Figure S13B). The PLCγ2 KO RNASeq dataset provides a good reference point to compare the data in this study. Of the total 780 DEGs identified in this study, 144 of those hits were also identified in the Andreone et al., study. It should be mentioned that the Andreone et al., study implemented a different media composition to differentiate their hiPSC-derived microglia. Therefore, both studies are not truly comparative. Principle component analysis (PCA) of both datasets is located in Figure S14.

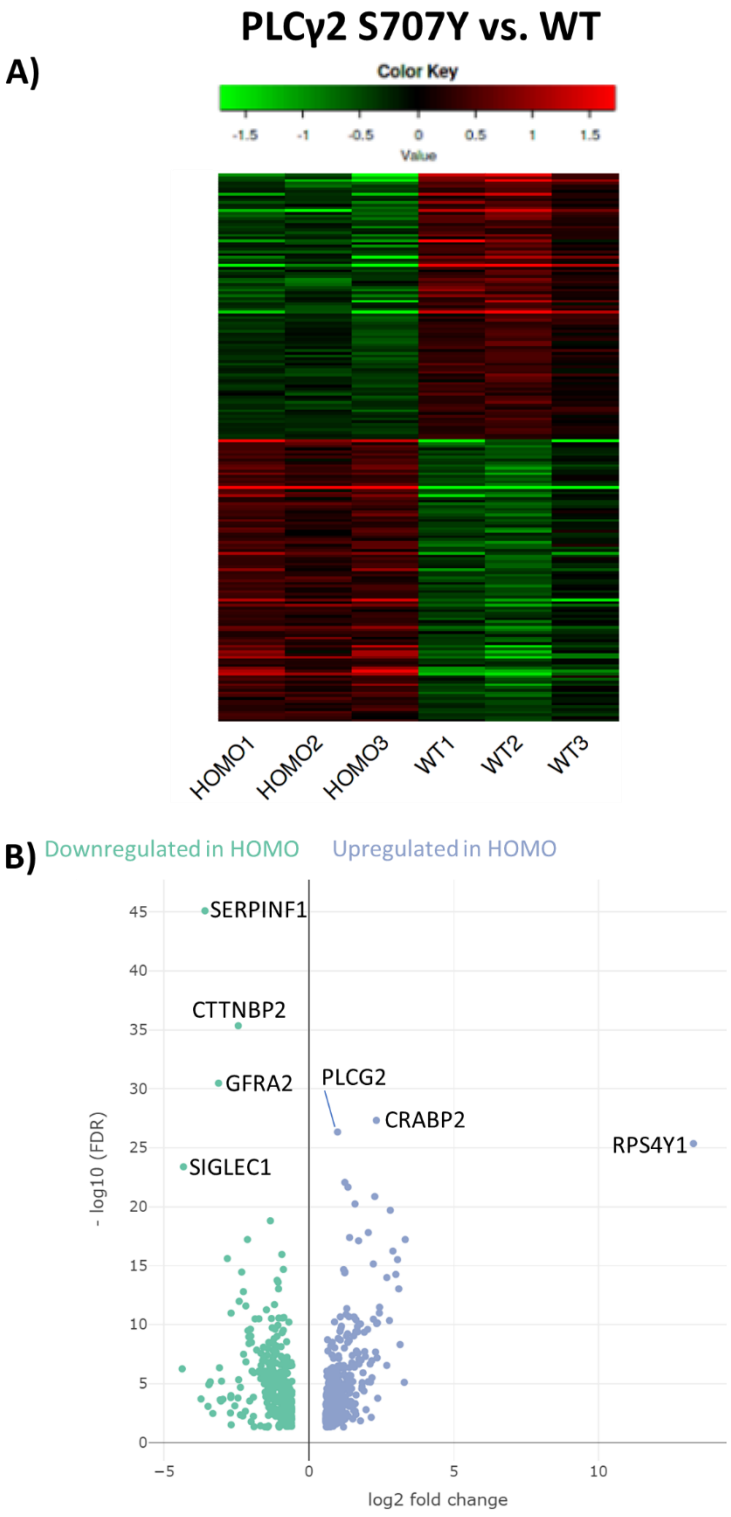

Figure 7.1 PLCγ2 S707Y hiPSC-derived microglia differentially expressed genes (DEGs). **A)** Heatmap of the DEGs downregulated (Green) and upregulated (Red) in the homozygous PLCγ2 S707Y hiPSC-derived microglia, compared to PLCγ2 WT hiPSC-derived microglia. **B)** Volcano plot displaying the DEGs downregulated and upregulated in the homozygous PLCγ2 S707Y hiPSC-derived microglia, compared to PLCγ2 WT hiPSC-derived microglia.

7.2.2 Pathway analysis

Gene ontology (GO) biological process enrichment analysis of the top 10 pathways in homozygous PLCγ2 S707Y hiPSC-derived microglia (compared to PLCγ2 WT hiPSC-derived microglia, Figure 7.2A), shows a upregulation in cell adhesion, but a downregulation in immune processes such as the immune system regulation, as well as immune and inflammatory responses (adj.Pval < 4.20E-10). Using the same analysis process for the Andreone et al., dataset, PLCγ2 KO hiPSC-derived microglia (compared to PLCγ2 WT hiPSC-derived microglia, Figure 7.2B) also displayed an downregulation in immune system processes and responses, as well as leukocyte processes and responses (adj.Pval < 4.70E-35).

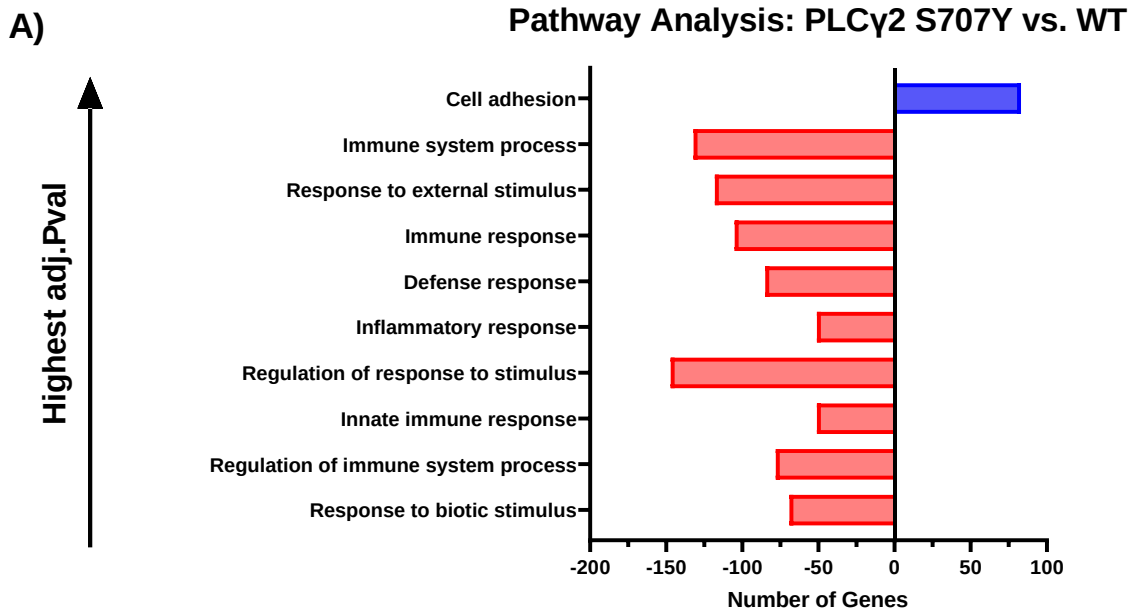

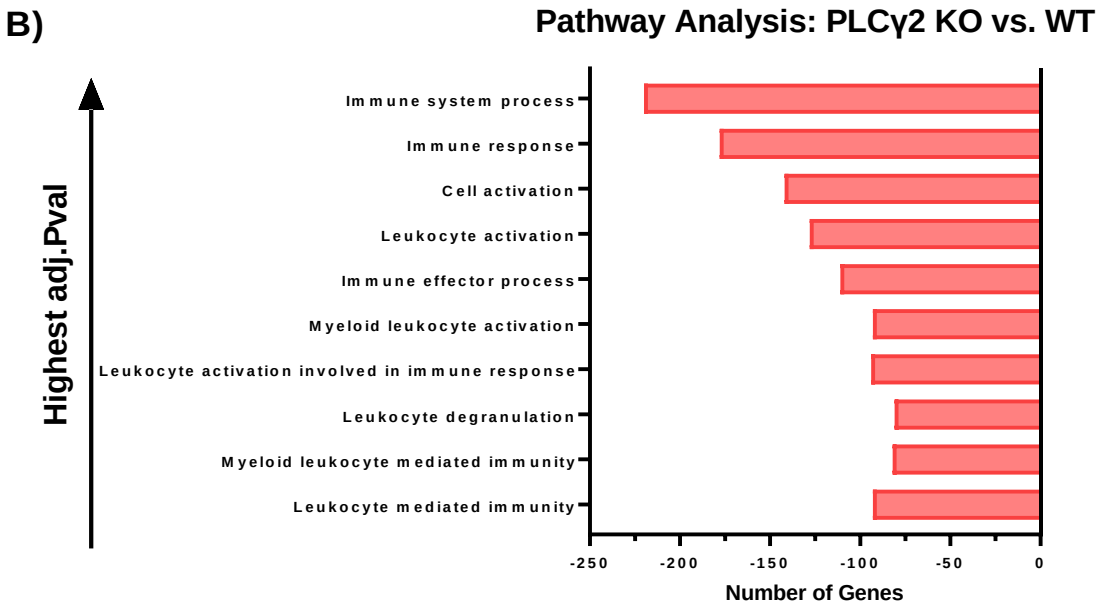

Figure 7.2 Gene Ontology (GO) biological process enrichment analysis of the top 10 upregulated (blue) and downregulated (red) pathways in PLCγ2 S707Y and KO hiPSC-derived microglia. **A)** GO of the homozygous PLCγ2 S707Y hiPSC-derived microglia, compared to PLCγ2 WT hiPSC-derived microglia (adj.Pval < 4.20E-10). **B)** GO of the PLCγ2 KO hiPSC-derived microglia, compared to PLCγ2 WT hiPSC-derived microglia (adj.Pval < 4.70E-35).

Gene Set Enrichment Analysis (GSEA) is a computational method that determines whether a defined set of genes shows statistically significant, concordant differences between two different samples. GSEA quantification of the top 10 pathways in the homozygous PLCγ2 S707Y hiPSC-derived microglia (compared to PLCγ2 WT hiPSC-derived microglia, Figure 7.3A), shows a downregulation of inflammatory and bacterium response (adj.Pval < 9.20E-03). When performing the same GSEA on the Andreone et al., dataset, PLCγ2 KO hiPSC-derived microglia (compared to PLCγ2 WT hiPSC-derived microglia, Figure 7.3B) displayed changes in cell migration, responsiveness and immunity (adj.Pval < 1.80E-03).

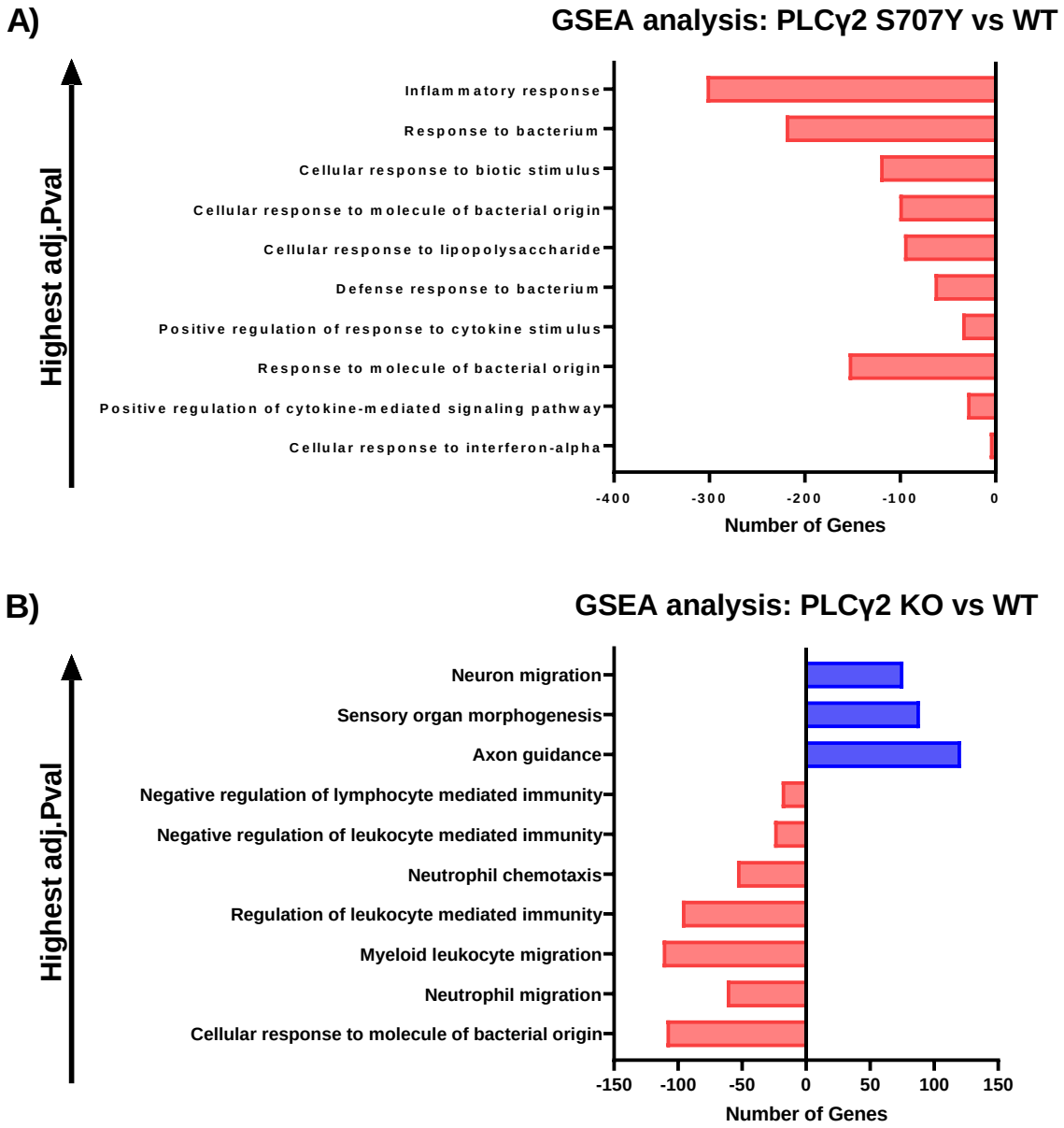

Figure 7.3 Gene Set Enrichment Analysis (GSEA) of the top 10 upregulated (blue) and downregulated (red) GO biological processes in PLCγ2 S707Y and KO hiPSC-derived microglia. **A)** Homozygous PLCγ2 S707Y hiPSC-derived microglia, compared to PLCγ2 WT hiPSC-derived microglia (adj.Pval < 9.20E-03). **B)** PLCγ2 KO hiPSC-derived microglia, compared to PLCγ2 WT hiPSC-derived microglia (adj.Pval < 1.80E-03)[133].

7.2.3 Top differentially expressed genes (DEGs)

Gene	Name	hiPSC-derived microglia PLCγ2 S707Y vs. WT log2 Fold Change	hiPSC-derived microglia PLCγ2 S707Y vs. WT adj.Pval	Description
RPS4Y1	Ribosomal Protein S4 Y-Linked 1	13.28	4.41E-26	The role of RPS4Y1 is unclear. It was demonstrated to be upregulated in pro-inflammatory monocytes[321]
CD163L1	Cluster Differentiation 163 Molecule Like 1	-4.37	5.64E-07	CD163L1 is an endocytic macrophage protein strongly regulated by mediators in the inflammatory response[322]
SIGLEC1	Sialoadhesin	-4.33	4.11E-24	Cell adhesion molecule that participates in antigen presentation and induction of adaptive immune responses[323,324]
FOLR2	Folate Receptor Beta (FRβ)	-3.72	2.02E-04	Mediates the uptake of folate in oxidized form into the cells via endocytosis[325]
SERPINF1	Serpin Family F Member 1 / Pigment Epithelium-Derived Factor (PEDF)	-3.59	8.06E-46	In microglia it is thought PEDF induces pro-inflammatory cytokine production[326]

Table 7.1 Top 5 DEGs (ranked by log2 Fold Change) of the homozygous PLCγ2 S707Y hiPSC-derived microglia, compared to PLCγ2 WT hiPSC-derived microglia. Values > 0 represent upregulation, and < 0 represent downregulation in the homozygous PLCγ2 S707Y hiPSC-derived microglia.

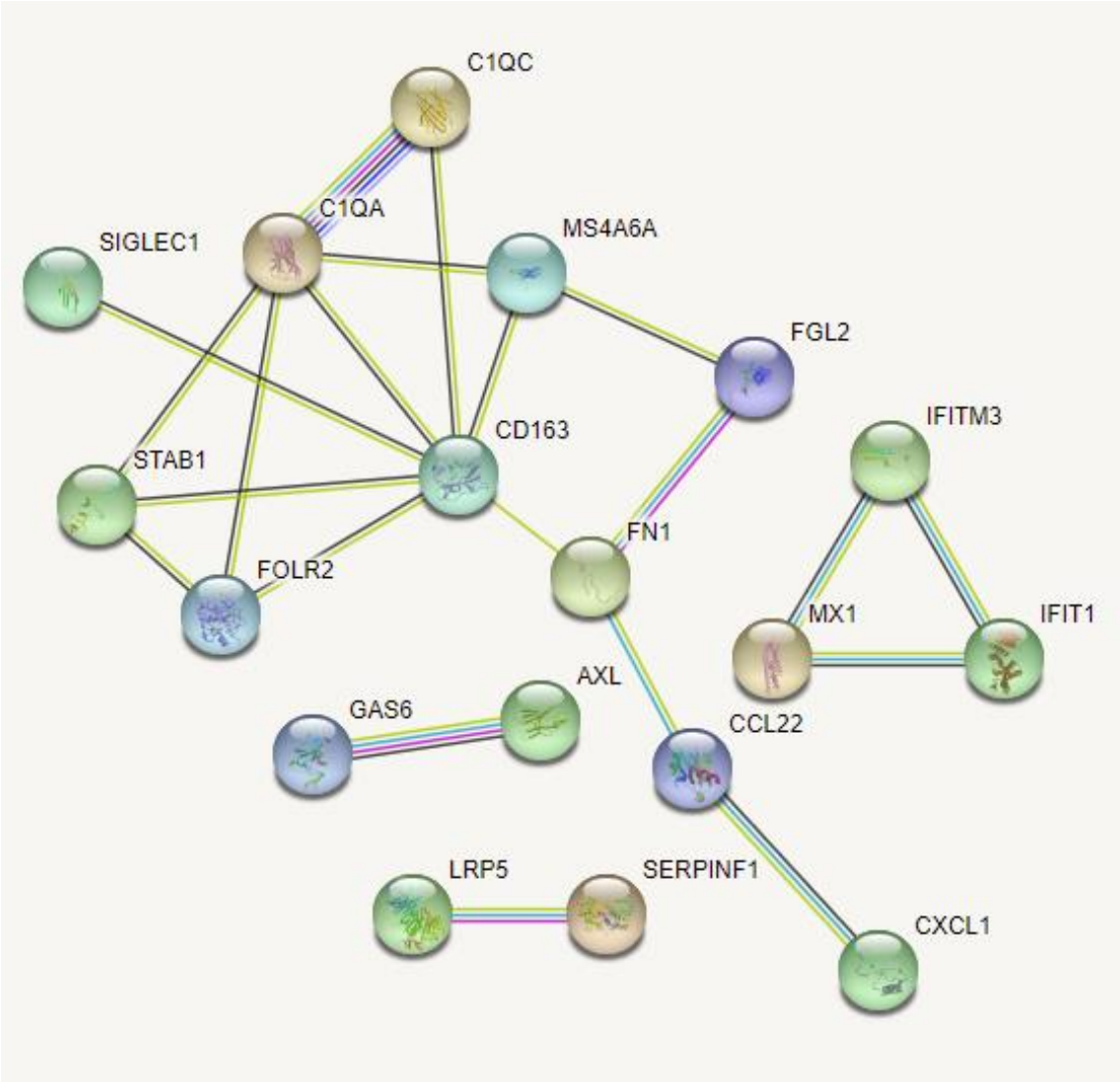

Figure 7.4 STRING (Search Tool for the Retrieval of Interacting Genes/Proteins) analysis of the top 73 DEGs (log2 Fold Change > 2, high confidence > 0.7) for the homozygous PLCγ2 S707Y hiPSC-derived microglia, compared to PLCγ2 WT hiPSC-derived microglia. Protein-protein interaction (PPI) enrichment p-value = 1.81E-12.

The log2 fold change values and Adj.Pval for the top 5 DEGs (ranked by log2 Fold Change) identified in the homozygous PLCγ2 S707Y hiPSC-derived microglia, compared to PLCγ2 WT hiPSC-derived microglia, are summarised in Table 7.1. The raw counts of the top 5 DEGs are located in Figure S15. Additionally, STRING (Search Tool for the Retrieval of Interacting Genes/Proteins) analysis of the top 73 DEGs (log2 Fold Change > 2) predicted multiple protein–protein interactions (PPI, Figure 7.4).

7.2.4 DEGs of interest

Gene	hiPSC-derived microglia PLCγ2 S707Y vs. WT log2 Fold Change	hiPSC-derived microglia PLCγ2 S707Y vs. WT adj.Pval	hiPSC-derived microglia PLCγ2 KO vs. WT log2 Fold Change	hiPSC-derived microglia PLCγ2 KO vs. WT adj.Pval
CD163	-2.18	2.59E-12	-0.94	7.06E-07
IFIT1	-2.70	1.56E-04	-	-
IFITM3	-2.26	3.25E-08	-	-
MX1	2.36	4.54E-03	-	-
GAS6	-2.41	1.05E-12	-	-
AXL	-2.26	1.60E-13	-	-
MERTK	-0.81	1.53E-03	-	-
P2RY6	-2.42	4.69E-06	-	-
C1QA	-2.07	4.04E-09	-0.72	4.04E-02
C1QB	-1.90	1.21E-06	-	-
C1QC	-2.10	3.23E-10	-	-
C3	-1.24	1.52E-08	-	-
C3AR1	-0.97	1.46E-06	-1.22	4.58E-04
LPL	1.20	4.85E-02	-2.55	9.78E-26
PLIN2	-1.63	1.37E-06	-	-

Table 7.2 DEGs of interest from homozygous PLCγ2 S707Y hiPSC-derived microglia, compared to PLCγ2 WT hiPSC-derived microglia. Function colour coded - Orange: Type I interferon signalling, Green: Phagocytosis receptors and proteins, Yellow: Complement proteins, and Grey: Lipid processing. (-) abbreviation indicates that the gene did not pass the threshold of analysis. The raw counts of the DEGs are located in Figure S16.

PLCγ2 KO hiPSC-derived microglia and macrophages display a reduction in phagocytic activity, compared to their PLCγ2 WT counterparts[133,183]. Additionally, PLCγ2 S707Y hiPSC-derived microglia also displayed similar deficiencies (Figure 6.6). Growth arrest specific 6 (GAS6) and its binding to the TAM family of receptor tyrosine kinases (TYRO3, AXL and MERTK) is crucial for cytoskeletal rearrangement and the phagocytic engulfment of apoptotic cells and Aβ plaques[327,328]. Additionally, the purinergic receptor P2Y6 (P2RY6) has been demonstrated to play a crucial role in the phagocytosis of stressed and damaged neurons[329]. Given the downregulation of GAS6, AXL, MERTK and P2RY6 observed for the PLCγ2 S707Y hiPSC-derived microglia, perhaps this downregulation is causative of the lack of phagocytosis observed (Table 7.2), as the cells are unable to respond effectively.

Network analysis of APOE, TREM2 and PLCγ2, known AD risk genes, revealed shared co-expression of biological processes related to immune system processes including the complement cascade activation: complement component 1qA (C1QA), complement component 1qB (C1QB) and complement component 3 (C3), suggesting that the complement pathway plays a role in AD pathogenesis[228]. PLCγ2 KO primary mouse microglia and hiPSC-derived microglia have also demonstrated downregulation in complement protein expression[133,311]. It is demonstrated here that the PLCγ2 S707Y variant also downregulates (C1QA, C1QB, C3, complement component 1qC (C1QC) and complement C3a receptor 1 (C3AR1)) complement protein expression (Table 7.2), suggesting that perhaps PLCγ2 plays a role in regulating the expression of complement proteins. As the complement pathway has been demonstrated to be vital for the phagocytosis of apoptotic cells[330], the downregulation of these proteins in the PLCγ2 S707Y hiPSC-derived microglia also could explain the effect on phagocytosis observed (Figure 6.6).

7.2.5 Microglial Identity

Mirroring the same genetic markers from Figure 5.2, the PLCγ2 WT and S707Y hiPSC-derived microglia were assessed for known microglia and myeloid markers. Overall, there appears to be good expression of known microglia and myeloid markers for the PLCγ2 WT and S707Y hiPSC-derived microglia, validating the model as physiologically relevant (Figure 7.5). iDEP analysis identified differences in SLC2A5, CD14, ITGAM and PLCγ2 expression between the PLCγ2 S707Y and WT hiPSC-derived microglia (Figure 7.5). Although differences in PLCγ2 RNA expression were

identified, it should be stated that RNA differences do not always correlate to protein expression[331,332]. It is clear from Figure 6.2 that the PLCγ2 protein expression does not correlate with the RNASeq data, as the homozygous S707Y hiPSC-derived microglia has decreased PLCγ2 expression relative to the WT. However, for SLC2A5, CD14 and ITGAM, protein expression would need to be characterised in order to validate the RNASeq findings.

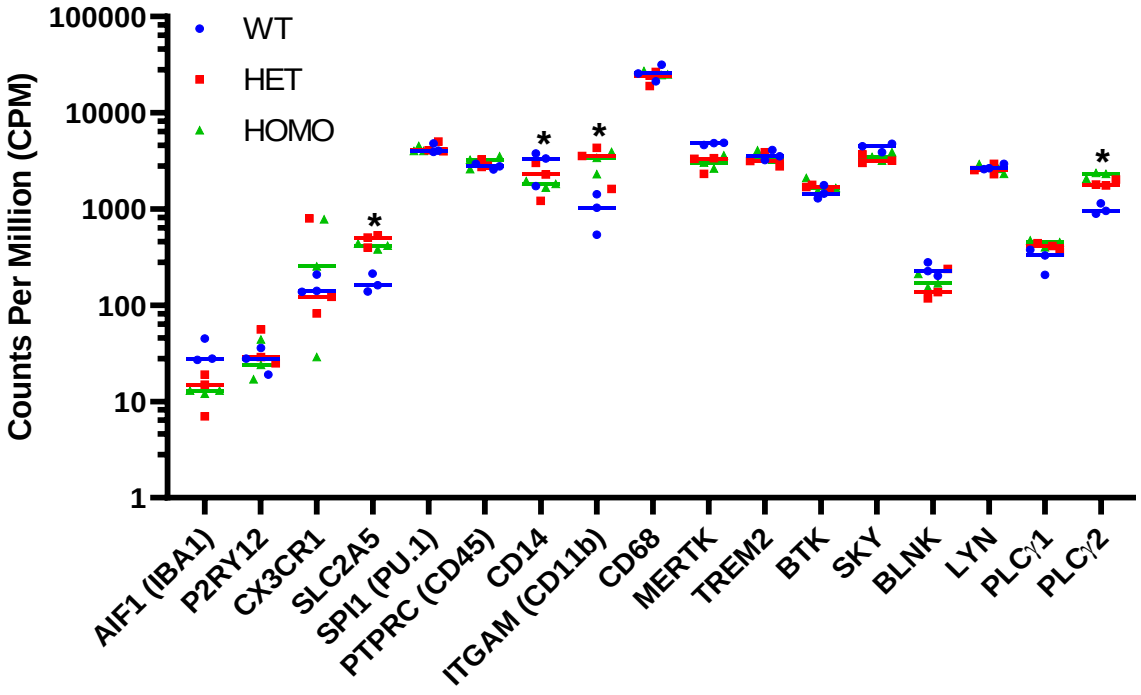

Figure 7.5 Comparison of the difference in gene expression between the PLCγ2 WT and S707Y heterozygous (HET) and homozygous (HOMO) hiPSC-derived microglia. The graphical line indicates the mean for three biological replicates (n=3). (*) symbol indicates statistical difference (adj.Pval < 5E-02) between the homozygous PLCγ2 S707Y and WT hiPSC-derived microglia.

7.3 Discussion

GO biological process enrichment analysis and GSEA of both PLCγ2 S707Y and KO hiPSC-derived microglia clearly show changes in pathways related to immune cell function (Figure 7.2 and Figure 7.3). This downregulation may explain the observed decreases in microglial response to apoptotic cells and LPS for the PLCγ2 S707Y hiPSC-derived microglia (Figure 6.6 and Figure 6.8), implicating PLCγ2 as a key mediator of microglia functionality.

Of the top 5 DEGs, the functions of ribosomal protein S4 Y-linked 1 (RPS4Y1), folate receptor beta (FOLR2) and serpin family F member 1 (SERPINF1) are not well

characterised, especially in the context of macrophage and microglial biology. Folate Receptor Beta (FRβ) has been suggested to act as a receptor or co-receptor for recognition of bacterial microbiota, similar to CD14, but further investigation is still needed[333]. Ribosomal proteins play an essential role in ribosome biogenesis and protein production[334]. However, it is believed that ribosomal proteins have ribosome-independent functions[334]. Although the specific ribosome-independent function of RPS4Y1 has yet to be characterised, other ribosomal proteins have been demonstrated to participate in the innate immune response by regulating NF-κB transcription[334]. Given the significant upregulation of RPS4Y1 in the PLCγ2 S707Y hiPSC-derived microglia, perhaps RPS4Y1 also plays a role in NF-κB regulation as p-NF-κB and NF-κB translocation was shown to be diminished (Figure 6.9 and Figure 6.10).

Even though cluster of differentiation 163 molecule like 1 (CD163L1) was identified as one of the top DEGs, STRING analysis also identified CD163 (cluster of differentiation 163) as an influential gene (Figure 7.4). CD163L1 exhibits similarities to CD163 in terms of structure and expression, but distinct differences in functionality e.g. bacterial binding do exist[322]. CD163 has long been considered a myeloid specific marker with an anti-inflammatory role, by regulating the secretion of IL-10 upon activation[335,336]. CD163 expression was shown to be downregulated by pro-inflammatory cytokines such as IL-1β, IL-8 and TNF-α[337]. Perhaps the increased secretion of these pro-inflammatory cytokines exhibited by the PLCγ2 S707Y hiPSC-derived microglia at the basal level (Figure 6.7), results in the downregulation of CD163 (Table 7.1), subsequently resulting in less IL-10 secretion upon activation, as observed in Figure 6.8. As mentioned previously, perhaps the decrease in secreted IL-10, mediated presumably by the downregulation of CD163, is indicative of the chronic pro-inflammatory state responsible for the peripheral APLAID clinical phenotype, as IL-10 is an anti-inflammatory cytokine involved in the resolution of inflammation[314]. Additionally, PLCγ2 KO hiPSC-derived microglia also exhibit similar downregulation of CD163 (Table 7.2), suggesting that perhaps CD163 expression is modulated by PLCγ2.

Additionally, sialic acid-binding immunoglobulin-type of lectin 1 (SIGLEC1, also known as sialoadhesin) was also identified as one of the top DEGs (Table 7.1). Sialoadhesin contains a long immunoglobulin domain that is thought to be important for cell adhesion and pathogen recognition[338]. Sialoadhesin expressing microglia have been suggested to serve as antigen-presenting cells that interact with CD8+ T cells to initiate the adaptive immune response[338]. Perhaps the downregulation of sialoadhesin exhibited

by the PLCγ2 S707Y hiPSC-derived microglia is causative of a lack of CD8+ T cell response, due to the lack of antigen presentation, resulting in a reduced adaptive immune response. Given that the PLCγ2 P522R LOAD protective variant has been reported to promote the recruitment of CD8+ T cells to the brain, perhaps PLCγ2 plays a role in the recruitment of CD8+ T cells to the brain[320]. However, it is not clear if this increased recruitment of CD8+ T cells is protective or damaging in the context of neurodegenerative disease, especially given that CD8+ T cells are also elevated in human AD brains[320,339].

STRING analysis identified a good correlation between interferon-induced protein with tetratricopeptide repeats 1 (IFIT1), interferon-induced transmembrane protein 3 (IFITM3) and MX dynamin like GTPase 1 (MX1), all of which are commonly induced by type I interferon signalling (Figure 7.4 and Table 7.2)[340,341]. Given that type I interferon signalling has been demonstrated to drive neuroinflammation and synapse loss in AD, perhaps PLCγ2 is a key mediator of this pathway[342]. However, further experiments would need to be performed.

With the cholesterol carrier APOE being an important genetic risk factor for AD, defective lipid clearance has been implicated as a central driver of AD pathogenesis[343]. RNASeq analysis of TREM2 KO and PLCG2 KO hiPSC derived-microglia showed downregulation of lipid processing genes, such as lipoprotein lipase (LPL) and perilipin 2 (PLIN2), resulting in an inability to clear cholesterol esters[133]. Contrary to the PLCγ2 KO hiPSC-derived microglia study, the PLCγ2 S707Y hiPSC-derived microglia displayed an upregulation of LPL (Table 7.2). Given the linear upregulation pattern of LPL gene transcription, PLCγ2 HOMO>WT>KO (Table 7.2), perhaps heightened basal PLCγ2 enzymatic activity results in greater lipoprotein processing due to the upregulation of LPL. However, PLIN2 was downregulated in PLCγ2 S707Y hiPSC-derived microglia (Table 7.2). Deficits in PLIN2 expression around Aβ plaques have also been reported in TREM2 R47H hiPSC-derived preMacs transplanted into mouse brain[344], suggesting that PLIN2 is a potential mediator of AD. Given that PLCγ2 appears to influence PLIN2 expression, perhaps its relationship needs to be further explored. Furthermore, Andreone et al,. cited the downregulation of multiple lipid processing genes for the PLCγ2 KO hiPSC-derived microglia. However, reanalysis of the RNASeq data only confirmed downregulation of LPL.

During development, C1q and C3 localise to neuronal synapses and mediate synapse elimination by phagocytic microglia[345]. Inhibition of C1q and C3 has been demonstrated to reduce the phagocytic capability of microglia, rescuing synaptic loss and dysfunction[346]. Moreover, C3aR1 has been suggested to be a major regulator of microglia reactivity and neuroinflammatory function, with expression of C3aR1 and C3 positively correlated with cognitive decline[347,348]. Interestingly, both PLCγ2 KO and S707Y hiPSC-derived microglia displayed significant downregulation of complement genes (Table 7.2). However, it is not clear from literature if this downregulation is beneficial or detrimental in the context of neurodegeneration[349]. In the case of the PLCγ2 S707Y hiPSC-derived microglia, perhaps the decreased phagocytic activity and cytokine production as shown in Figure 6.6 and Figure 6.8 is due to the downregulation of these complement proteins.

CD14 has been demonstrated to be essential for transporting LPS to the TLR4 signalling complex, as well as regulate TLR4 endocytosis[178]. Given the lack of cytokine secretion observed for the PLCγ2 S707Y hiPSC-derived microglia upon LPS stimulation (Figure 6.8), perhaps the downregulation of CD14 for the PLCγ2 S707Y hiPSC-derived microglia (Figure 7.5) is responsible for this phenotype. Additionally, PLCγ2 KO hiPSC-derived macrophages have been demonstrated to possess deficits in ITGAM expresison[183]. However, ITGAM was shown to be upregulated for the PLCγ2 S707Y hiPSC-derived microglia (Figure 7.5). Given that ITGAM expression is correlated with the activation state of microglia, it could suggest that hypermorphic PLCγ2 variants place microglia into a chronically activated state[350].

7.4 Summary

RNASeq pathway analysis clearly demonstrates that PLCγ2 has a regulatory role on microglia immune pathways and responses (Figure 7.2 and Figure 7.3). Analysis of the DEGs illustrates that PLCγ2 can influence many microglial cellular processes, specifically phagocytosis and the complement pathway (Table 7.2). As a result, the reduction in phagocytosis observed for the PLCγ2 S707Y hiPSC-derived microglia (Figure 6.6) may be due to the downregulation of complement proteins and TAM receptors, which are required for phagocytic function. Furthermore, the downregulation of genes related to bacterium response is perhaps causative of the reduction in cytokine production observed for PLCγ2 S707Y hiPSC-derived microglia (Figure 6.8). Other transcriptome differences were also identified from the PLCγ2 S707Y hiPSC-derived microglia, which require further confirmation and exploration.

Chapter 8 - Concluding remarks

8.1.1 Thesis overview

The aim of this thesis was to investigate the effect that disease-linked PLCγ2 variants have on enzymatic activity, as well as explore the role PLCγ2 has within microglia cell function. Recently, several rare and novel disease-linked PLCγ2 variants have been identified. However, there has been minimal characterisation into what effect each variant has on enzymatic activity and how this results in the APLAID phenotype. Through the use of a standard transient transfection assay to assess PLC mediated IP_1 accumulation, the enzymatic activity of the rare and novel Δ845-848, M1141K and V1103I PLCγ2 variants was assessed. Furthermore, as multiple PLCγ2 variants were assessed through same assay, it allowed for each tested PLCγ2 variant to be ranked based on activity (Table 4.1). The Δ845-848 and M1141K PLCγ2 variants displayed strong hypermorphic activity, whereas the PLCγ2 V1103I variant caused a mild increase in PLC activity. These findings, together with clinical data, support the concept that the increase in variant enzymatic activity contributes to the clinical APLAID phenotype.

From the generation of PLCγ2 KO and P522R hiPSC-derived microglia, PLCγ2 has been shown to have a key role within microglial functionality[133,226]. Recent publications have shown PLCγ2 to mediate microglial calcium signalling, cytokine production, phagocytosis and motility[133,183,204]. Characterisation of the LOAD protective PLCγ2 P522R variant shows it to be mildly hypermorphic under stimulated conditions, resulting in increased calcium flux[139,226]. However, how this increased enzymatic activity influences key microglial functions, such as phagocytosis, is still not clear as substrate-dependent phagocytic differences have been observed[226,227]. Despite the recent studies, there are still further questions regarding the effect the PLCγ2 P522R variant has on microglia, and more importantly, how it is protective against LOAD.

In order to better understand the role that hypermorphic PLCγ2 variants have within microglia function, as well as complement other studies, a human stem cell-derived microglia differentiation protocol was established to allow for the development and optimisation of functional assays to assess PLC enzymatic activity and PLC-mediated microglia functionality. As there are currently no specific small molecule compounds to selectively modulate PLCγ2 activity, the hypermorphic PLCγ2 S707Y variant was introduced into stem cell-derived microglia through genetic manipulation, to study the

effects of promoting chronic enzymatic activity on microglia function, as this variant elicits a more hypermorphic effect than the subtle effect produced by the PLCγ2 P522R variant.

Through the use of PLCγ2 WT and S707Y (heterozygous and homozygous) hiPSC-derived microglia, it was confirmed that enzymatic activity and calcium flux was elevated in PLCγ2 S707Y hiPSC-derived microglia under both basal and stimulated conditions (Figure 6.4 and Figure 6.5), as demonstrated in human PBMCs harbouring the polymorphism[215]. Furthermore, IL-1β, IL-8 and TNF-α secretion was shown to be elevated for the PLCγ2 S707Y hiPSC-derived microglia under basal conditions (Figure 6.7). However, following LPS exposure a reduction in IL-10, IL-8 and TNF-α secretion (Figure 6.8) was observed for the PLCγ2 S707Y hiPSC-derived microglia, likely due to the lack of NF-κB activation and translocation (Figure 6.9 and Figure 6.10). Additionally, a decrease in phagocytosis was observed for the PLCγ2 S707Y hiPSC-derived microglia following exposure to apoptotic pHrodo labelled SH-SY5Y cells (Figure 6.6)

RNASeq was performed to provide insight into the transcriptome differences between the PLCγ2 WT and S707Y hiPSC-derived microglia to suggest molecular changes underpinning functional differences, as well as enhance the interpretation of the phenotypic results. RNASeq analysis showed a downregulation in immune system regulation and responses in the PLCγ2 S707Y hiPSC-derived microglia compared to WT (Figure 7.2 and Figure 7.3), supporting the functional results. Together, this thesis demonstrates several novel phenotypic findings, and further emphasises the important role that PLCγ2 plays within microglia function.

8.1.2 The spectrum of protective vs. detrimental PLCγ2 polymorphisms

Literature shows that within the periphery strong hypermorphic PLCγ2 variants (e.g. S707Y) cause detrimental phenotypes that result in APLAID[216]. Perhaps the increased basal secretion of the IL-1β, IL-8 and TNF-α pro-inflammatory cytokines observed from the PLCγ2 S707Y hiPSC-derived microglia (Figure 6.7) could also translate to the PBMCs, whereby chronic inflammation caused by these pro-inflammatory cytokines results in the associated APLAID phenotype. Additionally, the lack of IL-10 cytokine secretion upon activation displayed from the PLCγ2 S707Y hiPSC-derived microglia (Figure 6.8) could result in an inability to control inflammation, thus facilitating chronic inflammation. Therefore, perhaps the combination of both the basal and activated

phenotypes contributes to APLAID for patients harbouring the PLCγ2 S707Y variant, as documented in the periphery[215].

RNASeq pathway analysis demonstrates that both the PLCγ2 S707Y and KO hiPSC-derived microglia display deficits in immune system processes and responses (Figure 7.2 and Figure 7.3), providing further evidence that PLCγ2 is a central node for immune cell function[204]. Given the partial overlap in effects produced by both the PLCγ2 KO and S707Y variant, perhaps strong hypermorphic PLCγ2 variants also place microglia in an unresponsive state, similar to the PLCγ2 KO. Literature has shown PLCγ2 KO hiPSC-derived microglia and macrophages to display deficits in IP_1 production, calcium response, CD11b (ITGAM) expression, cell adhesion, phagocytosis and lipid processing (e.g. downregulation of LPL)[133,183]. Amongst these phenotypes, PLCγ2 S707Y hiPSC-derived microglia also exhibit deficits in phagocytosis, despite the increased IP_1 accumulation and calcium flux. However, RNASeq analysis shows ITGAM and LPL expression (Figure 7.5 and Table 7.2), as well as cell adhesion pathways (Figure 7.2A) to be upregulated, suggesting that the PLCγ2 S707Y variant does not completely overlap with the PLCγ2 KO phenotype. However, the increase in mRNA expression may not correlate to protein expression[351], and as such further work into the role PLCγ2 S707Y has on lipid processing (through liquid chromatography-mass spectrometry), as well as cell adhesion needs to be investigated.

The question remains, given that PLCγ2 APLAID GOF variants promote a peripheral autoinflammatory phenotype, why when the PLCγ2 S707Y variant is introduced into hiPSC-derived microglia it appears to dampen the immune response upon activation? The majority of hypermorphic PLCγ2 variant characterisation has been performed in the context of the periphery, specifically B-cells, where the blocking of B-cell differentiation, as well as chronic inflammation accompanied by expansion of innate inflammatory cells, has been documented[204,207,215,352]. However, microglial machinery most likely differs from peripheral myeloid cells and leukocytes. For instance, increased IL-1β and TNF-α secretion was reported in LPS stimulated human PBMCs harbouring APLAID variants[217,222]. However, when repeated in the hiPSC-derived microglia, no change in IL-1β secretion, as well as a decrease in TNF-α secretion was observed (Figure 6.8). Therefore, PLCγ2 could be influencing different signalling cascades within microglial function compared to peripheral immune cells, or PLCγ2 modulation could be dependent on a different cellular environment and/or cell state.

RNASeq identified the downregulation of several complement pathway proteins (C1QA, C1QB, C1QC, C3 and C3AR1) and phagocytic receptors (AXL, MERTK and P2RY6) in the PLCγ2 S707Y hiPSC-derived microglia (Table 7.2). The complement pathway has been recognised as an essential component of microglial synaptic pruning and therefore brain development[353]. It has been postulated that a downregulation of synaptic pruning during development could contribute to neuronal hyperconnectivity and behavioural changed[353]. However, inhibition of C1q, C3 or the microglial complement receptor CR3 (consisting of ITGAM and CD18) has been shown to reduce the number of phagocytic microglia, as well as rescue synaptic loss and dysfunction in neurodegeneration[346]. Furthermore, activation of P2YR6 has been demonstrated to contribute to neurodegeneration through the phagocytosis of viable neurons, induced by Aβ and Tau[354]. P2YR6 knockout mice models have shown to counteract this effect, reducing neuronal loss and memory deficits induced by Aβ and Tau[354]. Due to the rarity of PLCγ2 GOF variants, the cognitive phenotypes of patients harbouring these variants has not been documented, nor explored[204]. Perhaps the drastic downregulation of proteins involved in the complement pathway, as well as P2YR6, exhibited from the PLCγ2 S707Y hiPSC-derived microglia might be protective against synapse loss. However, perhaps this dampened functional phenotype could also be detrimental as it could lead to ineffective toxic protein aggregate clearance, as well as dysfunctional brain development.

As mentioned previously in 1.6.3, the PLCγ2 P522R variant has been demonstrated to be protective against LOAD, as well as to correlate with human longevity. However, the mechanisms underlying the protective function are still not well understood. Substrate dependent differences in phagocytosis have been demonstrated for the PLCγ2 P522R variant[226]. Moreover, both an increase and a decrease in pHrodo-labelled-zymosan phagocytosis has been documented for the PLCγ2 P522R variant from two separate studies, further adding to the confusion[226,227]. Golde et al, suggested that perhaps pushing any system too far in one direction has the potential to do more harm than good for the treatment of neurodegenerative disorders[355]. Therefore, perhaps the PLCγ2 P522R variant lies in the “Goldilocks” zone (Figure 8.1), whereby the mild hypermorphic activity benefits immune function, but is not detrimentally impacting the immune response as observed for the strong hypermorphic PLCγ2 S707Y variant and the PLCγ2 deficient hiPSC-derived microglia (Figure 7.2 and Figure 7.3). Based off the experimental data generated for the PLCγ2 S707Y hiPSC-derived microglia, it may be

that the P522R variant protects by downregulating phagocytosis and inflammation. However, further studies would be needed.

It is well documented that the S707Y variant disrupts the PLCγ2 autoinhibitory mechanism, resulting in observed GOF enzymatic activity[155]. Although the P522R variant also demonstrates GOF activity, it is situated within the spPH-nSH2 linker region which does not lie on the autoinhibitory interface. Therefore, it is currently not clear how the P522R variant achieves its GOF activity. Given the potential difference in GOF mechanism, perhaps the data generated for the PLCγ2 S707Y cannot be extrapolated to the PLCγ2 P522R variant.

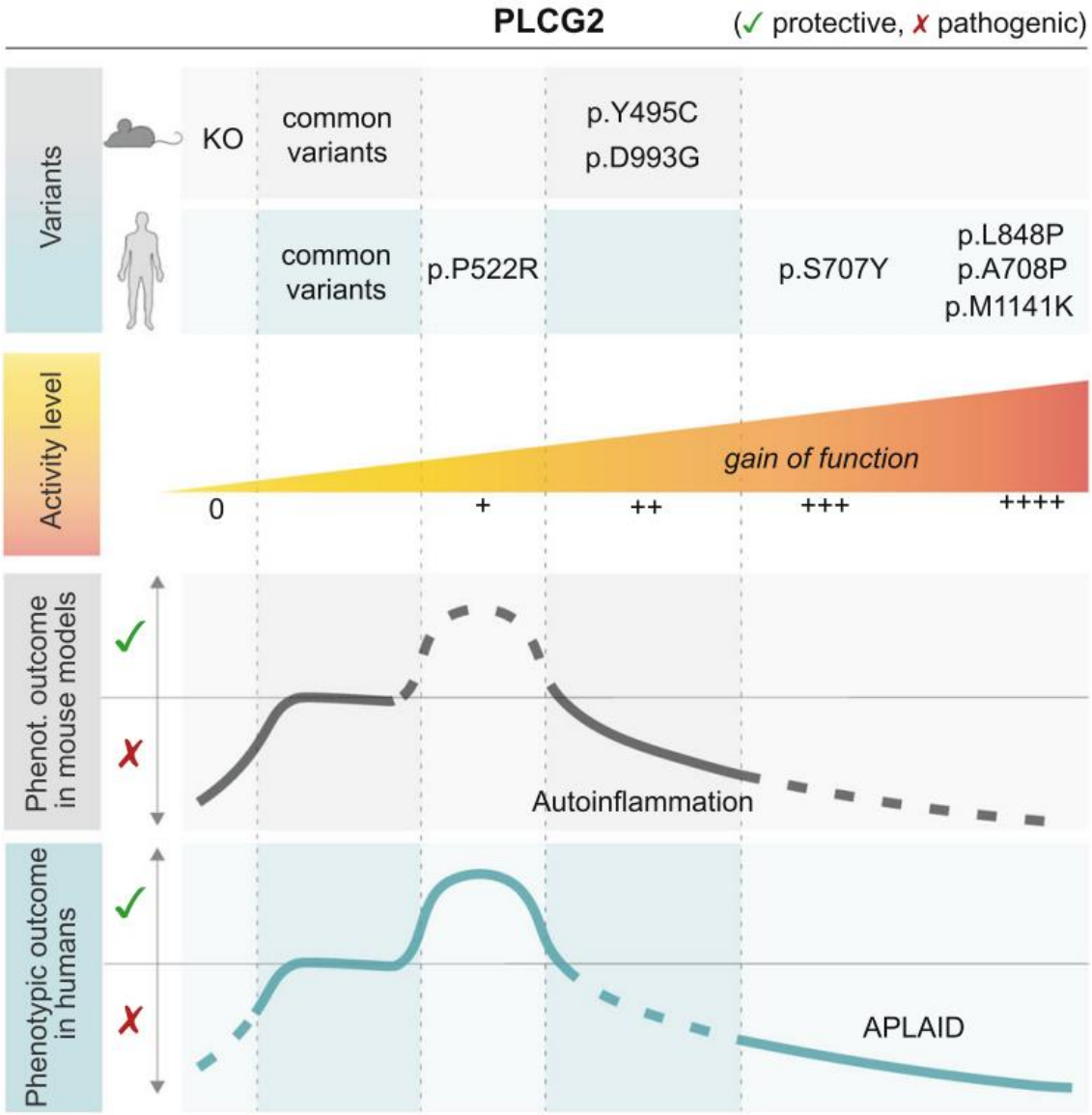

Figure 8.1 The disease spectrum of PLCγ2 variants. Summary of main PLCγ2 variants and the reported phenotypic consequences in both mouse models and humans. Filled lines represent characterised data from literature, whereas dotted line represents

unknown phenotype. Abbreviations: APLAID, autoinflammation and PLCγ2-associated antibody deficiency. Figure adapted from Magno et al[204].

8.2 Experimental/technical limitations of the work

Transient transfection efficiency can be influenced by factors such as the quantity of the nucleic acid, cell line health, number of passages, degree of confluency etc., and as a result variability between biological replicates is often observed. Therefore, statistical differences between PLCγ2 variant and PLCγ2 WT enzymatic activity were difficult to establish for some PLCγ2 variants.

The transient transfection of the HEK293T cells is a convenient system to characterise PLCγ2 variant enzymatic activity. However, this cellular system is artificial and clearly does not fully recapitulate the cellular machinery of physiologically relevant cells. Therefore, PLC activity could differ in a more relevant cell model, such as B cells or microglia. Although the differences in PLCγ2 expression were accounted for, the expression of the co-transfected EGFR was an experimental variable that could not adequately be normalised for, and as such was assumed to have equal expression for each experimental condition.

The reprogramming of human cells to generate hiPSCs can result in genetic alterations, and thus should be characterised[356]. Furthermore, it is unclear what influence the ARID2 heterozygous deletion to the kolf2 hiPSC line had on the experimental outcome and thus needs to be investigated further. Finally, it would be beneficial to evaluate multiple clones of each hiPSC line to be unequivocally sure that the phenotypic observations are due to the PLCγ2 variant alone.

Although hiPSC-derived microglia do recapitulate certain aspects of their native counterparts, there is currently no consensus on a unique proteomic, genetic or functional signature required to consider hiPSC-derived microglia truly representative of endogenous human microglia[251]. Additionally, the heterogeneity of hiPSC-derived microglia is still not currently known. Thus, it is unclear how close the hiPSC-derived microglia model is to their native human counterparts, especially as they are derived in isolation (monoculture). Moreover, hiPSC-derived microglia have been demonstrated to more closely resemble foetal than adult microglia, which may hinder the study of age-related neurodegeneration[251].

8.3 Future work

PIP_2 has been demonstrated to be vital for regulating actin binding proteins for actin cytoskeleton dynamics, as well as aid in the recruitment of proteins for endocytosis and exocytosis[306]. The PLCγ2 P522R variant has been shown to reduce PIP_2 availability following exposure to physiologically relevant stimuli[226]. Quantification of the availability of PIP_2 in the S707Y hiPSC-derived microglia could shed light into what role strong GOF PLCγ2 variants have on PIP_2 availability, as well as add further explanation of the observed experimental phenotypes. PIP_2 quantification through ICC fluorescence and liquid chromatography–mass spectrometry has been performed in literature and could be utilised[226,357]. Furthermore, the majority of experimental work has been focused on the PLCγ2-IP_3 pathway. Given that the PLCγ2-DAG-PKC pathway also likely influences microglia functionality[204], DAG sensors and p-PKC quantification through Western blotting should be utilised to better understand what effect strong GOF PLCγ2 variants have on microglial signalling and thus functionality.

Like any other brain cell monoculture model, hiPSC-derived microglia fail to fully recapitulate microglial biology due to the lack of interaction with other brain cell types. Perhaps more complex models, such as hiPSC-derived organoids, the transplantation of hiPSC-derived microglia in the brains of WT, as well as AD (e.g. 5xFAD) mouse models could provide better insight into what role strong PLCγ2 GOF variants, as well as the P522R variant, have on brain function and development e.g. synaptic pruning, and in AD[262]. Moreover, studying what role PLCγ2 GOF variants have on brain development and function in patients harbouring strong hypermorphic PLCγ2 variants will ultimately lead to better characterisation of the role PLCγ2 has within microglia functionality within the brain.

Further characterisation of the PLCγ2 P522R variant is still needed to better understand how this variant is protective against LOAD. It has been suggested that gene edited hiPSCs may not fully reproduce human pathology, as certain factors e.g. complicated genetic modifiers can only be provided by relevant donors[358]. Because of this, hiPSCs derived from donors harbouring the PLCγ2 P522R variant is necessary in order to better understand the protective function of the variants, with siblings or offspring that do not elicit the variant used as functional controls for experimentation. Therefore, future work should aim to profile the PLCγ2 P522R variant in donor-derived hiPSCs, performing the same phenotypic assays documented in this thesis to provide greater insight into the role of the variants within LOAD pathophysiology.

Further work is also required to address structural, mechanistic and signalling aspects of PLCγ2 function and dysregulation. Although there are good structural models of the PLCγ2 (AF-P16885-F1), based on PLCγ1 structures, further application of X-ray crystallography or cryo-electron microscopy should be utilised to solve the PLCγ2 structure and facilitate the development of drugs that either inhibit PLCγ2 functionality for people who harbour strong GOF PLCγ2 variants, or mimic the protective function of the P522R variant. Additionally, various unbiased proteomic approaches need to be performed to understand which adapter proteins and tyrosine kinases interact with PLCγ2 in microglia, to better understand the overall role PLCγ2 has within microglia signalling.

8.4 Conclusion

This thesis demonstrates a comprehensive enzymatic activity ranking of rare and novel PLCγ2 variants, leading to a greater understanding of how hypermorphic disease-linked PLCγ2 variants may be driving pathogenesis. Furthermore, despite the increase in enzymatic activity exhibited from the S707Y hiPSC-derived microglia, it would appear that strong GOF PLCγ2 variants dysregulate microglia cell function by altering cytokine secretion, decreasing phagocytosis, dampening NF-κB activation and translocation, as well as downregulating microglia immune pathways and responses, all of which has never been documented before. Furthermore, these findings highlight that therapies which aim to alter PLCγ2 enzymatic activity need to be able to precisely modulate function to promote beneficial and not detrimental effects.

Plasmid	Chromatogram
WT	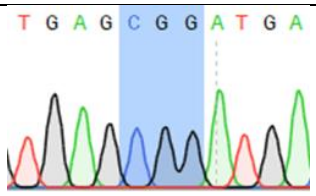 CGG (R)
R268W	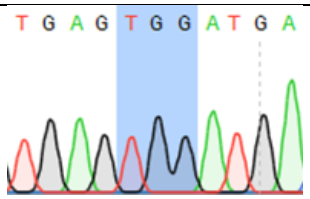 TGG (W)

Plasmid	Chromatogram
WT	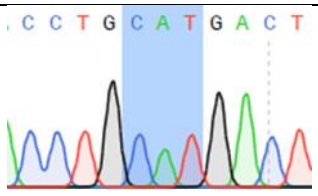 CAT (H)
H224R	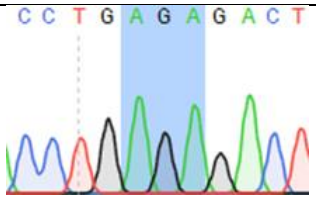 AGA (R)

Plasmid	Chromatogram
WT	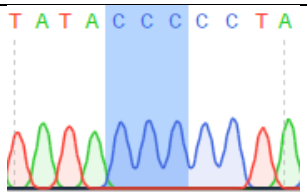 CCC (P)
P522R	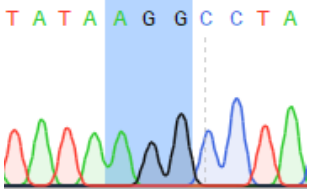 AGG (R)

Plasmid	Chromatogram
WT	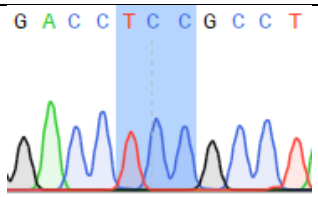 TCC (S)
S707Y	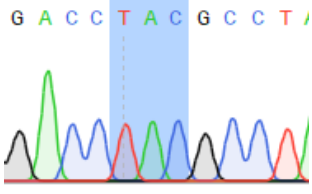 TAC (Y)

Plasmid	Chromatogram
WT	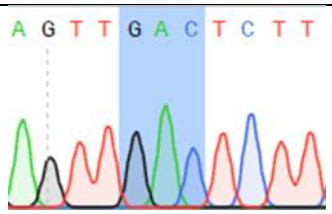 GAC (D)

Plasmid	Chromatogram
WT	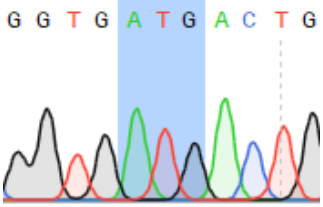 ATG (M)

D993G	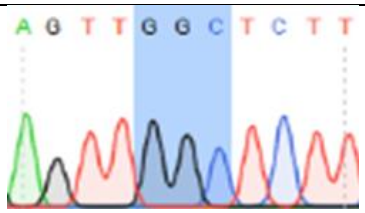 GGC (G)

M28L	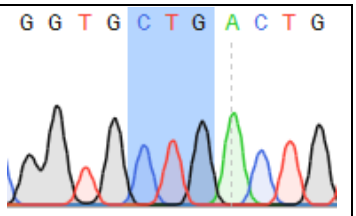 CTG (L)

Plasmid	Chromatogram
WT	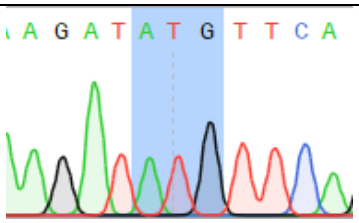 ATG (M)
M1141K	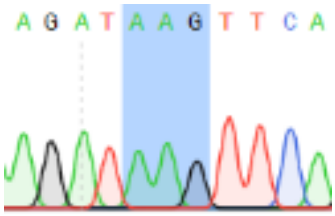 AAG (K)

Plasmid	Chromatogram
WT	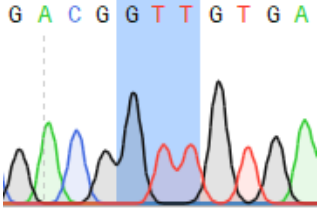 GTT (V)
V1103I	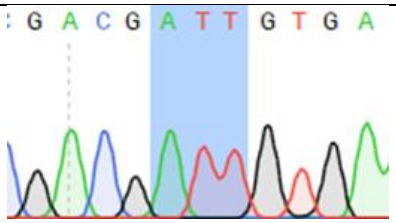 ATT (I)

Plasmid	Chromatogram	
WT	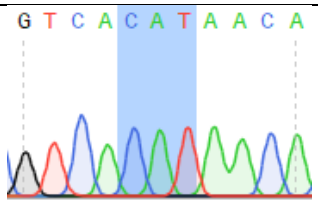 327: CAT (H)	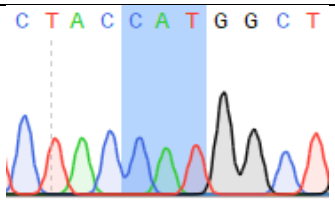 372: CAT (H)
H327/372F	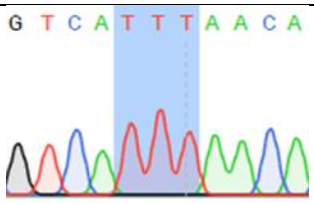 327: TTT (F)	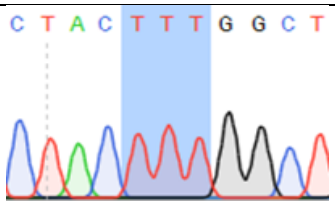 372: TTT (F)

Plasmid	Chromatogram				
WT	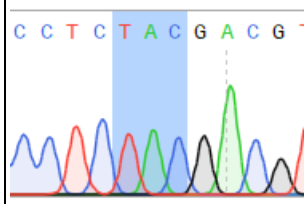 753: TAC (T)	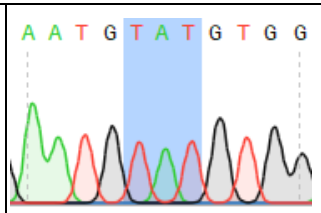 759: TAT (T)	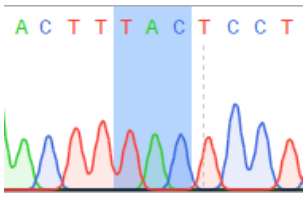 1197: TAC (T)	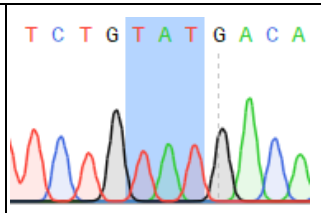 1217: TAT (T)	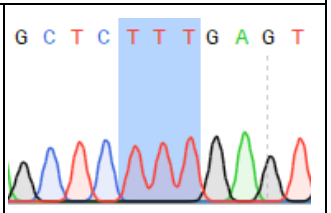 897: TTT (F)
T753/759/ 1197/1217F + F897Q (4F/F897Q)	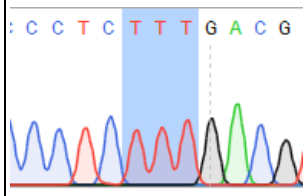 753: TTT (F)	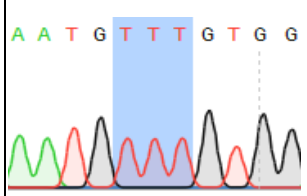 759: TTT (F)	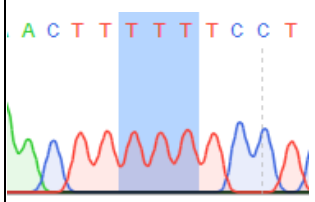 1197: TTT (F)	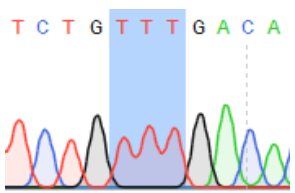 1217: TTT (F)	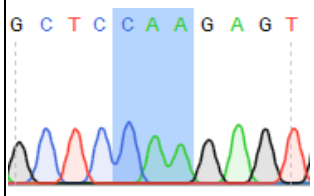 897: CAA (Q)

Figure S1 Chromatograms confirming the introduction of mutant alleles in PLCγ2 constructs by site-directed mutagenesis. Sequences from the wild-type (WT) constructs are shown in the top panels and mutant alleles in the bottom panels. Constructs were validated through Sanger sequencing.

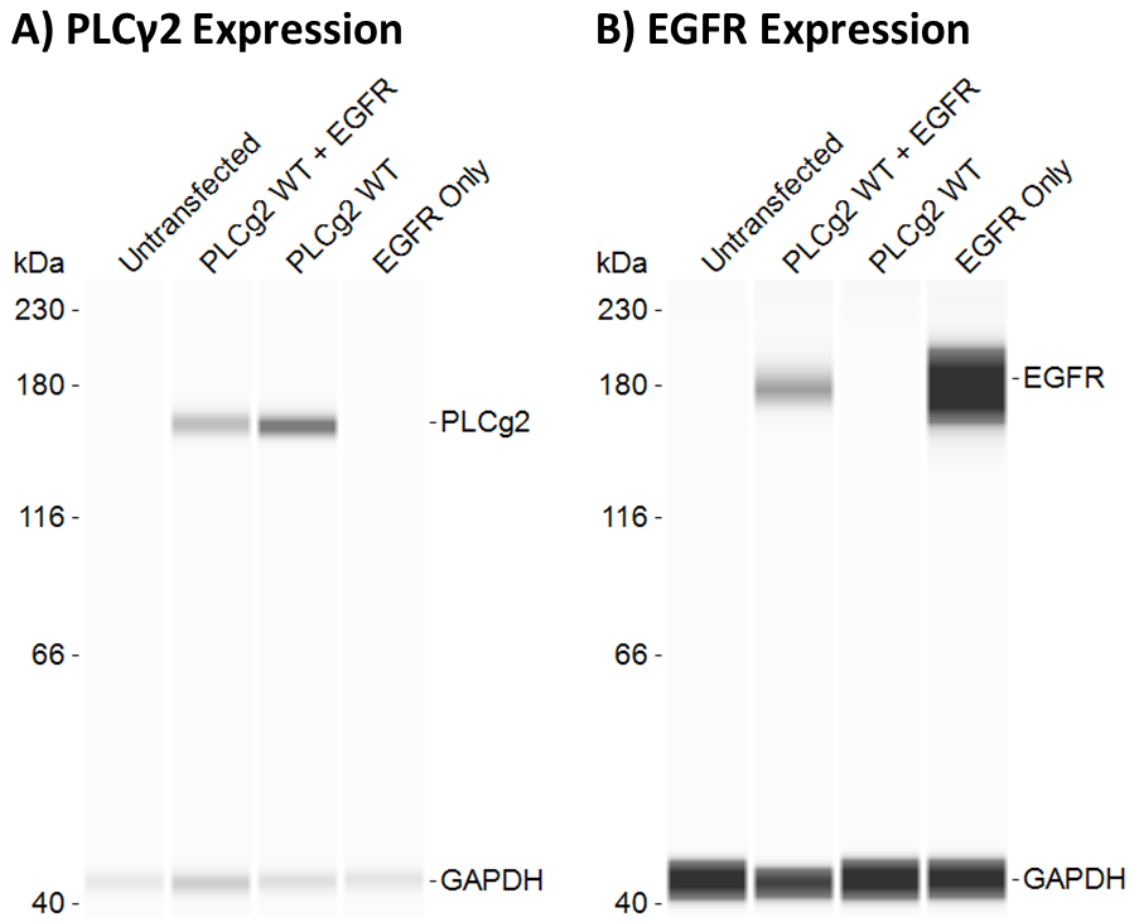

Figure S2 Comparison of EGFR and PLCγ2 protein expression in HEK293T transfected cells. Experimental WES Western blot from Figure 3.6. Transfection of a 1:1 EGFR:PLCγ2-GFP WT DNA ratio. **A**) Staining of PLCγ2 (150kDa, 1:50, Cell Signalling Technology, 3872s) and GAPDH (42kDa, 1:100, Cell Signalling Technology, 2118s) transfected HEK293T cells. **B**) Staining of EGFR (175KDa, 1:50, Cell Signalling Technology, 4267s) and GAPDH (42KDa, 1:100, Cell Signalling Technology, 2118s) staining of transfected HEK293T cells. The experiment consists of one biological replicate, with one experimental replicate (n=1).

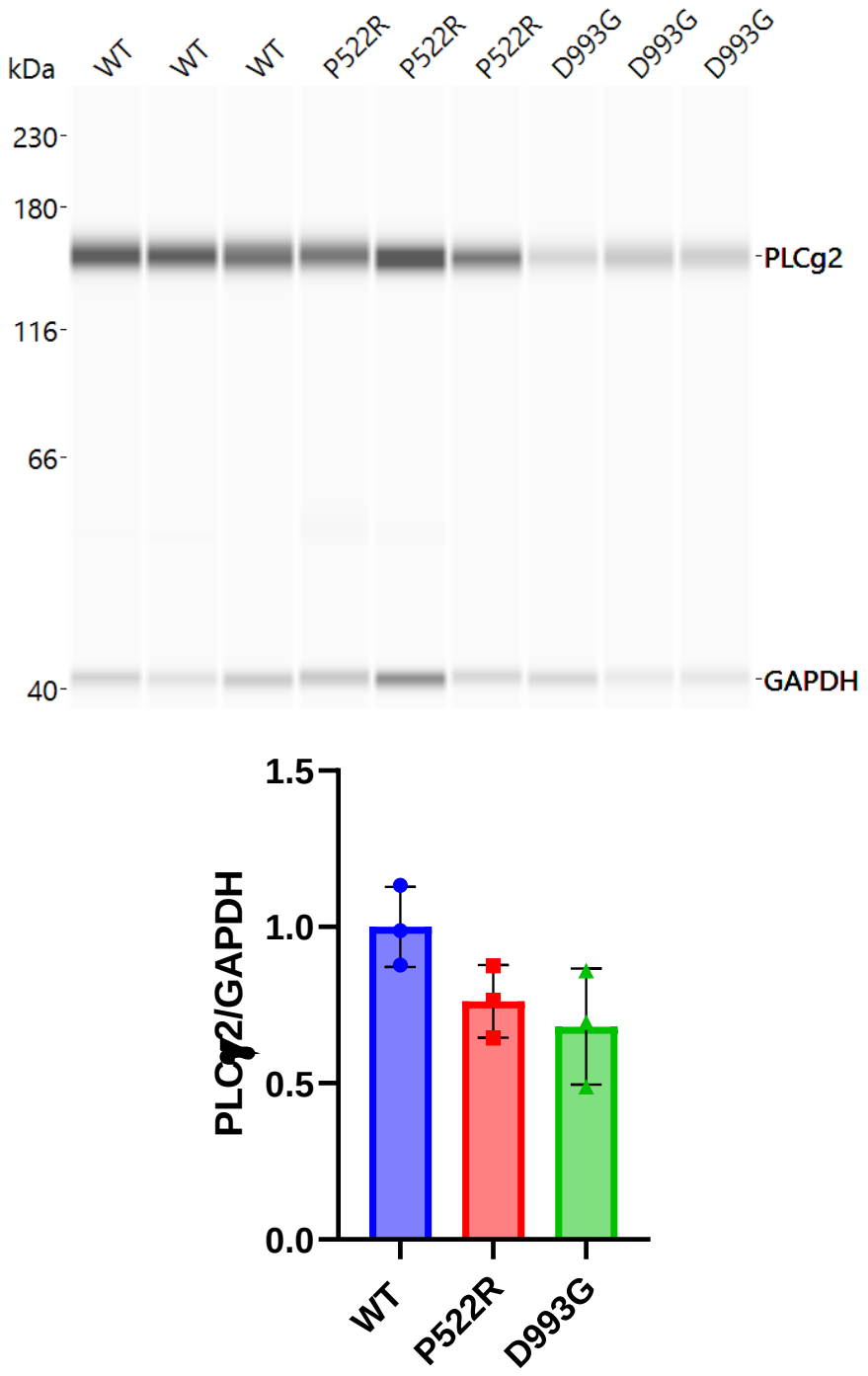

Figure S3 Experimental Western blot for IP_1 protein normalisation. PLCγ2 antibody (1:50, 150kDa, Cell Signaling Technology) staining of experimental IP_1 lysates, with expression normalised to GAPDH loading control (1:300, 42KDa, Cell Signaling Technology). Lysates were run through the WES Western blot and analysed using Compass (Protein Simple). Each lane represents each experimental replicate for EGF (150 ng/ul) stimulation. Comparison of PLCγ2/GAPDH expression displayed in the bar graph. Data represents mean value ± SD. The experiment consists of one biological replicate (n=1).

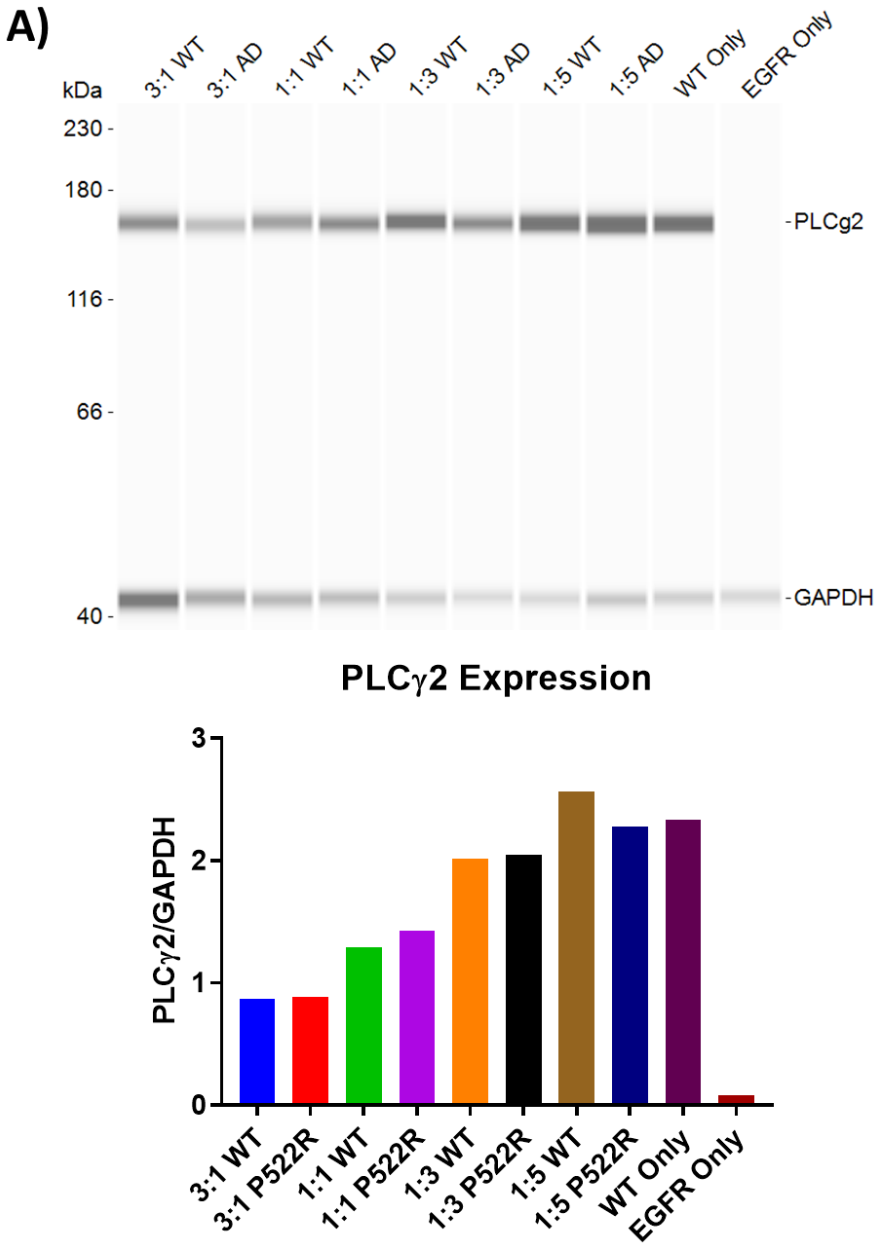
A)
kDa
3:1 WT
3:1 AD
1:1 WT
1:1 AD
1:3 WT
1:3 AD
1:5 WT
1:5 AD
WT Only
EGFR Only
230
180
116
66
40
PLCg2
GAPDH
PLCγ2 Expression
PLCγ2/GAPDH
3
2
1
0
3:1 WT
3:1 P522R
1:1 WT
1:1 P522R
1:3 WT
1:3 P522R
1:5 WT
1:5 P522R
WT Only
EGFR Only

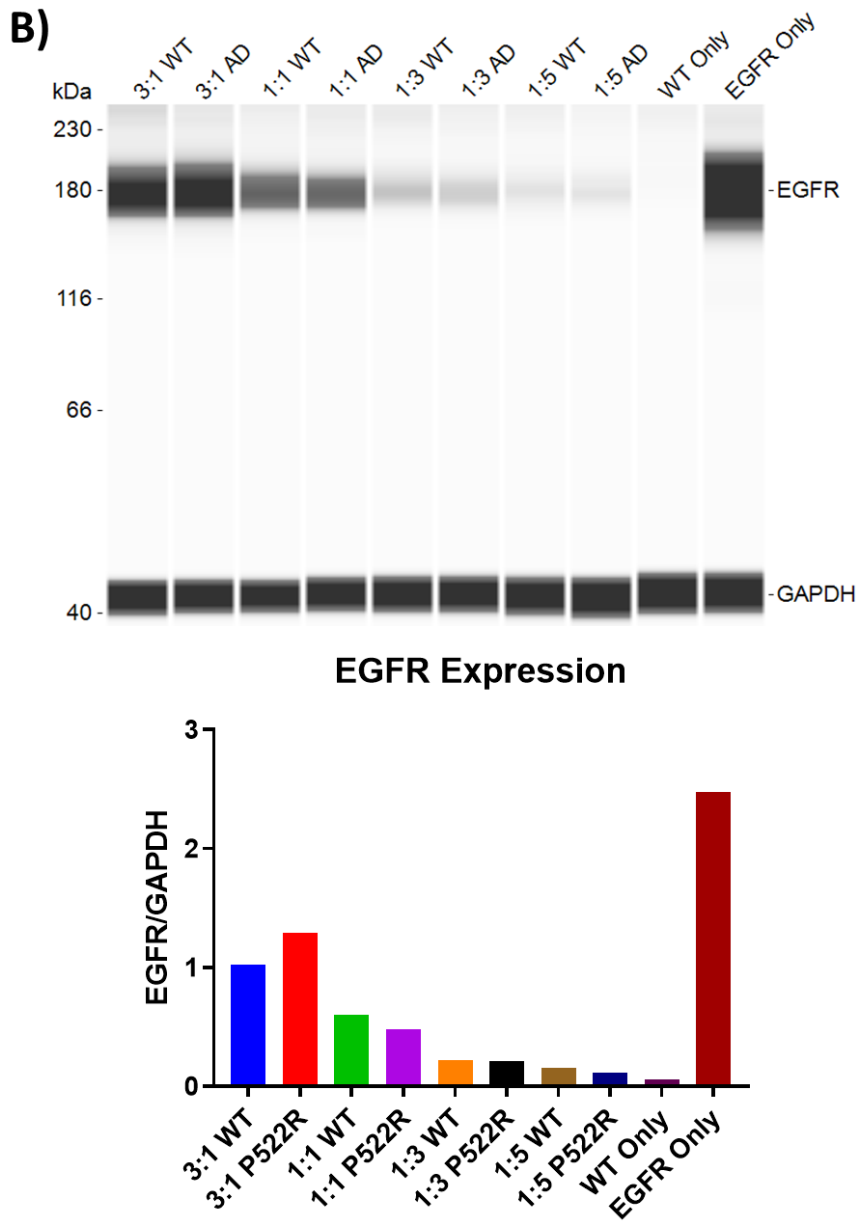

Figure S4 PLCγ2 and EGFR protein expression for titrated EGFR:PLCγ2 co-transfected HEK293T cells. DNA was fixed to a total volume of 0.4ug, with EGFR:PLCγ2-HIS titrated in favour of PLCγ2. **A)** Lysates were run through WES Western blotting and stained with a PLCγ2 antibody (1:50, 150kDa, Cell Signaling Technology), with expression normalised to GAPDH loading control (1:300, 42KDa, Cell Signaling Technology). **B)** Lysates were run through WES Western blotting and stained with a EGFR antibody (1:50, 150kDa, Cell Signaling Technology), with expression normalised to GAPDH loading control (1:300, 42KDa, Cell Signaling Technology). EGFR, PLCγ2 and GAPDH expression was analysed using Compass software (Protein Simple) and GAPDH normalised protein expression visualised in the bar graphs .The experiment consists of one biological replicate (n=1).

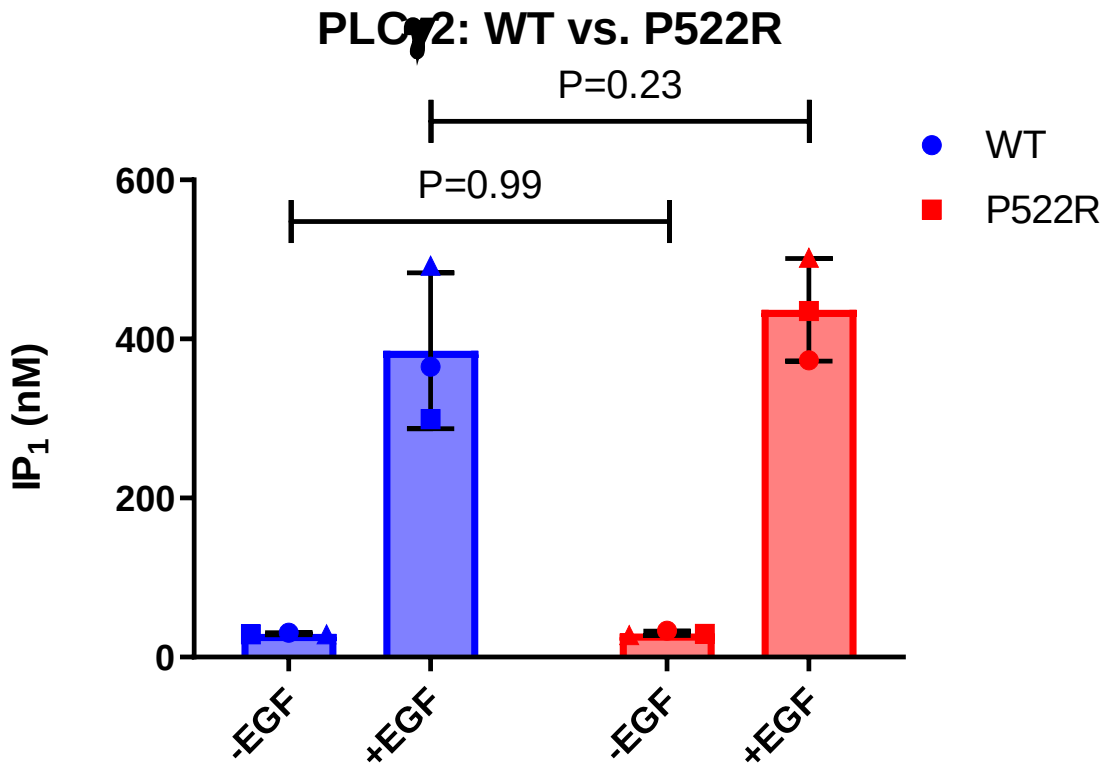

Figure S5 Example of the IP_1 variation observed for the PLCγ2 WT vs. P522R from protein normalisation between each biological replicate. Graphical symbol shape (triangle, square and circle) represents each set of biological replicates (Dunnett multiple comparisons two-way ANOVA, p-value displayed on the graph, n=3). Each biological replicate had at least three experimental replicates. Data represents mean value ± SD.

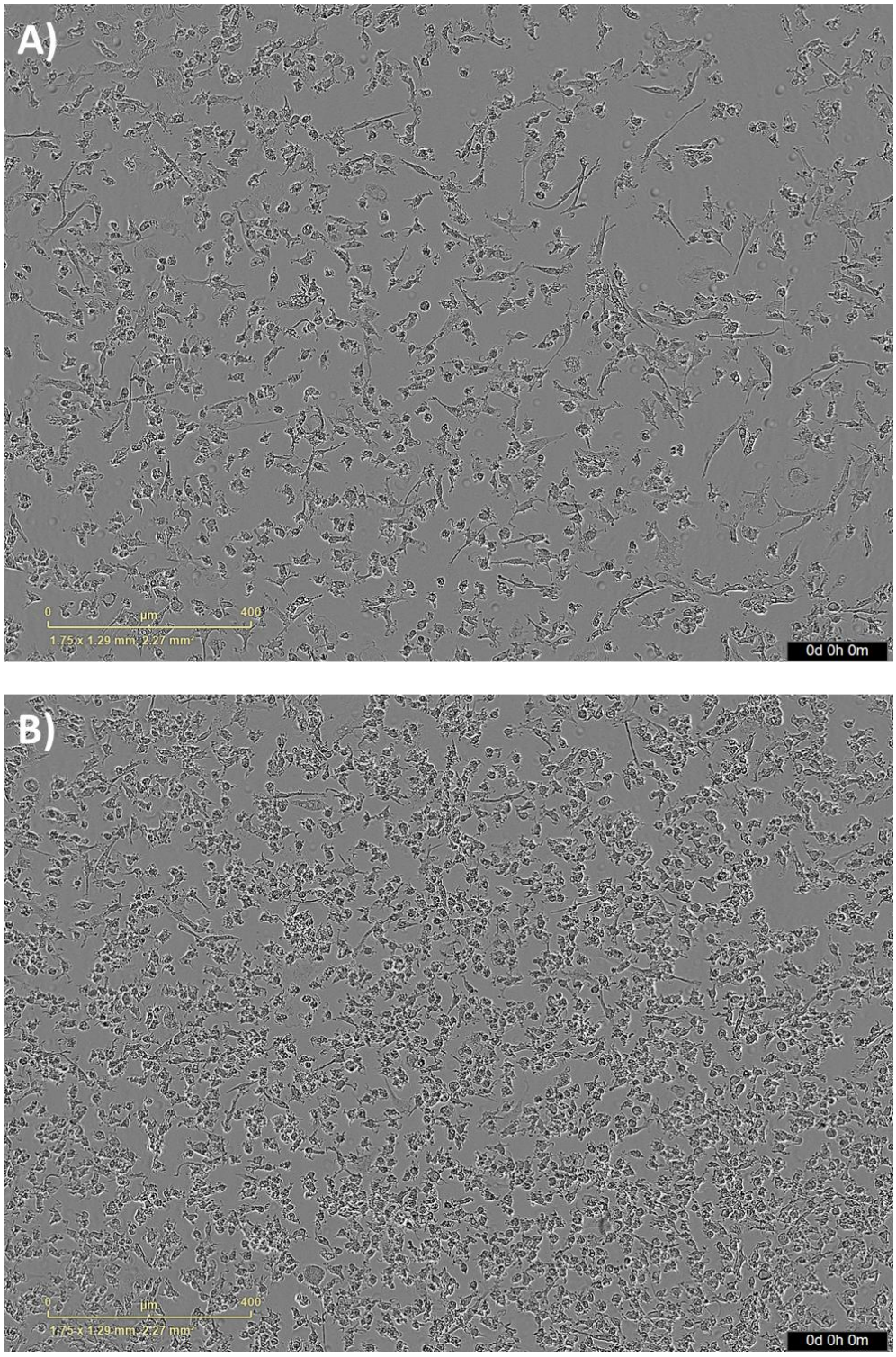

Figure S6 Cell confluency images of H9-derived microglia after 7 days of differentiation with an initial seeding density of **A**) 5k **B)** 10K. Images were captured on the IncuCyte S3 live-cell analysis system (Sartorius).

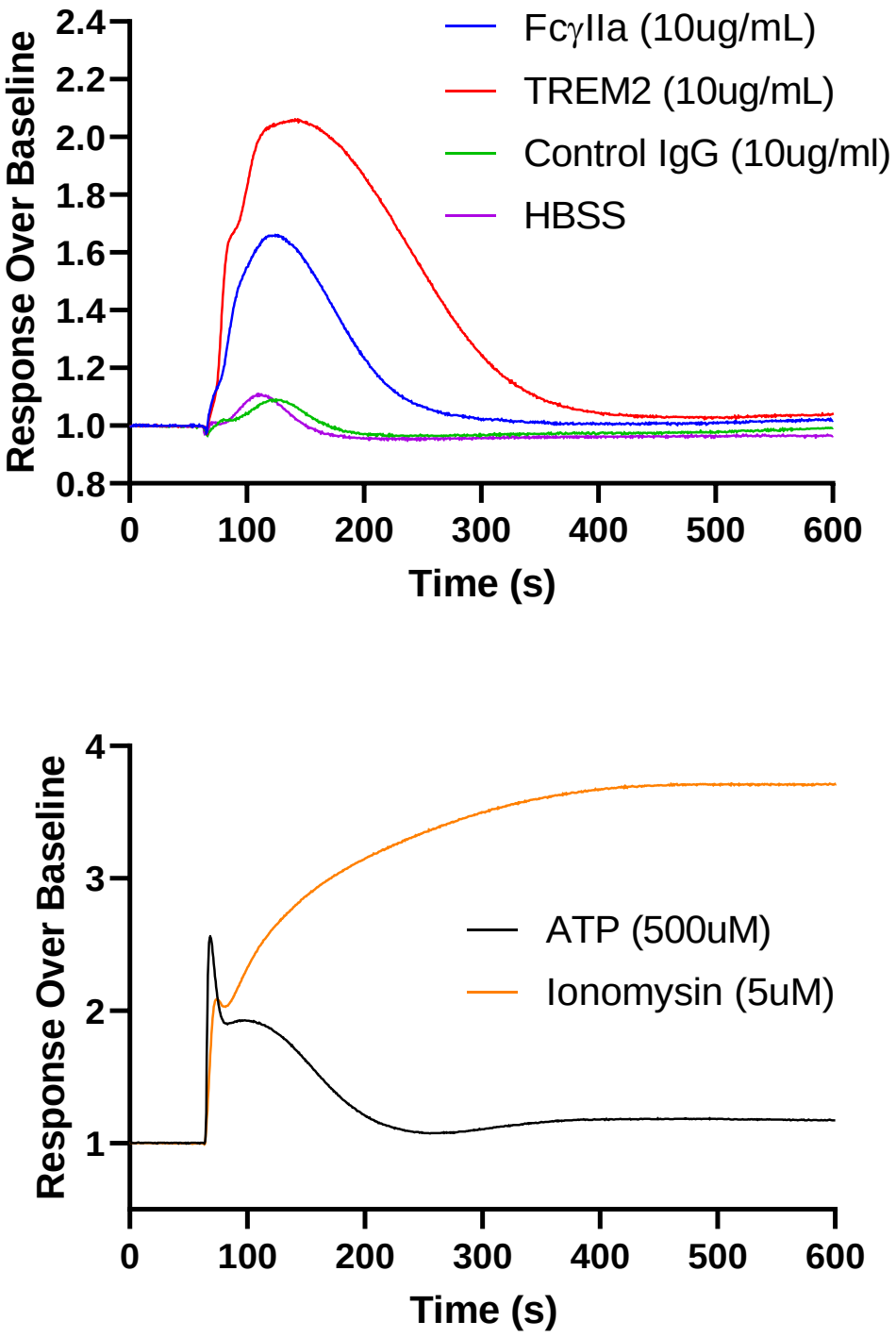

Figure S7 Representative calcium traces observed from stimulated H9-derived microglia. The cells were stimulated with either HBSS, 10 µg/mL control IgG, 1.25/2.5/5/10µg/mL of TREM2 or FCγRIIa antibody, 500µM ATP or 5µM Ionomycin before the relative fluorescence units (RFU) were measured on a FLIPR Tetra (Molecular Devices).

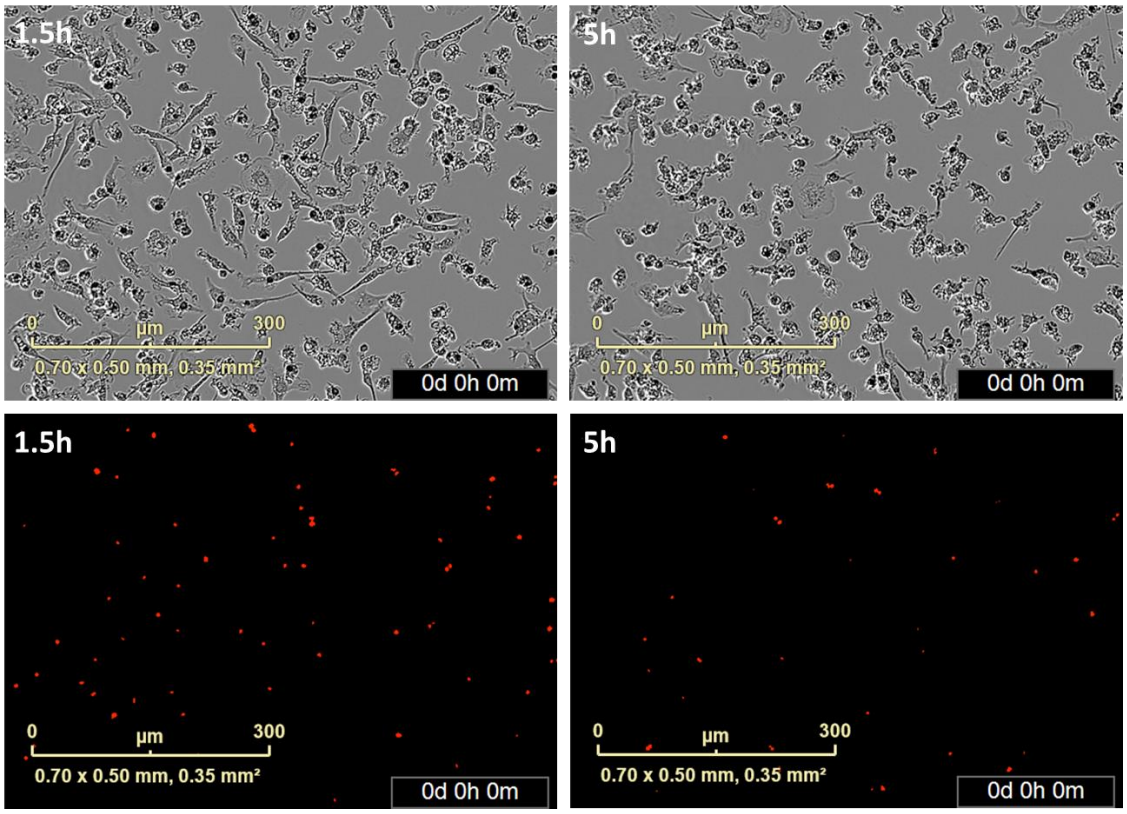

Figure S8 Representative images of H9-derived microglia phagocytosing pHrodo-labelled apoptotic SH-SY5Y cells after 1.5h and 5h. Brightfield and red fluorescence images were captured on the IncuCyte S3 live-cell analysis system (Sartorius).

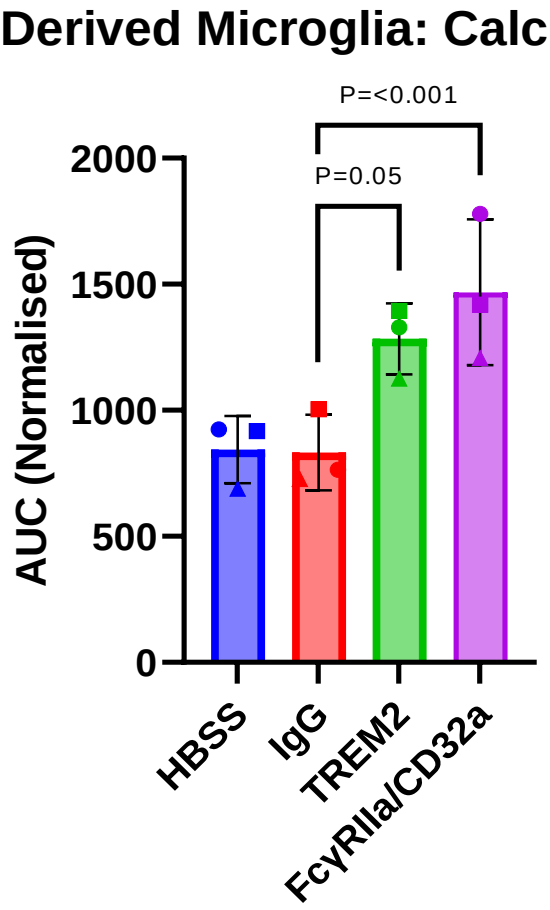

Figure S9 Validation of the calcium normalisation methodology with H9-derived microglia. Microglia were stimulated with either HBSS, 10µg/mL control IgG, 10µg/mL of TREM2 or FCγRIIa antibodies. After the calcium traces had returned to baseline each well was restimulated with 5uM Ionomycin. Experimental stimulated area under curve (AUC) calcium data was generated for each condition and normalised to the AUC of the Ionomycin re-stimulation. Graphical symbol shape (triangle, square and circle) represents each set of biological replicates (Dunnett multiple comparisons one-way ANOVA, p-value displayed on the graph, n=3). Each biological replicate had at least three experimental replicates. Data represents mean value ± SD.

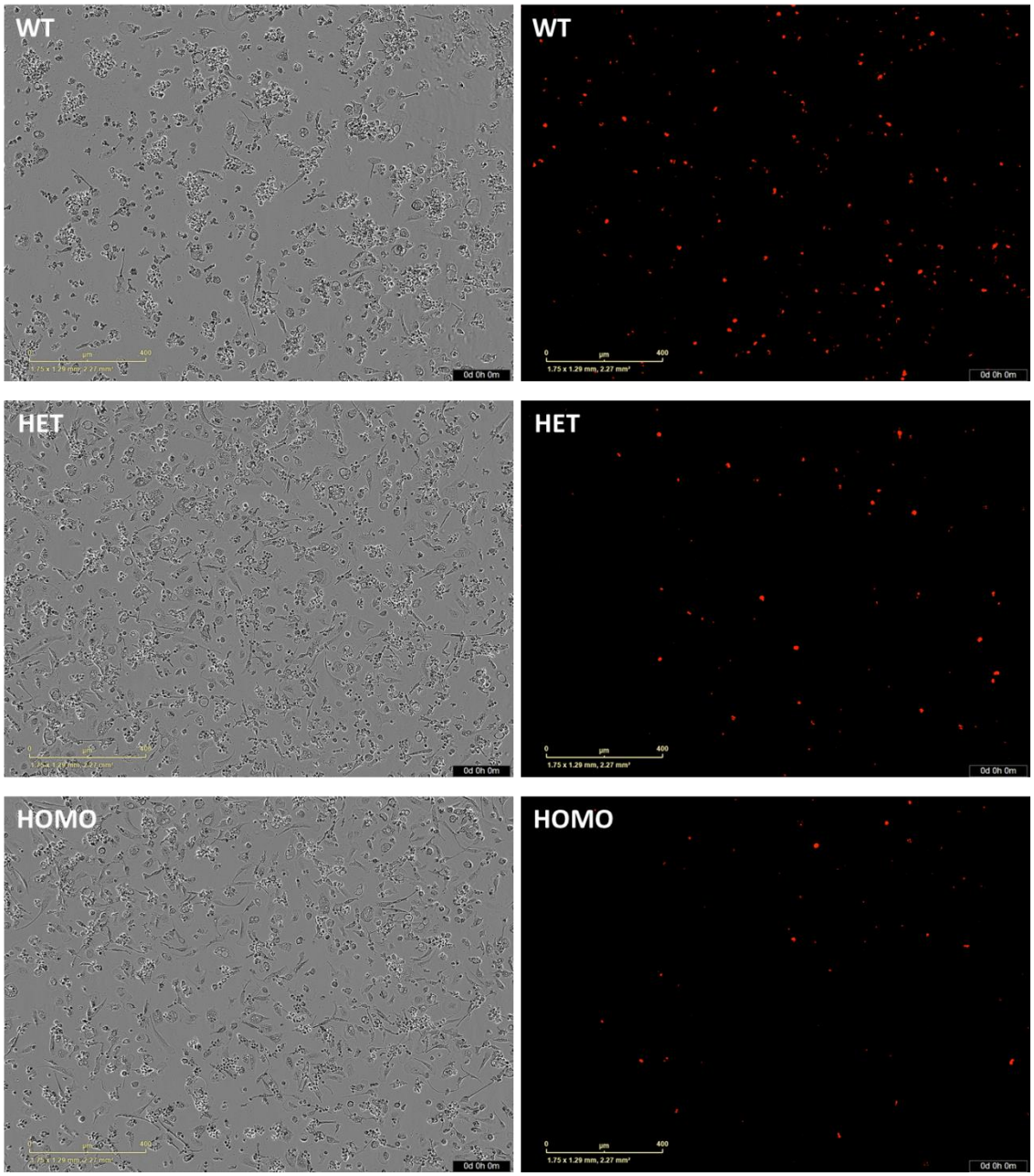

Figure S10 Representative images of PLCγ2 S707Y and WT hiPSC-derived microglia phagocytosing pHrodo-labelled apoptotic SH-SY5Y cells at 24h. Brightfield and red fluorescence images were captured on the IncuCyte S3 live-cell analysis system (Sartorius).

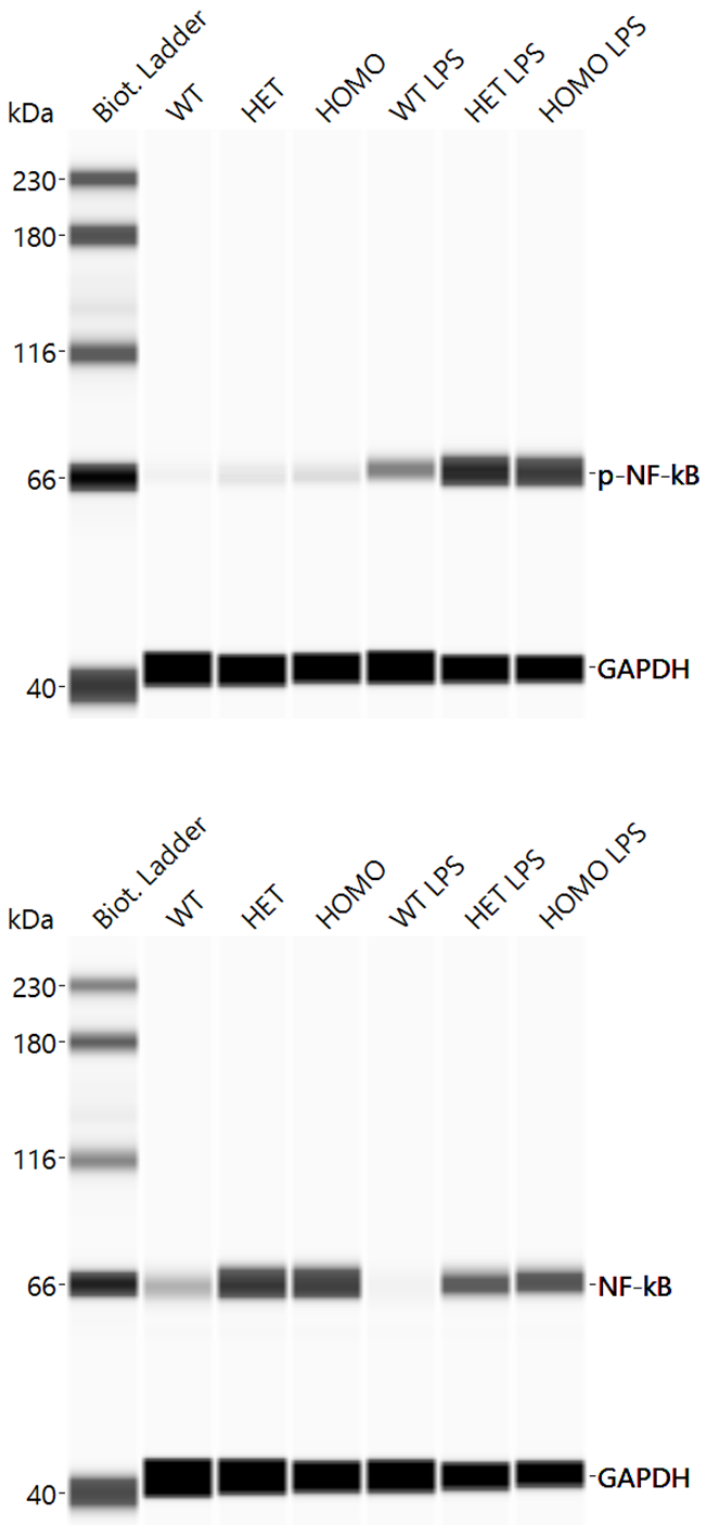

Figure S11 Representative image of the WES Western blot used for NF-κB p65 (1:40, Cell Signaling Technology) and S536 p-NF-κB p65 (1:40, Cell Signaling Technology) quantification of the homozygous and heterozygous PLCγ2 S707Y and WT hiPSC-derived microglia, following ± LPS (100ng/mL, 20min) exposure. The experiment consists of one biological replicate (n=1).

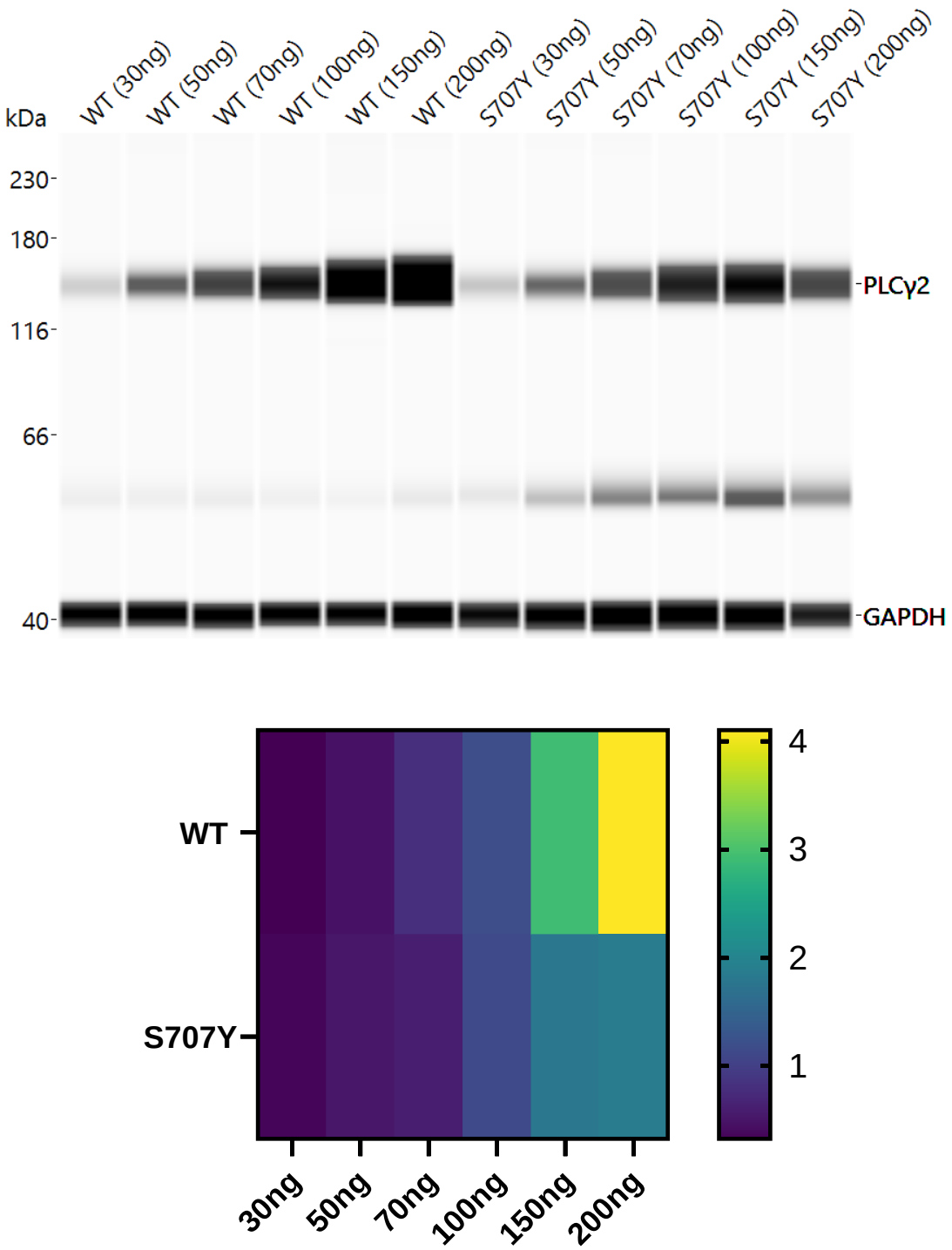

Figure S12 PLCγ2 expression of WT and S707Y variant from the HEK293T IP_1 assay. Lysates were run through WES Western blotting and stained with a PLCγ2 antibody (1:50, 150kDa, Cell Signaling Technology) and a GAPDH loading control (1:300, 42KDa, Cell Signaling Technology). PLCγ2 expression was normalised to GAPDH expression and represented as a heat map. The experiment consists of one biological replicate (n=1).

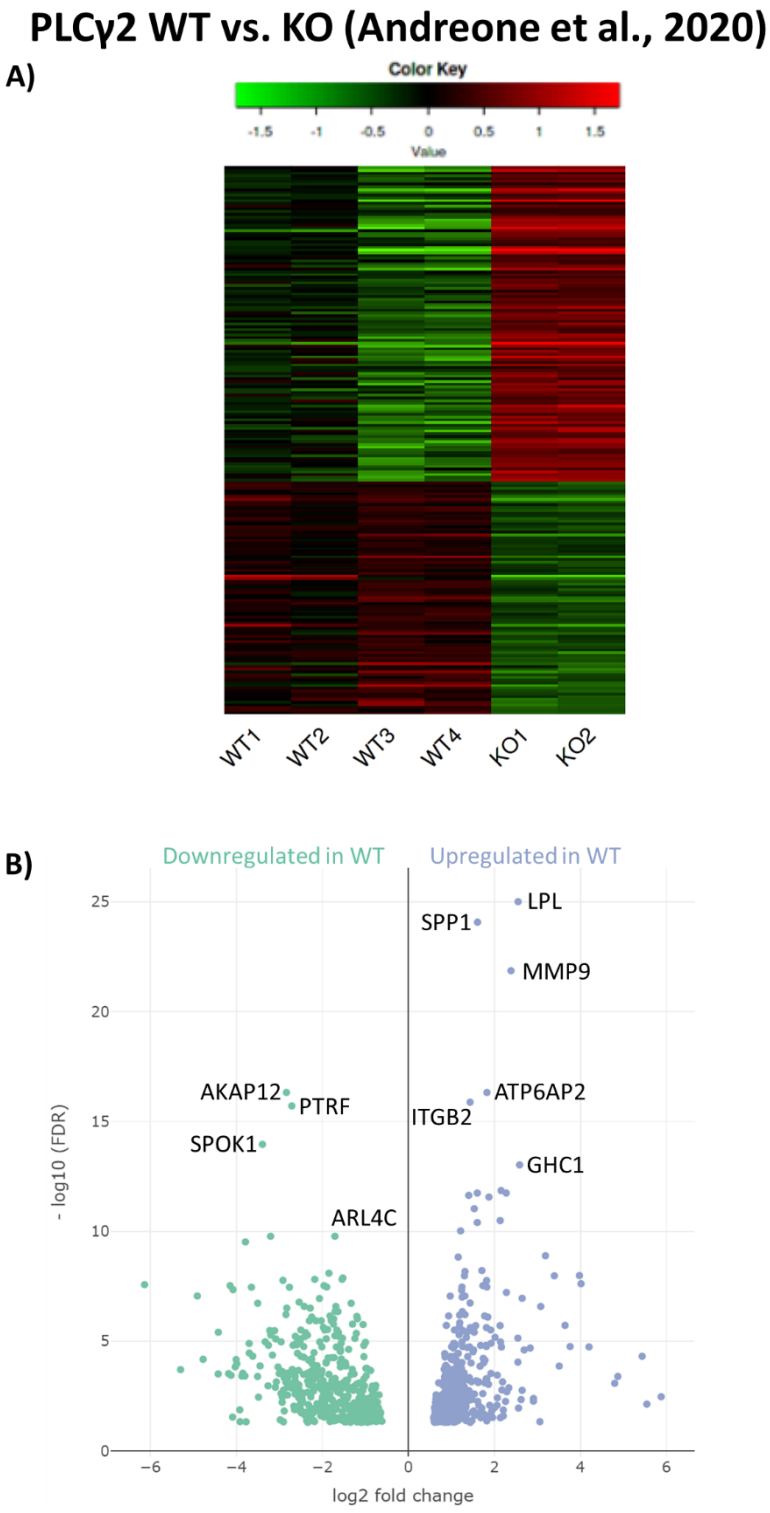

Figure S13 PLCγ2 S707Y hiPSC-derived microglia differentially expressed genes (DEGs). **A)** Heatmap of the DEGs downregulated (Green) and upregulated (Red) in the PLCγ2 KO hiPSC-derived microglia, compared to PLCγ2 WT hiPSC-derived microglia. **B)** Volcano plot displaying the DEGs downregulated and upregulated in PLCγ2 KO hiPSC-derived microglia, compared to PLCγ2 WT hiPSC-derived microglia. RNASeq dataset was acquired from Andreone et al[133].

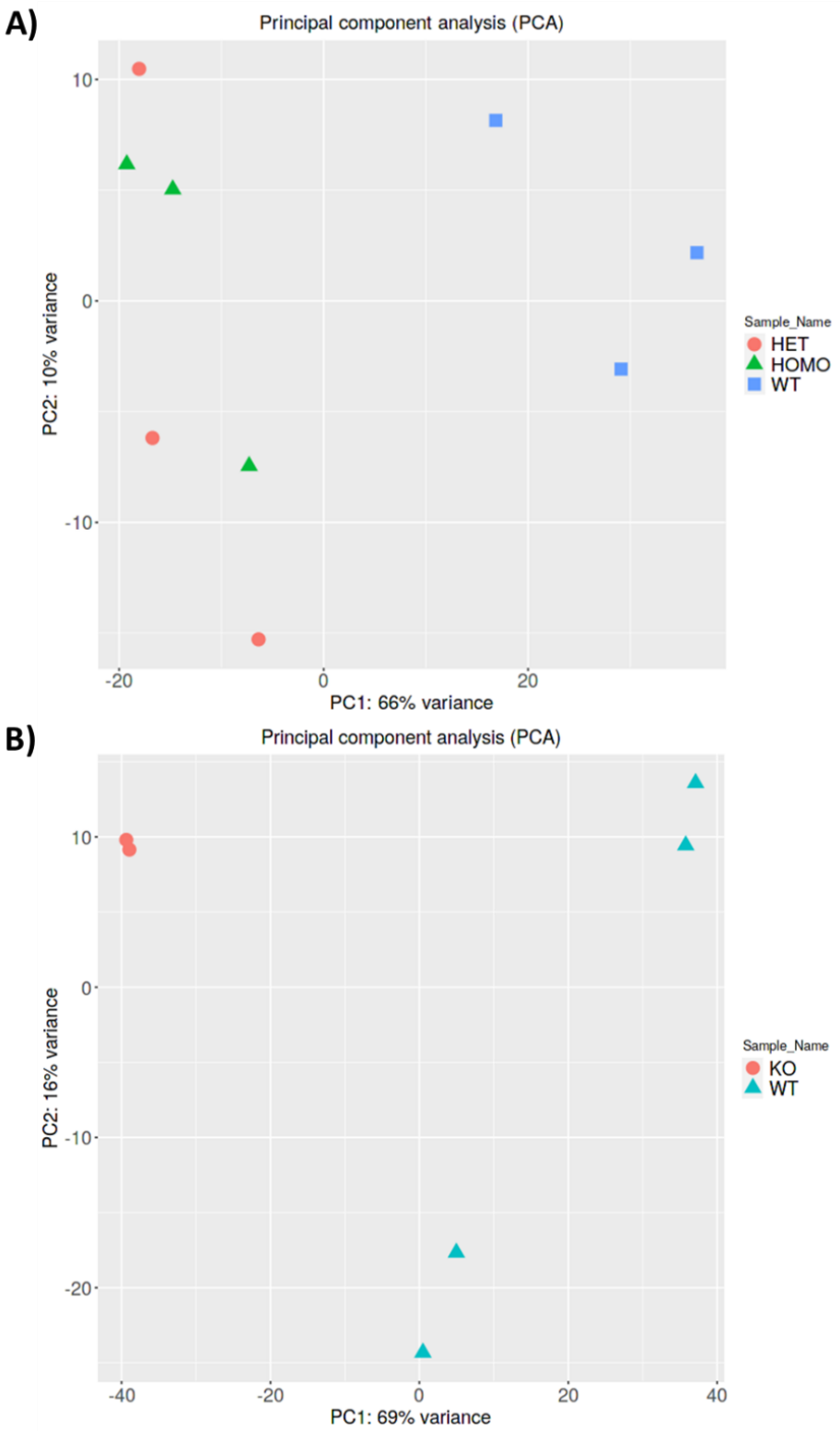

Figure S14 Principle component analysis (PCA) of **A)** PLCγ2 WT and S707Y (heterozygous and homozygous) hiPSC-derived microglia, and **B)** PLCγ2 WT and KO hiPSC-derived microglia, with RNASeq data taken from Andreone et al[133].

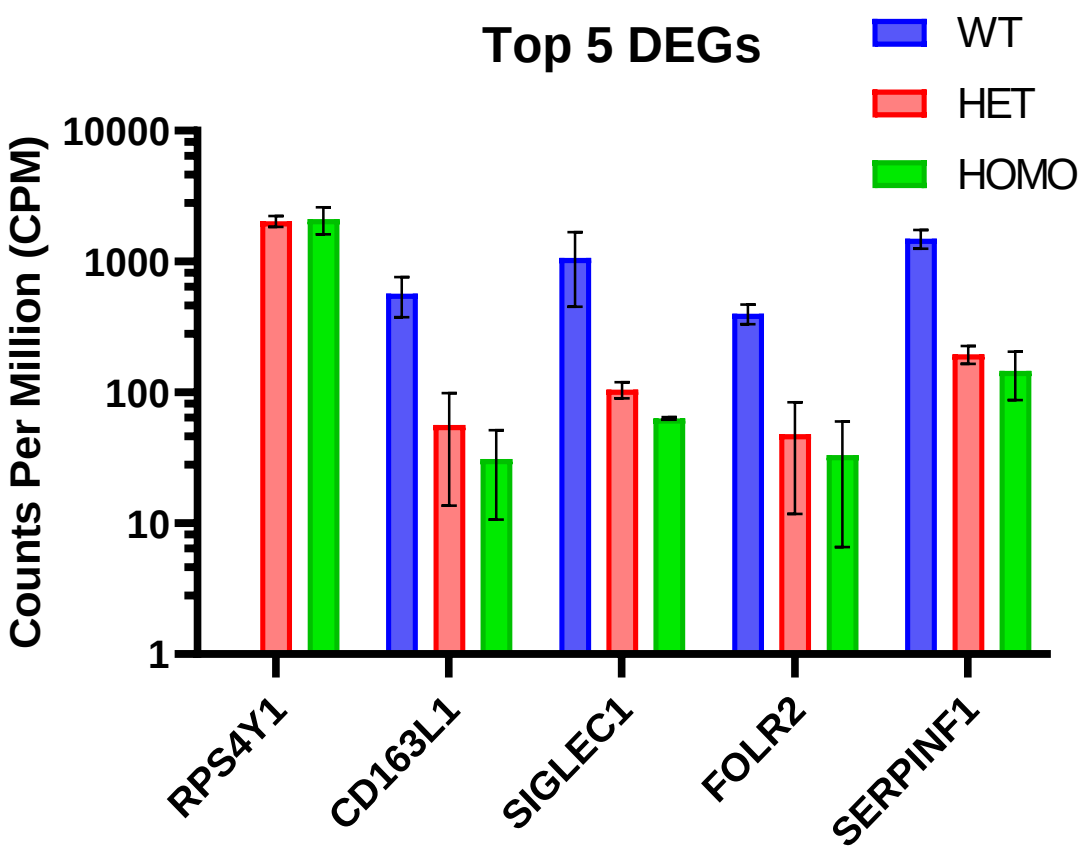

Figure S15 The raw counts per million (CPM) of the top 5 DEGs of the PLCγ2 S707Y hiPSC-derived microglia (compared to PLCγ2 WT).

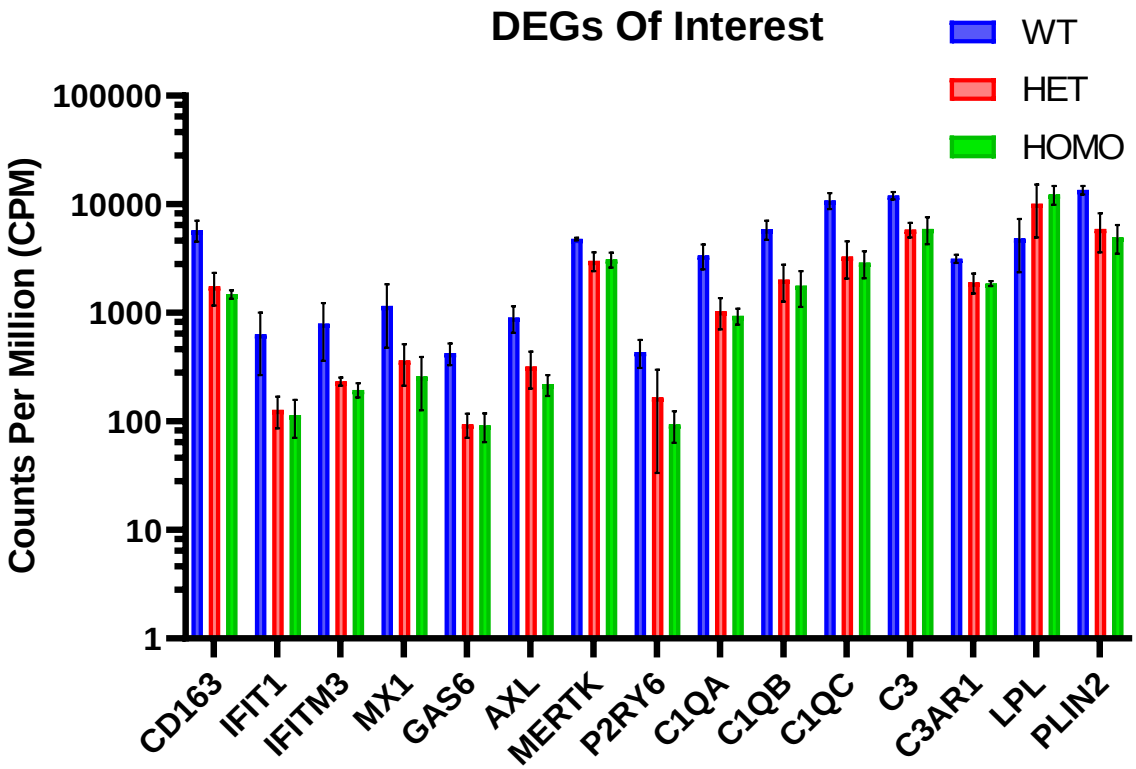

Figure S16 The raw counts per million (CPM) of the DEGs of interest from the PLCγ2 S707Y hiPSC-derived microglia (compared to PLCγ2 WT).

References

1. Chen, L. *et al.* Inflammatory responses and inflammation-associated diseases in organs. *Oncotarget* **9**, 7204–7218 (2018).

2. Chaplin, D. D. Overview of the immune response. *J. Allergy Clin. Immunol.* **125**, S3-23 (2010).

3. Nicholson, L. B. The immune system. *Essays Biochem.* **60**, 275–301 (2016).

4. Charles A Janeway, J., Travers, P., Walport, M. & Shlomchik, M. J. *Immunobiology: The Immune System in Health and Disease*. (Garland Science, 2001).

5. Marshall, J. S., Warrington, R., Watson, W. & Kim, H. L. An introduction to immunology and immunopathology. *Allergy, Asthma Clin. Immunol.* **14**, 49 (2018).

6. Theret, M., Mounier, R. & Rossi, F. The origins and non-canonical functions of macrophages in development and regeneration. *Development* **146**, (2019).

7. Wynn, T. A., Chawla, A. & Pollard, J. W. Macrophage biology in development, homeostasis and disease. *Nature* **496**, 445–55 (2013).

8. Hume, D. A. *et al.* The mononuclear phagocyte system revisited. *J. Leukoc. Biol.* **72**, 621–627 (2002).

9. Sheng, J., Ruedl, C. & Karjalainen, K. Most Tissue-Resident Macrophages Except Microglia Are Derived from Fetal Hematopoietic Stem Cells. *Immunity* **43**, 382–393 (2015).

10. Epelman, S. *et al.* Embryonic and Adult-Derived Resident Cardiac Macrophages Are Maintained through Distinct Mechanisms at Steady State and during Inflammation. *Immunity* **40**, 91–104 (2014).

11. Hoeffel, G. *et al.* C-Myb+ Erythro-Myeloid Progenitor-Derived Fetal Monocytes Give Rise to Adult Tissue-Resident Macrophages. *Immunity* **42**, 665–678 (2015).

12. Gomez Perdiguero, E. *et al.* Tissue-resident macrophages originate from yolk-sac-derived erythro-myeloid progenitors. *Nature* **518**, 547–551 (2015).

13. Epelman, S., Lavine, K. J. & Randolph, G. J. Origin and functions of tissue macrophages. *Immunity* **41**, 21–35 (2014).

14. Guilliams, M., Thierry, G. R., Bonnardel, J. & Bajenoff, M. Establishment and Maintenance of the Macrophage Niche. *Immunity* **52**, 434–451 (2020).

15. Shapouri-Moghaddam, A. *et al.* Macrophage plasticity, polarization, and function in health and disease. *J. Cell. Physiol.* **233**, 6425–6440 (2018).

16. Fujiwara, N. & Kobayashi, K. Macrophages in inflammation. *Curr. Drug Targets. Inflamm. Allergy* **4**, 281–286 (2005).

17. Nahrendorf, M. & Swirski, F. K. Abandoning M1/M2 for a Network Model of Macrophage Function. *Circ. Res.* **119**, 414–417 (2016).

18. Blériot, C., Chakarov, S. & Ginhoux, F. Determinants of Resident Tissue Macrophage Identity and Function. *Immunity* **52**, 957–970 (2020).

19. Tremblay, M.-È., Lecours, C., Samson, L., Sánchez-Zafra, V. & Sierra, A. From the Cajal alumni Achúcarro and Río-Hortega to the rediscovery of never-resting microglia. *Front. Neuroanat.* **9**, 45 (2015).

20. Sousa, C., Biber, K. & Michelucci, A. Cellular and Molecular Characterization of Microglia: A Unique Immune Cell Population. *Front. Immunol.* **8**, 198 (2017).

21. Rio-Hortega, P. El tercer elemento de los centos nerviosos. *Bol la Soc esp Biol* **9**, 69–120 (1919).

22. Lawson, L. J., Perry, V. H., Dri, P. & Gordon, S. Heterogeneity in the distribution and morphology of microglia in the normal adult mouse brain. *Neuroscience* **39**, 151–170 (1990).

23. Saijo, K. & Glass, C. K. Microglial cell origin and phenotypes in health and disease. *Nat. Rev. Immunol.* **11**, 775–787 (2011).

24. Ginhoux, F. *et al.* Fate Mapping Analysis Reveals That Adult Microglia Derive from Primitive Macrophages. *Science.* **330**, 841–845 (2010).

25. Ajami, B., Bennett, J. L., Krieger, C., Tetzlaff, W. & Rossi, F. M. V. Local self-renewal can sustain CNS microglia maintenance and function throughout adult life. *Nat. Neurosci.* **10**, 1538–1543 (2007).

26. Gautier, E. L. *et al.* Gene-expression profiles and transcriptional regulatory pathways that underlie the identity and diversity of mouse tissue macrophages. *Nat. Immunol.* **13**, 1118–1128 (2012).

27. Butovsky, O. *et al.* Identification of a unique TGF-β-dependent molecular and functional signature in microglia. *Nat. Neurosci.* **17**, 131–143 (2014).

28. Zhang, Y. *et al.* An RNA-sequencing transcriptome and splicing database of glia, neurons, and vascular cells of the cerebral cortex. *J. Neurosci.* **34**, 11929–11947 (2014).

29. Hickman, S. E. *et al.* The microglial sensome revealed by direct RNA sequencing. *Nat. Neurosci.* **16**, 1896–1905 (2013).

30. Gosselin, D. *et al.* Environment Drives Selection and Function of Enhancers Controlling Tissue-Specific Macrophage Identities. *Cell* **159**, 1327–1340 (2014).

31. Réu, P. *et al.* The Lifespan and Turnover of Microglia in the Human Brain. *Cell Rep.* **20**, 779–784 (2017).

32. Askew, K. *et al.* Coupled Proliferation and Apoptosis Maintain the Rapid Turnover of Microglia in the Adult Brain. *Cell Rep.* **18**, 391–405 (2017).

33. Cronk, J. C. *et al.* Peripherally derived macrophages can engraft the brain independent of irradiation and maintain an identity distinct from microglia. *J. Exp. Med.* **215**, 1627–1647 (2018).

34. Hanamsagar, R. *et al.* Generation of a microglial developmental index in mice and in humans reveals a sex difference in maturation and immune reactivity. *Glia* **66**, 460–460 (2018).

35. Thion, M. S. *et al.* Microbiome Influences Prenatal and Adult Microglia in a Sex-Specific Manner. *Cell* **172**, 500–516 (2018).

36. Schwarz, J. M., Sholar, P. W. & Bilbo, S. D. Sex differences in microglial colonization of the developing rat brain. *J. Neurochem.* **120**, 948–963 (2012).

37. Crain, J. M., Nikodemova, M. & Watters, J. J. Microglia express distinct M1 and M2 phenotypic markers in the postnatal and adult central nervous system in male and female mice. *J. Neurosci. Res.* **91**, 1143–1151 (2013).

38. Lenz, K. M., Nugent, B. M., Haliyur, R. & McCarthy, M. M. Microglia Are Essential to Masculinization of Brain and Behavior. *J. Neurosci.* **33**, 2761–2772 (2013).

39. Davalos, D. *et al.* ATP mediates rapid microglial response to local brain injury in vivo. *Nat. Neurosci.* **8**, 752–758 (2005).

40. Nimmerjahn, A., Kirchhoff, F. & Helmchen, F. Resting Microglial Cells Are Highly Dynamic Surveillants of Brain Parenchyma in Vivo. *Science.* **308**, 1314–1318 (2005).

41. Paolicelli, R. C. *et al.* Synaptic pruning by microglia is necessary for normal brain development. *Science.* **333**, 1456–1458 (2011).

42. Tremblay, M.-È., Lowery, R. L. & Majewska, A. K. Microglial Interactions with Synapses Are Modulated by Visual Experience. *PLoS Biol.* **8**, e1000527 (2010).

43. Schafer, D. P. *et al.* Microglia Sculpt Postnatal Neural Circuits in an Activity and Complement-Dependent Manner. *Neuron* **74**, 691–705 (2012).

44. Rogers, J. T. *et al.* CX3CR1 Deficiency Leads to Impairment of Hippocampal Cognitive Function and Synaptic Plasticity. *J. Neurosci.* **31**, 16241–16250 (2011).

45. Parkhurst, C. N. *et al.* Microglia Promote Learning-Dependent Synapse Formation through Brain-Derived Neurotrophic Factor. *Cell* **155**, 1596–1609 (2013).

46. Gemma, C. & Bachstetter, A. D. The role of microglia in adult hippocampal neurogenesis. *Front. Cell. Neurosci.* **22**, 229 (2013).

47. Bachstetter, A. D. *et al.* Fractalkine and CX3CR1 regulate hippocampal neurogenesis in adult and aged rats. *Neurobiol. Aging* **32**, 2030–44 (2011).

48. Sierra, A. *et al.* Microglia Shape Adult Hippocampal Neurogenesis through Apoptosis-Coupled Phagocytosis. *Cell Stem Cell* **7**, 483–495 (2010).

49. Hughes, A. N. & Appel, B. Microglia phagocytose myelin sheaths to modify developmental myelination. *Nat. Neurosci.* **23**, 1055–1066 (2020).

50. Sipe, G. O. *et al.* Microglial P2Y12 is necessary for synaptic plasticity in mouse

visual cortex. *Nat. Commun.* **7**, 10905 (2016).

51. Schafer, D. P., Lehrman, E. K. & Stevens, B. The “quad-partite” synapse: Microglia-synapse interactions in the developing and mature CNS. *Glia* **61**, 24–36 (2013).

52. Li, Q. & Barres, B. A. Microglia and macrophages in brain homeostasis and disease. *Nat. Rev. Immunol.* **18**, 225–242 (2017).

53. Gosselin, D. *et al.* An environment-dependent transcriptional network specifies human microglia identity. *Science.* **356**, (2017).

54. Grabert, K. *et al.* Microglial brain region-dependent diversity and selective regional sensitivities to aging. *Nat. Neurosci.* **19**, 504–16 (2016).

55. Böttcher, C. *et al.* Human microglia regional heterogeneity and phenotypes determined by multiplexed single-cell mass cytometry. *Nat. Neurosci.* **22**, 78–90 (2019).

56. Doorn, K. J. *et al.* Brain region-specific gene expression profiles in freshly isolated rat microglia. *Front. Cell. Neurosci.* **9**, 84 (2015).

57. Stratoulias, V., Venero, J. L., Tremblay, M.-È. & Joseph, B. Microglial subtypes: diversity within the microglial community. *EMBO J.* **38**, e101997 (2019).

58. Hammond, T. R. *et al.* Single-Cell RNA Sequencing of Microglia throughout the Mouse Lifespan and in the Injured Brain Reveals Complex Cell-State Changes. *Immunity* **50**, 253–271 (2019).

59. De Schepper, S., Crowley, G. & Hong, S. Understanding microglial diversity and implications for neuronal function in health and disease. *Dev. Neurobiol.* **81**, 507–523 (2021).

60. World Health Organisation. *Dementia fact sheet*. https://www.who.int/news-room/fact-sheets/detail/dementia (2017).

61. Crous-Bou, M., Minguillón, C., Gramunt, N. & Molinuevo, J. L. Alzheimer’s disease prevention: from risk factors to early intervention. *Alzheimers. Res. Ther.* **9**, 71 (2017).

62. Dubois, B. *et al.* Preclinical Alzheimer’s disease: Definition, natural history, and

diagnostic criteria. *Alzheimer's Dement.* **12**, 292–323 (2016).

63. De Strooper, B. & Karran, E. The Cellular Phase of Alzheimer's Disease. *Cell* **164**, 603–615 (2016).

64. Pennanen, C. *et al.* Hippocampus and entorhinal cortex in mild cognitive impairment and early AD. *Neurobiol. Aging* **25**, 303–310 (2004).

65. Desikan, R. S. *et al.* Automated MRI measures identify individuals with mild cognitive impairment and Alzheimer's disease. *Brain* **132**, 2048–2057 (2009).

66. Liu, C.-C., Liu, C.-C., Kanekiyo, T., Xu, H. & Bu, G. Apolipoprotein E and Alzheimer disease: risk, mechanisms and therapy. *Nat. Rev. Neurol.* **9**, 106–18 (2013).

67. Farrer, L. A. *et al.* Effects of age, sex, and ethnicity on the association between apolipoprotein E genotype and Alzheimer disease. A meta-analysis. APOE and Alzheimer Disease Meta Analysis Consortium. *JAMA* **278**, 1349–56 (1997).

68. Kinney, J. W. *et al.* Inflammation as a central mechanism in Alzheimer's disease. *Alzheimer's Dement. Transl. Res. Clin. Interv.* **4**, 575 (2018).

69. Chen, G. *et al.* Amyloid beta: structure, biology and structure-based therapeutic development. *Acta Pharmacol. Sin. 2017 389* **38**, 1205–1235 (2017).

70. Medina, M. & Avila, J. The role of extracellular Tau in the spreading of neurofibrillary pathology. *Front. Cell. Neurosci.* **8**, 113 (2014).

71. Schneider, L. S. *et al.* Clinical trials and late-stage drug development for Alzheimer's disease: an appraisal from 1984 to 2014. *J. Intern. Med.* **275**, 251–83 (2014).

72. Guzman-Martinez, L. *et al.* Neuroinflammation as a common feature of neurodegenerative disorders. *Front. Pharmacol.* **10**, 1008 (2019).

73. Seyedian, S. S., Nokhostin, F. & Malamir, M. D. A review of the diagnosis, prevention, and treatment methods of inflammatory bowel disease. *J. Med. Life* **12**, 113–122 (2019).

74. Collaborators GBD 2017 Inflammatory Bowel Disease. The global, regional, and national burden of inflammatory bowel disease in 195 countries and territories,

1990-2017: a systematic analysis for the Global Burden of Disease Study 2017. *lancet. Gastroenterol. Hepatol.* **5**, 17–30 (2020).

75. Podolsky, D. K. Inflammatory Bowel Disease. *N. Engl. J. Med.* **347**, 417–429 (2002).

76. Heyman, M. B. *et al.* Children with early-onset inflammatory bowel disease (IBD): Analysis of a pediatric IBD consortium registry. *J. Pediatr.* **146**, 35–40 (2005).

77. Stokkers, P. C. F. & Hommes, D. W. New cytokine therapeutics for inflammatory bowel disease. *Cytokine* **28**, 167–173 (2004).

78. Szigethy, E., McLafferty, L. & Goyal, A. Inflammatory Bowel Disease. *Child Adolesc. Psychiatr. Clin. N. Am.* **19**, 301–318 (2010).

79. Chudy-Onwugaje, K. O., Christian, K. E., Farraye, F. A. & Cross, R. K. A State-of-the-Art Review of New and Emerging Therapies for the Treatment of IBD. *Inflamm. Bowel Dis.* **25**, 820–830 (2019).

80. Na, Y. R., Stakenborg, M., Seok, S. H. & Matteoli, G. Macrophages in intestinal inflammation and resolution: a potential therapeutic target in IBD. *Nat. Rev. Gastroenterol. Hepatol.* **16**, 531–543 (2019).

81. Cho, J. H. & Brant, S. R. Recent insights into the genetics of inflammatory bowel disease. *Gastroenterology* **140**, 1704–12 (2011).

82. Zhang, B. *et al.* Inflammatory bowel disease is associated with higher dementia risk: a nationwide longitudinal study. *Gut* **70**, 85–91 (2021).

83. Laria, A. *et al.* The macrophages in rheumatic diseases. *J. Inflamm. Res.* **9**, 1–11 (2016).

84. Perry, V. H., Nicoll, J. A. R. & Holmes, C. Microglia in neurodegenerative disease. *Nat. Rev. Neurol.* **6**, 193–201 (2010).

85. Rivollier, A., He, J., Kole, A., Valatas, V. & Kelsall, B. L. Inflammation switches the differentiation program of Ly6Chi monocytes from anti-inflammatory macrophages to inflammatory dendritic cells in the colon. *J. Exp. Med.* **209**, 139 (2012).

86. Kunkle, B. W. *et al.* Genetic meta-analysis of diagnosed Alzheimer's disease identifies new risk loci and implicates Aβ, tau, immunity and lipid processing. *Nat. Genet.* **51**, 414–430 (2019).

87. Witoelar, A. *et al.* Genome-wide Pleiotropy Between Parkinson Disease and Autoimmune Diseases. *JAMA Neurol.* **74**, 780–792 (2017).

88. Lambert, J.-C. *et al.* Meta-analysis of 74,046 individuals identifies 11 new susceptibility loci for Alzheimer's disease. *Nat. Genet.* **45**, 1452–1458 (2013).

89. Cowan, M. & Petri, W. A. Microglia: Immune regulators of neurodevelopment. *Front. Immunol.* **9**, 2576 (2018).

90. Gupta, S. *et al.* Transcriptome analysis reveals dysregulation of innate immune response genes and neuronal activity-dependent genes in autism. *Nat. Commun.* **5**, 5748 (2014).

91. Suzuki, K. *et al.* Microglial Activation in Young Adults With Autism Spectrum Disorder. *JAMA Psychiatry* **70**, 49 (2013).

92. Voineagu, I. *et al.* Transcriptomic analysis of autistic brain reveals convergent molecular pathology. *Nature* **474**, 380–384 (2011).

93. Morgan, J. T. *et al.* Microglial Activation and Increased Microglial Density Observed in the Dorsolateral Prefrontal Cortex in Autism. *Biol. Psychiatry* **68**, 368–376 (2010).

94. Vargas, D. L., Nascimbene, C., Krishnan, C., Zimmerman, A. W. & Pardo, C. A. Neuroglial activation and neuroinflammation in the brain of patients with autism. *Ann. Neurol.* **57**, 67–81 (2005).

95. Tetreault, N. A. *et al.* Microglia in the Cerebral Cortex in Autism. *J. Autism Dev. Disord.* **42**, 2569–2584 (2012).

96. Sekar, A. *et al.* Schizophrenia risk from complex variation of complement component 4. *Nature* **530**, 177–183 (2016).

97. Schafer, D. P. *et al.* Microglia contribute to circuit defects in Mecp2 null mice independent of microglia-specific loss of Mecp2 expression. *Elife* **5**, e15224 (2016).

98. Hellwig, S., Heinrich, A. & Biber, K. The brain's best friend: microglial neurotoxicity revisited. *Front. Cell. Neurosci.* **7**, 71 (2013).

99. Hansen, D. V., Hanson, J. E. & Sheng, M. Microglia in Alzheimer's disease. *J. Cell Biol.* **217**, 459–472 (2018).

100. Liddelow, S. A. *et al.* Neurotoxic reactive astrocytes are induced by activated microglia. *Nature* **541**, 481–487 (2017).

101. Cherry, J. D., Olschowka, J. A. & O'Banion, M. K. Neuroinflammation and M2 microglia: the good, the bad, and the inflamed. *J. Neuroinflammation* **11**, 98 (2014).

102. Hong, S., Dissing-Olesen, L. & Stevens, B. New insights on the role of microglia in synaptic pruning in health and disease. *Curr. Opin. Neurobiol.* **36**, 128 (2016).

103. Koenigsknecht-Talboo, J. & Landreth, G. E. Microglial phagocytosis induced by fibrillar beta-amyloid and IgGs are differentially regulated by proinflammatory cytokines. *J. Neurosci.* **25**, 8240–8249 (2005).

104. Krasemann, S. *et al.* The TREM2-APOE Pathway Drives the Transcriptional Phenotype of Dysfunctional Microglia in Neurodegenerative Diseases. *Immunity* **47**, 566–581 (2017).

105. Keren-Shaul, H. *et al.* A Unique Microglia Type Associated with Restricting Development of Alzheimer's Disease. *Cell* **169**, 1276–1290 (2017).

106. Pulido-Salgado, M., Vidal-Taboada, J. M., Barriga, G. G.-D., Solà, C. & Saura, J. RNA-Seq transcriptomic profiling of primary murine microglia treated with LPS or LPS + IFNγ. *Sci. Rep.* **8**, 16096 (2018).

107. Sala Frigerio, C. *et al.* The Major Risk Factors for Alzheimer's Disease: Age, Sex, and Genes Modulate the Microglia Response to Aβ Plaques. *Cell Rep.* **27**, 1293–1306 (2019).

108. Sobue, A. *et al.* Microglial gene signature reveals loss of homeostatic microglia associated with neurodegeneration of Alzheimer's disease. *Acta Neuropathol. Commun.* **9**, 1 (2021).

109. Mathys, H. *et al.* Single-cell transcriptomic analysis of Alzheimer's disease.

Nature **570**, 332–337 (2019).

110. Olah, M. *et al.* Single cell RNA sequencing of human microglia uncovers a subset associated with Alzheimer's disease. *Nat. Commun.* **11**, 6129 (2020).

111. Srinivasan, K. *et al.* Alzheimer's Patient Microglia Exhibit Enhanced Aging and Unique Transcriptional Activation. *Cell Rep.* **31**, 107843 (2020).

112. Bromberg, Y. & Rost, B. Correlating protein function and stability through the analysis of single amino acid substitutions. *BMC Bioinformatics* **10**, S8 (2009).

113. Kruglyak, L. & Nickerson, D. A. Variation is the spice of life. *Nat. Genet.* **27**, 234–236 (2001).

114. Ng, P. C. & Henikoff, S. Predicting the Effects of Amino Acid Substitutions on Protein Function. *Annu. Rev. Genomics Hum. Genet.* **7**, 61–80 (2006).

115. Shastry, B. S. SNPs: Impact on Gene Function and Phenotype. in *Single Nucleotide Polymorphisms* 3–22 (Humana Press, Totowa, NJ, 2009).

116. Sims, R. *et al.* Rare coding variants in PLCG2, ABI3, and TREM2 implicate microglial-mediated innate immunity in Alzheimer's disease. *Nat. Genet.* **49**, 1373–1384 (2017).

117. Hollingworth, P. *et al.* Common variants at ABCA7, MS4A6A/MS4A4E, EPHA1, CD33 and CD2AP are associated with Alzheimer's disease. *Nat. Genet.* **43**, 429–435 (2011).

118. Miyashita, A. *et al.* SORL1 Is Genetically Associated with Late-Onset Alzheimer's Disease in Japanese, Koreans and Caucasians. *PLoS One* **8**, e58618 (2013).

119. Seshadri, S. Genome-wide Analysis of Genetic Loci Associated With Alzheimer Disease. *JAMA* **303**, 1832 (2010).

120. Bertram, L. *et al.* Genome-wide Association Analysis Reveals Putative Alzheimer's Disease Susceptibility Loci in Addition to APOE. *Am. J. Hum. Genet.* **83**, 623–632 (2008).

121. Naj, A. C. *et al.* Common variants at MS4A4/MS4A6E, CD2AP, CD33 and EPHA1 are associated with late-onset Alzheimer's disease. *Nat. Genet.* **43**, 436–

441 (2011).

122. Johnson, E. C. B. *et al.* Large-scale proteomic analysis of Alzheimer's disease brain and cerebrospinal fluid reveals early changes in energy metabolism associated with microglia and astrocyte activation. *Nat. Med.* **26**, 769–780 (2020).

123. Nott, A. *et al.* Brain cell type-specific enhancer-promoter interactome maps and disease - risk association. *Science.* **366**, 1134–1139 (2019).

124. Bellenguez, C. *et al.* New insights into the genetic etiology of Alzheimer's disease and related dementias. *Nat. Genet.* **54**, 412–436 (2022).

125. Humphrey, M. B., Xing, J. & Titus, A. The TREM2-DAP12 signaling pathway in Nasu-Hakola disease: a molecular genetics perspective. *Res. Reports Biochem.* **5**, 89 (2015).

126. Guerreiro, R. *et al.* TREM2 Variants in Alzheimer's Disease. *N. Engl. J. Med.* **368**, 117–127 (2013).

127. Jonsson, T. *et al.* Variant of TREM2 Associated with the Risk of Alzheimer's Disease. *N. Engl. J. Med.* **368**, 107–116 (2013).

128. Jay, T. R. *et al.* Disease Progression-Dependent Effects of TREM2 Deficiency in a Mouse Model of Alzheimer's Disease. *J. Neurosci.* **37**, 637–647 (2017).

129. Neumann, H. & Takahashi, K. Essential role of the microglial triggering receptor expressed on myeloid cells-2 (TREM2) for central nervous tissue immune homeostasis. *J. Neuroimmunol.* **184**, 92–99 (2007).

130. Wang, Y. *et al.* TREM2 Lipid Sensing Sustains the Microglial Response in an Alzheimer's Disease Model. *Cell* **160**, 1061–1071 (2015).

131. Yeh, F. L., Wang, Y., Tom, I., Gonzalez, L. C. & Sheng, M. TREM2 Binds to Apolipoproteins, Including APOE and CLU/APOJ, and Thereby Facilitates Uptake of Amyloid-Beta by Microglia. *Neuron* **91**, 328–340 (2016).

132. Yuan, P. *et al.* TREM2 Haplodeficiency in Mice and Humans Impairs the Microglia Barrier Function Leading to Decreased Amyloid Compaction and Severe Axonal Dystrophy. *Neuron* **90**, 724–739 (2016).

133. Andreone, B. J. *et al.* Alzheimer's-associated PLCγ2 is a signaling node required for both TREM2 function and the inflammatory response in human microglia. *Nat. Neurosci.* **23**, 927–938 (2020).

134. Piers, T. M. *et al.* A locked immunometabolic switch underlies TREM2 R47H loss of function in human iPSC-derived microglia. *FASEB J.* **34**, 2436–2450 (2020).

135. Cheng-Hathaway, P. J. *et al.* The Trem2 R47H variant confers loss-of-function-like phenotypes in Alzheimer's disease. *Mol. Neurodegener.* **13**, 29 (2018).

136. Hall-Roberts, H. *et al.* TREM2 Alzheimer's variant R47H causes similar transcriptional dysregulation to knockout, yet only subtle functional phenotypes in human iPSC-derived macrophages. *Alzheimers. Res. Ther.* **12**, 151 (2020).

137. Tsai, A. P.-Y. *et al. PLCG2 as a Risk Factor for Alzheimer's Disease*. (2020).

138. de Lange, K. M. *et al.* Genome-wide association study implicates immune activation of multiple integrin genes in inflammatory bowel disease. *Nat. Genet.* **49**, 256–261 (2017).

139. Magno, L. *et al.* Alzheimer's disease phospholipase C-gamma-2 (PLCG2) protective variant is a functional hypermorph. *Alzheimers. Res. Ther.* **11**, 16 (2019).

140. Eyster, K. M. The membrane and lipids as integral participants in signal transduction: lipid signal transduction for the non-lipid biochemist. *Adv. Physiol. Educ.* **31**, 5–16 (2007).

141. Park, J. B. *et al.* Phospholipase signalling networks in cancer. *Nat. Rev. Cancer* **12**, 782–792 (2012).

142. Wang, X., Devaiah, S., Zhang, W. & Welti, R. Signaling functions of phosphatidic acid. *Prog. Lipid Res.* **45**, 250–278 (2006).

143. Suh, P.-G. *et al.* Multiple roles of phosphoinositide-specific phospholipase C isozymes. *BMB Rep.* **41**, 415–34 (2008).

144. Murakami, M. *et al.* Recent progress in phospholipase A2 research: From cells to animals to humans. *Prog. Lipid Res.* **50**, 152–192 (2011).

145. Aoki, J., Inoue, A., Makide, K., Saiki, N. & Arai, H. Structure and function of extracellular phospholipase A1 belonging to the pancreatic lipase gene family. *Biochimie* **89**, 197–204 (2007).

146. Hajicek, N. *et al.* Structural basis for the activation of PLC-γ isozymes by phosphorylation and cancer-associated mutations. *Elife* **8**, e51700 (2019).

147. Liu, Y. *et al.* Structural insights and activating mutations in diverse pathologies define mechanisms of deregulation for phospholipase C gamma enzymes. *EBioMedicine* **51**, 102607 (2020).

148. Singh, S. M. & Murray, D. Molecular modeling of the membrane targeting of phospholipase C pleckstrin homology domains. *Protein Sci.* **12**, 1934 (2003).

149. Kouchi, Z. *et al.* The Role of EF-hand Domains and C2 Domain in Regulation of Enzymatic Activity of Phospholipase Cζ. *J. Biol. Chem.* **280**, 21015–21021 (2005).

150. Bunney, T. D. *et al.* Structural Insights into Formation of an Active Signaling Complex between Rac and Phospholipase C Gamma 2. *Mol. Cell* **34**, 223–233 (2009).

151. Braiman, A., Barda-Saad, M., Sommers, C. L. & Samelson, L. E. Recruitment and activation of PLCγ1 in T cells: a new insight into old domains. *EMBO J.* **25**, 774 (2006).

152. Wang, J., Sohn, H., Sun, G., Milner, J. D. & Pierce, S. K. The autoinhibitory C-terminal SH2 domain of phospholipase C-γ2 stabilizes B cell receptor signalosome assembly. *Sci. Signal.* **7**, 89 (2014).

153. Yablonski, D., Kadlecek, T. & Weiss, A. Identification of a Phospholipase C-γ1 (PLC-γ1) SH3 Domain-Binding Site in SLP-76 Required for T-Cell Receptor-Mediated Activation of PLC-γ1 and NFAT. *Mol. Cell. Biol.* **21**, 4208–4218 (2001).

154. Poissonnier, A. *et al.* CD95-Mediated Calcium Signaling Promotes T Helper 17 Trafficking to Inflamed Organs in Lupus-Prone Mice. *Immunity* **45**, 209 (2016).

155. Koss, H., Bunney, T. D., Behjati, S. & Katan, M. Dysfunction of phospholipase Cγ in immune disorders and cancer. *Trends Biochem. Sci.* **39**, 603–11 (2014).

156. Zerbino, D. R. *et al.* Ensembl 2018. *Nucleic Acids Res.* **46**, D754–D761 (2018).

157. Wilde, J. I. & Watson, S. P. Regulation of phospholipase C gamma isoforms in haematopoietic cells: why one, not the other? *Cell. Signal.* **13**, 691–701 (2001).

158. Ji, Q. S. *et al.* Essential role of the tyrosine kinase substrate phospholipase C-gamma1 in mammalian growth and development. *Proc. Natl. Acad. Sci.* **94**, 2999–3003 (1997).

159. Katan, M. Families of phosphoinositide-specific phospholipase C: structure and function. *Biochim. Biophys. Acta - Mol. Cell Biol. Lipids* **1436**, 5–17 (1998).

160. Regunathan, J. *et al.* Differential and nonredundant roles of phospholipase Cgamma2 and phospholipase Cgamma1 in the terminal maturation of NK cells. *J. Immunol.* **177**, 5365–5376 (2006).

161. Liao, H.-J. *et al.* Absence of erythrogenesis and vasculogenesis in Plcg1-deficient mice. *J. Biol. Chem.* **277**, 9335–9341 (2002).

162. Seo, J. B., Jung, S. R., Huang, W., Zhang, Q. & Koh, D. S. Charge Shielding of PIP2 by Cations Regulates Enzyme Activity of Phospholipase C. *PLoS One* **10**, e0144432 (2015).

163. Xu, C. *et al.* A PI(4,5)P2-derived "gasoline engine model" for the sustained B cell receptor activation. *Immunol. Rev.* **291**, 75–90 (2019).

164. Philips, T. E. J. *et al.* The Alzheimer's disease protective R522 variant of PLCg2, consistently enhances PLCγ2 activation, depleting PI(4,5)P2 levels and altering cell function in in vitro and in vivo assays. *Alzheimer's Dement.* **16**, e047404 (2020).

165. Huang, Y. H. & Sauer, K. Lipid signaling in T-cell development and function. *Cold Spring Harb. Perspect. Biol.* **2**, a002428 (2010).

166. Kadamur, G. & Ross, E. M. Mammalian Phospholipase C. *Annu. Rev. Physiol.* **75**, 127–154 (2013).

167. Gresset, A., Sondek, J. & Harden, T. K. The Phospholipase C Isozymes and Their Regulation. *Subcell. Biochem.* **58**, 61–94 (2012).

168. Eichmann, T. O. & Lass, A. DAG tales: the multiple faces of diacylglycerol--

stereochemistry, metabolism, and signaling. *Cell. Mol. Life Sci.* **72**, 3931–3952 (2015).

169. Desfougères, Y., Wilson, M. S. C., Laha, D., Miller, G. J. & Saiardi, A. ITPK1 mediates the lipid-independent synthesis of inositol phosphates controlled by metabolism. *Proc Natl Acad Sci U S A.* **116**, 24551–24561 (2019).

170. Kim, Y. J., Sekiya, F., Poulin, B., Bae, Y. S. & Rhee, S. G. Mechanism of B-Cell Receptor-Induced Phosphorylation and Activation of Phospholipase C-γ2. *Mol. Cell. Biol.* **24**, 9986–9999 (2004).

171. Walliser, C. *et al.* Functional characterization of phospholipase C-γ2 mutant protein causing both somatic ibrutinib resistance and a germline monogenic autoinflammatory disorder. *Oncotarget* **9**, 34357–34378 (2018).

172. Falasca, M. *et al.* Activation of phospholipase C gamma by PI 3-kinase-induced PH domain-mediated membrane targeting. *EMBO J.* **17**, 414 (1998).

173. Watanabe, D. *et al.* Four Tyrosine Residues in Phospholipase C-γ2, Identified as Btk-dependent Phosphorylation Sites, Are Required for B Cell Antigen Receptor-coupled Calcium Signaling. *J. Biol. Chem.* **276**, 38595–38601 (2001).

174. Piechulek, T. *et al.* Isozyme-specific Stimulation of Phospholipase C-γ2 by Rac GTPases. *J. Biol. Chem.* **280**, 38923–38931 (2005).

175. Nakamura, Y. & Fukami, K. Regulation and physiological functions of mammalian phospholipase C. *J. Biochem.* **161**, 94 (2017).

176. Walliser, C. *et al.* The Phospholipase Cγ2 Mutants R665W and L845F Identified in Ibrutinib-resistant Chronic Lymphocytic Leukemia Patients Are Hypersensitive to the Rho GTPase Rac2 Protein. *J. Biol. Chem.* **291**, 22136–22148 (2016).

177. Bourgin-Hierle, C., Gobert-Gosse, S., Thérier, J., Grasset, M.-F. & Mouchiroud, G. Src-family kinases play an essential role in differentiation signaling downstream of macrophage colony-stimulating factor receptors mediating persistent phosphorylation of phospholipase C-γ2 and MAP kinases ERK1 and ERK2. *Leukemia* **22**, 161–169 (2008).

178. Zanoni, I. *et al.* CD14 Controls the LPS-Induced Endocytosis of Toll-like

Receptor 4. *Cell* **147**, 868–880 (2011).

179. Wonerow, P., Pearce, A. C., Vaux, D. J. & Watson, S. P. A critical role for phospholipase Cgamma2 in alphaIIbbeta3-mediated platelet spreading. *J. Biol. Chem.* **278**, 37520–37529 (2003).

180. Inoue, O., Suzuki-Inoue, K., Dean, W. L., Frampton, J. & Watson, S. P. Integrin α2β1 mediates outside-in regulation of platelet spreading on collagen through activation of Src kinases and PLCγ2. *J. Cell Biol.* **160**, 769–780 (2003).

181. Wen, R., Jou, S.-T., Chen, Y., Hoffmeyer, A. & Wang, D. Phospholipase Cγ2 Is Essential for Specific Functions of FcεR and FcγR. *J. Immunol.* **169**, 6743–6752 (2002).

182. Wang, D. *et al.* Phospholipase Cγ2 Is Essential in the Functions of B Cell and Several Fc Receptors. *Immunity* **13**, 25–35 (2000).

183. Obst, J. *et al.* PLCγ2 regulates TREM2 signalling and integrin-mediated adhesion and migration of human iPSC-derived macrophages. *Sci. Rep.* **11**, 19842 (2021).

184. Mócsai, A. *et al.* The immunomodulatory adapter proteins DAP12 and Fc receptor γ-chain (FcRγ) regulate development of functional osteoclasts through the Syk tyrosine kinase. *Proc. Natl. Acad. Sci. U. S. A.* **101**, 6158 (2004).

185. Crotti, T. N. *et al.* The immunoreceptor tyrosine-based activation motif (ITAM) - related factors are increased in synovial tissue and vasculature of rheumatoid arthritic joints. *Arthritis Res. Ther.* **14**, R245 (2012).

186. Galson, D. L. & Roodman, G. D. Origins of Osteoclasts. in *Osteoimmunology* 7–41 (Academic Press, 2011).

187. Burger, J. A. & Wiestner, A. Targeting B cell receptor signalling in cancer: preclinical and clinical advances. *Nat. Rev. Cancer* **18**, 148–167 (2018).

188. Woyach, J. A., Johnson, A. J. & Byrd, J. C. The B-cell receptor signaling pathway as a therapeutic target in CLL. *Blood* **120**, 1175 (2012).

189. Kania, E., Roest, G., Vervliet, T., Parys, J. B. & Bultynck, G. IP3 Receptor-Mediated Calcium Signaling and Its Role in Autophagy in Cancer. *Front. Oncol.* **7**, 140 (2017).

190. Mebratu, Y. & Tesfaigzi, Y. How ERK1/2 activation controls cell proliferation and cell death: Is subcellular localization the answer? *Cell cycle* **8**, 1168–1175 (2009).

191. Konishi, H. & Kiyama, H. Microglial TREM2/DAP12 signaling: A double-edged sword in neural diseases. *Front. Cell. Neurosci.* **12**, 206 (2018).

192. N'Diaye, E.-N. *et al.* TREM-2 (triggering receptor expressed on myeloid cells 2) is a phagocytic receptor for bacteria. *J. Cell Biol.* **184**, 215 (2009).

193. Kawabori, M. *et al.* Triggering Receptor Expressed on Myeloid Cells 2 (TREM2) Deficiency Attenuates Phagocytic Activities of Microglia and Exacerbates Ischemic Damage in Experimental Stroke. *J. Neurosci.* **35**, 3384 (2015).

194. Zhong, L. *et al.* Amyloid-beta modulates microglial responses by binding to the triggering receptor expressed on myeloid cells 2 (TREM2). *Mol. Neurodegener.* **13**, 15 (2018).

195. Lanier, L. L., Corliss, B. C., Wu, J., Leong, C. & Phillips, J. H. Immunoreceptor DAP12 bearing a tyrosine-based activation motif is involved in activating NK cells. *Nature* **391**, 703–707 (1998).

196. Call, M. E., Wucherpfennig, K. W. & Chou, J. J. The structural basis for intramembrane assembly of an activating immunoreceptor complex. *Nat. Immunol.* **11**, 1023–1029 (2010).

197. Bouchon, A., Hernández-Munain, C., Cella, M. & Colonna, M. A Dap12-Mediated Pathway Regulates Expression of Cc Chemokine Receptor 7 and Maturation of Human Dendritic Cells. *J. Exp. Med.* **194**, 1111–1122 (2001).

198. Lanier, L. L. & Bakker, A. B. . The ITAM-bearing transmembrane adaptor DAP12 in lymphoid and myeloid cell function. *Immunol. Today* **21**, 611–614 (2000).

199. Stefano, L. *et al.* The surface-exposed chaperone, Hsp60, is an agonist of the microglial TREM2 receptor. *J. Neurochem.* **110**, 284–294 (2009).

200. Otero, K. *et al.* Macrophage colony-stimulating factor induces the proliferation and survival of macrophages via a pathway involving DAP12 and β-catenin. *Nat. Immunol.* **10**, 734–743 (2009).

201. Peng, Q. *et al.* TREM2- and DAP12-dependent activation of PI3K requires DAP10 and is inhibited by SHIP1. *Sci. Signal.* **3**, ra38 (2010).

202. Liu, W. *et al.* Trem2 promotes anti-inflammatory responses in microglia and is suppressed under pro-inflammatory conditions. *Hum. Mol. Genet.* **29**, 3224–3248 (2020).

203. Colonna, M. & Wang, Y. TREM2 variants: new keys to decipher Alzheimer disease pathogenesis. *Nat. Rev. Neurosci.* **17**, 201–207 (2016).

204. Magno, L., Bunney, T. D., Mead, E., Svensson, F. & Bictash, M. N. TREM2/PLCγ2 signalling in immune cells: function, structural insight, and potential therapeutic modulation. *Mol. Neurodegener.* **16**, 22 (2021).

205. Everett, K. L. *et al.* Characterization of Phospholipase Cγ Enzymes with Gain-of-Function Mutations. *J. Biol. Chem.* **284**, 23083–23093 (2009).

206. Abe, K. *et al.* A novel N-ethyl-N-nitrosourea-induced mutation in phospholipase Cγ2 causes inflammatory arthritis, metabolic defects, and male infertility in vitro in a murine model. *Arthritis Rheum.* **63**, 1301–1311 (2011).

207. Yu, P. *et al.* Autoimmunity and Inflammation Due to a Gain-of-Function Mutation in Phospholipase Cγ2 that Specifically Increases External Ca2+ Entry. *Immunity* **22**, 451–465 (2005).

208. Bunney, T. D. *et al.* Structural and Functional Integration of the PLCγ Interaction Domains Critical for Regulatory Mechanisms and Signaling Deregulation. *Structure* **20**, 2062–2075 (2012).

209. Wang, D. *et al.* Phospholipase Cgamma2 is essential in the functions of B cell and several Fc receptors. *Immunity* **13**, 25–35 (2000).

210. Maltseva, N. *et al.* Cold urticaria – What we know and what we do not know. *Allergy* **76**, 1077–1094 (2021).

211. Ombrello, M. J. *et al.* Cold Urticaria, Immunodeficiency, and Autoimmunity Related to PLCG2 Deletions. *N. Engl. J. Med.* **366**, 330–338 (2012).

212. Milner, J. D. PLAID: a Syndrome of Complex Patterns of Disease and Unique Phenotypes. *J. Clin. Immunol.* **35**, 527–530 (2015).

213. Aderibigbe, O. M. *et al.* Distinct Cutaneous Manifestations and Cold-Induced Leukocyte Activation Associated With PLCG2 Mutations. *JAMA Dermatology* **151**, 627–634 (2015).

214. Gandhi, C., Healy, C., Wanderer, A. A. & Hoffman, H. M. Familial atypical cold urticaria: Description of a new hereditary disease. *J. Allergy Clin. Immunol.* **124**, 1245–1250 (2009).

215. Zhou, Q. *et al.* A Hypermorphic Missense Mutation in PLCG2 , Encoding Phospholipase Cγ2, Causes a Dominantly Inherited Autoinflammatory Disease with Immunodeficiency. *Am. J. Hum. Genet.* **91**, 713–720 (2012).

216. Neves, J. F. *et al.* Novel PLCG2 Mutation in a Patient With APLAID and Cutis Laxa. *Front. Immunol.* **9**, 2863 (2018).

217. Chae, J. J. *et al.* Connecting two pathways through Ca 2+ signaling: NLRP3 inflammasome activation induced by a hypermorphic PLCG2 mutation. *Arthritis Rheumatol.* **67**, 563–567 (2015).

218. Zhao, Z. *et al.* A novel role of NLRP3-generated IL-1β in the acute-chronic transition of peripheral lipopolysaccharide-elicited neuroinflammation: Implications for sepsis-associated neurodegeneration. *J. Neuroinflammation* **17**, 64 (2020).

219. Ahn, I. E. *et al.* Clonal evolution leading to ibrutinib resistance in chronic lymphocytic leukemia. *Blood* **129**, 1469–1479 (2017).

220. Albitar, A. *et al.* Using high-sensitivity sequencing for the detection of mutations in BTK and PLCγ2 genes in cellular and cell-free DNA and correlation with progression in patients treated with BTK inhibitors. *Oncotarget* **8**, 17936–17944 (2017).

221. Burger, J. A. *et al.* Clonal evolution in patients with chronic lymphocytic leukaemia developing resistance to BTK inhibition. *Nat. Commun.* **7**, 11589 (2016).

222. Martín-Nalda, A. *et al.* Severe Autoinflammatory Manifestations and Antibody Deficiency Due to Novel Hypermorphic PLCG2 Mutations. *J. Clin. Immunol.* **40**, 987 (2020).

223. Read, J. A., Rozmus, J. & Hannibal, M. C. PLCG2 gene calcium-binding C2 domain variant results in autoinflammation and phospholipase C-gamma-2-associated antibody deficiency and immune dysregulation phenotype. *J. Clin. Immunol.* **38**, 330–444 (2018).

224. Novice, T. *et al.* A Germline Mutation in the C2 Domain of PLCγ2 Associated with Gain-of-Function Expands the Phenotype for PLCG2-Related Diseases. *J. Clin. Immunol.* **40**, 267–276 (2020).

225. Parker, L. *et al.* Phospholipase C-Gamma 2 Activity in Familial Steroid-Sensitive Nephrotic Syndrome. *Pediatr. Res.* **85**, 719–723 (2019).

226. Maguire, E. *et al.* PIP2 depletion and altered endocytosis caused by expression of Alzheimer's disease-protective variant PLCγ2 R522. *EMBO J.* **40**, e105603 (2021).

227. Takalo, M. *et al.* The Alzheimer's disease-associated protective Plcγ2-P522R variant promotes immune functions. *Mol. Neurodegener.* **15**, 52 (2020).

228. Kleineidam, L. *et al.* PLCG2 protective variant p.P522R modulates tau pathology and disease progression in patients with mild cognitive impairment. *Acta Neuropathol.* **139**, 1025–1044 (2020).

229. Karikari, T. K. *et al.* Blood phosphorylated tau 181 as a biomarker for Alzheimer's disease: a diagnostic performance and prediction modelling study using data from four prospective cohorts. *Lancet Neurol.* **19**, 422–433 (2020).

230. van der Lee, S. J. *et al.* A nonsynonymous mutation in PLCG2 reduces the risk of Alzheimer's disease, dementia with Lewy bodies and frontotemporal dementia, and increases the likelihood of longevity. *Acta Neuropathol.* **138**, 237–250 (2019).

231. Tsai, A. P. *et al. PLCG2 as a Risk Factor for Alzheimer's Disease*. *bioRxiv* (2020).

232. Mao, D., Epple, H., Uthgenannt, B., Novack, D. V & Faccio, R. PLCgamma2 regulates osteoclastogenesis via its interaction with ITAM proteins and GAB2. *J. Clin. Invest.* **116**, 2869–2879 (2006).

233. Wert, G. d. & Mummery, C. Human embryonic stem cells: research, ethics and

policy. *Hum. Reprod.* **18**, 672–682 (2003).

234. Chin, M. H. *et al.* Induced pluripotent stem cells and embryonic stem cells are distinguished by gene expression signatures. *Cell Stem Cell* **5**, 111–123 (2009).

235. Yu, J. & Thomson, J. A. Induced Pluripotent Stem Cells. in *Principles of Tissue Engineering* 581–594 (Academic Press, 2014).

236. Takahashi, K. *et al.* Induction of Pluripotent Stem Cells from Adult Human Fibroblasts by Defined Factors. *Cell* **131**, 861–872 (2007).

237. Lowry, W. E. *et al.* Generation of human induced pluripotent stem cells from dermal fibroblasts. *Proc. Natl. Acad. Sci. U. S. A.* **105**, 2883–2888 (2008).

238. Wilson, K. D. *et al.* MicroRNA Profiling of Human-Induced Pluripotent Stem Cells. *Stem Cells Dev.* **18**, 749–758 (2009).

239. Guenther, M. G. *et al.* Chromatin Structure and Gene Expression Programs of Human Embryonic and Induced Pluripotent Stem Cells. *Cell Stem Cell* **7**, 249 (2010).

240. Narsinh, K. H., Plews, J. & Wu, J. C. Comparison of Human Induced Pluripotent and Embryonic Stem Cells: Fraternal or Identical Twins? *Mol. Ther.* **19**, 635–638 (2011).

241. Wynn, T. A., Chawla, A. & Pollard, J. W. Origins and Hallmarks of Macrophages: Development, Homeostasis, and Disease. *Nature* **496**, 445 (2013).

242. Haenseler, W. *et al.* A Highly Efficient Human Pluripotent Stem Cell Microglia Model Displays a Neuronal-Co-culture-Specific Expression Profile and Inflammatory Response. *Stem Cell Reports* **8**, 1727–1742 (2017).

243. Gutbier, S. *et al.* Large-Scale Production of Human iPSC-Derived Macrophages for Drug Screening. *Int. J. Mol. Sci.* **21**, 4808 (2020).

244. Friedman, B. A. *et al.* Diverse Brain Myeloid Expression Profiles Reveal Distinct Microglial Activation States and Aspects of Alzheimer's Disease Not Evident in Mouse Models. *Cell Rep.* **22**, 832–847 (2018).

245. Dawson, T. M., Golde, T. E. & Lagier-Tourenne, C. Animal models of neurodegenerative diseases. *Nat. Neurosci.* **21**, 1370–1379 (2018).

246. Hasselmann, J. & Blurton-Jones, M. Human iPSC-derived microglia: A growing toolset to study the brain's innate immune cells. *Glia* **68**, 721–739 (2020).

247. Galatro, T. F. *et al.* Transcriptomic analysis of purified human cortical microglia reveals age-associated changes. *Nat. Neurosci.* **20**, 1162–1171 (2017).

248. Smith, A. M. & Dragunow, M. The human side of microglia. *Trends Neurosci.* **37**, 125–135 (2014).

249. Rustenhoven, J. *et al.* Isolation of highly enriched primary human microglia for functional studies. *Sci. Rep.* **6**, 19371 (2016).

250. Bohlen, C. J. *et al.* Diverse Requirements for Microglial Survival, Specification, and Function Revealed by Defined-Medium Cultures. *Neuron* **94**, 759–773 (2017).

251. Speicher, A. M., Wiendl, H., Meuth, S. G. & Pawlowski, M. Generating microglia from human pluripotent stem cells: novel in vitro models for the study of neurodegeneration. *Mol. Neurodegener.* **14**, 46 (2019).

252. Muffat, J. *et al.* Efficient derivation of microglia-like cells from human pluripotent stem cells. *Nat. Med.* **22**, 1358–1367 (2016).

253. Abud, E. M. *et al.* iPSC-derived human microglia-like cells to study neurological diseases. *Neuron* **94**, 278 (2017).

254. Livak, K. J. & Schmittgen, T. D. Analysis of Relative Gene Expression Data Using Real-Time Quantitative PCR and the 2−ΔΔCT Method. *Methods* **25**, 402–408 (2001).

255. Ge, S. X., Son, E. W. & Yao, R. iDEP: an integrated web application for differential expression and pathway analysis of RNA-Seq data. *BMC Bioinformatics* **19**, 534 (2018).

256. Jensen, L. J. *et al.* STRING 8—a global view on proteins and their functional interactions in 630 organisms. *Nucleic Acids Res.* **37**, D412–D416 (2009).

257. Trinquet, E. *et al.* d-myo-Inositol 1-phosphate as a surrogate of d-myo-inositol 1,4,5-tris phosphate to monitor G protein-coupled receptor activation. *Anal. Biochem.* **358**, 126–135 (2006).

258. Thomas, P. & Smart, T. G. HEK293 cell line: A vehicle for the expression of recombinant proteins. *J. Pharmacol. Toxicol. Methods* **51**, 187–200 (2005).

259. Newton, P., Harrison, P. & Clulow, S. A novel method for determination of the affinity of protein: Protein interactions in homogeneous assays. *J. Biomol. Screen.* **13**, 674–682 (2008).

260. Caraux, A. *et al.* Phospholipase C-γ2 is essential for NK cell cytotoxicity and innate immunity to malignant and virally infected cells. *Blood* **107**, 994–1002 (2006).

261. Burns, T. C., Li, M. D., Mehta, S., Awad, A. J. & Morgan, A. A. Mouse models rarely mimic the transcriptome of human neurodegenerative diseases: A systematic bioinformatics-based critique of preclinical models. *Eur. J. Pharmacol.* **759**, 101–117 (2015).

262. Mancuso, R. *et al.* Stem-cell-derived human microglia transplanted in mouse brain to study human disease. *Nat. Neurosci.* **22**, 2111–2116 (2019).

263. Collins, H. Y. & Bohlen, C. J. Isolation and Culture of Rodent Microglia to Promote a Dynamic Ramified Morphology in Serum-free Medium. *J. Vis. Exp.* **133**, 57122 (2018).

264. Cahoy, J. D. *et al.* A Transcriptome Database for Astrocytes, Neurons, and Oligodendrocytes: A New Resource for Understanding Brain Development and Function. *J. Neurosci.* **28**, 264–278 (2008).

265. Zeisel, A. *et al.* Cell types in the mouse cortex and hippocampus revealed by single-cell RNA-seq. *Science.* **347**, 1138–1142 (2015).

266. Ma, X. *et al.* Structural Basis for the Dual Recognition of Helical Cytokines IL-34 and CSF-1 by CSF-1R. *Structure* **20**, 676–687 (2012).

267. Lin, H. *et al.* Discovery of a Cytokine and Its Receptor by Functional Screening of the Extracellular Proteome. *Science.* **320**, 807–811 (2008).

268. Wei, S. *et al.* Functional overlap but differential expression of CSF-1 and IL-34 in their CSF-1 receptor-mediated regulation of myeloid cells. *J. Leukoc. Biol.* **88**, 495–505 (2010).

269. Wang, Y. *et al.* IL-34 is a tissue-restricted ligand of CSF1R required for the development of Langerhans cells and microglia. *Nat. Immunol.* **13**, 753–760 (2012).

270. Greter, M. *et al.* Stroma-Derived Interleukin-34 Controls the Development and Maintenance of Langerhans Cells and the Maintenance of Microglia. *Immunity* **37**, 1050–1060 (2012).

271. Mizuno, T. *et al.* Interleukin-34 selectively enhances the neuroprotective effects of microglia to attenuate oligomeric amyloid-β neurotoxicity. *Am. J. Pathol.* **179**, 2016–2027 (2011).

272. Elmore, M. R. P. *et al.* Colony-Stimulating Factor 1 Receptor Signaling Is Necessary for Microglia Viability, Unmasking a Microglia Progenitor Cell in the Adult Brain. *Neuron* **82**, 380–397 (2014).

273. Reich, M. *et al.* Alzheimer's Risk Gene TREM2 Determines Functional Properties of New Type of Human iPSC-Derived Microglia. *Front. Immunol.* **11**, 3918 (2021).

274. Haage, V. *et al.* Comprehensive gene expression meta-analysis identifies signature genes that distinguish microglia from peripheral monocytes/macrophages in health and glioma. *Acta Neuropathol. Commun.* **7**, 20 (2019).

275. Jurga, A. M., Paleczna, M. & Kuter, K. Z. Overview of General and Discriminating Markers of Differential Microglia Phenotypes. *Front. Cell. Neurosci.* **14**, 198 (2020).

276. Shen, K. *et al.* Multiple sclerosis risk gene Mertk is required for microglial activation and subsequent remyelination. *Cell Rep.* **34**, 108835 (2021).

277. Sasaki, Y., Ohsawa, K., Kanazawa, H., Kohsaka, S. & Imai, Y. Iba1 Is an Actin-Cross-Linking Protein in Macrophages/Microglia. *Biochem. Biophys. Res. Commun.* **286**, 292–297 (2001).

278. Mazaheri, F. *et al.* TREM2 deficiency impairs chemotaxis and microglial responses to neuronal injury. *EMBO Rep.* **18**, 1186–1198 (2017).

279. Woollacott, I. O. C. *et al.* Microglial burden, activation and dystrophy patterns in

frontotemporal lobar degeneration. *J. Neuroinflammation* **17**, 234 (2020).

280. Daily , N. J., Santos, R., Vecchi , J., Kemanli , P. & Wakatsuki , T. Calcium Transient Assays for Compound Screening with Human iPSC-derived Cardiomyocytes: Evaluating New Tools. *J. Evol. stem cell Res.* **1**, 11 (2017).

281. Morgan, A. J. & Jacob, R. Ionomycin enhances Ca2+ influx by stimulating store-regulated cation entry and not by a direct action at the plasma membrane. *Biochem. J.* **300**, 665–672 (1994).

282. Petersen, O. H. & Verkhratsky, A. Calcium and ATP control multiple vital functions. *Philos. Trans. R. Soc. B Biol. Sci.* **371**, 20150418 (2016).

283. Yin, J., Valin, K. L., Dixon, M. L. & Leavenworth, J. W. The Role of Microglia and Macrophages in CNS Homeostasis, Autoimmunity, and Cancer. *J. Immunol. Res.* **2017**, 5150678 (2017).

284. Hall-Roberts, H., Di Daniel, E., James, W. S., Davis, J. B. & Cowley, S. A. In vitro Quantitative Imaging Assay for Phagocytosis of Dead Neuroblastoma Cells by iPSC-Macrophages. *JoVE (Journal Vis. Exp.* e62217 (2021).

285. Bull, D., Schweitzer, C., Bichsel, C., Britschgi, M. & Gutbier, S. Generation of an hiPSC-Derived Co-Culture System to Assess the Effects of Neuroinflammation on Blood–Brain Barrier Integrity. *Cells* **11**, 419 (2022).

286. Zhou, X., Yang, W. & Li, J. Ca2+- and Protein Kinase C-dependent Signaling Pathway for Nuclear Factor-κB Activation, Inducible Nitric-oxide Synthase Expression, and Tumor Necrosis Factor-α Production in Lipopolysaccharide-stimulated Rat Peritoneal Macrophages. *J. Biol. Chem.* **281**, 31337–31347 (2006).

287. Liu, T., Zhang, L., Joo, D. & Sun, S.-C. NF-κB signaling in inflammation. *Signal Transduct. Target. Ther.* **2**, 17023 (2017).

288. Minematsu, H. *et al.* Nuclear presence of nuclear factor of activated T cells (NFAT) c3 and c4 is required for Toll-like receptor-activated innate inflammatory response of monocytes/macrophages. *Cell. Signal.* **23**, 1785 (2011).

289. Parameswaran, N. & Patial, S. Tumor Necrosis Factor-α Signaling in

Macrophages. *Crit. Rev. Eukaryot. Gene Expr.* **20**, 87 (2010).

290. Xu, R. *et al.* Human iPSC-derived mature microglia retain their identity and functionally integrate in the chimeric mouse brain. *Nat. Commun.* **11**, 1577 (2020).

291. Cengiz, P. *et al.* Developmental differences in microglia morphology and gene expression during normal brain development and in response to hypoxia-ischemia. *Neurochem. Int.* **127**, 137 (2019).

292. Mildner, A., Huang, H., Radke, J., Stenzel, W. & Priller, J. P2Y12 receptor is expressed on human microglia under physiological conditions throughout development and is sensitive to neuroinflammatory diseases. *Glia* **65**, 375–387 (2017).

293. Morillas, A. G., Besson, V. C. & Lerouet, D. Microglia and Neuroinflammation: What Place for P2RY12? *Int. J. Mol. Sci.* **22**, 1636 (2021).

294. Jung, S. *et al.* Analysis of Fractalkine Receptor CX3CR1 Function by Targeted Deletion and Green Fluorescent Protein Reporter Gene Insertion. *Mol. Cell. Biol.* **20**, 4106–4114 (2000).

295. Banerjee, P. *et al.* Generation of pure monocultures of human microglia-like cells from induced pluripotent stem cells. *Stem Cell Res.* **49**, 102046 (2020).

296. Dräger, N. M. *et al. A CRISPRi/a platform in iPSC-derived microglia uncovers regulators of disease states*. *bioRxiv* (2022).

297. Lively, S. & Schlichter, L. C. Microglia responses to pro-inflammatory stimuli (LPS, IFNγ+TNFα) and reprogramming by resolving cytokines (IL-4, IL-10). *Front. Cell. Neurosci.* **12**, 215 (2018).

298. Hildebrandt, M. R. *et al.* Precision Health Resource of Control iPSC Lines for Versatile Multilineage Differentiation. *Stem Cell Reports* **13**, 1126 (2019).

299. Jiang, H. *et al.* Chromatin remodeling factor ARID2 suppresses hepatocellular carcinoma metastasis via DNMT1-Snail axis. *Proc. Natl. Acad. Sci. U. S. A.* **117**, 4770–4780 (2020).

300. Schmunk, G. *et al.* High-throughput screen detects calcium signaling dysfunction

in typical sporadic autism spectrum disorder. *Sci. Rep.* **7**, 40740 (2017).

301. Mizoguchi, Y. & Monji, A. Microglial intracellular Ca2+ signaling in synaptic development and its alterations in neurodevelopmental disorders. *Front. Cell. Neurosci.* **11**, 69 (2017).

302. Ishijima, T. & Nakajima, K. Inflammatory cytokines TNFα, IL-1β, and IL-6 are induced in endotoxin- stimulated microglia through different signaling cascades. *Sci. Prog.* **104**, 368504211054985 (2021).

303. Wan, F. & Lenardo, M. J. The Nuclear Signaling of NF-κB – Current Knowledge, New Insights, and Future Perspectives. *Cell Res.* **20**, 24 (2010).

304. Fond, A. M. & Ravichandran, K. S. *Clearance of dying cells by phagocytes: mechanisms and implications for disease pathogenesis*. *Advances in experimental medicine and biology* vol. 930 (NIH Public Access, 2016).

305. Hammond, G. R. V. & Burke, J. E. Novel roles of phosphoinositides in signaling, lipid transport, and disease. *Curr. Opin. Cell Biol.* **63**, 57 (2020).

306. Katan, M. & Cockcroft, S. Phosphatidylinositol(4,5)bisphosphate: diverse functions at the plasma membrane. *Essays Biochem.* **64**, 513–531 (2020).

307. Johnson, C. M. & Rodgers, W. Spatial Segregation of Phosphatidylinositol 4,5-Bisphosphate (PIP2) Signaling in Immune Cell Functions. *Immunol. Endocr. Metab. Agents Med. Chem.* **8**, 349 (2008).

308. Jung, Y. J., Tweedie, D., Scerba, M. T. & Greig, N. H. Neuroinflammation as a Factor of Neurodegenerative Disease: Thalidomide Analogs as Treatments. *Front. Cell Dev. Biol.* **7**, 313 (2019).

309. Ashutosh *et al.* CXCL8 protects human neurons from amyloid-β-induced neurotoxicity: Relevance to Alzheimer's disease. *Biochem. Biophys. Res. Commun.* **412**, 565–571 (2011).

310. Liu, X. & Quan, N. Microglia and CNS interleukin-1: Beyond immunological concepts. *Front. Neurol.* **9**, 8 (2018).

311. Tsai, A. P. *et al.* PLCG2 is associated with the inflammatory response and is induced by amyloid plaques in Alzheimer's disease. *Genome Med.* **14**, 17 (2022).

312. Zhou, Y., Chen, Y., Xu, C., Zhang, H. & Lin, C. TLR4 Targeting as a Promising Therapeutic Strategy for Alzheimer Disease Treatment. *Front. Neurosci.* **14**, 1291 (2020).

313. Zhou, J. *et al.* Imbalance of Microglial TLR4/TREM2 in LPS-Treated APP/PS1 Transgenic Mice: A Potential Link Between Alzheimer's Disease and Systemic Inflammation. *Neurochem. Res.* **44**, 1138–1151 (2019).

314. Couper, K. N., Blount, D. G. & Riley, E. M. IL-10: The Master Regulator of Immunity to Infection. *J. Immunol.* **180**, 5771–5777 (2008).

315. Bluemn, T. *et al.* Arid2 regulates hematopoietic stem cell differentiation in normal hematopoiesis. *Exp. Hematol.* **94**, 37–46 (2021).

316. Kukurba, K. R. & Montgomery, S. B. RNA Sequencing and Analysis. *Cold Spring Harb. Protoc.* **2015**, 951 (2015).

317. Alsema, A. M. *et al.* Profiling Microglia From Alzheimer's Disease Donors and Non-demented Elderly in Acute Human Postmortem Cortical Tissue. *Front. Mol. Neurosci.* **13**, 134 (2020).

318. Wan, Y. W. *et al.* Meta-Analysis of the Alzheimer's Disease Human Brain Transcriptome and Functional Dissection in Mouse Models. *Cell Rep.* **32**, 107908 (2020).

319. McQuade, A. *et al.* Gene expression and functional deficits underlie TREM2-knockout microglia responses in human models of Alzheimer's disease. *Nat. Commun.* **11**, 5370 (2020).

320. Claes, C. *et al.* The P522R protective variant of PLCG2 promotes the expression of antigen presentation genes by human microglia in an Alzheimer's disease mouse model. *Alzheimer's Dement.* (2022).

321. Hu, Y. *et al.* Genetic landscape and autoimmunity of monocytes in developing Vogt-Koyanagi-Harada disease. *Proc. Natl. Acad. Sci. U. S. A.* **117**, 25712–25721 (2020).

322. Moeller, J. B. *et al.* CD163-L1 Is an Endocytic Macrophage Protein Strongly Regulated by Mediators in the Inflammatory Response. *J. Immunol.* **188**, 2399–2409 (2012).

323. Zheng, Q. *et al.* Siglec1 suppresses antiviral innate immune response by inducing TBK1 degradation via the ubiquitin ligase TRIM27. *Cell Res.* **25**, 1121–1136 (2015).

324. Linnartz-Gerlach, B., Kopatz, J. & Neumann, H. Siglec functions of microglia. *Glycobiology* **24**, 794–799 (2014).

325. Kumar, P., Huo, P. & Liu, B. Formulation Strategies for Folate-Targeted Liposomes and Their Biomedical Applications. *Pharmaceutics* **11**, 381 (2019).

326. Sanagi, T., Yabe, T. & Yamada, H. The regulation of pro-inflammatory gene expression induced by pigment epithelium-derived factor in rat cultured microglial cells. *Neurosci. Lett.* **380**, 105–110 (2005).

327. Myers, K. V., Amend, S. R. & Pienta, K. J. Targeting Tyro3, Axl and MerTK (TAM receptors): implications for macrophages in the tumor microenvironment. *Mol. Cancer* **18**, 94 (2019).

328. Huang, Y. *et al.* Microglia use TAM receptors to detect and engulf amyloid β plaques. *Nat. Immunol.* **22**, 586–594 (2021).

329. Koizumi, S. *et al.* UDP acting at P2Y6 receptors is a mediator of microglial phagocytosis. *Nature.* **446**, 1091–1095 (2007).

330. Butler, C. A. *et al.* Microglial phagocytosis of neurons in neurodegeneration, and its regulation. *J. Neurochem.* **158**, 621–639 (2021).

331. De Sousa Abreu, R., Penalva, L. O., Marcotte, E. M. & Vogel, C. Global signatures of protein and mRNA expression levels. *Mol. Biosyst.* **5**, 1512–1526 (2009).

332. Vogel, C. & Marcotte, E. M. Insights into the regulation of protein abundance from proteomic and transcriptomic analyses. *Nat. Rev. Genet.* **13**, 227–232 (2012).

333. Samaniego, R. *et al.* Folate Receptor β (FRβ) Expression in Tissue-Resident and Tumor-Associated Macrophages Associates with and Depends on the Expression of PU.1. *Cells* **9**, 1445 (2020).

334. Zhou, X., Liao, W. J., Liao, J. M., Liao, P. & Lu, H. Ribosomal proteins:

functions beyond the ribosome. *J. Mol. Cell Biol.* **7**, 92 (2015).

335. Van Gorp, H., Delputte, P. L. & Nauwynck, H. J. Scavenger receptor CD163, a Jack-of-all-trades and potential target for cell-directed therapy. *Mol. Immunol.* **47**, 1650–1660 (2010).

336. Han, X. *et al.* TREM2 and CD163 Ameliorate Microglia-Mediated Inflammatory Environment in the Aging Brain. *J. Mol. Neurosci.* **72**, 1075–1084 (2022).

337. Zhu, Z. *et al.* Lipopolysaccharide Downregulates CD163 Expression to Inhibit PRRSV Infection via TLR4-NF-κB Pathway. *Front. Microbiol.* **11**, (2020).

338. Siew, J. J. & Chern, Y. Microglial lectins in health and neurological diseases. *Front. Mol. Neurosci.* **11**, 158 (2018).

339. Gate, D. *et al.* Clonally expanded CD8 T cells patrol the cerebrospinal fluid in Alzheimer's disease. *Nature* **577**, 399–404 (2020).

340. Li, H. *et al.* Expression and Prognostic Value of IFIT1 and IFITM3 in Head and Neck Squamous Cell Carcinoma. *Am. J. Clin. Pathol.* **153**, 618–629 (2020).

341. Borden, E. C. Interferons. in *The Molecular Basis of Cancer: Fourth Edition* 739-752.e7 (W.B. Saunders, 2015).

342. Roy, E. R. *et al.* Type I interferon response drives neuroinflammation and synapse loss in Alzheimer disease. *J. Clin. Invest.* **130**, 1912–1930 (2020).

343. Marschallinger, J. *et al.* Lipid-droplet-accumulating microglia represent a dysfunctional and proinflammatory state in the aging brain. *Nat. Neurosci.* **23**, 194–208 (2020).

344. Claes, C. *et al.* Plaque-associated human microglia accumulate lipid droplets in a chimeric model of Alzheimer's disease. *Mol. Neurodegener.* **16**, 50 (2021).

345. Stevens, B. *et al.* The Classical Complement Cascade Mediates CNS Synapse Elimination. *Cell.* **131**, 1164–1178 (2007).

346. Hong, S. *et al.* Complement and microglia mediate early synapse loss in Alzheimer mouse models. *Science.* **352**, 712–716 (2016).

347. Litvinchuk, A. *et al.* Complement C3aR Inactivation Attenuates Tau Pathology and Reverses an Immune Network Deregulated in Tauopathy Models and

Alzheimer's Disease. *Neuron* **100**, 1337–1353 (2018).

348. Harder, J. M. *et al.* Complement peptide C3a receptor 1 promotes optic nerve degeneration in DBA/2J mice. *J. Neuroinflammation* **17**, 336 (2020).

349. Schartz, N. D. & Tenner, A. J. The good, the bad, and the opportunities of the complement system in neurodegenerative disease. *J. Neuroinflammation* **17**, 354 (2020).

350. Roy, A., Fung, Y. K., Liu, X. & Pahan, K. Up-regulation of Microglial CD11b Expression by Nitric Oxide. *J. Biol. Chem.* **281**, 14971 (2006).

351. Koussounadis, A., Langdon, S. P., Um, I. H., Harrison, D. J. & Smith, V. A. Relationship between differentially expressed mRNA and mRNA-protein correlations in a xenograft model system. *Sci. Rep.* **5**, 10775 (2015).

352. Yu, M. *et al.* PLCγ-dependent mTOR signalling controls IL-7-mediated early B cell development. *Nat. Commun.* **8**, 1457 (2017).

353. Gomez-Arboledas, A., Acharya, M. M. & Tenner, A. J. The Role of Complement in Synaptic Pruning and Neurodegeneration. *ImmunoTargets Ther.* **10**, 373 (2021).

354. Puigdellívol, M. *et al.* The microglial P2Y6 receptor mediates neuronal loss and memory deficits in neurodegeneration. *Cell Rep.* **37**, 110148 (2021).

355. Golde, T. E. Harnessing Immunoproteostasis to Treat Neurodegenerative Disorders. *Neuron* **101**, 1003–1015 (2019).

356. Liang, G. & Zhang, Y. Genetic and epigenetic variations in iPSCs: potential causes and implications for application. *Cell Stem Cell* **13**, 149 (2013).

357. Ogiso, H. & Taguchi, R. Reversed-phase LC/MS method for polyphosphoinositide analyses: Changes in molecular species levels during epidermal growth factor activation in A431 cells. *Anal. Chem.* **80**, 9226–9232 (2008).

358. Kim, C. iPSC technology-Powerful hand for disease modeling and therapeuticscreen. *BMB Rep.* **48**, 256 (2015).